

Tuning the Reactivity of Mononuclear Tridentate Platinum (II) Complexes:

*A detailed Kinetic and Mechanistic Approach using Azole
Nucleophiles*

By

Slindokuhle V Nkabinde

BSc (Honours) (University of KwaZulu-Natal)

Master of Science



**UNIVERSITY OF
KWAZULU-NATAL**

**INYUVESI
YAKWAZULU-NATALI**

School of Chemistry and Physics

Pietermaritzburg

March 2014

Tuning the Reactivity of Mononuclear Tridentate Platinum (II) Complexes:

*A detailed Kinetic and Mechanistic Approach using Azole
Nucleophiles*

By

Slindokuhle V Nkabinde

BSc (Honours) (University of KwaZulu-Natal)

Submitted in fulfilment of the academic requirements for the degree of
Master in Science

School of Chemistry and Physics

Pietermaritzburg

March 2014

Declaration

I hereby declare that this thesis reports results from original work investigated in the School of Chemistry and Physics, University of KwaZulu-Natal, Pietermaritzburg, and has not been submitted for the fulfilment of any degree at any University.

.....

Slindokuhle V. Nkabinde

I hereby certify that this statement is correct.

.....

Prof. D. Jaganyi (supervisor)

School of Chemistry & Physics
University of KwaZulu-Natal
Pietermaritzburg
November 2013

Dedication

This is dedicated to my late father, a loving and wise man.

I thank God for blessing me with the time and memories I spent with him.

Abstract

The kinetic substitution reactions of two different sets of mononuclear Platinum(II) complexes with heterocyclic bio-relevant azole nucleophiles, *viz.* Imidazole (**Im**), 1-methylimidazole (**MIm**), 1,2-Dimethylimidazole (**DIm**), 1,2,4-triazole (**Trz**) and pyrazole (**Pyz**). All substitution reactions were studied under *pseudo*-first order conditions as a function of the incoming nucleophiles concentration and temperature using stopped-flow techniques and UV/Visible spectroscopy.

The first set of complexes included the tridentate polypyridine complexes, Pt(II)(2,2':6,2''-terpyridine)Cl]Cl.2H₂O, (**PtL1**) Pt(II)(1,3-di(2-pyridyl)benzene)Cl, (**PtL2**) Pt(II)(2,6-di-(2'-quinolinyl)pyridine)Cl](Cl), (**PtL3**) and Pt(II)(1,3-di-(2'-quinolinyl)benzene)Cl (**PtL4**). The substitution of these complexes with the previously mentioned azoles showed that tuning electronic communication of the Pt(II) centre towards substitution through quinoline moieties has an opposed effect to that obtained through pyridine moieties, and verified that the *trans*-effect of a phenyl ring is much greater than that of a pyridine ring. The reactivity trend among the complexes was **PtL2** > **PtL4** > **PtL1** > **PtL3**. Once the nucleophiles were categorised into two groups based on their structural similarities, reactivity trend observed amongst the nucleophiles was generally **Im** > **Pyz** > **Trz**, based on the basicity (electronic effects) and **MIm** > **Im** > **DIm** based on steric effects.

The second series of complexes were tridentate [Pt(bis(2-pyridylmethyl)amine)OH₂](ClO₄)₂, **Ptdpa** and [Pt(bis(2-pyridylmethyl)sulfide)OH₂](ClO₄)₂, **Ptdps** of which the kinetics were studied in an aqua medium and at constant ionic strength (0.1 M). **Ptdps** was found to be more reactive (three magnitude higher) than **Ptdpa**. The rate of substitution of the aqua ligand is dependent on the strength of the σ -donor character and the π -acceptability of the atom situated *trans* to the leaving group. The observed reactivity for the azoles followed the trend, **MIm** > **Im** > **DIm** > **Trz** > **Pyz**. This reactivity trend is in accordance with the basicity, and reflects steric and electrophilic effects of the nucleophiles. This was supported by DFT calculations and the X-ray crystal structure of **Ptdps**_Cl.

For all substitution reactions, the temperature dependent studies showed an associative activation. It is envisaged that the findings of this project will provide useful information for designing new drugs as part of a protracted search of effective anticancer drugs with a wider spectrum.

Table of Content

Acknowledgement	i
Poster Presentation	ii
List of Abbreviations	iii
List of Figures	v
List of Tables	viii
Chapter 1: Platinum Chemistry	1
1.1. Introduction to Cancer	1
1.2. Cancer Treatments	1
1.3. Platinum Chemistry and Properties	2
1.3.1. Anticancer Activity of Pt(II) Complexes	3
1.3.1.1. Mechanism of Action of Cisplatin	4
1.3.1.1.1. Cellular Uptake	4
1.3.1.1.2. Reactivity of Cisplatin with DNA	6
1.3.1.2. Cisplatin Resistance	8
1.3.2. New and Non-classical Pt-containing Anticancer Agents	8
1.3.2.1. Second Generation Cisplatin Analogues	8
1.3.2.2. Multi-nuclear Platinum Complexes	10
1.3.3. Current Findings on Anticancer Platinum(II) Drugs	11
1.3.3.1. Terpyridine/tridentate Donor Platinum(II) Complexes	11
1.3.3.1.1. Their Role in Bioinorganic Chemistry	11
1.4. Azoles	13
1.4.1. Azoles in Biological Systems	13
1.5. Aim of Current Study	14
1.6. References	15
Chapter 2: Substitution Reactions	19
2.1. Introduction to Substitution Reactions	19
2.2. Mechanism of Ligand Substitution Reactions for Square Planar Complexes	20
2.2.1. Association Mechanism, <i>A</i>	21
2.2.2. Interchange Mechanism, <i>I</i>	22
2.2.2.1. Associative Interchange mechanism, <i>I_a</i> ,	22
2.2.2.2. Dissociative Interchange mechanism, <i>I_d</i>	22

2.3.	Substitution Reactions of Square Planar Complexes	22
2.3.1.	Kinetics and Mechanisms of Substitution Reactions	24
2.4.	Factors Influencing the Rate of Substitution	26
2.4.1.	The Effect of the Entering Nucleophile	26
2.4.2.	The effect of the non-labile ligand (spectator Ligands)	30
2.4.2.1.	The <i>trans</i> -Effect	31
2.4.2.1.1.	The π -Bonding Theory	32
2.4.2.1.2.	The Molecular Orbital Theory for σ - and π - <i>trans</i> Effect	33
2.4.2.2.	The <i>cis</i> -Effect	35
2.4.3.	The Steric Effect	36
2.4.4.	Effect of the Leaving Group	38
2.4.5.	Solvent Effect	39
2.5.	References	41
Chapter 3: Reaction Kinetics		43
3.1.	Introduction	43
3.2.	The Rate Law	44
3.3.	Integration Rate Expressions	45
3.3.1.	First Order Reactions	45
3.3.2.	Reversible First order reactions	46
3.3.3.	Second Order Reactions	47
3.3.4.	Reversible Second Order reactions	49
3.4.	Activation Parameters	51
3.4.1.	The effect of Pressure on the Volume of Activation	53
3.5.	Experimental kinetic Techniques	54
3.5.1.	UV/ Visible Spectroscopy	54
3.5.2.	Flow Methods	56
3.6.	References	58
Chapter 4: Mechanistic Behaviour of Platinum(II) Complexes with Quinolyl and Pyridyl Moieties Using a Series of Bio-relevant Azole Nucleophiles		60
4.0.	Abstract	60
4.1.	Introduction	61
4.2.	Experimental	63
4.2.1.	Materials and procedures	63

4.2.2.	Synthesis of Ligands	63
4.2.3.	Synthesis of Platinum(II) Complexes	64
4.2.4.	Preparation of Complexes and Nucleophile Solutions for Kinetic Analysis	66
4.2.5.	Physical Measurements and Instrumentation	67
4.2.6.	Computational modelling	67
4.2.7.	X-ray Crystallography	67
4.2.8.	Kinetic measurements	69
4.3.	Results	70
4.3.1.	Computational Studies	70
4.3.2.	Kinetic and Mechanistic Studies	73
4.4.	Discussion	79
4.5.	Conclusion	83
4.6.	References	84
4.7.	Supporting Information	87
 Chapter 5: A Detailed Kinetic and Mechanistic Study of the Substitution Reactions of Platinum(II) Complexes with N^NN- and N^SN-donor Chelates using Azole Nucleophiles. Crystal structure of [Pt(bis(2-pyridylmethyl)sulfide)Cl]ClO₄		109
5.0.	Abstract	109
5.1.	Introduction	110
5.2.	Experimental	112
5.2.1.	Chemicals and reagents	112
5.2.2.	Synthesis of (bis(2-pyridylmethyl) sulphide), dps	113
5.2.3.	Synthesis of Pt(II) complexes	113
5.2.3.1.	Synthesis of [Pt(bis(2-pyridylmethyl) amine)Cl](ClO ₄), Ptdpa-Cl	113
5.2.3.2.	Synthesis of [Pt(bis(2-pyridylmethyl) sulfide)Cl](ClO ₄), Ptdps-Cl	113
5.2.3.3.	Crystallization of [Pt(bis(2-pyridylmethyl) sulphide)Cl](ClO ₄)·CH ₃ NO ₂ , Ptdps-Cl	114
5.2.4.	Preparation of aqua complex solutions	114
5.2.5.	Instrumentation & Physical Measurements	114
5.2.6.	Determination of the p <i>K</i> _a value of Ptdps	115
5.2.7.	Computational Details	116

5.2.8. X ray Crystallography	116
5.2.9. Kinetic measurements	117
5.3. Results	118
5.3.1. Computational Studies	118
5.3.2. Kinetic Studies	121
5.3.3. Crystal Structure of [Pt(dps-Cl)](ClO ₄)·CH ₃ NO ₂	126
5.4. Discussion	128
5.5. Conclusion	131
5.6. References	133
5.7. Supporting Information	136
Chapter 6: Summary and Future Work	161
6.1. Summary	161
6.2. Future Work	162
6.3. References	163

Acknowledgements

I would like to thank my supervisor Professor D. Jaganyi for the opportunity to study under his supervision, his financial support from time to time and for his continuous guidance throughout this project.

I also express my deepest appreciation to the following people:

- Dr Allen Mambanda, Dr Grace Kinunda and Dr Isaac Wekesa for the input and mentorship they offered towards write-up.
- I am also grateful for the support I have received from all the members of our kinetic research group, Dr D. Reddy, Dr Aishath Shaira, Tshephiso Rose Papo, Meshack Sitati and Asman Panyako.
- Im also thankful to Msa Ngubane for his support, assistance and encouragement throughout the course of my study.
- Thanks to Bilaal Ismail for helping me arrange and analyse my X-ray data.
- To my family, all my sisters and all the New Generation harvest City Church members whom I love and appreciate dearly.
- To my close friends Veve Zungu and Mthokozisi Mbanjwa for their invaluable friendship.
- All my friends and colleagues at the school of chemistry who helped provide a good working and joyful environment.

I would also like to acknowledge the following:

- Mr Craig Grimmer for his assistance with NMR analysis and technical issues. As well as Mrs Caryl J. van Rensburg for her help with Mass spectra and CHN analysis.
- The National Research foundation of South Africa and the University of KwaZulu-Natal for their financial assistance throughout this degree.
- Dr M. P. Akerman and Prof. O. Q. Munro for their assistance in determining X-ray crystal structures.
- All the academic and technical staff in the school of chemistry and physics for their assistance and support.

Poster Presentation

16th Biennial South Africa Chemical Institute (SACI 2013) Inorganic Chemistry Conference. Incorporating the Carman Physical Chemistry Symposium, Southern Sun Elangeni Hotel Durban, South Africa, 30 June to 4 July 2013, entitled: *A kinetic and Mechanistic Study of Pt(II) Complexes containing S/N trans-donor chelates with Azole Nucleophiles.*

List of Abbreviations

A	Absorbance
A	Arrhenius pre-exponential factor (as indicated)
A	Associative mechanism
Å	Angstrom (10^{-10} m)
AgCl	Silver chloride
bpma	bis(2-pyridylmethyl)amine
CDCl ₃	deuterated chloroform
C	Celsius
cisplatin	cis-diaminedichloroplatinum(II)
dien	diethylenetriamine
Dim	1,2-dimethylimidazole
D	dissociative
DFT	Density functional theory
d	doublet
dd	doublet of dooublet
DMSO	Dimethyl Sulfoxide
DNA	Deoxyribonucleic acid
E _a	Arrhenius activation energy
ΔE	Energy gap between the HOMO and LUMO
ε	Extinction coefficient
EtOH	Ethanol
G	Gibbs free energy
h	Planck's constant
ΔH [‡]	Change in enthalpy of activation
HET	2-hydroxyethanethiol
His	histidine
HOMO	Highest occupied molecular orbital
I	Ionic strength
I	Interchange
I _a	Associatively activated interchange
I _d	Dissociatively activated interchange
Im	Imidazole

IR	Infrared
k_1, k_{-1}, k_2, k_{-2}	rate constants
K_b	Boltzmann constant ($1.3807 \times 10^{-23} \text{ JK}^{-1}$)
K	Equilibrium constant
K	Kelvin
k_{obs}	observed pseudo first-order constant
l	pathlength
LFER	Linear free energy relationship
LUMO	Lowest Unoccupied Molecular Orbital
MeOH	Methanol
M	Molarity (mol dm^{-3}) or metal
MIm	1-methylimidazole
NBO	Natural bond orbital
n°_{Pt}	Nucleophilicity of the incoming group Pt
NER	Nucleotide excision repair
nm	nanometer
NMR	nuclear magnetic resonance
Nu	Nucleophile
ppm	Parts per million
py	pyridine
Pyz	pyrazole
R	Gas constant ($8.3145 \text{ JK}^{-1} \text{ mol}^{-1}$)
RNA	ribonucleic acid
s	nucleophilic discrimination factor
s	singlet or strong
ΔS^{\ddagger}	change in Activation entropy
T	Temperature
T	Transmittance
UV	Ultraviolet
vis	Visible
vs	very strong
vw	very weak
w	weak
ν	frequency
ΔV^{\ddagger}	Change in partial molar volume change

List of Figures

Figure 1.1	Molecular structures of the Pt complexes investigated for antitumour activity in the bacterial cells.	3
Figure 1.2	Proposed reaction pathway for cisplatin in the cell and binding to the target DNA.	5
Figure 1.3	X-ray and NMR structures showing interactions of cisplatin with double stranded DNA leading to the formation of various adducts. (a). Cisplatin 1,2-d(GpG) intrastrand cross-link, (b). Cisplatin 1,3-d(GpTpG) intrastrand crosslink, (c). cisplatin interstrand crosslink and d. monofunctional adduct bound to a protein.	6
Figure 1.4	Diagram illustrating the development of monofunctional platinum-based drugs that are clinically used worldwide.	10
Figure 1.5	Structures of some platinum terpyridine complexes responsible for DNA intercalation in certain tumour cells.	12
Figure 1.6	Diagram showing mechanism for oxygen binding to deoxyhaemoglobin to produce oxyhemoglobin.	13
Figure 1.7	Structures and corresponding abbreviations for the sets of platinum(II) complexes used in this study.	14
Figure 2.1	The potential energy profile diagrams illustrating the various substitution mechanisms in terms of the Langford-Gary nomenclature.	20
Figure 2.2	Potential energy profiles for an associative substitution mechanism illustrating the relationship between the intermediate and the transition states: (a) shows the bond-breaking transition state at a higher energy, whereas (b) Shows the bond-breaking transition state at a higher energy.	21
Figure 2.3	Scheme showing the energy profile and possible steric changes during an associative substitution of the leaving ligand, X by the entering nucleophile, Y of a square planar complex. The transition state energies are represented by all the even numbers and all the intermediates are represented by the odd numbers.	23
Figure 2.4	Schematic representation of the direct and solvolysis paths of an associative substitution.	25
Figure 2.5	Plot of reaction rates of <i>trans</i> -Pt(py) ₂ Cl ₂ against concentration of various nucleophiles in methanol at 30 °C.	26

Figure 2.6	Illustrates the correlation of the rate constants of and <i>trans</i> -Pt(Et ₃) ₂ Cl ₂ (▲) with various nucleophiles in water at 35 °C and <i>trans</i> -Pt(py) ₂ Cl ₂ (●) in methanol at 30 °C as a reference.	30
Figure 2.7	Schematic diagram representing the labilization of the leaving group, X by the <i>trans</i> ligand, T .	31
Figure 2.8	Charge distribution in induced dipoles in the coordinate, L-Pt-X .	32
Figure 2.9	Schematic diagram of the Pt-PR₃ double bond. if ligands PR₃ and X are in the <i>xy</i> plane and the <i>d</i> orbitals shown are either <i>d_{xy}</i> or <i>d_{yz}</i> .	32
Figure 2.10	Activated trigonal bipyrimidal complex for PtL₂TXY , where T is a π-bonding ligand.	33
Figure 2.11	Molecular orbital diagram of PtCl ₄ ²⁻ .	34
Figure 2.12	Diagram showing the σ-bonding of T-Pt-X using the σ _x MO. (a) The equal σ-bond strengths of T and X . (b) The σ-bonding strength of the <i>trans</i> -ligand, T is greater than that of X thus weakening the Pt-X bond.	34
Figure 2.13	The steric effect of the aryl square planar complex and trigonal bipyrimidal intermediate of the <i>cis</i> isomer and <i>trans</i> isomer.	38
Figure 3.1	Schematic diagram of a UV/Visible Spectrometer.	55
Figure 3.2	Schematic diagram of a Stopped-flow mixing apparatus.	57
Figure 4.1	Molecular structure of the ligand, L4 with thermal ellipsoids at the 50 % probability level.	69
Figure 4.2	UV/Vis spectra for the reaction of PtL3 (5.18 x10 ⁻⁵ M) and MIm (1.04 x10 ⁻³ M) at an ionic strength of 0.1 M (LiCF ₃ SO ₃ and 0.01 M LiCl) , at 298 K. <i>Inset</i> : kinetic trace at 370 nm.	74
Figure 4.3	Typical stopped flow trace for the reaction between PtL2 (3.70 x10 ⁻⁵ M) and DIm (5.55 x10 ⁻³ M) in methanol followed at 318 nm, <i>I</i> = 0.1 M (LiCF ₃ SO ₃ , LiCl) at T = 298 K.	75
Figure 4.4	Concentration dependence of <i>k</i> _{obs} for the displacement of the chloro ligand in PtL4 by theazole nucleophiles at <i>I</i> = 0.1 M, T = 298 K.	76
Figure 4.5	Plot of ln(<i>k</i> ₂ /T) versus 1/T for PtL4 with theazole nucleophiles in the temperature range 15 – 35 °C, <i>I</i> = 0.1 M.	77
Figure 5.1	UV/Vis spectra for the titration of 0.1 mM Ptdps with NaOH, pH range 1–10, T = 298 K. <i>Inset</i> : Plot of absorbance vs. pH at 300 nm.	116
Figure 5.2	Density functional theoretical (DFT) minimum energy structures, HOMO and LUMO frontier molecular orbitals for the complexes Ptdpa and Ptdps .	121
Figure 5.3	UV/ Vis absorbance spectra for Ptdpa (1.032 x10 ⁻⁴ M) and Trz (1.03 x 10 ⁻³ M) at an ionic strength of 0.1 M (NaClO ₄), at 298 K. <i>Inset</i> : kinetic trace at	122

	275 nm.	
Figure 5.4	Stopped-flow kinetic trace at 285 nm for the substitution reaction of Pyz with Ptdps at 298 K.	122
Figure 5.5	Concentration dependence plot for the displacement of the aqua ligand from Ptdps (1.04×10^{-4} M) by azole nucleophiles at 298 K.	123
Figure 5.6	Temperature dependence of $k_2/ \text{M}^{-1} \text{s}^{-1}$, for the displacement of the aqua ligand in Ptdps (1.04×10^{-4} M) by a series of azole nucleophiles.	123
Figure 5.7	Thermal ellipsoid diagram (50% probability surfaces) of the molecular structure of Ptdps-Cl (ClO₄) · CH₃NO₂ .	126
Figure 5.8	Top edge view of the monocation, Ptdps-Cl showing the <i>trans</i> S-donor atom being out-of-plane.	127
Figure 5.9	Plots of $\log k_2$ achieved from the substitution reactions of the Pt(II) complexes against the $\text{p}K_a$ values of the nucleophiles investigated.	131
Figure 6.1	Sulfur-containing Biological Nucleophiles.	162
Figure 6.2	Two additional complexes to extend on Chapter 5 .	

List of Tables

Table 2.1	A selection of n°_{Pt} values listed according to donor atoms for Pt(py) ₂ Cl ₂	29
Table 2.2	Estimated σ - and π - <i>trans</i> effects of selected ligands.	35
Table 2.3	The effect of <i>trans</i> ligand, T on the reactivity rate of <i>cis</i> - Pt(PEt ₃) ₂ TCl with py.	36
Table 2.4	Steric effects on the rate constants for the chloride substitution by pyridine in <i>cis</i> - and <i>trans</i> -[Pt(PEt ₃) ₂ (L)Cl].	37
Table 2.5	The effect of the nature of the leaving group on the rate of substitution of [Pt(dien)X] ⁺ in water at 25 °C.	39
Table 2.6	Solvent Effect on the ³⁶ Cl ⁻ substitution reaction rates with Pt(II) complex, <i>trans</i> -Pt(py) ₂ Cl ₂ at 25 °C.	40
Table 4.1	Crystal data and structural refinement for 1,3-di-(2'-quinoliny)benzene, L4 .	68
Table 4.2	A summary of the DFT calculated parameters for the investigated platinum(II) complexes.	71
Table 4.3	DFT calculated (B3LYP/LANL2DZ) diagrams showing the HOMOs, LUMOs, electrostatic potential mappings and the planarity of the tridentate Pt(II) complexes.	72
Table 4.4	DFT-calculated geometry-optimised structures of PtL3 and PtL4 coordinated DIm to compare levels of steric conflicts due to ion interactions.	73
Table 4.5	Second-order rate constants at 25 °C and the activation parameters for the chloride substitution from tridentate Pt(II) complexes by Im , MIm , DIm , Trz and Pyz azole nucleophiles in methanol [<i>I</i> = 0.1 M (0.09 M LiCF ₃ SO ₃ + 0.01 M LiCl)].	78
Table 4.6	DFT-calculated NBO charges of investigated azole nucleophiles	79
Table 5.1	Crystallographic data and structure refinement for [Ptdps-Cl](ClO ₄)·CH ₃ NO ₂ .	117
Table 5.2	A summary of the DFT calculated structural data for the investigated tridentate Pt(II) complexes, Ptdpa and Ptdps at B3LYP/LANL2DZ level of theory.	120

Table 5.3	Rate constants and activation parameters for substitution reactions of Ptdpa and Ptdps with azole nucleophiles at $T = 298$ K, pH = 2 (Ptdpa) or 3 (Ptdps), $I = 0.1$ M (HClO ₄ adjusted with NaClO ₄).	125
Table 5.4	Selected X-ray determined bond lengths (Å) and angles (°) for Ptdps-Cl .	127
Table 5.5	The pK_a values and NBO charges for the donor atoms of the nucleophiles studied.	128

CHAPTER 1

Platinum Chemistry

1.1. Introduction to Cancer

Cancer is defined as the uncontrolled growth of abnormal cells in the body,^{1,2} it is initiated when one or more cells amongst the 50 trillion normal, healthy cells begins to grow and multiply too much leading to the formation of a solid mass called a malignant tumour or neoplasm (new growth).¹⁻⁴ Cancer is caused by a mutational damage of a gene in particular cells preventing them from reproducing normally as instructed by other cells in their vicinity.^{3,5,6} These rebellious cells (benign tumours) eventually develop the ability to spread out from region where they originated and begin to invade nearby tissues and eventually other organs (malignant tumours) through the blood and the lymphatic systems. This process is called metastasis.^{3,5,7,8} There are more than 200 different kinds of cancers known to affect humans and they can arise from almost any organ or tissue in the body and each type has its unique features even though the basic processes that resulted in these diverse tumours happen to be quite similar.^{1,2,3,5} Cancer is one of the leading causes of death in the world apart from heart-related illnesses, and it does not discriminate based on age, gender or race it may develop in anyone.⁹ These genetic defects which later lead to cancer cells are only (5 – 10%) hereditary from generation to generation and are mostly caused by environmental and lifestyle factors (90 – 95 %) such as drinking alcohol, smoking tobacco and exposure to pollutants.^{1-3,5,10,11} Cancer is responsible for 23 % of total deaths worldwide with lung cancer being the leading cancer type in males, claiming 17 % of total deaths followed by stomach, liver, colorectal, oesophagus and prostate cancer. While in females the most common type of cancer leading to mortality in females is breast cancer, which is responsible for 23% of the total cancer deaths. This is followed by lung, stomach, colorectal and cervical cancer.^{5,9,10} Various treatment methods have been developed to treat different types of cancer with the aim of prolonged the life of cancer patients.

1.2. Cancer Treatments

Nowadays, cancer can be treated using any of these procedures, namely: surgery, radiotherapy, chemotherapy, or by a combination of any of the mentioned techniques.

Surgery:

Is a procedure involving cutting into the patient's body to remove the cancerous part. However, this can be agonizing to some patients and is ineffective for cancer which has spread to other parts or organs of the body.¹²

Radiotherapy:

This works by damaging the DNA responsible for growth and division in the cancerous cells of the exposed tissue using high energies such as gamma rays, x-rays, and charged particles.¹³ This is able to shrink tumours and kills cancer cells. Similar to surgery, radiation therapy is a local treatment since it focuses on one area of the body.

Chemotherapy:

Is the use of drugs to treat any diseases but this term is normally used in cancer treatment. Chemotherapy is different from the other treatments because the drug travels throughout the body to reach the cancer cells or it can be administered directly to treat one part of the body which has cancer.^{14,15} Chemotherapeutic drugs are able to destroy rapidly dividing cells and this includes normal rapidly dividing cells thus leading to side effects. Chemotherapy drugs can be divided into various groups based on their structure, mechanism and similarities with other anti-cancer agents. These include alkylating agents, antimetabolites, antitumour antibiotics and mitotic inhibitor.¹⁴ Alkylating agents in particular, are able to alkylate with many nucleophilic groups under cell conditions. They form covalent bonds with biomolecules such as DNA thus impeding DNA replication and directly damaging the DNA of cells preventing the cancer cells from reproducing.⁷ This consists of metal-based drugs such as the potent platinum(II) anticancer agents, cisplatin and its analogues, carboplatin and oxaliplatin. Modern research now focuses on developing metal-based anti-cancer agents that will target tumour cells and have less damage on normal healthy cells.

Cancer treatment using this group of anti-cancer drugs has drastically accelerated over the years ever since the discovery of the potent anticancer active drug cisplatin.¹⁶

1.3. Platinum Chemistry and Properties

Currently the use of platinum in the medical field has escalated enormously, their use as the major component for a variety of medical devices such as pacemakers, catheters and neuromodulation devices.¹⁷ However, it is the anticancer therapeutic activity of Platinum(II) and Platinum(IV) complexes that has allowed platinum to place its mark in the biomedical field. Platinum-based anticancer drugs are now one of the most extensively used anticancer drugs worldwide ever since the anti-tumour active compound, *cis*-diaminedichloroplatinum(II)

(cisplatin), was first administered to cancer patients in 1971.^{18,19} From then, the field was developed into a thriving area of research.

1.3.1. Anticancer Activity of Pt(II) Complexes

Cisplatin's potent anti-cancer activity was discovered by Barnett Rosenberg in the early 1960's during an experiment to investigate the effect of an applied electric field on cellular growth of *Escherichia coli* (*E. coli*) in a solution of ammonium chloride using a set of platinum electrodes.^{20,21} During this experiment, the platinum electrode rods electrolyzed and the platinum released from the rods reacted with the ammonium chloride solution in the growth chamber to form compounds which resulted in cessation of cell division and induced filamentous growth (300 times its original length) in the bacterial rods.²⁰⁻²³ Further experiments were conducted to determine the complexes liable for this intriguing cell growth behaviour in the *E. coli*, detailed chemical analysis identified four neutral platinum (II) and Platinum(IV) complexes among others, namely: *cis*-[Pt(NH₃)₂Cl₂], *trans*-[Pt(NH₃)₂Cl₂], *cis*-[Pt(NH₃)₂Cl₄] and *trans*-[Pt(NH₃)₂Cl₄] (structures are shown in **Figure 1.1**). After numerous tests of these complexes, it was revealed that only the two *cis*-isomers were found to be active against bacterial cell growth and both the *trans* isomers were inactive.

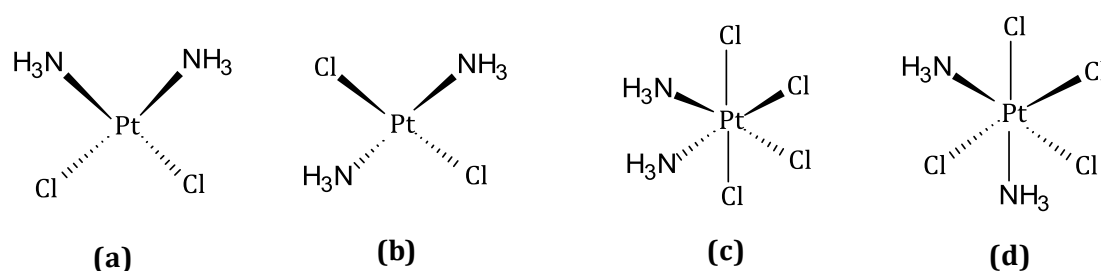


Figure 1.1: Molecular structures of the Pt complexes investigated for antitumour activity in the bacterial cells.

One of the active complexes *cis*-[Pt(NH₃)₂Cl₂] was identified as *cis*-dichlorodiammineplatinum(II), a complex known as Peyrone's chloride since 1845.^{21,22} In 1968 *cis*-dichlorodiammineplatinum(II), also known as cisplatin was administered to mice with solid Sarcoma-180 tumours and was found to be effective at reducing the cancerous tumour indicating that the drug is antitumour active.²¹ Since then, the remarkable discovery of cisplatin's anticancer activity led to its clinical trials in 1971 and its approval by the United States Food and Drug Administration, US FDA in 1978.^{16,21-24} This contributed tremendously to cancer chemotherapy, changing the treatment of an extensive range of solid tumour cancers such as testicular, ovarian, bladder, lung, neck and head cancer as well as cervical cancer.^{16,21,25} Cisplatin has the ability to cure over 90% patients suffering from testicular cancer, improve

endurance in patients diagnosed with advanced ovarian cancer. In addition, it is one of the first cures for small-cell lung cancer.^{7,21} Cisplatin became the first member of a class of platinum-based anti-cancer drugs and has been used ever since to treat tumour cells.²¹⁻²⁴

1.3.1.1. Mechanism of Action of Cisplatin

Cisplatin is a square planar complex containing two non-labile neutral ammonia ligands and two labile anionic chloride ligands. Regardless of the simplicity of its structure, cisplatin is one of the most potent anticancer drugs. Unfortunately its efficacy against cancer is restricted by the severe side effects that emanate from treatments with cisplatin thus limiting its clinical application.²⁶ These include nausea and vomiting, neurotoxicity (kidney damage), nephrotoxicity (renal failure), ototoxicity (Hearing loss) and myelosuppression (reduced bone marrow activity).^{4,16,21,27-29}

The innovative and intense research contributed to this field over the past few decades has led to substantial knowledge about platinum-based drugs such as cisplatin, however the mechanistic details as to how such drugs actually kills cancer cells are still indistinct.

One of the challenges researchers were faced with, was to identify the foremost target of cisplatin. Since the antitumor drug was able to reduce cell division without inhibiting growth in *E. coli*, and was able to inhibit DNA synthesis, DNA was suspected to being the cellular target of platinum-based drugs. Also, the numerous experiments conducted have provided evidence which support DNA to being the major cellular target of Pt-based drugs.^{15,16,21-26}

1.3.1.1.1. Cellular Uptake

Cisplatin is administered to cancer patients intravenously as a saline solution due to its limited water solubility, to minimise side effects such as nephrotoxicity, and to prevent the drug from being hydrolysed in the stomach or any other part besides before reaching the target site.³⁰ From the injected amount, about 50% of the drug is transported through the blood to various tissues while the other half of the platinum complex is eventually excreted through urine.¹⁶

The drug is a neutrally charged complex, making it easier for cisplatin to pass through the lipid bilayer of the cell membrane.²⁵ Previous studies have suggested cisplatin to enter the cell mainly through passive diffusion due to its uptake proceeding linearly with time over 60 minutes.³⁰⁻³³ However in recent studies, there has been an increased amount of evidence which supports the involvement of an active transport mechanism, the copper transporters (CTR 1) which are known for its contribution in copper homeostasis are suggested to be mediators in the cisplatin uptake process.^{22,33-39} From the information gathered over the years, it is appropriately proposed that cisplatin accumulation within the cell occurs by a combination of both passive

and active uptake.²⁹ The presence of a relatively high chloride concentration in extracellular fluids (100 mM) suppress the formation of the mono- and di-aqua species, it is only when cisplatin enters the cell that the activated aqua species are formed.

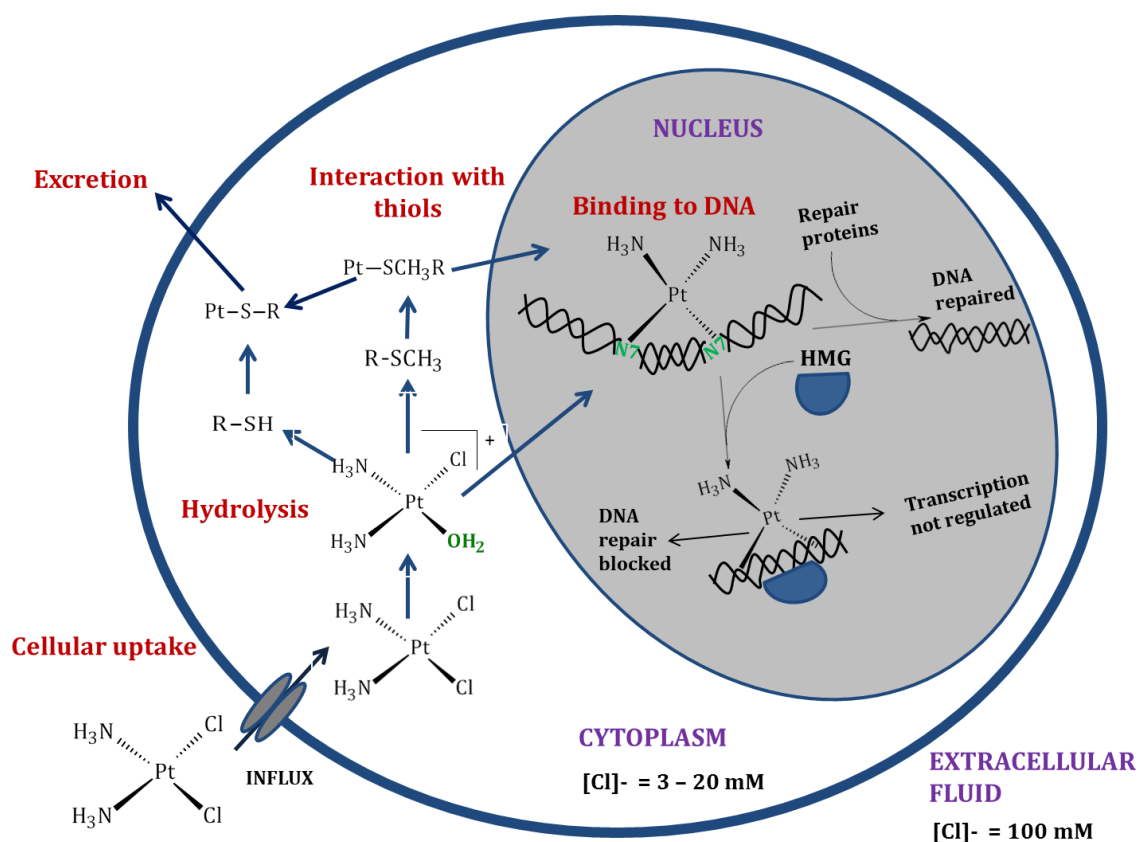


Figure 1.2: Proposed reaction pathway for cisplatin in the cell and binding to the target DNA.^{36,37,38}

Within the cell, the chloride concentration is much lower (2 – 30 mM) and this stimulates the rapid replacement of the first chloride ion with an aqua ligand to mainly form the potent mono-aqua species, $cis-[Pt(H_2O)Cl(NH_3)_2]^+$ (see **Figure 1.2**) with a pK_a of ~ 6.5 .^{34,39} The complex is consecutively ionized further until the second chloro-group is replaced by an aqua group to form a moderately active species, $cis-[Pt(H_2O)_2(NH_3)_2]^{2+}$.^{24,25,40}

Within the cytosol, they are susceptible to cytoplasmic interactions with intercellular components, such as RNA, microfilaments, as well as thiol-containing peptides and proteins such as methionine, metallothionein and glutathione (GSH).^{23,26} Due to a relatively high concentration of SH-containing biomolecules ($\sim 10 \text{ mM}$), the drug can be rapidly deactivated and this could lead to the development of negative pharmacological properties such as resistance and toxicity.^{30,40} Approximately 75 – 85% of cisplatin binds to proteins and other non-DNA cellular components and only 5 – 10% actually reaches, DNA which is assumed to be the target site.^{30,33,40}

1.3.1.1.2. Reactivity of Cisplatin with DNA

It has been generally established that the antitumour properties of cisplatin lie on its ability to bind to DNA and form a various structural adducts.^{21,23,41} The N7 position of the imidazole ring of the purine nucleotide guanosine and to a lesser extent adenine situated in the major groove of the DNA double helix have been identified as the principal cellular target for cisplatin. This is because the N7-position of guanosine is the most nucleophilic and accessible of DNA suitable for platinum to coordinate.^{21,41,42} When cisplatin interacts with DNA to form a variety of either monofunctional or bifunctional adducts which block replication and/or prevent transcription. These adducts include intrastrand crosslinks, interstrand cross-links, protein-DNA adducts or monofunctional adducts.

It has been established that the predominant adducts forming 60 – 65% of cisplatin with DNA is the 1,2-d(GpG) intrastrand cross-links followed by the 1,2-d(ApG) intrastrand cross-links with 20 – 25% of all adducts. The other less frequently occurring adducts such as 1,3-d(GpXpG)-intrastrand cross-links (where there is another base in between the two G-bases), interstrand cross-links and protein-DNA cross-links on guanine each contributed a much smaller percentage of ~ 2 % of all adducts.^{23,33,40,41} Shown in **Figure 1.3** are examples of cisplatin cross-links.

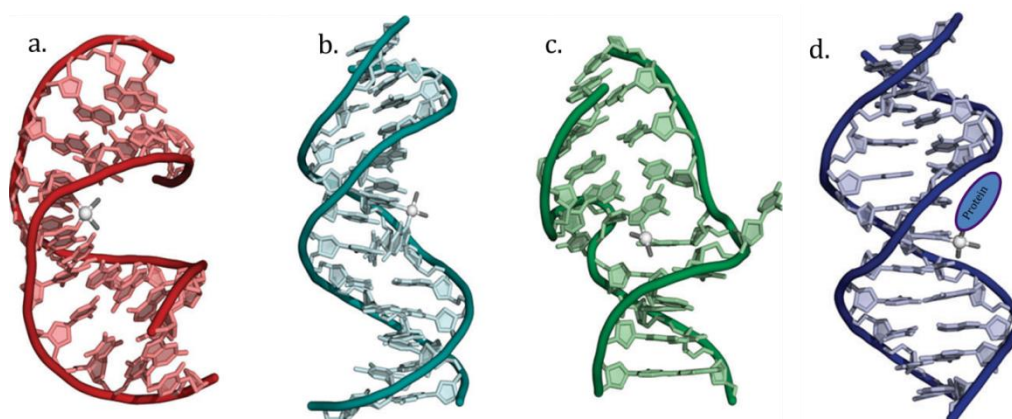


Figure 1.3: X-ray and NMR structures showing interactions of cisplatin with double stranded DNA leading to the formation of various adducts. (a). Cisplatin 1,2-d(GpG) intrastrand cross-link, (b). Cisplatin 1,3-d(GpTpG) intrastrand crosslink, (c). cisplatin interstrand crosslink and d. monofunctional adduct bound to a protein.²⁹

The 1,2-intrastrand adducts are the most preferred cross-links for cisplatin to coordinate to DNA, this is mostly ascribed because it involves two purine bases with the shortest distance between each other. Also, guanine is the most nucleophilic base and its N7 atom is the most

exposed site for Pt-drugs to coordinate. Furthermore, it is suggested that bis-guanine complex, $cis-[Pt(NH_3)_2(Gua)_2]^{2+}$ is more stable than the mono-aqua complex, $cis-[Pt(NH_3)_2(H_2O)Gua]^{2+}$.

Interestingly, when cisplatin covalently binds to two adjacent purines, there is a severe distortion on the double helical structure by causing a bend (between 30 and 60°) of the helix towards the major groove thus widening and flattening the minor groove in the area of the adduct resulting in a destabilization of the double helix.²¹ This deformation alters the natural interactions of DNA with other cellular components such as protein and prevents replication and transcription. This is believed to be the cause of cisplatin's cytotoxicity and is regarded as a crucial step for the antitumour activity of Pt-based drugs.

In some studies conducted with the *trans*-isomer, transplatin was proven to being inactive during *in vivo* antitumour experiments and showed reduced *in vitro* cytotoxicity.³⁰ However, since both transplatin and cisplatin covalently bind to the N7 atom of the purine bases of DNA, therefore reasons as to why the *trans*-isomer was inactive and the *cis*-isomer was active against tumours was due to the different adducts formed because of geometric constrains existing with the *trans*-isomer.²¹ Transplatin is inability to form the 1,2-intrastrand d(GpG) or d(ApG) adducts between adjacent purine bases pairs which are believed to be the active lesions in anticancer activity of Pt-based drugs. Transplatin mainly forms 1,3-intrastands and interstrand adducts instead.^{23,30,43,44} This supports the reasoning that the conformational changes of the duplex DNA associated with the produced adducts are responsible for the anticancer properties of the drug.

The damage on the helical structure caused by the cisplatin-DNA adducts can be recognised by a class of repair cellular proteins. These types of proteins involved in different pathways are able to decide whether the damage is adequate for repair or extensive enough for cell suicide. Several protein types have been associated with recognition of induced-cisplatin-DNA damage but only a few have shown to be of great significance, Nucleotide-excision repair (NER), mismatch repair (MMR) and high-mobility group (HMG) proteins. Of the mentioned proteins, the HMG proteins are those that are able to bind to cisplatin-DNA adducts. These proteins are responsible for repairing the damaged DNA by either cutting out the Pt-adducts and re-constructing DNA at the exposed site, or not repairing the DNA thus preventing DNA replication and transcription and initiating apoptosis (programmed cell death).^{7,22} The NER pathway is regarded as the most versatile system since most types of DNA lesions are removed by them. However, the details of these pathways and the cellular mechanism which would explain and describe the complete processing of DNA lesions are still vague.

Nevertheless, various studies have revealed some of these protein groups to be overexpressed in cell lines which acquire cisplatin resistance during treatment; this supports the thoughts of their involvement in inducing cytotoxicity.^{21-24,30}

1.3.1.2. Cisplatin Resistance

Drug resistance is one of the disadvantages of chemotherapeutic treatment of most common forms of solid tumours. As far as cisplatin is concerned, it's the major setbacks in its clinical applications. This resistance can either be due to pre-existing (intrinsic) mutants of tumour cells that fail to respond to the effects of the drug, or due to induced (acquired) resistance developed by tumour cells to a particular drug or group of drugs as a result of chronic drug exposure during treatment.^{25,45-49} The mechanism leading to cytotoxic effects of cisplatin is still indistinct, however, it has been established that intercellular events that interfere with any stage between the drug uptake step and the final programmed death stage of the entire process will inhibit apoptosis and lead to drug resistance. This includes the following:^{21,24,25,50-52}

- Reduced cellular uptake and/or increased drug efflux by resistant cells resulting in low drug accumulation within the cell.
- Increased repair of cisplatin treatment of DNA lesions (mostly through NER machinery) and signalling promoting cell survival.
- Increased tolerance of cisplatin-DNA adducts.
- Degradation and deactivation of cisplatin by intracellular thiol containing proteins leading to lower levels of the drug reaching the targeted DNA.

1.3.2. New and Non-classical Pt-containing Anticancer Agents

The determination of these biochemical influences that lead to cisplatin resistance in various cancer types such as, ovarian, bladder, cervical, head and neck, and small-cell and non-small-cell lung chemotherapy. This has provided the basis for the design and development of new improved platinum analogues which are able to circumvent cisplatin resistance, display fewer and more bearable side effects and/or broaden the range of treatable cancer types.^{7,22}

1.3.2.1. Second Generation Cisplatin Analogues

Although several platinum analogues have been synthesised and screened for anticancer activities, only a few compounds showed admirable characteristics to be clinically approved by the FDA. These include [*cis*-diaminecyclobutanedicarboxylatoplatinum(II)] (carboplatin), {[*(1R,2R)*-diaminocyclohexane]oxalatoplatinum(II)}[*(1,2)*-diaminocyclohexane]}, oxaliplatinazane; *cis*-Amminedichloro (2-Methylpyridine), (picoplatin or ZD0473) and (*OC*-6-

43)-bis(acetato)amminedichloro(cyclohexylamine)platinum, (satraplatin or JM216) shown in **Figure 1.4**

Out of the mentioned anticancer drugs, carboplatin is the only one active against similar cancer cell lines as the parent drug, cisplatin. The compound consists of two inert *cis*-coordinated amine groups and a stable bidentate leaving group, 1,1'-cyclobutanedicarboxylate (see **Figure 1.4**) which delays the hydrolysis process better than cisplatin (rate constant difference of $\sim 10^{-3}$) thus reducing cell toxicity.^{53,54} This low reactivity of carboplatin, the rate at which the Pt-drug binds to other competing deactivating biomolecules in the cell decreases and higher concentration doses can be administered to patients without concerns about major cisplatin-related drawbacks.^{26,45} However, once carboplatin is aquated, the produced active species is the same as that of cisplatin. This explains why both drugs are active against the same cancer types such as ovarian cancer.^{21,54} Carboplatin has been clinically approved in many countries and has recently been involved in Phase II and III trials for salivary gland cancer treatment.^{54,55}

Oxaliplatin, on the other hand is the first cisplatin analogue to succeed with cisplatin resistant carcinomas. Due to its non-labile bidentate (1*R*,2*R*)-1,2-diaminocyclohexane, (DACH) ligand it is able to form different GpG adducts with DNA. The massive hydrophobic DACH ligand is directed into the major groove preventing DNA repair proteins from binding to the Pt centre.^{54,56} Oxaliplatin also consists of an oxalate leaving group which helps minimize side effects. Currently this drug is extensively used to treat adjuvant and metastatic colorectal carcinomas when combined with other drugs such as flouropyridines and leucovorin.^{21,54,57}

Another successful drug worth mentioning is platinum(IV) octahedral complex, Satraplatin, also known as JM216. Due to its neutral charge, high solubility in aqueous solutions and its adequate lipophilicity, it is one of the first orally administered drugs since it is able to remain stable in the stomach to reach the cancerous cells.⁵⁸ Satraplatin is currently under phase III of the clinical trials for ovarian and small cancers.

Another orally administered cisplatin analogue is *cis*-dichloroamine-(2-methyl)pyridineplatinum(II) also known as picoplatin (ZD0473). It was rationally designed as a sterically hindered Pt(II) complex to resist suppress deactivating thiol-containing components such as glutathione and methionine in order to overcome resistance. X-ray structure data of picoplatin have shown the 2-methyl pyridine ring is tilted 102.7° relative to the coordination square-plane. This obstructs axial approach of the incoming nucleophile to one side of the plane and slows down the hydrolysis process.^{54,59-62} The structural design of this complex demonstrates how reactivity tuning can be used to benefit the biological reactivity (mode of action) of drugs either during delivery or on the site of action.

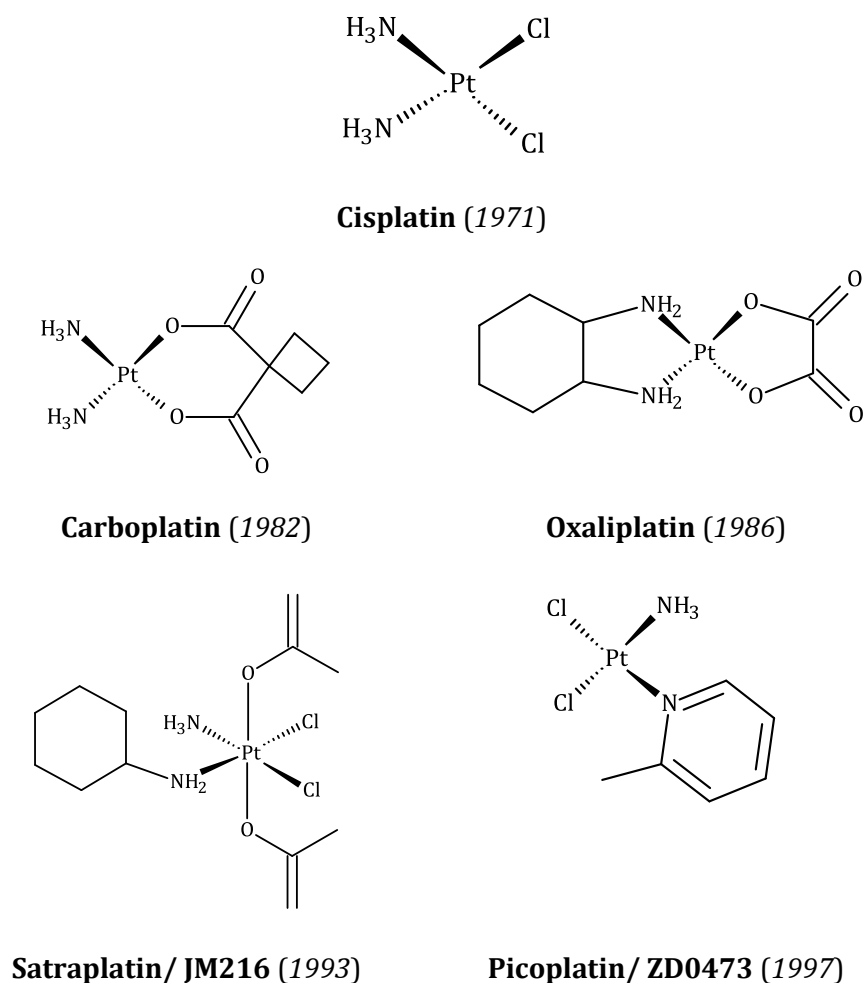


Figure 1.4: Diagram illustrating the development of monofunctional platinum-based drugs that are clinically used worldwide.²²

1.3.2.2. Multi-nuclear Platinum Complexes

Although there has been some improvement in decreasing the severity of the side effects and overcoming resistance, not much progress has been done to reduce cytotoxicity or broadening the spectrum of treatable cancer cell lines. This led to the discovery of non-classical platinum complexes which violate the postulation of platinum(II) complexes to have a *cis*-geometry and two anionic leaving groups in order for it to be anti-tumor active, and multinuclear complexes. Multi-nuclear complexes are platinum complexes which contain two or more linked platinum centres each of which can covalently bind to DNA to give DNA-Pt inter and intrastrand adducts which are structurally different from those of cisplatin and its analogues.⁶³⁻⁶⁶ These adducts have potential to escape recognition by the DNA repair machinery.

1.3.3. Current Findings on Anticancer Platinum(II) Drugs

The antitumour properties of cisplatin and its second generation analogues have paved the way and provided sufficient information about anticancer properties of platinum-based drugs. This has opened a new perspective for the rational design and development of a variety of alternative and extremely diverse metal-based complexes currently being explored by researchers. Still the aim is to develop anticancer drugs with higher activity, increased solubility, circumvent resistant and reduced toxicity. These include *trans*-geomers, charged (both cationic and anionic) and even non-H-amine ligand containing Pt(II) complexes. Recently much focus has been directed to Pt(II) complexes containing non-labile ligands such as pyridine, quinolines

1.3.3.1. Terpyridine/tridentate Donor Platinum(II) Complexes

However, to design metal-based drugs that are applicable as anticancer agents during chemotherapy has been a challenge over the past years for inorganic researchers in this field. Thus any candidate for anticancer agent needs to demonstrate positive substitution reaction abilities with bioinorganic nucleophiles that mimic various fragments of the targeted bimolecular components the drug could possibly coordinate to within the cell, such as thiol-containing proteins and DNA.

The substitution reactions of Pt(II) complexes containing tridentate non-labile ligand systems are the most studied due to their kinetic stability and solubility in aqua solutions with terpyridine platinum(II) complexes and derivatives being the most commonly studied in the bioinorganic chemistry and medical field.

1.3.3.1.1. Their Role in Bioinorganic Chemistry

Synthesis of the first 2,2':6',2''-terpyridine Platinum(II) complex, [Pt(terpy)(Cl)]⁺, was published in 1934.^{67,68} Interest on these square planar complexes comes from their ability to intercalate to DNA. This is the insertion of a planar aromatic heterocyclic ligand of appropriate size and charge between adjacent base pairs of DNA. The perpendicular base pairs distort the helical structure by moving 3.4 Å apart in order to accommodate the intercalator.^{69,70} The resulting DNA-complex intercalation product is stabilised by hydrogen bonds existing between the cationic ligand and the polyanionic nucleic acids.⁶⁹ This is the phenomenon that gives rise to the chemotherapeutic activity of polypyridine complex. For instance, the monocationic Pt(II) terpy derivative, [Pt(terpy)(HET)]⁺, where HET = 2-hydroxyethanethiolate, is known to intercalate to calf thymus DNA with a binding constant of $(1.2 \pm 0.2) \times 10^6 \text{ M}^{-1}$ at pH 6.8 in a $3 \times 10^3 \text{ M}$ sodium chloride solution.^{71,72}

Based on these findings, numerous studies have been conducted with other platinum(II) terpyridine complexes and of which most of them have shown DNA intercalation against tumour cells. The dicationic pyridine complex, $[\text{Pt}(\text{terpy})(4\text{-picoline})]^{2+}$ intercalates to DNA much stronger than the latter complex due to the charge increase, with a binding constant of $(1.8 \pm 0.5) \times 10^7 \text{ M}^{-1}$. While $[\text{Pt}(\text{terpy})(2\text{-picoline})]^{2+}$ had much lower binding constant of 3.0×10^3 compared to $[\text{Pt}(\text{terpy})(4\text{-picoline})]^{2+}$. It was then established that electron donation of the 4-picoline moiety promotes intercalation whereas steric hindrance 2-picoline moiety in $[\text{Pt}(\text{terpy})(2\text{-picoline})]^{2+}$ inhibits intercalation.^{72,73} **Figure 1.5** shows some platinum(II) terpyridine intercalators that have been studied.

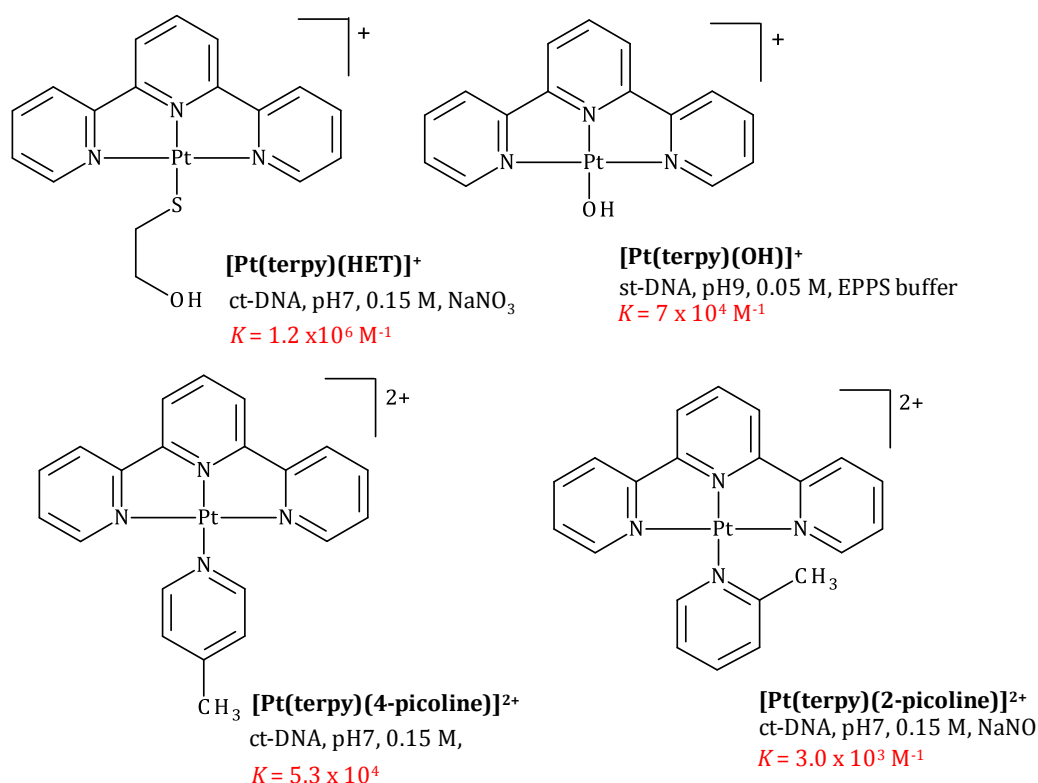


Figure 1.5: Structures of some platinum terpyridine complexes responsible for DNA intercalation in certain tumour cells.^{72,74,75}

A related study conducted by Lowe *et al.*⁷⁶ on the cytotoxicity of a range of platinum(II) 2,2':6',2''-terpyridine derivatives, including the complexes $[\text{Pt}(\text{terpy})(\text{imidazole})]^+$ and $[\text{Pt}(\text{terpy})(\text{thiazole})]^+$, which showed to have antiprotozoal activity in vitro tests against *Leishmania donovani*, *Trypanosoma cruzi* and *Trypanosoma brucei*.⁷⁶ The involvement of bioinorganic components like imidazole and other related azoles on intercalation and cytotoxicity studies was of interest in the current study.

1.4. Azoles

Azoles are five-membered nitrogen-heterocyclic aromatic rings with at least one other atom being a nitrogen, sulfur or oxygen.⁷⁷ Due to their structural similarities with DNA nucleic acids they are important in substitution reactions of Platinum(II) complexes as they give an idea of how such antitumour active Pt(II) complexes with interact with DNA.

1.4.1. Azoles in Biological Systems

Previous studies have shown Platinum complexes prefer to covalently bind or intercalate to the N7-position of guanosine which forms part of an azole ring.^{21,23,72} Also, it has been deduced that imidazole derivatives has an important role in histidine which is one of the ligands in most hemeproteins.^{78,79,80,81}

Hemeproteins comprise of an iron(II) centre coordinated planar to a porphyrin (heme) and axially to a histidine ligand. Depending on the versatility of the heme group and the different interactions it has with other protein scaffolds in different environments, these protein complexes are responsible for various activities, such as electron transfer, catalysis, oxygen transport and storage, ligand binding, signal transduction, and control of gene expression in plants and/or animals.⁸² Hemoglobin and myoglobin are the hemeproteins responsible for oxygen transport and storage, respectively.^{79,82} **Figure 1.6** shows the production of oxyhemoglobin from deoxyhemoglobin.

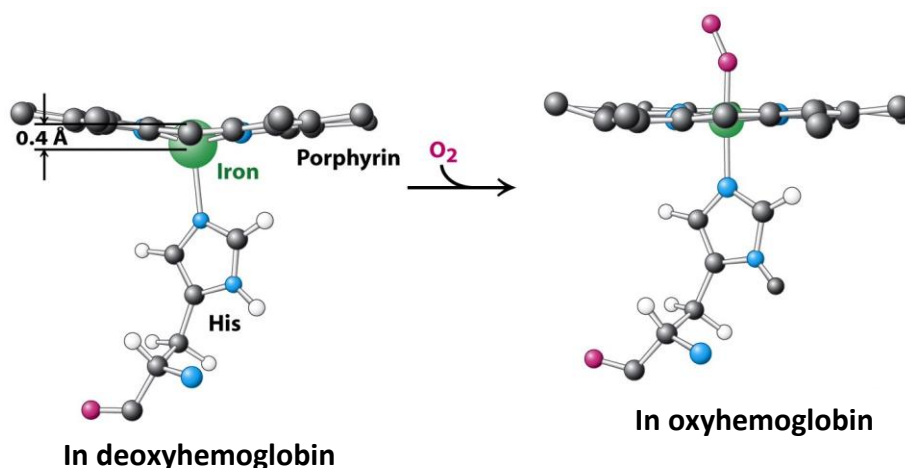


Figure 1.6: Diagram showing mechanism for oxygen binding to deoxyhaemoglobin to produce oxyhemoglobin.⁸³

The functions of azoles in the biological system highlighted above are just a selection of the use of azoles. However, the mentioned uses were the most appealing from a kinetic perspective and they motivated the use of azoles as nucleophiles in this study.

1.5. Aim of Current Study

This study involves the kinetic and mechanistic investigation of two sets of mononuclear Pt(II) complexes structurally designed to provide further understanding on the effects of altering electronic and steric factors on ligand substitution reactions. The first set consists of two Pt(II) aqua complexes bearing *cis*-2-pyridylmethyl ligands chelated to either a *trans*-amine group or a *trans*-sulfide group. For this part of the study we seek to gain a better understanding of the difference in *trans*-effect of the sulfide group as to that of the amine group. Moreover, the effect provided in-depth understanding of the π -acceptor and σ -donor properties of the *trans*-ligands in the presence of *cis*-2-pyridylmethyl ligands. The second set comprises of Pt(II) complexes with either *cis*-pyridine and *cis*-quinoline ligand systems in order to understand on the role of extended π -conjugated systems on substitution reactions. In addition, the *trans* ligand is varied from a pyridine ring to a phenyl ring in order to understand the effect of the *trans* changes combined with the extended conjugation affect the reactivity of the Pt(II) centre. Since Pt(II) complexes are known to prefer binding to the N7 guanine site of DNA, five membered heterocyclic nitrogen donor rings called azoles were chosen as nucleophiles in this study due to their similarities with the targeted binding site and other biological components such as histidine. The five azole nucleophiles used differed in the number of nitrogen atom in the ring, their position in the ring and the number of substituents of the donor atoms. This was to vary the basicity and the steric demands of the nucleophiles and to understand how these changes influences the substitution reactions. **Figure 1.7** shows the chemical structures of all the investigated complexes.

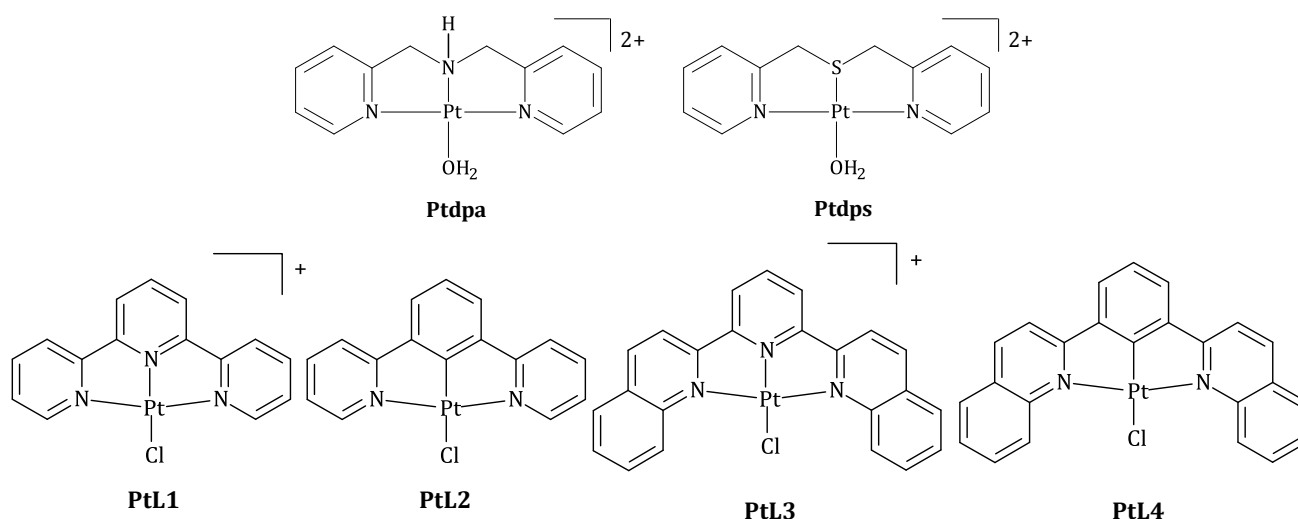


Figure 1.7: Structures and corresponding abbreviations for the sets of platinum(II) complexes used in this study.

Specific aims of the study

1. To extend our understanding on the factors influencing substitution reactivity when one changes the *trans*-amine group of a chelated Pt(II) complex, [Pt(bis(2-pyridylmethyl)amine)(H₂O)](ClO₄)₂ to a *trans*-sulfide group of the chelated complex, [Pt(bis(2-pyridylmethyl) sulphide)H₂O](ClO₄)₂.
2. Is to investigate the role of extended π-conjugation on ligand substitution reactions of mononuclear tridentate Pt(II) complexes by using complexes with *cis*-2-pyridyl or *cis*-2'-quinolinyl ligand systems and to determine how this π-conjugation extension influences the *trans*-effect when the *trans* ligand is a stronger π-accepting pyridine ring and when it is changed to a stronger σ-donating phenyl ring. The result obtained were compared to those of complex, [Pt(2,2':6',2''-terpyridine)Cl]Cl.⁸⁴

1.6. References

1. J. A. Moscow, K. H. Gowan, *Biology of Cancer*. L. Ingoldman, A.L. Schafer, eds., Cecil Medicine. 24th ed. Philadelphia, Pa: Saunders Elsevier, **2011**: Ch 185.
2. M. J. Thun., A. Jemal, *Epidemiology of Cancer*. Goldman L. Schafer A.L., eds., Cecil Medicine. 24th ed. Philadelphia, Pa: Saunders Elsevier, **2011**: Ch 183.
3. R. A. Weinberg, *How Cancer Arises: Sc. Am.*, **1996**, 275, 62 – 70.
4. D. E. Thurston, *Chemistry and Pharmacology of Anti-cancer Drugs*, CRC Press Taylor & Francis Group, USA, **2007**, p. 1 - 27, 61 - 73.
5. J. Cairns, *Cancer Science and Society*, W. H. Freeman and Company, US, **1978**, p. 15-31, 35-39.
6. K. Sandeep, Shweta, S. Nisha, S. M. Munjanath, Ariti, *J. of Drug Delivery & Therapeutics*, **2012**, 2, 3, 97 - 105.
7. Y-P. Ho, S. C. F. Au-Yeung and K. K. W. To, *Medical Res. Rev.*, **2003**, 23, 5, 633 - 655.
8. M. Pan and C. Ho, *Chem. Soc. Rev.*, **2008**, 37, 2558.
9. A. Jemal, F. Bray, M. M. Center, J. Ferlay, E. Ward and D. Forman, *Global Cancer, CA: Cancer J. Clin.*, **2011**, 61, 69 - 90.
10. P. Anand, A. B. Kunnamakara, C. Sundaram, K. B. Harikumar, S. T. Tharakah, O. S. Lai, B. Sung and B. B. Aggarwal, *Pharmaceutical Research*, **2008**, 25, 9, 2097 - 2116.
11. G. N. Wogan, S. S. Hecht, J. S. Felton, A. H. Conney, L. A. Loeb, *Seminars in Cancer Biology*, **2004**, 14, 473 - 486.

12. Fleming, ID. Surgical therapy. In: Lenhard RE, Osteen RT, Gansler T, eds. *Clinical Oncology*. Atlanta, Ga: American Cancer Society, **2001**, 160 - 165.
13. (<http://www.cancer.org/treatment/treatmentsandsideeffects/treatmenttypes/radiation/index>). Retrieved on 30/04/2013.
14. (<http://www.cancer.org/treatment/treatmentsandsideeffects/treatmenttypes/chemotherapy/index>). Retrieved on 30/04/2013.
15. T. Boulikas, A. Pantos, E. Bellis and P. Christofis, *Cancer Therapy*, **2007**, 5, 537 – 538.
16. A. Sigel and H. Sigel, *Metal ions in Biological systems volume 11*, Marcel Dekker Inc., New York, **1996**, 339.
17. A. Cowley and B. Woodward, *Platinum Metal Rev.*, **2011**, 55, 2, 98 - 107.
18. D. Lebowitz and R. Canetta, *Eur. J. Cancer*, **1998**, 34, 10, 1522 - 1534.
19. T. W. Hambley, *J. Chem. Soc., Dalton Trans.*, **2001**, 2711 - 2718.
20. B. Rosenberg, E. Renshaw, L. Vancamp, J. Hartwick and J. Drobnik, *J. of Bacteriology*, **1967**, 93, 2, 716 - 721.
21. B. Lippert, *Cisplatin: Chemistry and Biochemistry of a leading Anticancer Drug*, Wiley-VCH, New York, **1999**, p. 3 - 100, 184 - 190.
22. L. Kelland, *The Resurgence of Platinum-based Cancer Chemotherapy*, **2007**, 573 - 584.
23. E. R. Jamieson and S. J. Lippard, *Chem. Rev.*, **1999**, 99, 2467 - 2498.
24. T. Boulikas and M. Vougiouka, *Oncology Reports*, **2003**, 10, 1663 - 1682.
25. Z. H. Siddik, *Oncogene*, **2003**, 22, 7265 - 7279.
26. S. E. Sherman and S. J. Lippard, *Chem. Rev.*, **1987**, 87, 1153 - 1181.
27. F. Huq, H. Dagheriri, J. Q. Yu, H. Tayyem, P. Beale and M. Zhang, *Eur. J. Med. Chem.*, **2004**, 39, 947.
28. P. J. Loehrer and L.H. Einhorn, *Ann. Intern. Med.*, **1984**, 100, 704 - 713.
29. R. C. Todd and S. J. Lippard, *Metallomics*, **2009**, 1, 4, 280 - 291.
30. V. Cepeda, M. A. Fuertes, J. Castilla, C. Alonso, C. Quevedo and J. M. Pérez, *Anti-Cancer Agents in Medical Chemistry*, **2007**, 7, 3 - 18.
31. D. P. Gately and S. B. Howell, *Cellular accumulation of the anticancer agent cisplatin: a review. Br. J. Cancer*, **1993**, 67, 1171 – 1176.
32. D. Wong and S. J. Lippard, *Nature Rev. Drug Disc.*, **2005**, 4, 307 - 320.
33. S. Ahmad, *Trans. Metal Chem.*, **2006**, 31, 1003 - 1016.
34. J. Reedijk, *Proc. Natl. Acad. Sci., USA*, **2003**, 100, 7, 3611 - 3616.
35. S. Ishida, J. Lee, D. J. Thiele and I. Herskowitz, *Proc. Natl Acad. Sci. USA*, **2002**, 99, 14298 - 14302.
36. J. Reedijk, *J. Eur. J. Inorg. Chem.* **2009**, 10, 1303 - 1312.

37. J.-M. Teuben, M. R. Zubiri and J. Reedijk, *J. Chem. Soc., Dalton Trans.*, **2000**, 369.
38. R. R. Crichton, *Biological Inorganic Chemistry: An Introduction*, Elsevier, New York, **2008**, p. 1, 341 - 344.
39. S. J. Berners-Price, T. A. Frenkiel, U. Frey, J. D. Ranford and P. J. Sadler, *J. Chem. Soc. Chem. Commun.*, **1992**, 789 - 791.
40. M. A. Fuertes, C. Alonso and J. M. Pérez, *Chem. Rev.*, **2003**, *103*, 3, 645 - 662.
41. A. M. Fichtinger-Schepman, J. L. van der Veer, J. H. den Hartog, P. H. Lohman and J. Reedijk, *Biochemistry*, **1985**, *24*, 707 - 713.
42. X-L. Yang & A. H-J. Wang, *Pharmacol. & Ther.*, **1999**, *83*, 181 - 215.
43. C. A. Lepre, K. G. Strothkamp and S. J. Lippard, *Biochemistry*, **1987**, *26*, 5651 - 5657.
44. A. Eastman, M.M. Jennerwein and D.L. Nagel, *Chem. Biol. Interact.*, **1988**, *67*, 71 - 81.
45. S. J. Lippard, *Pure & Appl. Chem.*, **1987**, *59*, 6, 731 - 742.
46. J. Reedijk, *Platinum Metals Rev.*, **2008**, *52*, 1, 2 - 11.
47. M. Kartalou and J. M. Essigmann, *Mutat. Res.*, **2001**, *478*, 23 - 43.
48. G. Giaccone and H. M. Pinedo, *The Oncologist: Drug Resistance*, **1996**, *1*, 82 - 87.
49. M.M. Gottesman, *Mechanism of Cancer Drug Resistance: Annu. Rev. Med.*, **2002**, *53*, 615 - 627.
50. L.R. Kelland, N.P. Farrell, *Platinum-Based Drugs in Cancer Therapy*, Humana Press Inc, Totowa NJ, **2000**, p. 321-337.
51. J. Reedijk, *Chem. Rev.*, **1999**, *99*, 2499.
52. C. H. Versantvoort, H. J. Broxterman, T. R. Badrij, J. Scheper and P. R. Twentyman, *J. Cancer*, **1995**, *72*, 82.
53. U. Frey, J. D. Ranford and P. J. Sadler, *Inorg. Chem.*, **1993**, *32*, 1333 - 1340.
54. N. J. Wheate, S. Walker, G. E. Craig and R. Oun, *Dalton Trans.*, **2010**, *39*, 8113 - 8127.
55. S. A. Laurie, L. L. Siu, E. Winqvist, A. Maksymiuk, E. L. Harnett, W. Walsh, D. Tu and W. R. Parkulekar, *Cancer*, **2010**, *116*, 362 - 368.
56. J. Kasparkova, M. Vojtiskova, G. Natile and V. Brabec, *Chem.-Eur. J.*, **2008**, *14*, 1330 - 1341.
57. F. Levi, G. Metzger, C. Massari and G. Milano, *Clin. Pharmakin.*, **2000**, *38*, 1 - 21.
58. E. Wong and C. M. Giandomenico, *Chem. Rev.*, **1999**, *99*, 2451 - 2466.
59. F. I. Raynaud, F. E. Boxall, P. M. Goddard, M. Valenti, M. Jones, B. A. Murrer, M. Abrams and L. R. Kelland, *Clin. Cancer Res.*, **1997**, *3*, 2063 - 2074.
60. J. Holford, F. Raynaud, B. A. Murrer, K. Grimald, J. A. Hartley, M. Abrams and L. R. Kelland, *Anticancer Drug Des*, **1998**, *13*, 1, 1 - 18.
61. Y. Chen, Z. Guo, S. Parsons and P. J. Sadler, *J. Chem. Eur.*, **1998**, *4*, 672.

62. N. J. Wheate, J. G. Collins, *Coordi. Chem. Rev.*, **2003**, *241*, 133 - 145.
63. M. J. Cleare and J. D. Hoeschele, *Platinum Met.Rev.*, **1973**, *17*, 3.
64. M. J. Cleare and J. D. Hoeschele, *Bioinorg. Chem.*, **1973**, *2*, 187.
65. N. J. Wheate and J. D. Collins, *Curr. Med. Chem. -Anti-Cancer Agents*, **2005**, *5*, 267 - 279.
66. N. Farrell, *Comments Inorg. Chem.*, **1995**, *16*, 6, 373 - 389.
67. G. T. Morgan and F. H. Burstall, *J. Chem. Soc.*, **1934**, 1498.
68. B. W. J. Harper, M. van Holst and J. Aldrich-wright, *Platinum(II) Intercalating Complexes based on 2,2':6',2''-Terpyridine*, **2011**, p. 101 - 102.
69. L. S. Lerman, *J. Mol. Biol.*, **1961**, *3*, 18.
70. K. W. Jennette, J. T. Gill, J. A. Sadownick and S. J. Lippard, *J. Am. Chem. Soc.*, **1976**, 6160 - 6168.
71. K. W. Jennette, S. J. Lippard, G. A. Vassiliades and W. R. Bauer, *Proc. Nat. Acad. Sci. USA*, **1974**, *71*, *10*, 3839 - 3843.
72. S. D. Cummings, *Coord. Chem. Rev.*, **2009**, *253*, 1495 - 1516.
73. M. Cusumano, M. L. Di Pietro and A. Giannetto, *Inorg. Chem.*, **1999**, *38*, 1754.
74. L. Messori, G. Marcon, A. Innocenti, E. Gallori, M. Franchi and P. Orioli, *Bioinorg. Chem. Appl.*, **2005**, *3*, 239.
75. C.S. Peyratout, T.K. Aldridge, D.K. Crites and D.R. McMillin, *Inorg. Chem.* **1995**, *34*, 4484.
76. G. Lowe, A. S. Droz, T. Vilaivan, G. W. Weaver, L. Tweedale, J. M. Pratt, P. Rock, V. Yardley and S. L. Croft, *J. Med. Chem.*, **1999**, *42*, 999 - 1006.
77. T. L. Gilchrist, *Heterocyclic Chemistry 3rd edition*, Addison Wesley Longman, England, **1998**, p. 295 - 298.
78. P. Banerjee, *Coord. Chem.*, **1999**, 190-192, 19-28.
79. W. Kaim and B. Schwederski, *Bioinorganic Chemistry: Inorganic Elements in the Chemistry of Life*, first edition, John Wiley & Sons, New York, **1994**, p. 16-35, 106-123.
80. R.J. Sundberg and R. B. Martin, *Chem. Rev.*, **1974**, *74*, 471.
81. Z. D. Bugarcic, S. T. Nandibewoor, M. S. A. Hamza, F. Heinemann and R. van Eldik, *Dalton Trans.*, **2006**, 2984.
82. M. Paoli, J. Marles-Wright and A. Smith, *DNA and Cell Biol.*, **2002**, *21*, *4*, 271 - 280.
83. J. M. Berg, J. L. Tymoczko and L. Stryer, *Biochemistry 6th edition*, **2006**, W. H. Freeman New York, Chapter 7.
84. A. Shaira, D. Reddy and D. Jaganyi, *Dalton Trans.*, **2013**, *42*, 8426.

CHAPTER 2

Substitution Reactions

2.1. Introduction to Substitution Reactions

In order to rationally design new and improved anticancer therapeutics it is important to have an in-depth understanding of the kinetics associated with the interactions of the Pt drug with the targeted DNA molecule.^{1,2} Since majority of the transition metal complexes which poses anticancer activity are in the d^8 electronic configuration, their ligand substitution rates should reveal more about their anticancer properties.

A substitution reaction is known as the replacement of a ligand from the coordination shell of a metal centre by another ligand from the direct surroundings.^{3,4,5} However, if there is no temporary change in oxidation state of the metal centre the process is defined as a simple substitution reaction.^{3,5} Also characteristic of a simple substitution is that the bond breaking and bond formation process is associated with a brief change in the coordination number of the reaction centre.³ Ingold and Hughes⁶ were able to categorize the substitution reactions of carbon as either homolytic or heterolytic depending on how the bond breaking process occurs.^{3,5,7} Homolytic substitution is when both the reactive centre and the leaving group take one electron from the former bond.⁵ The heterolytic substitution reactions can be further divided into two subgroups, electrophilic heterolysis (the reactive centre keeps the electron pair from the bond) and nucleophilic heterolysis (the leaving group leaves with the electron pair).³



Also, established by Ingold and Hughes for organic reactions are the terms nucleophilic substitution, S_N , and electrophilic substitution, S_E .^{7,8} Nucleophilic reactions can be divided further into S_N1 or S_N2 nucleophilic reactions depending on the pathway of the substitution. A S_N1 reaction involves a unimolecular rate-determining step whereas for S_N2 reactions, a bimolecular step is rate-determining.^{3,5,8,9} Most inorganic complexes undergo nucleophilic substitution reactions and there are different ways in which a coordinated leaving group can be replaced by a nucleophile. The previously explained terms are seldomly used in inorganic reaction since they do not describe the substitution reaction mechanism in detail.³

2.2. Mechanism of Ligand Substitution Reactions for Square Planar Complexes

Following the terminology introduced by Langford and Gary to categorize inorganic substitution reactions based on stoichiometric mechanisms, three main classes of mechanism were proposed.^{4,10,11,12,13}

- I. **Dissociative mechanism (D)**: Contains an identifiable intermediate with a reduced coordination number. The mechanism is similar to S_N1 pathways.
- II. **Associative mechanism (A)**: Contains an identifiable intermediate with an increased coordination number. The reaction mechanism is similar to S_N2 pathways.
- III. **Interchange mechanisms (I)**: No distinguishable intermediate is detected owing to the rapidly exchanging activated complex.

Thus the type of activation mechanism depends on the detection of an intermediate. The interchange mechanism can be classified further into two groups based on intimate mechanisms.^{3,4}

- I. Dissociatively activated interchange mechanism (I_d): The transition state shows no direct interaction between the metal centre and the entering group, only a weak bond exists.
- II. Associatively activated interchange mechanism (I_a): The transition state consists of a bond between the metal centre and the entering group.

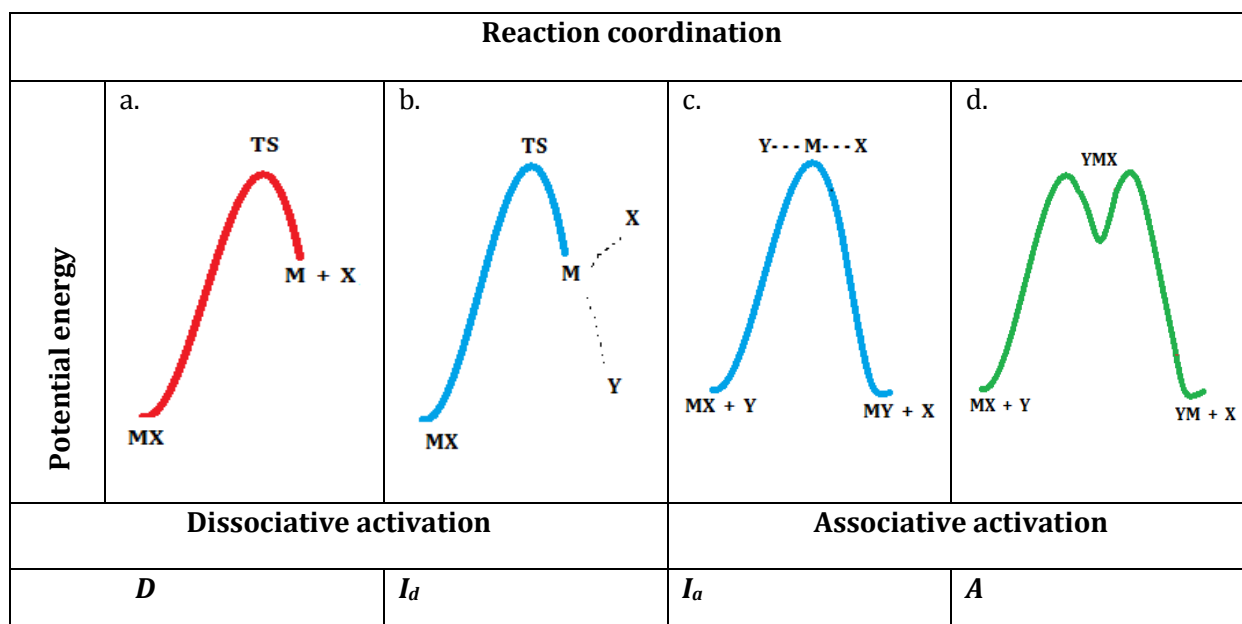


Figure 2.1: The potential energy profile diagrams illustrating the various substitution mechanisms in terms of the Langford-Gary nomenclature.^{3,4,10}

During a dissociative activation, the bond between the leaving group and the metal centre, **M-X**, breaks completely before the bond between the metal and the entering group, **M-Y**, begins to form.^{4,13} The reaction profile of this mechanism consists of one transition state and one intermediate (**Figure 2.1**). The 14-electron intermediate has a lower coordination number than either reactant or product which is able to withstand countless molecular collisions in order to equilibrate its surroundings fully before it coordinates with the incoming group.^{4,14} The rate of reaction is dependent only on the nature of the leaving group and independent of the nature and the amount of entering nucleophile in solution.^{4,10,15} As a consequence, the rate-determining step for this mechanism is the breaking of the bond between the metal and the leaving group.^{4,12}

2.2.1. Association Mechanism, A

In this mechanism, the formation of the bond between the metal centre and the entering group, **M-Y**, occurs before the bond between the metal centre and the leaving group, **M-X**, breaks. An associative pathway is distinguished by a single intermediate of higher coordination number than the reactant or product existing in between two transition states, the bond-making transition state, and the bond-breaking transition state.⁴ The energies of the mentioned transition states are degenerate when there is no net chemical change and can only be set apart by the identity of the leaving and entering groups. However, when there is a net chemical change one of the transition state lies at a higher potential energy than other and the deeper the energy of the formed intermediate, the more stable (see **Figure 2.2**).⁴

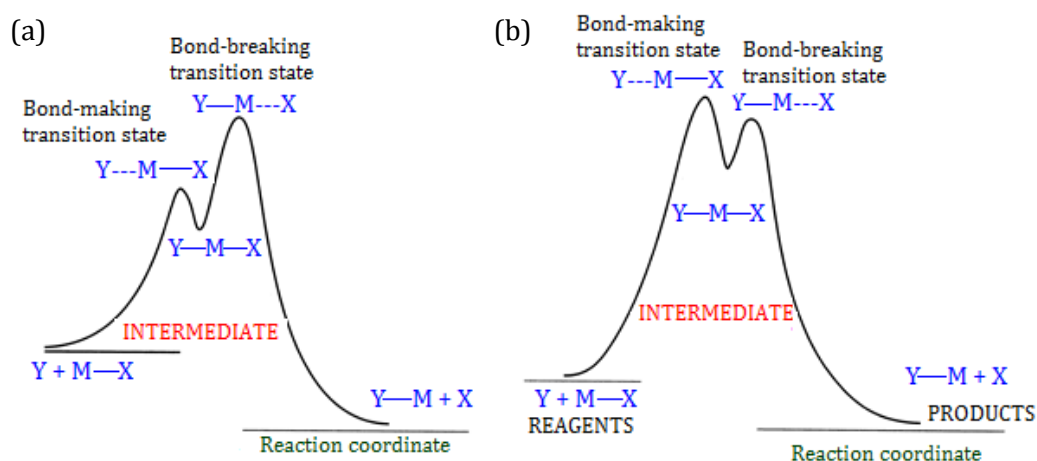


Figure 2.2: Potential energy profiles for an associative substitution mechanism illustrating the relationship between the intermediate and the transition states: (a) shows the bond-breaking transition state at a higher energy, whereas (b) Shows the bond-breaking transition state at a higher energy.¹⁴

2.2.2. Interchange Mechanism, *I*

This mechanism involves reactions where the bond breaking of the metal and the leaving group as well as the bond forming of the metal and entering group proceed concurrently. It contains one transition state and no distinguishable intermediate is detected owing to the rapidly exchanging activated complex. The interchange mechanisms consist of all grey area between **A** and **D** mechanisms and can be further divided into two subgroups, associative interchange, I_a and dissociative interchange, I_d mechanistic pathways.^{4,13}

2.2.2.1. Associative Interchange mechanism, I_a

This is the mechanism that covers the differences between interchange and association mechanisms. The bond forming step is more noticeable than the bond breaking step. As the entering group approaches the metal centre, the already bound leaving group does not rapidly responds and maintains the hold on its reactive centre until the entering group is completely bound.¹³ Thus, rate of reactions undergoing this type of mechanism is more dependent on the nature of the entering group as to that of the leaving group.^{4,5,11}

2.2.2.2. Dissociative Interchange mechanism, I_d

It accounts for the differences between the interchange and dissociation mechanisms. During this mechanism, the transition state consists of two very weak bonds existing between the metal centre with both leaving group and entering group. This is because when the leaving group departs, it moves from the inner coordination shell to the outer coordination shell while the entering group moves into the inner coordination shell from the outer coordination shell. However, the bond between the metal centre and the leaving group is weakened prior to the entering group being tightly bound, making the bond breaking step more prominent in the transition state formation.^{4,5,11,12}

2.3. Substitution Reactions of Square Planar Complexes

Square planar geometry is one of the four-coordinate configuration and with restricted occurrence. Mostly, square planar geometry coordinates complexes with low-spin d^8 configuration, such as, nickel (II), palladium (II), rhodium (I), iridium (I), gold (III) and platinum (II).^{5,14} Out of the few studies conducted with d^8 configuration metal complexes, it was accomplished that some of them are not relevant for square planar substitution reactions.^{5,14} For instance, square planar complexes of Rh(I) and Ir(I) with some ligands are prone to oxidative addition reactions. Ni(II) complexes tend to favour other geometries such as

octahedral over square planar and their substitution reactions those that do form square planar are mostly too rapid to fully analyse.^{4,5,14} Au(III), on the other hand forms square planar complexes but can be easily reduced to other forms of lower oxidation states such as Au(I) or Au(0). However, Pt(II) square planar complexes are the most favoured and studied of the square planar complexes, due to their stability during redox reactions and to their relatively low reactivity making it easier to kinetically study their substitution reactions.^{4,5,14,16,17} Synthesis of Pt(II) complexes dates back to over 50 years ago and has been tremendous development has been made ever since. Recently, the design and synthesis of novel Pt(II) complexes has focused on the kinetic and mechanistic studies of their substitution reactions and their application in other square planar metal complexes such as Pd(II).^{10,12,13,18} From the few studies comparing the substitution reaction rate of palladium(II) to platinum(II) complexes, it has been discovered that the rate of substitution of some Pd(II) complexes is five orders of magnitude greater than that of Pt(II) complexes with the same ligand system.^{17,19-21} Square planar complexes have an unsaturated 16-electron coordinate valence shell thus the energetics supports an associative pathway involving a 18-electron transition state. During this mechanistic pathway the relatively low energy of the vacant p_z orbital of Pt(II) allows the metal centre to extend its coordinate from four to five by accepting an extra pair of electron from the entering group resulting in a trigonal bipyramidal transition state geometry.^{4,10,12-14} This is illustrated in **Figure 2.3**.

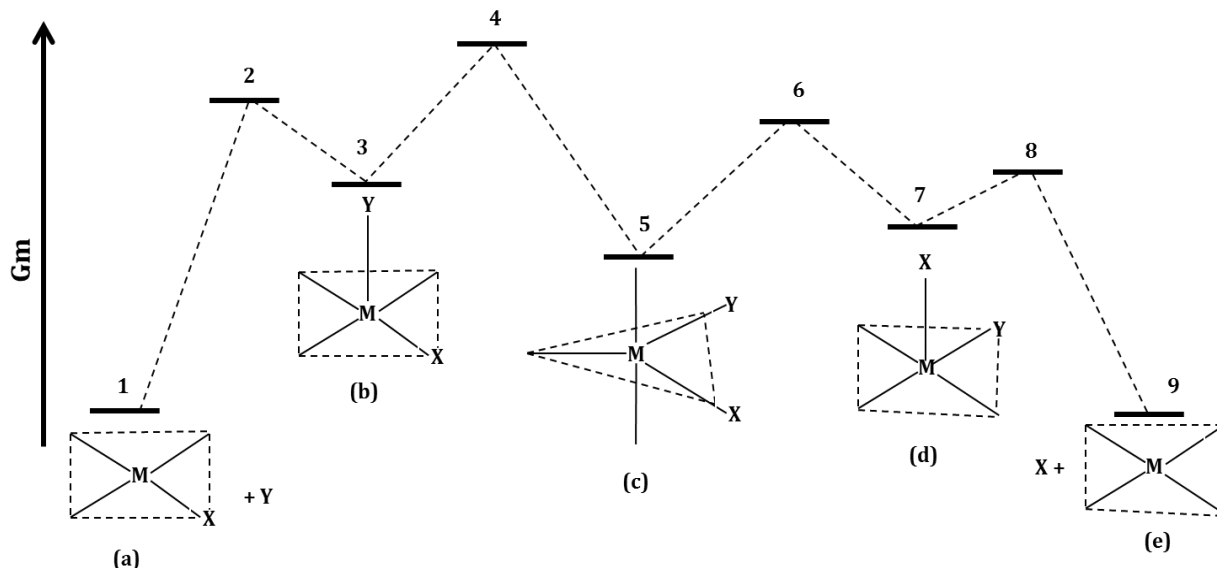
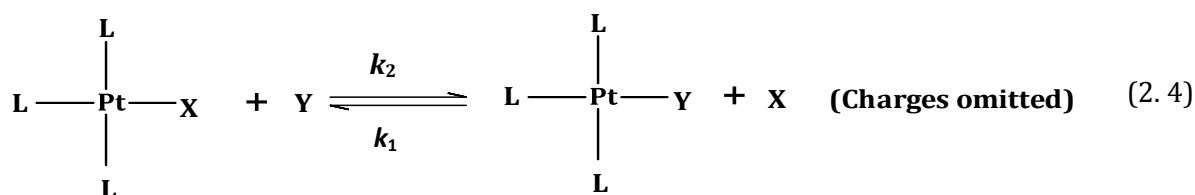


Figure 2.3: Scheme showing the energy profile and possible steric changes during an associative substitution of the leaving ligand, X by the entering nucleophile, Y of a square planar complex. The transition state energies are represented by all the even numbers and all the intermediates are represented by the odd numbers.¹²

2.3.1. Kinetics and Mechanisms of Substitution Reactions

In order to give a detailed mechanistic pathway for square planar substitution reactions, one has to determine how the nature of the reactants and/or solvent used affects the kinetics and mechanism of the reaction.⁴ Consider the following coordination reaction:



The rate law can be expressed as:

$$\begin{aligned} -\frac{d[\text{PtL}_3\text{X}]}{dt} &= k_1[\text{PtL}_3\text{X}] + k_2[\text{PtL}_3\text{X}][\text{Y}] \\ &= (k_1 + k_2[\text{Y}])[\text{PtL}_3\text{X}] \end{aligned} \quad (2.5)$$

where k_1 is first-order rate constant independent of the entering group, Y , and k_2 is the second-order rate constant dependent of Y (for a specific solvent at constant temperature).^{4,8,14}

The associative pathway that is independent of the entering group, Y , represented by the rate constant, k_1 , generally involves a solvolysis step prior to the nucleophilic attack of Y , thus this step becomes the rate-determining step. Whereas the pathway dependent of Y and is characterised by k_2 , whose the rate-determining step is the direct nucleophilic attack along the z -axis. The extra set of electrons contributed by Y to the square planar complex results in a saturated 18-electron five-coordinate intermediate. Both associative pathways are shown in **Figure 2.4**.

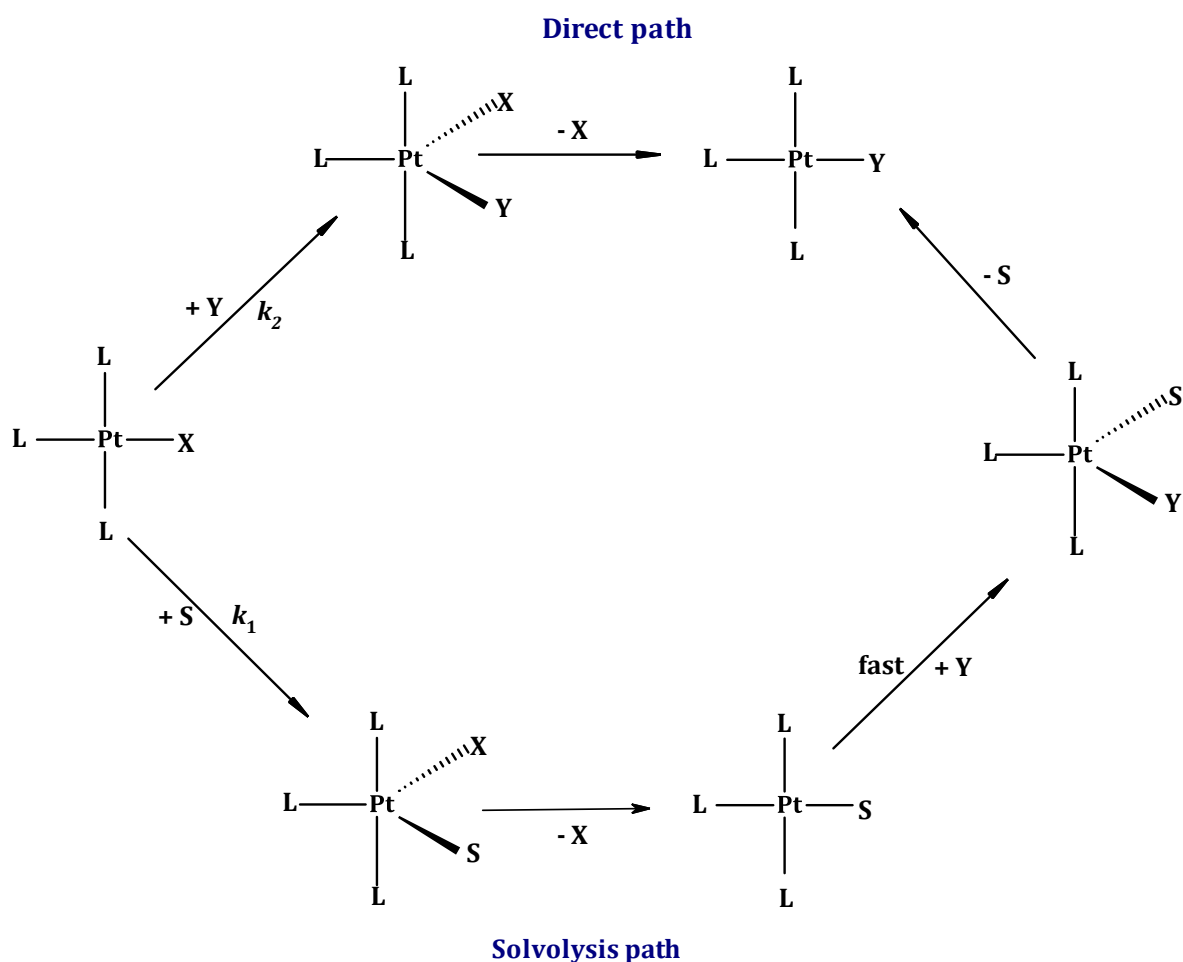


Figure 2.4: Schematic representation of the direct and solvolysis paths of an associative substitution.^{4,5}

Most kinetic studies of substitution reactions of square planar complexes are performed under *pseudo* first-order conditions; this is when the concentration of the entering nucleophile is at least 10 fold excess over the metal complex concentration to maintain first-order conditions and to ensure the reaction goes to completion. Accordingly, the rate of the reaction represented by *Equation 2.5* can be simplified to:

$$\text{Rate} = k_{\text{obs}} [\text{PtL}_3\text{X}] \quad (2.6)$$

$$k_{\text{obs}} = k_1 + k_2[\text{Y}] \quad (2.7)$$

where k_{obs} is the observed *pseudo* first-order rate constant.

A plot of k_{obs} against the concentration of **Y** gives the value of k_2 as the slope and the value of k_1 as the y -intercept. **Figure 2.5** shows a plot of observed first-order rate constants, k_{obs} , against various entering nucleophiles for the substitution reaction of *trans*-Pt(py)₂Cl₂.^{8,14,16}

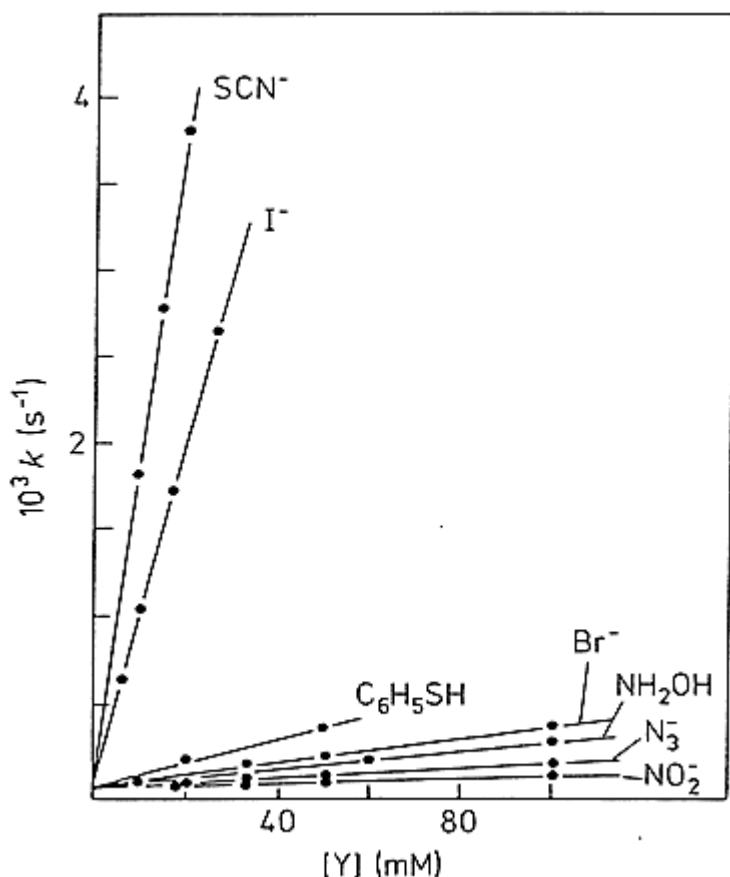


Figure 2.5: Plot of reaction rates of *trans*-Pt(py)₂Cl₂ against concentration of various nucleophiles in methanol at 30 °C.^{8,9,14,22}

Figure 2.5 provides substantial evidence of the sensitivity of k_2 on the nature of the entering group since the slope is different for each nucleophile. However for the same Pt(II) complex, the value of k_1 does not change for all nucleophiles verifying that its value is independent of the nature of the entering nucleophile.⁸

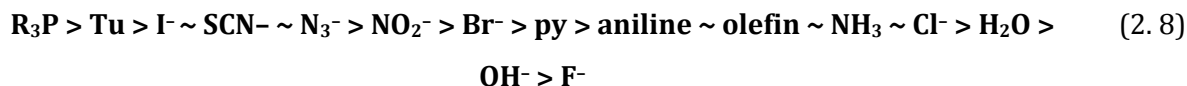
2.4. Factors Influencing the Rate of Substitution

The rate of substitution of square planar complexes involving associative mechanistic pathways is affected by several factors. All the ligands involved in the five-coordinate transition state have the potential to affect the energetics and reactivity of the Pt(II) complex. The following factors play a crucial role on the reactivity of square planar Pt(II) complexes.

2.4.1. The Effect of the Entering Nucleophile

The nucleophilicity of the entering group in associatively activated substitution reactions is mostly measured by the magnitude of the second-order rate constant, k_2 .^{4,5} Nucleophilicity is a

quantitative measure of the efficiency of the nucleophile towards electrophilic centres. The more effective the nucleophile, the larger the rate constant value for that particular substitution reaction.^{4,5,10} Previous studies conducted on Pt(II) complexes with various nucleophiles allowed the establishment of a general nucleophilicity scale that ranks the reactivity order of some of the common nucleophiles.^{8,22,23,24}



This reactivity trend (*Equation 2.8*) is mostly dependent on the polarizability (softness) of the entering nucleophile than it is on their base strength.^{8,14,25} Soft nucleophiles prefer soft metal centre as their substrate, such as platinum and gold whereas harder (non-polarizable) nucleophiles prefer harder substrates.^{14,26}

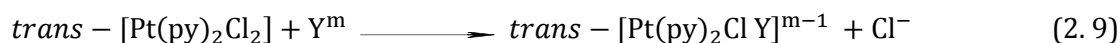
In order to define the nature of a nucleophile, one need to relate the reactivity of the nucleophile with other properties of the nucleophile, this is called a linear free energy relationship (LFER).^{14,22,27}

The nucleophilicity of the entering group is mostly influenced by several factors:^{8,11,12}

- a. Base Strength: Base strength of a nucleophile is determined by its pK_a value, the magnitude of the pK_a determines the nucleophilicity of the entering towards a metal centre.⁸
- b. Polarizability: Polarizability illustrates the strength of a ligand as an electron donor group to a metal centre. It is best defined using the *Hard Soft Acid Base* (HSAB) theory invented by Pearson in the 1960's.^{26,28} The Polarizability of a nucleophile is more significant reflection of the reactivity rates than for equilibria of the reaction.
- c. Oxidizability: Oxidizability is determined by the electrode reduction potential. Readily oxidized ligands (i.e. strong reducing agents) are regarded as good nucleophiles.^{8,11}
- d. Solvation Energy: Ligands that are easily solvated are considered as weak nucleophiles because it requires substantial energy for a ligand to break through the solvated shell and coordinate to a metal centre.

- e. Metal Centre: The effectiveness of a nucleophile highly depends on the nature of the metal centre. Heavier elements are more polarised in the transition state.

A study investigating the relative reactivity of nucleophiles involved the substitution of the chloride ligand from *trans*-Pt(py)₂Cl₂ in methanol with various nucleophiles (*Equation 2.9*).^{4,5,8,14}



where **Y** is the nucleophile and *m* is the charge of **Y**.

This was according to the rate law:^{4,5}

$$\text{rate} = (k_1 + k_2[\text{Y}^m])[\text{Pt}(\text{py})_2\text{Cl}] \quad (2.10)$$

Thus, for the standard reaction represented by *Equation 2.9*, the nucleophilicity constant, n°_{Pt} can be defined as:^{5,14,22}

$$\log \frac{k_Y}{k_S} = n^\circ_{\text{Pt}} \quad (2.11)$$

where k_Y is the second order rate constant of the entering group for the reaction and k_S is the rate constant of the attack of the solvent (methanol) on the Pt(II) complex.

At 30 °C, the concentration of methanol is 24.3 mol dm⁻³. Hence, this is simplified to:^{4,5}

$$n^\circ_{\text{Pt}} = n_{\text{Pt}} + \log 24.3 = n_{\text{Pt}} + 1.39 \quad (2.12)$$

Table 2.1 below summarises the nucleophilicity data, n°_{Pt} , obtained for *Equation 2.9* with various nucleophiles, **Y**.

Table 2.1: A selection of n°_{Pt} values listed according to donor atoms for $Pt(py)_2Cl_2$.^{4,5,22,27}

Nucleophile	Donor atom	n°_{Pt}
CH ₃ OH	O	0
C ₅ H ₅ N	N	3.13
imidazole	N	3.44
NH ₃	N	3.06
pyridine	N	3.19
(C ₆ H ₅) ₂ S	S	4.38
S=C(NH ₂) ₂	S	7.17
(CH ₃) ₂ S	S	4.87
SCN ⁻	S	5.75
SO ₃ ²⁻	S	5.79
Cl ⁻	Cl (halogen)	3.04
Br ⁻	Br (halogen)	4.18
I ⁻	I (halogen)	5.46
(C ₆ H ₅)P	P	8.79
(C ₂ H ₅) ₃ P	P	8.85
(CH ₃)Se	Se	5.70
(C ₆ H ₅ CH ₂) ₂ Se	Se	5.53
CN ⁻	C	7.14
C ₆ H ₁₁ NC	C	6.34

Since the reactivity of a nucleophile towards a Pt(II) centre is determined by the magnitude of the nucleophilicity constant, it is seen from **Table 2.1** that the nucleophilicity of the halogens follow the decreasing trend, I⁻ > Br⁻ > Cl⁻. Furthermore, phosphine and sulfur-donor groups have the most reactive nucleophiles towards Pt(II) centre due to their high nucleophilicity constant values. The plot of $\log k_y$ for a given nucleophile, versus the n°_{Pt} value for most Pt(II) complexes gives a LFER given by the following:^{8,14}

$$\log k_y = S n^{\circ}_{Pt} + C \quad (2.13)$$

Where S , is the complex specific slope called the *nucleophilic discrimination factor*, whose purpose is to measure the sensitivity of the Pt(II) centre to the nucleophilicity of the entering group. The intercept, C , is called the *intrinsic reactivity* which is equal to $\log k_s$, where k_s represents the rate constant of the weakest nucleophile in a solution.^{4,5,8} **Figure 2.6** shows the linear relationship $\log k_y$ and n°_{Pt} .²²

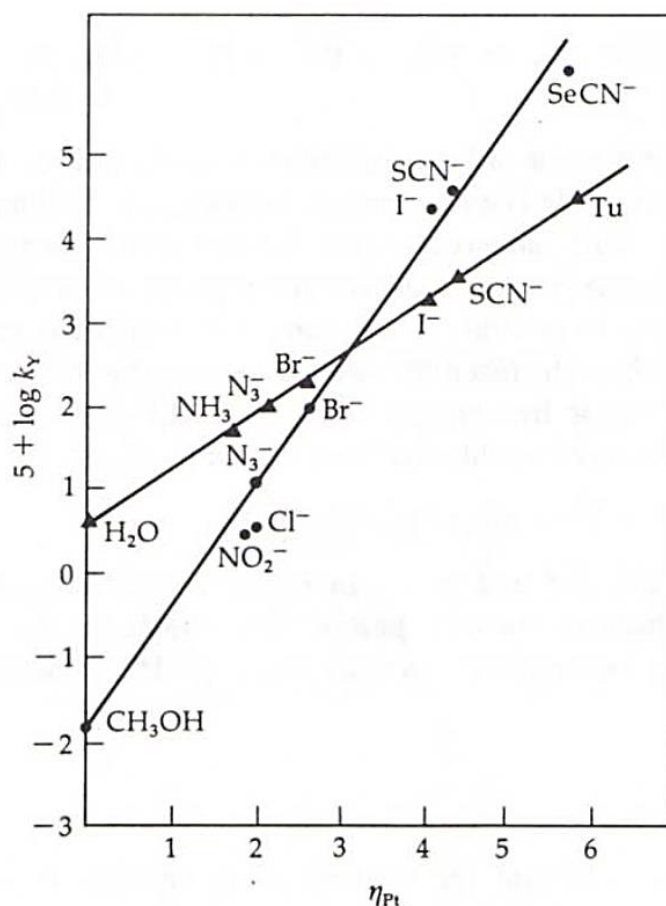


Figure 2.6: Illustrates the correlation of the rate constants of and $trans\text{-Pt}(\text{Et}_3)_2\text{Cl}_2$ (\blacktriangle) with various nucleophiles in water at 35 °C and $trans\text{-Pt}(\text{py})_2\text{Cl}_2$ (\bullet) in methanol at 30 °C as a reference.²⁹

From **Figure 2.6**, the reference complex, $trans\text{-Pt}(\text{py})_2\text{Cl}_2$, has a S value that is equal to 1.¹⁴ Thus, if $S > 1$ for a certain complex towards a set of nucleophiles, the reactivity increases relative to the reference.

2.4.2. The effect of the non-labile ligand (spectator Ligands)

Apart from the influence of the entering and the leaving groups, substitution reactions of square planar complexes are also affected by the nature of the non-labile ligands positioned *cis* and *trans* to the leaving group.^{4,5,8} the transition state of an associative mechanism involves a trigonal bipyramidal intermediate which consists of the leaving group, entering group and *trans* ligand in the trigonal plane and the two *cis* ligands in the axial positions.^{4,8} Hence, the effect of the *trans* ligand is expected to be different from that of the two *cis* ligands, so for that reason they have to be discussed separately. Recent studies on the substitution reactions of square planar complexes involve modifications of the *cis* and/or *trans* groups of complexes to investigate their effect on reactivity.³⁰⁻³⁸

2.4.2.1. The *trans*-Effect

The *trans*-effect refers to the effect caused by a coordinated ligand on the substitution rate of ligands opposite to it in a metal complex.^{8,9} It was first recognised by Werner and better understood as the *trans effect* from the work reported by Chernayev and his co-workers on square planar Pt(II) complexes.^{4,14,26} The influence of a *trans* non-labile ligand on the rate of substitution is important. **Figure 2.7** shows the effects of the *trans* ligand, **T** on the leaving group, **X**.

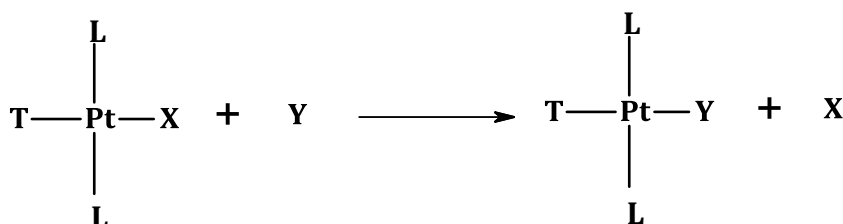
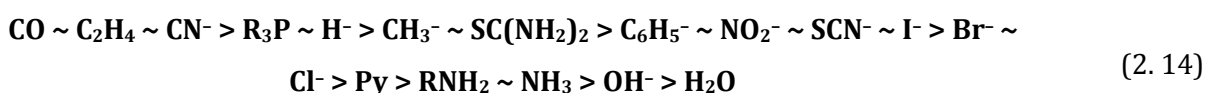


Figure 2.7: Schematic diagram representing the labilization of the leaving group, **X** by the *trans* ligand, **T**.^{8,24}

However, the extent of labilization of the leaving group, **X** is dependent on the *trans* ligand, **T**. The greater the *trans* effect of a particular ligand, the greater the *trans*-labilization of the leaving group and the larger the rate constant for that substitution reaction. Several studies investigating the *trans* effect of various ligands on the substitution rate of Pt(II) complexes using different nucleophiles found that the *trans* effect decreases in the order shown by *Equation 2.14*.^{4,8,12,14,18}



Kinetic studies have shown that the difference in rate of substitution between complexes containing a strong *trans* ligand and that containing a weak *trans* ligand is a factor of 10^6 or more. The increase or decrease in rate arising from the *trans* effect of a ligand is due to changes occurring in the ground state and/or the transition state. This is a kinetic phenomenon since it affects the rate of substitution of the leaving group positioned *trans* to it.^{8,14}

Another phenomenon typical to square planar Pt(II) complexes is the *trans* influence, which is purely a thermodynamic effect. It is described as the effect of the *trans* ligand on the ground state measurements like bond lengthening (X-ray determinations) and vibrational bond stretches (IR frequencies) meaning it only concerns the ground state and not the transition state.^{8,14}

Many theories have been developed with the aim of coming up with an explanation of the *trans* effect, but only a few succeeded. One was the polarization theory, and it is based on bond weakening of the **Pt-X** bond (see **Figure 2.8**). This was postulated by Grinberg³⁹ and is explained using charge distribution in induced dipoles in the **L-Pt-X** coordinate, where **L** is the *trans* ligand and **X** is the leaving group in **Figure 2.8**.

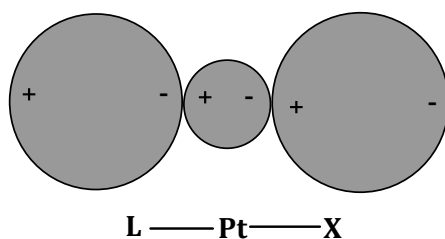


Figure 2.8: Charge distribution in induced dipoles in the coordinate, **L-Pt-X**.⁸

However, out of the many developed theories only two were most successful in accounting for the *trans* effect and they involve π - and σ -bonding properties. Thus it is important to understand both σ - and π -bonding when discussing the *trans* effect.^{8,11,14}

2.4.2.1.1. The π -Bonding Theory

This theory suggests that the π -bonding ligands, CO, C₂H₄ and R₃P, which are found higher in the *trans* effect series (see *Equation 2.14*) because they are able to stabilize the transition state as they are stronger π -acceptor ligands for electron density from the metal centre.^{8,11} This theory was made known by Pauling in order to justify for the short Ni-C bond distance of the complex, Ni(CO)₄. **Figure 2.9** shows bonding of phosphorus to the Pt(II) metal centre.

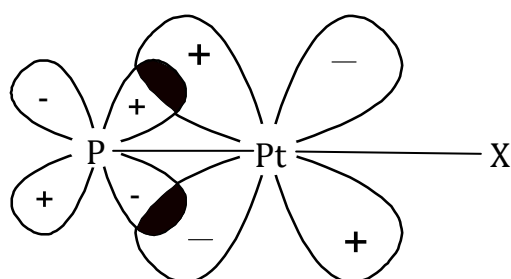


Figure 2.9: Schematic diagram of the **Pt-PR₃** double bond. if ligands **PR₃** and **X** are in the *xy* plane and the *d* orbitals shown are either *d_{xy}* or *d_{yz}*.⁸

From **Figure 2.9**, a pair of electrons is donated from phosphorus to the platinum orbitals thus a σ -bond is formed. Also, due to an overlap of the filled *d*-orbitals of platinum with a vacant *d*-orbital of phosphorus a π -bond is formed.^{8,13}

The withdrawal of electrons from the orbitals of the Pt centre to the vacant orbitals of the ligand weakens the **Pt-X** bond in the presence of most good *trans* directors. Except for the case of olefins where electron donation (σ -bonding) is more important than electron withdrawing (π -bonding).⁸ However, bond weakening in the ground state was considered inadequate to account for the effect of most good *trans* activators, and that the increase in rate of substitution had to involve stabilization of the transition state.⁸ This was proposed by Chatt *et al.*⁴⁰ and Orgel⁴¹ individually. They suggested that the *trans* effect is due to π -bonding stabilizing the activated trigonal bipyrimidal complex. Chatt *et al.* highlighted that electron withdrawal from Pt(II) *via* π -back bonding of the *trans* ligand, **T**, enhances the addition of the entering group, **Y**, thus increasing the rate.⁴⁰ Whereas, Orgel emphasised that the increase in stability of the transition state which results in higher rate constant values is due to π -back bonding because electron density on the Pt(II) decreased along the **Pt-X** and **Pt-Y** directions.⁴¹ **Figure 2.10** shows the activated trigonal bipyrimidal complex.⁸

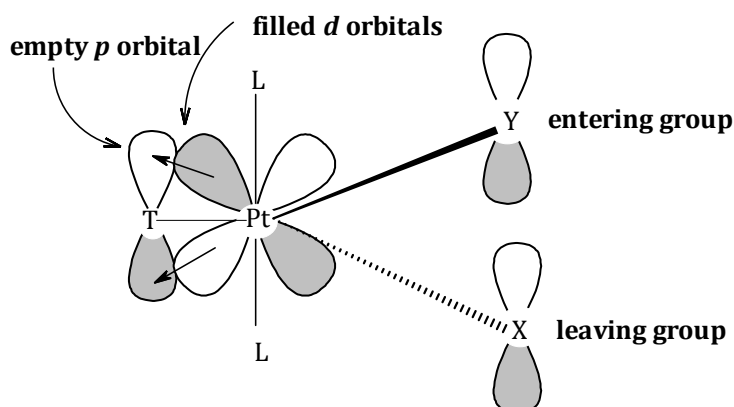


Figure 2.10: Activated trigonal bipyrimidal complex for PtL_2TXY , where **T** is a π -bonding ligand.⁸

2.4.2.1.2. The Molecular Orbital Theory for σ - and π -*trans* Effect

The molecular orbital (MO) theory is the most successful explanations for the σ - and π -*trans* effect as it explains the bonding of these systems.^{8,42}

a. σ -*trans* effect

Figure 2.11 shows a basic MO diagram of $[\text{PtCl}_4]^{2-}$. From this diagram, it is seen that the most stable orbitals are the σ -bonding orbitals found mainly on the chloride ligands. The next in stability are the π -bonding orbitals followed by the relatively stable anti-bonding σ and π molecular orbitals, π_{xz}^* , π_{yz}^* , σ_z^{2*} and π_{xy}^* and then the relatively unstable $\sigma_{x^2-y^2}^*$.^{8,42} At higher energies the anti-bonding σ orbitals, σ_s^* , σ_x^* , σ_y^* and σ_z^* , are located.⁸

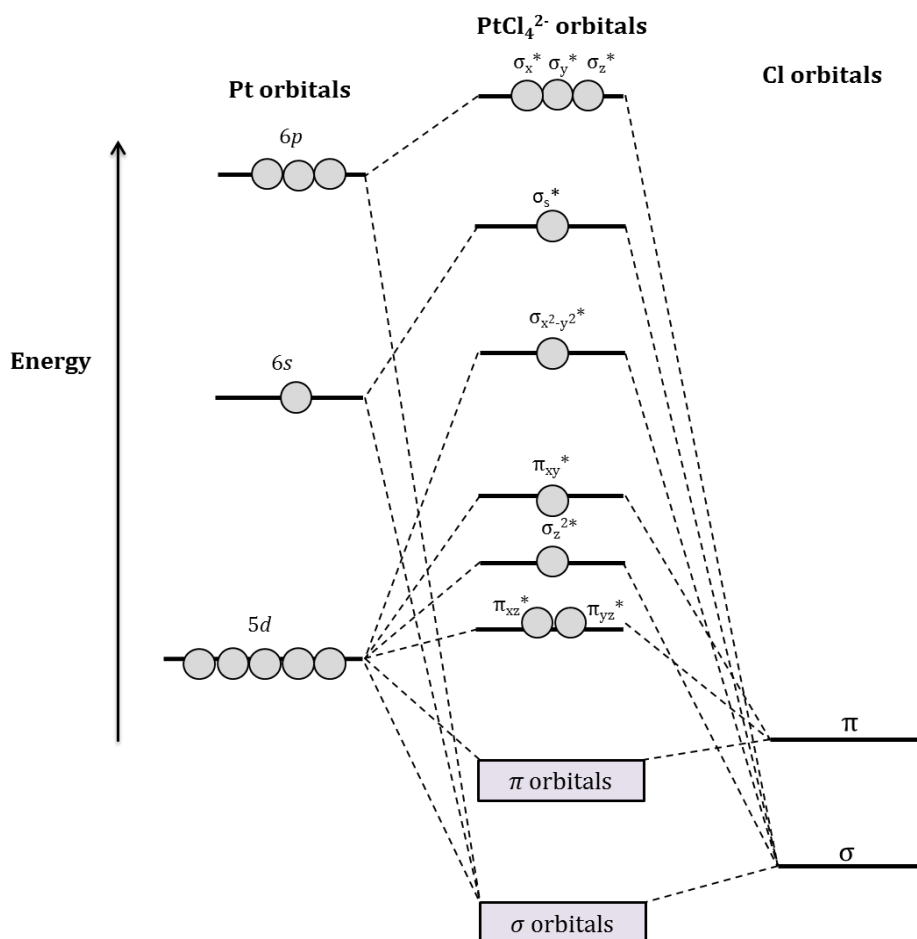


Figure 2.11: Molecular orbital diagram of PtCl_4^{2-} .^{8,42}

In square planar complexes such as these, it is noted that out of the four Pt valence atomic orbitals ($d_{x^2-y^2}$, s , p_x and p_y) involved in σ -bonding, only the two p -orbitals have *trans* directional properties because of their geometry.^{8,42} Therefore in the overall MO arrangement, the *trans* ligand, **T** and the leaving group, **X** of the complex PtL_2TX share the same σ_x orbital.⁸ Thus, the strong σ -bonding ligand, **T**, has a larger portion of the MO orbital and the leaving group, **X**, has less resulting in a weakened **Pt-X** bond due to limited electrons available for bonding accounting for the increase in rate of substitution of **X** (see **Figure 2.12**).⁸

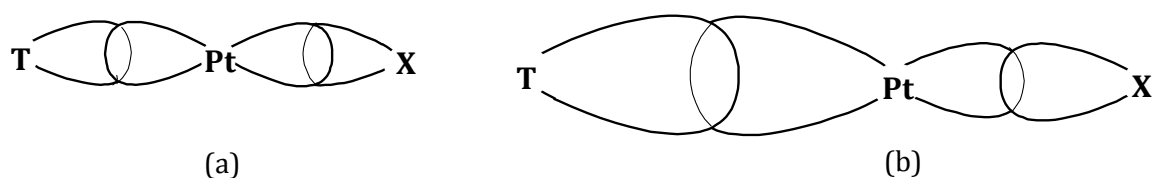


Figure 2.12: Diagram showing the σ -bonding of **T-Pt-X** using the σ_x MO. (a) The equal σ -bond strengths of **T** and **X**. (b) The σ -bonding strength of the *trans*-ligand, **T** is greater than that of **X** thus weakening the **Pt-X** bond.^{8,11,14}

b. π -*trans* effect

Square planar complexes with ligands that form strong π -bonds and are good *trans* directors, such as C_2H_4 , CO and CN^- , only three MOs (π_{xy}^* , π_{yz}^* and π_{xz}^*) have geometries suitable for π -bonding. Once the entering group has coordinated to the Pt centre and a trigonal bipyramidal structure is attained, four MOs (π_{xz}^* , π_{yz}^* , π_{xy}^* and $\pi_{x^2-y^2}^*$) with the appropriate symmetry for π -bonding result. Thus, there is a greater transition state stabilization if the *trans* ligand, **T**, is able to π -bond to the Pt centre because the electronic charge delocalised to the ligand results in a lower energy.^{8,11} Therefore, reactions of Pt(II) complexes with good *trans* π -acceptor ligands have a lower activation energy.^{8,32,36,43} A study attempting to assess the σ - and π -*trans* effects of several ligands and the qualitative results obtained are represented in **Table 2.2**.

Table 2.2: Estimated σ - and π -*trans* effects of selected ligands.⁸

Ligand	σ -effect [§]	π -effect [§]
C_2H_4	w	vs
CO	m	vs
CN^-	m	s
PR_3	s	m
H^-	vs	vw
I^-	m	m
CH_3^-	s	vw
SCN^-	m	m
$C_6H_5^-$	m	w
Br^-	m	w
Cl^-	m	vw
Pyridine	w	w
OH^-	vw	vw

2.4.2.2. The *cis*-Effect

Apart from sensitivity of substitution reactions to the *trans* ligand, they are also sensitive to *cis* ligands even though it is to a lesser extent than that of the *trans* ligand. The *cis* effect of the reaction is highly linked to steric hindrance in the *cis*-position.⁴ It has been established from previous studies that the *trans* effect is approximately 10^3 - 10^6 orders of magnitude greater to

[§] vs = very strong, s = strong, m = medium, w = weak, vw = very weak.

that of the *cis* effect.^{12,36} Due to the *cis* effect being smaller, most studies investigating the *cis* effect also involve varying the *trans* effect.

For instance, a kinetic study performed with *cis*-Pt(PEt₃)₂TCl and pyridine (Equation 2.15) showed the same trend as its isomeric complex, *trans*-Pt(PEt₃)₂TCl, with pyridine when the *trans* ligand, **T** was changed. Results are represented in **Table 2.3**.

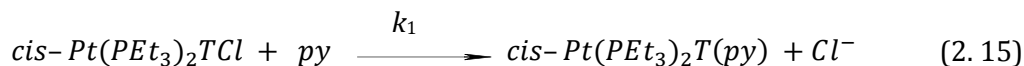


Table 2.3: The effect of *trans* ligand, **T** on the reactivity rate of *cis*-Pt(PEt₃)₂TCl with py.⁴⁴

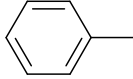
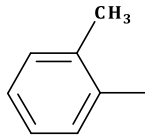
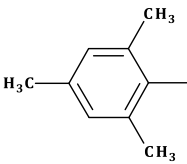
<i>trans</i> ligand, T	k ₁ / s ⁻¹
Cl ⁻	170
C ₆ H ₆ ⁻	380
CH ₃ ⁻	600

2.4.3. The Steric Effect

The transition state of associatively activated square planar reactions is more *sterically hindered* than the ground state since it comprises of a five-coordinate intermediate.⁵ Also, it is expected that if the ligands of a specific Pt(II) complex are sterically bulky than the associative substitution reaction may be retarded, while a dissociative substitution reaction may be accelerated due to steric strain being relieved during bond dissociation.^{5,8,11,12} The steric retardation of associative mechanisms is due to the electron density repulsion of the congested group of atoms coordinated to the metal centre. This steric effect can be brought about by introduction of a sterically bulk entering nucleophile or the presence of a sterically bulk spectator ligand, especially if the sterically hindered groups are on the *cis*-positions relative to the leaving group.^{4,5}

For instance, a study investigating the steric effects on the chloride substitution using *cis*-/*trans*-[Pt(PEt₃)₂(L)Cl] where **L** = phenyl, *o*-tolyl, mesityl and pyridine (**py**) as the nucleophile. The rate constant data is shown in **Table 2.4**.

Table 2.4: Steric effects on the rate constants for the chloride substitution by pyridine in *cis*- and *trans*-[Pt(PEt₃)₂(L)Cl].^{5,8,11}

Ligand, L	<i>k</i> _{obs} (s ⁻¹)	
	<i>cis</i> - (0 °C)	<i>trans</i> - (25 °C)
L = phenyl 	8.0 x 10 ⁻²	1.2 x 10 ⁻⁴
L = <i>o</i> -tolyl 	2.0 x 10 ⁻⁴	1.7 x 10 ⁻⁵
L = mesityl 	1 x 10 ⁻⁶ (25 °C)	3.4 x 10 ⁻⁶

The increase in steric bulk decreases the reaction rate from phenyl to mesityl. However, the decrease in reactivity from phenyl to mesityl is greater for the *cis*-complexes (a factor of 1/80 000) than it is with the *trans*-complexes (a factor of 1/36).⁸ This is because when the Pt complexes forms a trigonal bipyramidal geometry in the transition state, the *cis*-groups occupy the axial positions while the leaving group and entering group are in the equatorial positions (see **Figure 2.13**). Therefore, in the case of the *cis*-isomers, L is in the axial position in the transition state hence there is a greater steric repulsion between the *cis*-ligand and the leaving group than when it is in the equatorial position for the *trans* complex.¹¹

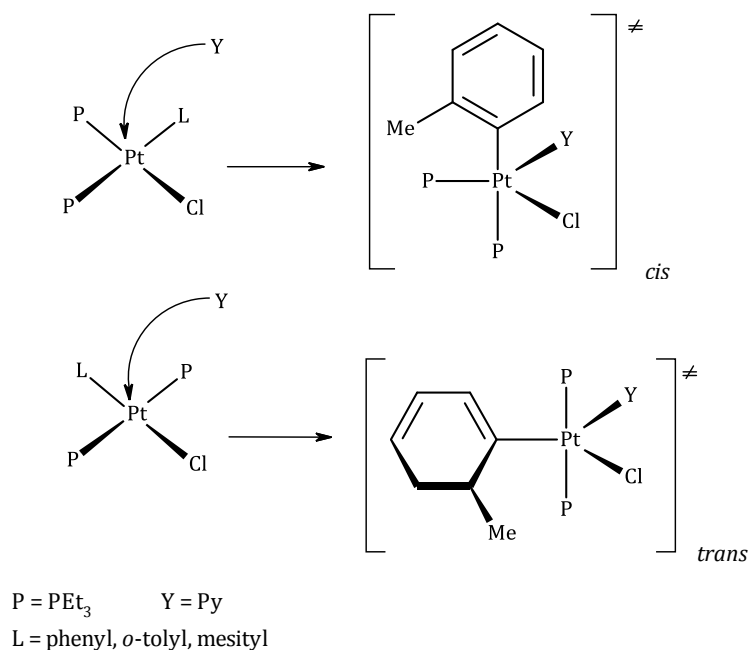


Figure 2.13: The steric effect of the aryl square planar complex and trigonal bipyramidal intermediate of the *cis* isomer and *trans* isomer.¹¹

Steric effects may also cause the mechanism to change from associative to dissociative by a favourable change from square planar to a three-coordinate T-shaped intermediate. However, this usually occurs when the Pt(II) complex has two bulky groups on the *cis* positions.^{11,13}

2.4.4. Effect of the Leaving Group

The effect of the leaving group is not as influential as that of the entering group on the rate of substitution in associatively activated square planar complexes. However, there have reports that showed some substitution reaction rates of some square planar complexes to be dependent on the nature of leaving group.^{4,5,8,12,14} However, in order to determine the effect of the leaving group on the rate, the *cis* and *trans* ligands must be kept constant.

The reaction represented by *Equation 2.16* has been extensively studied and the obtained kinetic data (**Table 2.5**) shows the effect of the leaving group on the rate.

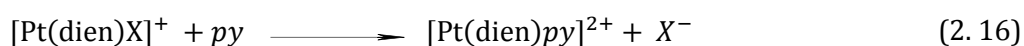
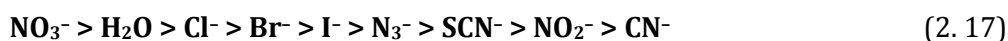


Table 2.5: The effect of the nature of the leaving group on the rate of substitution of $[\text{Pt}(\text{dien})\text{X}]^+$ in water at 25 °C.^{8,16,23}

Ligand, X	$10^6 k_{\text{obs}}/\text{s}^{-1}$
NO_3^-	Very fast
H_2O	1900
Cl^-	35
Br^-	23
I^-	10
N_3^-	0.83
SCN^-	0.30
NO_2^-	0.050
CN^-	0.017

The rate of substitution of the leaving group, **X** decreases in the following order:



From this it is seen that the rate constant values, k_{obs} of the associative mode of substitution of various leaving groups is influenced by the nature of the leaving group.^{4,5} In most cases, the effect of the leaving group is related to the strength of the metal-ligand bond, **Pt-X** because the bond breaking process affects the transition state formation.⁸ However, it is easier to replace a leaving group which has a lower nucleophilicity than the entering group to allow the formation of a five-coordinate intermediate instead of a four-coordinate intermediate.⁸

2.4.5. Solvent Effect

It is well-known that some square-planar reactions follow a solvent path. This involves the direct attack of the solvent on the reactive centre. Some studies have shown this alternative path to have a contribution to the overall rate of the reaction that is proportional to the coordination ability of the solvent.⁸ This involvement of a solvolysis pathway in substitution reactions of square planar complexes results in a second order rate law (See *Chapter 3*). This is in accordance with the experimental data (**Table 2.6**) attained for the solvent effect on the reactivity rate of the chloride substitution reactions for *trans*-Pt(py)₂Cl₂ represented by *Equation 2.18*

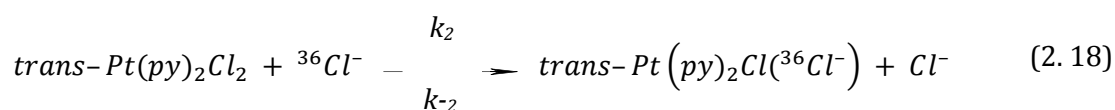


Table 2.6: Solvent Effect on the $^{36}\text{Cl}^-$ substitution reaction rates with Pt(II) complex, *trans*-Pt(py) $_2\text{Cl}_2$ at 25 °C.^{8,11,45}

Coordination Solvent	$k_{-2} / (10^{-5} \text{ s}^{-1})$	Weakly coordinating solvents	$k_{2(\text{Cl}^-)} / \text{M}^{-1} \text{ s}^{-1}$
DMSO	380	CCl_4	10^4
H_2O	3.5	C_6H_6	10^2
CH_3NO_2	3.2	<i>i</i> -BuOH	10^{-1}
$\text{C}_2\text{H}_5\text{OH}$	1.4	Me_2CO	10^{-2}
<i>n</i> - $\text{C}_3\text{H}_7\text{OH}$	0.42	DMF	10^{-3}

Reactions conducted in coordinating solvents such as DMSO, have reactivity rates that show a direct dependence on the nucleophilicity of the solvent, while substitution reactions conducted in weakly coordinating solvents have rates that show no dependence on the solvent used.^{8,14}

The rate constant value for coordinating solvents, k_{-2} , shown in **Table 2.6** increases in the following order: ROH < $\text{H}_2\text{O} \sim \text{CH}_3\text{NO}_2$ < DMSO. The significantly larger exchange rate of DMSO compared to H_2O verifies that the Pt(II) centre is better suited to coordinate to the more polarised and larger S-atom of DMSO than it does with the O-atom of H_2O . This also signifies that the Pt-solvent bond formation step is of great importance in the transition state.⁸ As far as weakly coordinating solvents are concerned, the rate of a reaction is larger for non-polar solvents like CCl_4 where the chloride is solvated therefore highly reactive $k_{2(\text{Cl}^-)}[^{36}\text{Cl}^-] > k_{-2}$. The opposite applies for polar solvents such as DMF where the chloride leaving group is not solvated.^{8,14}

2.5. References

1. J. Reedijk, *Chem. Rev.*, **1999**, *99*, 2499.
2. J. Reedijk, *PNAS*, **2003**, *100*, 7, 3611.
3. L. Arnaut, S. Formosinho and H. Burrows, *Chemical Kinetics From Molecular Structure to Chemical Reactivity*, Elsevier, New York, **2007**, p. 273 - 294.
4. M. L. Tobe and J. Burgess, *Inorganic Reaction Mechanisms*, Addison Wesley Longman Limited, New York, **1999**, p. 30 - 43, 70 - 112.
5. M. L. Tobe, *Inorganic Reaction Mechanisms Studies in Modern Chemistry*, Nelson, London, **1972**, p.17 - 23, 42 - 68.
6. K. F. Purcell and J. C. Kotz, *Inorganic Chemistry*, W. B. Saunders Co., Philadelphia, **1977**, p. 393 - 401.
7. C. K. Ingold, *Structure and Mechanism in Organic Chemistry 2nd edition*, Cornell University Press, Ithaca, New York, **1969**, p. 241.
8. F. Basolo and R. G. Pearson, *Mechanisms of Inorganic Reactions, 2nd edition*. Wiley, New York, **1967**, p. 124 - 128, 351 - 453.
9. D. Benson, *Mechanisms of inorganic reactions in solution*, McGraw-Hill, London, **1968**, p. 19 - 31.
10. C. H. Langford, H. B. Gray, *Ligand Substitution Dynamics*, Benjamin, New York, **1965**, p. 18 - 48.
11. R. B. Jordan, *Reaction Mechanisms of Inorganic and Organometallic Systems*, Oxford University Press Inc, New York, **1991**, p. 23 - 30, 47 - 54, 58 - 60.
12. S. Ašperger, *Chemical Kinetics and Inorganic Reaction Mechanisms, 2nd edition.*, Kluwer Academic/Plenum Publisher, New York, **2003**, p. 38 - 39, 105 - 106, 140 - 153.
13. R. A. Henderson, *The Mechanisms of Reactions at Transition Metal Sites*, Oxford University Press, Oxford, **1993**, p. 1 - 4, 10 - 22.
14. J. D. Atwood, *Inorganic and Organic Reaction Mechanisms, 2nd edition*, Wiley- VCH Inc., New York, **1997**, p. 32-34, 43-61
15. P. Atkins, T. Overton, J. Rourke, M. Weller and F. Armstrong, *Shriver & Atkins Inorganic Chemistry 4th edition*, Oxford University Press, New York, **2006**.
16. F. Basolo, H. B. Gray and R.G. Pearson, *J. Am. Chem. Soc* **1960**, *82*, 4200.
17. D. Jaganyi, D. Reddy, J. A. Gerterbach, A. Hofmann and R. van Eldik, *J. Chem. Soc., Dalton Trans*, **2004**, 299.
18. R. G. Wilkins, *Kinetics and Mechanisms of Reactions of Transition Metal Complexes, 2nd edition*, VCH, Weinheim, **1991**, p. 199- 201, 232- 237.

19. Ž. D. Bugarčić, S. T. Nandibewoor, M. S. A. Hamza, F. Heinemann and R. van Eldik, *Dalton Trans.*, **2006**, 2984.
20. Ž. D. Bugarčić, G. Liehr and R. van Eldik, *J. Chem. Soc., Dalton Trans.*, **2002**, 951.
21. D. Jaganyi, F. Tiba, O.Q. Munro, B. Petrović and Z. D. Bugarčić, *Dalton Trans.*, **2006**, 2943-2949.
22. U. Belluco, L. Cattalini, F. Basolo, R.G. Pearson and A. Turco, *J. Am. Chem. Soc.*, **1965**, 87, 241.
23. H. B. Gray, *J. Am. Chem. Soc.*, **1962**, 84, 1548.
24. D. Banerjea, F. Basolo and R. G. Pearson, *J. Am. Chem. Soc.*, **1957**, 79, 4055.
25. R. K. Murmann, R. T. M. Fraser and J. Bauman, *Mechanisms of Inorganic Reactions*, Washington, D. C, **1965**, p. 20 - 23, 81 - 97
26. R. G. Pearson, *J. Am. Chem. Soc.*, **1963**, 85, 3533.
27. R. G. Pearson, H. Sobel and J. Songstad, *J. Am. Chem. Soc.*, **1968**, 90, 319.
28. R. G. Pearson, *J. Chem. Educ.*, **1968**, 45, 643.
29. H. B. Gray and R. J. Olcott, *Inorg. Chem*, **1962**, 1, 481.
30. P. Ongoma and D. Jaganyi, *Dalton Trans.*, **2012**, 41, 10724.
31. A. Shaira, D. Reddy and D. Jaganyi, *Dalton Trans.*, **2013**, 42, 8426 – 8436.
32. A. Hofmann, D. Jaganyi, O. Q. Munro, G. Liehr and R. van Eldik, *Inorg. Chem.*, **2003**, 42, 1688 – 1700.
33. Ž. D. Bugarčić, G. Liehr and R. van Eldik, *J. Chem. Soc., Dalton Trans.*, **2002**, 951.
34. D. Jaganyi, K-L. De Boer, J. Gertenbach, J. Perils, *Int. J. Chem. Kinet.*, **2008**, 40, 808 – 818.
35. D. Jaganyi, F. Tiba, O.Q. Munro, B. Petrović and Z. D. Bugarčić, *Dalton Trans.*, **2006**, 2943.
36. A. Hofmann, L. Dahlenburg and R. van Eldik, *Inorg. Chem.*, **2003**, 42, 6528.
37. A. Mambanda and D. Jaganyi, *Dalton Trans.*, **2011**, 40, 79.
38. D. Reddy, K. J. Akerman, M. P. Akerman, D. Jaganyi, *Transition Met. Chem.*, **2011**, 36, 593.
39. A. A. Grinberg, *Acta Physicochim*, **1935**, 3, 573.
40. J. Chatt, L. A. Duncanson and L. M. Venanzi, *J. Chem. Soc.*, **1955**, 4456.
41. L. E. Orgel, *J. Inorg. Nucl. Chem*, **1956**, 2, 137.
42. U. Belluco, *Organometalic Coordination Chemistry of Platinum*, Academic Press, London, **1974**, p. 40-53, 138-160, 220-221.
43. B. Pitteri, M. Bortoluzzi and G. Marangoni, *Transition. Met. Chem.*, **2005**, 30, 1008
44. F. Basolo, J. Chatt, H. B. Gray, R. G. Pearson and B. L. Shaw, *J. Chem. Soc.*, **1961**, 2207
45. R. G. Pearson, H. B. Gray and F. Basolo, *J. Am. Chem. Soc.*, **1960**, 82, 787.

CHAPTER 3

Reaction Kinetics

3.1. Introduction

Chemical reaction kinetics deals with the rates of various chemical processes, it determines how fast or how slow a chemical reaction is occurring.^{1,2} These chemical processes are usually simplified into sequential single-step processes referred to as elementary reactions in order to deal with the kinetics of each individual step as these steps usually involve a single reactive collision between two molecules, this is known as a bimolecular step.³ The rate of a chemical reaction is defined as the rate at which certain amount of the reactants are used up, or equivalently the rate at which products are formed.^{1,4} This can be expressed in terms of the concentrations of the *stoichiometric* reactants and products making it independent of the size of the sample but dependent on the molecular collisions between the reactants. However, experimentally the rate at which a chemical reaction occurs depends on a variety of factors.⁴ By observing how these factors are influenced by such factors, kineticists can describe what occurs at the molecular level. These include: concentration of reactants and/or products, temperature, pressure, ionic strength of a solution, pH (if applicable), solvent, and whether or not a catalyst is being used.^{3,5}

- The **concentration** of the reactants is mostly used to determine the rate of a chemical reaction. If the concentration of the reactants is high, thus more collisions between the different reactant molecules will occur and the rate at which the reaction takes place increases.
- An increase in **temperature** results in an increased chemical reaction rate. From temperature dependent studies, the activation parameters, enthalpy and entropy (discussed later in this chapter) can be determined.
- The **solvent** used in a chemical reaction causes an effect only if the solvent molecules interact with the reactant molecules in a manner that alters the kinetics of the reaction and thus the rate.
- The **pH** only becomes a factor when working in an aqua medium. Once the pK_a values of the reacting species are known, one can determine the appropriate pH at which the

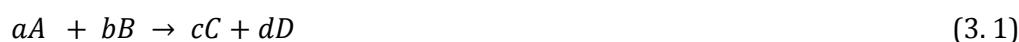
reacting species are in the deprotonated form. These two forms of the molecules have different reactivity rates.

- A **catalyst's** primary aim is to speed up a chemical reaction. Thus the rate obtained in the presence of a catalyst is greater than that obtained with no catalyst.

As mentioned above, the concentration of the reactants is the most important factor as it is used to study the kinetics of a chemical reaction while all the other factors are kept constant.

3.2. The Rate Law

For the chemical reaction represented below:



Where the chemical compounds are represented by the capital letters and the stoichiometry is represented by smaller letters. The rate of a reaction is conveyed in a manner independent of the amount of sample used and the units are usually reflected as $M s^{-1}$.^{6,7}

$$Rate = \frac{-d[Reactant]}{dt} = \frac{d[product]}{dt} \quad (3.2)$$

where the negative sign signifies that the concentration of the reactant becomes reduced with time.

The rate law on the other hand, can be referred to as the study of the dependence of the reaction rates and the rate constants on the concentrations of the various reactants in a reaction.^{1,7} Using the concentration of all the components, the rate can be expressed as:

$$Rate = -\frac{1}{a} \cdot \frac{d[A]}{dt} = -\frac{1}{b} \cdot \frac{d[B]}{dt} = \frac{1}{c} \cdot \frac{d[C]}{dt} = \frac{1}{d} \cdot \frac{d[D]}{dt} \quad (3.3)$$

The rate law is generally represented as:

$$Rate = -k \prod_i [A_i]^{\alpha_i} [X_j]^{\beta_j} \quad (3.4)$$

where A_i are the reactant, k is the rate constant, X_j are any other species (catalysts) that may affect the rate while α and β are the reactant orders.

The reaction order on the other hand is defined as:

The units of the rate constant, k are dependent on the reaction order.

$$\text{reaction order} = \sum_i \alpha_i \quad (3.5)$$

3.3. Integration Rate Expressions

A rate law is a differential equation that refers to the rate of change of a reactant (or product) concentration with time. If we integrate the rate law then we obtain an expression for the concentration as a function of time, which is usually the type of data obtained from experimentally.

3.3.1. First Order Reactions

Mostly reactions are first order or are performed under conditions that resemble first order reactions because these types of reactions are easier to understand.¹ When considering the first order reaction.



The rate can be given by the following

$$\text{Rate} = k[A] = \frac{-d[A]}{dt} \quad (3.7)$$

which rearranges to give:

$$\frac{-d[A]}{[A]} = k_1 dt \quad (3.8)$$

Integrating from $t = 0$ to $t = t$, (A_t) gives

$$\int_{[A]_0}^{[A]_t} \frac{d[A]}{[A]} = -k_1 \int_0^t dt \quad (3.9)$$

$$\ln \frac{[A]_t}{[A]_0} = -k_1 t \quad (3.10)$$

$$\ln[A]_t = -k_1 t + \ln[A]_0 \quad (3.11)$$

where $[A] = [A]_0$ at time $t = 0$ and $[A] = [A]_t$ at time $t = t$

This is in a linear equation form ($y = mx + c$) with $y = \ln[A]_t$, $x = t$ and $c = \ln [A]_0$. Thus, a plot of $\ln[A]_t$ versus t yields a straight line and from the slope of the graph $-k_1$ can be determined.^{1,7}

Equation 3.11 can be expressed as:

$$\frac{[A]_t}{[A]_0} = e^{-k_1 t} \quad (3.12)$$

and simplified to:

$$[A]_t = [A]_0 e^{-k_1 t} \quad (3.13)$$

Furthermore, *Equation 3.13* indicates that a plot of $[A]_t$ against time varies exponentially.

3.3.2. Reversible First order reactions

Some reactions do not go to completion and form an equilibrium between the reactants and products under certain reaction conditions. Such reactions are termed reversible.



The rate law for the reaction represented by *Equation 3.14* is

$$\text{rate} = \frac{-d[B]}{dt} = \frac{-d[A]}{dt} = -k_1[A]_t - k_{-1}[B]_t \quad (3.15)$$

At $t = 0$, $B = 0$, and $[A]_t = [A]_0$, at any time

$$[B]_t = [A]_0 - [A]_t \quad (3.16)$$

Substituting *Equation 3.16* into *Equation 3.15* gives:

$$\frac{-d[A]}{dt} = k_1[A]_t - k_{-1}([A]_0 - [A]_t) \quad (3.17)$$

At equilibrium no overall reaction occurs, thus

$$-\frac{d[A]}{dt} = 0 \quad (3.18)$$

Applying *Equation 3.18* to *Equation 3.15* leads

$$k_1[A]_{eq} = k_{-1}[B]_{eq} = k_{-1}([A]_0 - [A]_{eq}) \quad (3.19)$$

which can be simplified to:

$$[A]_0 = \frac{k_1 + k_{-1}}{k_{-1}} [A]_{eq} \quad (3.20)$$

Substitution of *Equation 3.20* into *Equation 3.17* produces

$$\frac{-d[A]}{dt} = (k_1 + k_{-1})[A] - (k_1 + k_{-1})[A]_{eq} \quad (3.21)$$

Separation of the variables and integration eventually leads to

$$\int_{[A]_0}^{[A]_t} \frac{d[A]}{([A]_t - [A]_{eq})} = -(k_1 + k_{-1}) \int_0^t dt \quad (3.22)$$

gives

$$\ln \left(\frac{[A]_0 - [A]_{eq}}{[A]_t - [A]_{eq}} \right) = (k_1 + k_{-1})t \quad (3.23)$$

Rearrangement of Equation 3.23 leads to

$$\ln ([A]_t - [A]_{eq}) = -(k_1 + k_{-1})t + \ln([A]_0 - [A]_{eq}) \quad (3.24)$$

A plot of $\ln([A]_t - [A]_{eq})$ against time gives a linear fit with a slope of $-(k_1 + k_{-1})$. To determine each individual rate constant, k_1 or k_{-1} it's crucial to evaluate the equilibrium constant, K_{eq} .^{1,5,7}

The equilibrium constant is a ratio of the concentration of the remaining reactant and the formed product which can be correlated to the distinctive rate constant as follows:

$$K_{eq} = \frac{[B]_{eq}}{[A]_{eq}} = \frac{k_1}{k_{-1}} \quad (3.25)$$

This provides two equations with two unknowns. However treating reversible first order reactions can be difficult and may lead to inaccurate measurement of $[A]_{eq}$. Furthermore, the observed rate constant, k_{obs} , is equal to the sum of the rate constant of the forward and reverse reaction, *i.e.*

$$k_{obs} = k_1 + k_{-1} \quad (3.26)$$

3.3.3. Second Order Reactions

Second order rate laws are among the most encountered in reaction kinetic studies. Reactions that are second-order with respect to one of the reactant and reactions that are first-order with respect to two different reactants fall under second order reactions. When considering the reaction equation described below:



The rate law can be given as:

$$\text{Rate} = k[A][B] \quad (3.28)$$

$$\text{Rate} = \frac{d[C]}{dt} = -\frac{d[A]}{dt} = -\frac{d[B]}{dt} = k_2[A]_t[B]_t \quad (3.29)$$

If at $t = 0$, the initial concentration of A and B are $[A]_0$ and $[B]_0$, and at a particular time t , the concentration of A is reduced to $[A]_0 - x$, and concentration of B would be reduced to $[B]_0 - x$, where x is the amount of reactants that has reacted to form the product C. Therefore the rate equation can be written as:⁸

$$-\frac{d[A]}{dt} = k_2([A]_0 - x)([B]_0 - x) \quad (3.30)$$

Since $[A]_t = [A]_0 - x$, hence $\frac{dx}{dt} = -\frac{d[A]}{dt} = -\frac{d[B]}{dt}$ and thus the rate law shown in Equation 3.30 can be written as:

$$\frac{dx}{dt} = k_2([A]_0 - x)([B]_0 - x) \quad (3.31)$$

Separation of the variables gives:

$$\frac{dx}{([A]_0 - x)([B]_0 - x)} = k_2 dt \quad (3.32)$$

Integration of Equation 3.32 between limits $x = 0$ to $x = x$ and $t = 0$ to $t = t$ can be expressed as:

$$\int_0^x \frac{dx}{([A]_0 - x)([B]_0 - x)} = k_2 \int_0^t dt \quad (3.33)$$

Giving the following expression (provided $[A]_0 \neq [B]_0$):

$$\frac{1}{[A]_0 - [B]_0} \ln \frac{[B]_0 ([A]_0 - x)}{[A]_0 ([B]_0 - x)} = k_2 t \quad (3.34)$$

This expression can be simplified to give

$$\frac{1}{[A]_0 - [B]_0} \ln \frac{[B]_0 [A]_t}{[A]_0 [B]_t} = k_2 t \quad (3.35)$$

By using Equation 3.35, the second-order rate constant can only be determined if the values of $[A]_0$, $[B]_0$, $[A]_t$ and $[B]_t$ are known. This means that the kinetic experiment has to involve many complicated and time-consuming steps.^{1,5,7} Therefore, second-order reactions are often studied under *pseudo* first-order conditions. This is accomplished by having one of the reagents in large excess (at least 10-fold excess) such that its concentration remains constant during the reaction.

For instance if $[B]_0 \gg [A]_0$ then the concentration of B remains relatively constant. Supposing that the reaction order with respect to A is one, then the rate law in *Equation 3.29* can be written as:

$$\begin{aligned} -\frac{d[A]}{dt} &= k_2[A]_t[B]_t \\ &= (k_2[B]_0)[A]_t \\ &= k_{obs}[A]_t \end{aligned} \quad (3.36)$$

where k_{obs} , is the observed rate constant with units of s^{-1} and is equal to $k_2[B]_0$.

A plot of $\ln [A]_t$ against time gives a linear fit with the observed rate constant, k_{obs} , as the slope. To determine the second-order rate constant, k_2 , a series of k_{obs} values have to be obtained at varying concentrations of B in excessive amounts. This generates a number of values for $[B]_0$. Thus k_{obs} from *Equation 3.36* can be expressed as:

$$k_{obs} = k_2[B]_0 \quad (3.37)$$

A plot of k_{obs} versus time, gives the second-order rate constant, k_2 with units $M^{-1} s^{-1}$

3.3.4. Reversible Second Order reactions

As with some first order reactions, some second order reactions also result in an equilibrium being established instead of going to completion. Consider the following equilibrium reaction:



By applying *pseudo* first-order conditions, the rate law can be expressed as:

$$-\frac{d[A]}{dt} = -\frac{d[B]}{dt} = \frac{d[C]}{dt} = k_2[A]_t[B]_t - k_{-2}[C]_t \quad (3.39)$$

Assuming that there is no product present initially and that the stoichiometric ratio of the reaction is 1:1:1, the mass balances at any time, t are:

$$\begin{aligned} [A]_t &= [A]_0 - [C]_t \\ \text{and } [B]_t &= [B]_0 - [C]_t \end{aligned} \quad (3.40)$$

At equilibrium

$$[A]_{eq} = [A]_0 - [C]_{eq}$$

$$\text{and } [B]_{eq} = [B]_0 - [C]_{eq} \quad (3.41)$$

At equilibrium the rate of the forward reaction is equal to the rate of the reverse reaction, as indicated by *Equation 3.42*.

$$-\frac{d[A]}{dt} = k_2[A]_{eq}[B]_{eq} - k_{-2}[C]_{eq} = 0 \quad (3.42)$$

Hence

$$k_2[A]_{eq}[B]_{eq} = k_{-2}[C]_{eq} \quad (3.43)$$

By substituting for $[C]_{eq}$ in *Equation 3.43*, using value from *Equation 3.41* and rearranging the following was obtained:

$$k_{-2}[A]_0 = k_2[A]_{eq}[B]_{eq} + k_{-2}[A]_{eq} \quad (3.44)$$

Substitution of $[C]_t$ from *Equation 3.40* with the term $[A]_0 - [A]_t$, and substitution into *Equation 3.39* gives the rate as:

$$\begin{aligned} -\frac{d[A]}{dt} &= k_2[A]_t[B]_t - k_{-2}([A]_0 - [A]_t) \\ &= k_2[A]_t[B]_t - k_{-2}[A]_0 = k_2[A]_t \end{aligned} \quad (3.45)$$

The combination of *Equations 3.44* and *Equation 3.45* gives:

$$-\frac{d[A]}{dt} = k_2[A]_t[B]_t - k_2[A]_{eq}[B]_{eq} - k_{-2}[A]_{eq} + k_{-2}[A]_t \quad (3.46)$$

Applying *pseudo* first order conditions where $[B]_0 \gg [A]_0$ *Equation 3.46* can be represented as:

$$\begin{aligned} -\frac{d[A]}{dt} &= k_2[A]_t[B]_0 - k_2[A]_{eq}[B]_0 - k_{-2}[A]_{eq} + k_{-2}[A]_t \\ &= (k_2[B]_0 + k_{-2})([A]_t - [A]_{eq}) \end{aligned} \quad (3.47)$$

Separation of the variables and integration of *Equation 3.47* gives:

$$\int_{[A]_0}^{[A]_t} \frac{d[A]}{([A]_t - [A]_{eq})} = -(k_2[B]_0 + k_{-2}) \int_0^t dt$$

$$\ln \left(\frac{[A]_t - [A]_{eq}}{[A]_0 - [A]_{eq}} \right) = - (k_2 [B]_0 + k_{-2})t$$

$$= -k_{obs}t$$

where $k_{obs} = k_2[B]_0 + k_{-2}$ (3. 48)

Hence, a plot of k_{obs} versus $[B]_0$ gives a straight line fit with k_2 as the slope and k_{-2} as the intercept. *Pseudo* first order conditions of this kind are mostly used in kinetic studies of square planar complex.

The equilibrium constant, K , can be determined by calculating the ratio:⁸

$$K_{eq} = \frac{k_2}{k_{-2}} \quad (3. 49)$$

Also, if a reaction mechanism proceed in two parallel pathways where one is independent of $[B]_0$ and the second involves solvolysis, this type of rate law can occur.^{1,5,7}

3.4. Activation Parameters

As much as kinetic studies are about determining the rate at which a reaction occurs, it is also necessary to deduce the mechanistic pathway in which a reaction takes place, especially for inorganic reaction mechanisms. That is often accomplished by determining the activation parameters of the reaction through temperature dependent studies.¹ These values provide a link between kinetic and thermodynamic aspects.^{1,7,9} The activation parameters can be obtained from temperature dependence measurements analysed using the Transition State theory or the Arrhenius equation.^{1,10,11}

Arrhenius determined the temperature dependence of reaction rate constants using an empirical relationship based on van't Hoff's suggestion.^{1,6,7,12}

$$k = Ae^{\left(\frac{-E_a}{RT}\right)} \quad (3. 50)$$

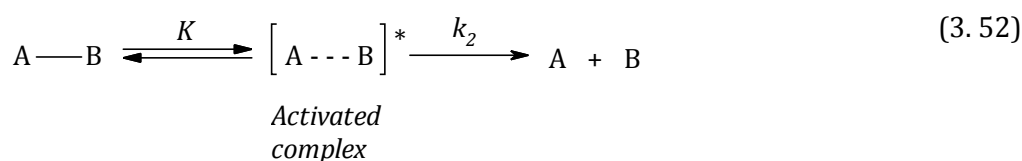
where, k is *rate constant* for the reaction, A is *Arrhenius pre-exponential factor* in $M^{-1}s^{-1}$, E_a is *Arrhenius activation energy* in $J mol^{-1}$, R is the *gas constant* (equal to $8.315 J K^{-1} mol^{-1}$), and T = absolute temperature in K.

By experimentally determining the rate constant at varying temperatures, one is able to plot a graph of $\ln k$ versus $\frac{1}{T}$ according to the following equation:

$$\ln k = \ln A - \frac{E_a}{R} \left(\frac{1}{T} \right) \quad (3.51)$$

The rate constant value is expected to increase with an increase in temperature.^{1,7} The Arrhenius equation is often used in kinetic reactions.

The transition state theory on the other hand, also known as the absolute rate theory and the activated complex theory, is most preferred treatment for reaction rates.^{5,13} The theory originates from the assumption that majority of the complex reactions proceed *via* the formation of a quasi-equilibrium between the reactants and the transition state.^{5,7,14} Consider the reaction described below using this theory:



The reaction rate can be represented as

$$\frac{d[A]}{dt} = k_2 \{A \cdots B\}^* = \frac{k_b T}{h} K^\ddagger [A][B] \quad (3.53)$$

where k_b = Boltzmann's constant whose value is $1.38 \times 10^{-23} \text{ J K}^{-1}$

T = temperature in kelvin

h = Plank's constant which is equal to $6.626 \times 10^{-34} \text{ J s}^{-1}$

K^\ddagger = equilibrium constant.

The experimental second-order rate constant, k_{expt} can be expressed as:

$$k_{\text{expt}} = \frac{k_b T}{h} K^\ddagger \quad (3.54)$$

The Gibbs free energy of activation, ΔG^\ddagger , is expressed as:

$$\Delta G^\ddagger = -RT \ln K^\ddagger \quad (3.55)$$

$$= \Delta H^\ddagger - T\Delta S^\ddagger$$

where ΔH^\ddagger is the change in enthalpy of activation and ΔS^\ddagger is the change in entropy of activation.

Substituting Equation 3.55 into Equation 3.54 affords the following expression:

$$k_{\text{expt}} = \frac{k_b T}{h} e^{\left(-\frac{\Delta G^\ddagger}{RT}\right)} = e^{\left(-\frac{\Delta H^\ddagger}{RT}\right)} e^{\left(\frac{\Delta S^\ddagger}{R}\right)} \quad (3.56)$$

Applying the natural logarithm on Equation 3.73 affords:

$$\ln\left(\frac{k_{\text{expt}}}{T}\right) = \ln\left(\frac{k_b}{h}\right) - \frac{\Delta H^\ddagger}{RT} + \frac{\Delta S^\ddagger}{R} \quad (3.57)$$

Simplifying the Equation 3.57 and representing it in linear form gives:

$$\ln\left(\frac{k_{\text{expt}}}{T}\right) = \frac{-\Delta H^\ddagger}{R} \cdot \frac{1}{T} + \left(\ln\frac{k_b}{h} + \frac{\Delta S^\ddagger}{R}\right) \quad (3.58)$$

where

$$\ln\frac{k_b}{h} = 23.8 \quad (3.59)$$

Thus from a plot of $\ln\left(\frac{k_{\text{expt}}}{T}\right)$ versus $\frac{1}{T}$, the enthalpy of activation, ΔH^\ddagger , is obtained from the slope and the entropy of activation, ΔS^\ddagger , is determined from the y-intercept of the graph. This plot is referred to as the Eyring plot.^{1,7,11} Mostly, ΔS^\ddagger values are obtained by extrapolating along the y-axis of the graph, hence values are accompanying with larger errors, normally three times higher than that of ΔH^\ddagger .⁵

The activation parameters are essential for determining reactions in solution as they reveal a lot about the mechanism pathway. For instance, large and negative values of the entropy of activation signifies an associative mechanism whereas large positive values of the entropy of activation are indicative of a dissociative mechanism since disorder increases due to bond breaking before complex formation.^{1,7,15}

3.4.1. The effect of Pressure on the Volume of Activation

Fortunately, temperature is not the only variable which can be varied in kinetic studies; pressure can also affect the rate of the reaction. The volume of activation, ΔV^\ddagger for a reaction can be determined from varying pressure-dependence rate constants which is very useful in assigning the mechanism, especially if entropy and enthalpy of activation values are not giving meaningful results.^{1,7,16} The rate constant also increases with an increase in pressure at constant temperature. This effect is described by the following equation:

$$\left(\frac{d \ln k_2}{dP}\right) = -\frac{\Delta V^\ddagger}{RT} \quad (3.60)$$

The volume of activation, ΔV^\ddagger , is the difference in partial molar volume between the transition state and the reacting species.¹⁷

This integrates to give:

$$\ln k = - \left(\frac{\Delta V^\ddagger}{RT} \right) P \quad (3.61)$$

A plot of $\ln k$ versus P gives a linear curve and the volume of activation can be calculated from the slope of the graph. Negative values for ΔV^\ddagger indicate an associative mechanism whereas positive ΔV^\ddagger values indicate a dissociative mechanism. The volume of activation changes with mechanism in the same way as the entropy.

3.5. Experimental kinetic Techniques

There are various experimental techniques and methods used to study kinetic reactions and each involves the measuring or controlling of certain physical properties such as absorbance, temperature, concentration, pressure, conductivity and ρ /density.¹² However, the mostly used methods involve measuring the concentration of either the reactants or products with time. The data obtained is then used to determine the rate law using previously mentioned theoretical kinetic processes. Selecting an experimental method by which kinetic data is obtained depends on whether or not the reaction is fast or slow.

Reactions that are too fast (reach completion in 60 seconds to 10^{-14} seconds) need specialised instrumentation and techniques for rapid mixing of the reagents and rapid data collection.⁵ Under such conditions the reaction has to be quenched or the instrument used to collect the data must be programmed to continuously record the concentration.^{18,19}

If the reactions occur with slow rates, the kinetics can be studied by mixing the reagents and determining their concentration profile over time using suitable conventional techniques.²⁰ However, over the past years many experimental techniques and instruments have been developed which are used in kinetic studies. These include, pulse methods, nuclear magnetic resonance (NMR), UV/Visible spectrophotometry and stopped-flow analysis. Of the mentioned methods only two are employed in this study, UV/Visible spectrophotometry and stopped-flow analysis.

3.5.1. UV/Visible Spectroscopy

UV/Visible spectroscopy is a sensitive instrument that detects sample concentrations ranging from 10^{-4} to 10^{-6} M.²⁰ It is the most often used technique for kinetic studies involving absorption spectra.^{1,17} It consists of a light source, (usually deuterium is used for UV radiation and tungsten is used for visible light), through the slit light enters the monochromator where it strikes a dispersing prism and exits through another slit. Eventually radiation reaches the sample and reference

solutions contained in quartz or fused silica cuvettes that allow UV radiation to pass through to the detecting system. Photomultiplier tubes are the most frequently used detectors in UV/Vis spectroscopy as it comprises of photoemissive cathode, a number of dynodes and an anode. Once the radiation photons have passed through the detector, an absorbance spectra ranging from 190 nm to 800 nm can be recorded.²¹

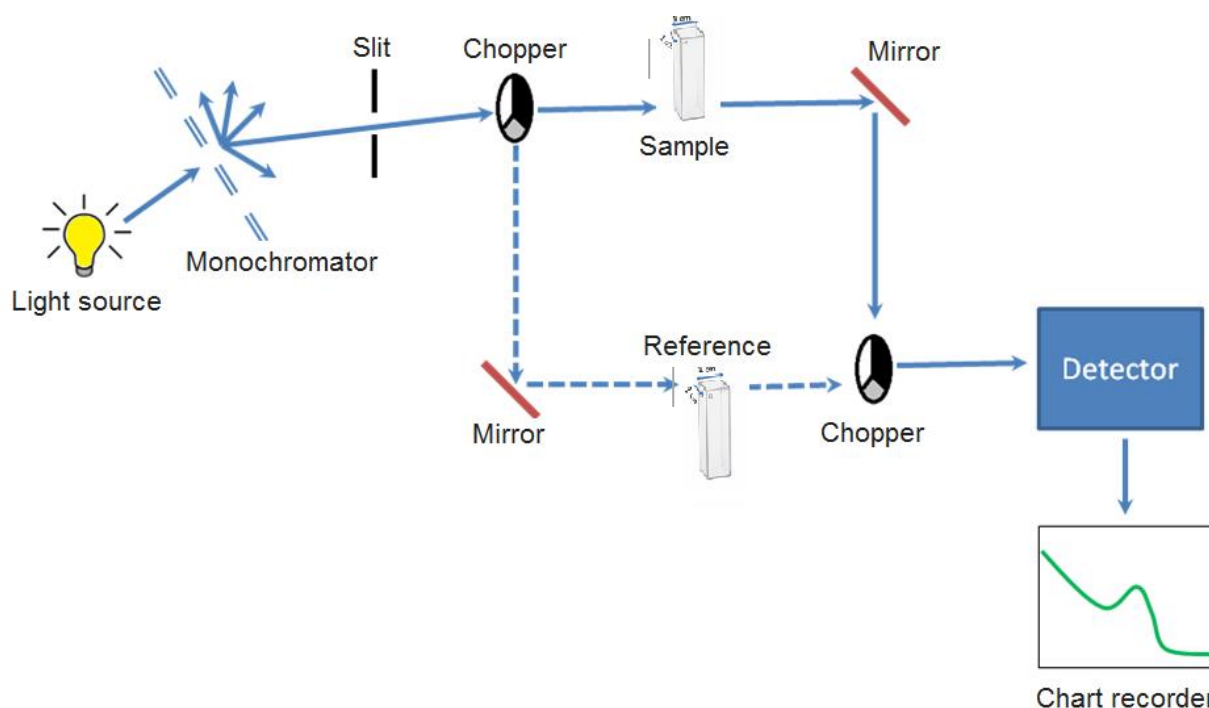


Figure 3.1: Schematic diagram of a UV/Visible Spectrometer.¹

UV/Vis spectrophotometers are designed to measure the light passing through the sample, this is known as the transmittance, T , and is given by:^{12,18}

$$T = \frac{I}{I_0} \quad (3.62)$$

where I is the intensity of the transmitted light (*sample intensity*) and I_0 is the intensity of the incident light (*reference intensity*).

The absorbance, on the other hand can be obtained from the intensities as follows:

$$A = \log\left(\frac{I_0}{I}\right) = -\log T \quad (3.63)$$

In order to compare different samples, factors affecting the absorbance must be kept constant leaving only the sample. This is accomplished by using Beer's law given in *Equation 3.81* as it shows a direct proportionality of the absorbance with the concentration of the sample.^{12,18,19}

$$A = \varepsilon cl \quad (3.64)$$

where A is the absorbance, c is the concentration of the sample (in mol dm^{-3}), l is the path length (in cm), ε is the molar absorptivity or the extinction coefficient (in $\text{M}^{-1} \text{cm}^{-1}$).

For the first-order reaction, represented by *Equation 3.6*, at any time t , the absorbance is

$$A_t = \varepsilon_X [X]_t + \varepsilon_Y [Y]_t \quad (3.65)$$

where A_t is the absorption at any time t , and $\varepsilon_X, \varepsilon_Y$ are the molar absorptivity of X and Y respectively.

Once the reaction has reached completion, the absorbance becomes

$$A_\infty = \varepsilon_X [X]_0 + \varepsilon_Y [Y]_0 \quad (3.66)$$

For kinetic analysis, the following expression is obtained from the absorbances:

$$\ln \frac{[X]_0}{[X]_t} = \ln \left(\frac{A_0 - A_\infty}{A_t - A_\infty} \right) = k_1 t \quad (3.67)$$

In kinetic studies, the absorbance of a reaction is taken over a wide wavelength range and at a certain period of time. A kinetic trace of absorbance versus time is obtained at a particular wavelength and is used to determine the observed rate constant of the reaction. By reacting the same procedure at different concentrations of the one reactant, the rate constant of the reaction at that specific temperature can be determined.

3.5.2. Flow Methods

Since not all chemical reactions occur at rates convenient enough to be studied using normal kinetic techniques such as the UV/Vis spectroscopy. Some reactions occur too fast and require less time to be spent on mixing the reactants. For such reactions special techniques that allow the reactants to mix rapidly in the reaction vessel are found in conventional flow methods.¹⁸ Flow methods involve the flow of the reactant solutions under pressure into a mixing chamber and then to an observation chamber. The progress of the reaction can be determined by measuring certain physical property at a fixed point along the observation chamber in which a variety of flow rates are required, or an alternative would be to measure a certain physical property, mostly the concentration of the reactants or products, at various positions along the chamber as a function of time.² There are two types of flow methods, continuous and stopped-flow methods. Stopped-flow is currently more popular in kinetic studies as it is modified from continuous flow methods to be more efficient since it uses less solution.^{2,19} From the diagram shown in **Figure 3.2**, syringes S1 and S2 are delivering the respective reactant solutions at constant temperature from two separate reservoirs with the aid of a concerted pressure on the plungers. They pass through the mixing chamber, M, where they

immediately react (for approximately 0.001 seconds) and proceed through the observation chamber then to a stop syringe S3.^{18,19} Where detection by the UV/Visible light source takes place and results are recorded.^{11,12,18}

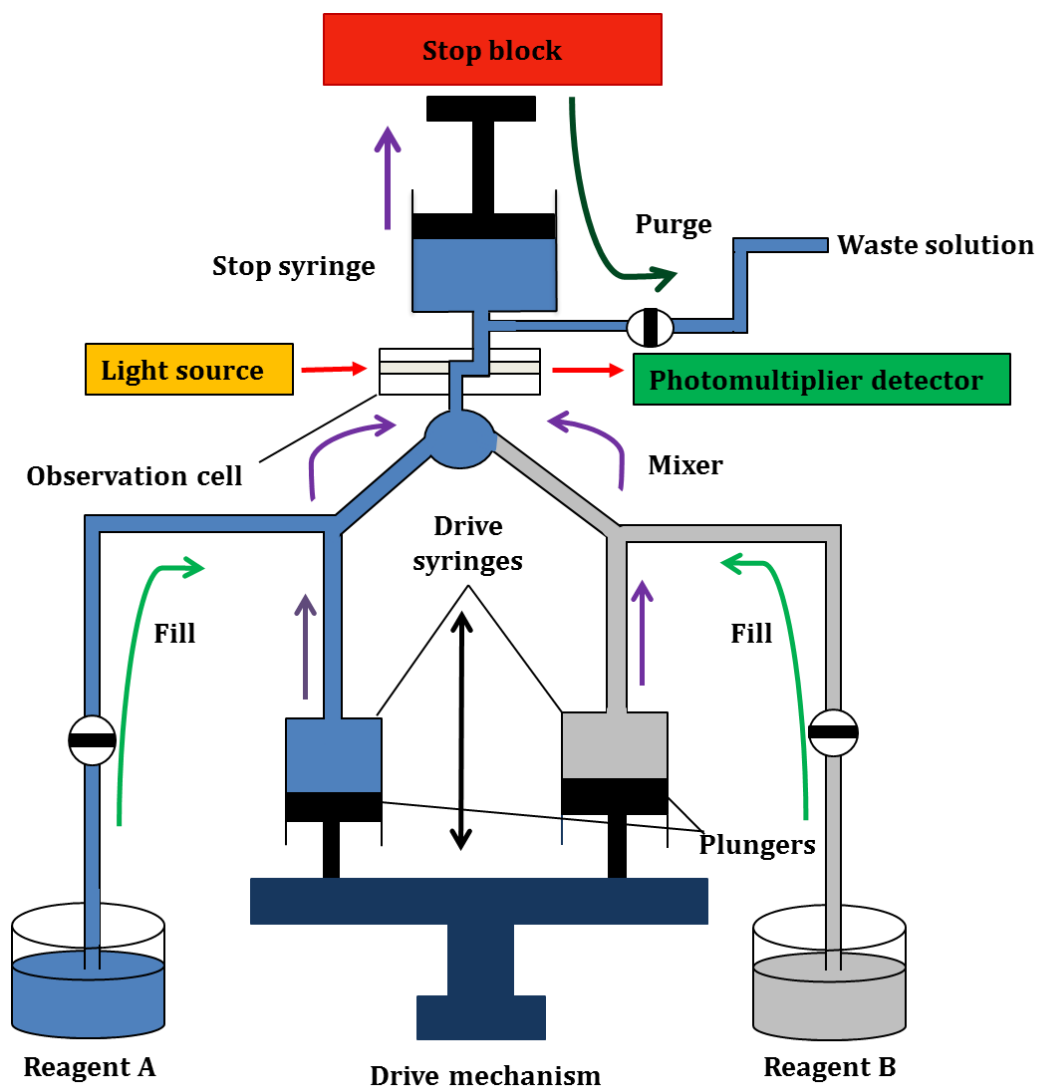


Figure 3.2: Schematic diagram of a Stopped-flow mixing apparatus.¹⁸

3.6. References

1. J. D. Atwood, *Inorganic and Organic Reaction Mechanisms*, 2nd edition, Wiley- VCH Inc., New York, **1997**, p. 1-32.
2. A. G. Skyes, *Kinetics of Inorganic Reactions*, Pergamon Press Ltd. London, **1966**, p. 1 – 21.
3. <http://vallance.chem.ox.ac.uk/pdfs/KineticsLectureNotes.pdf>. Retrieved 23/08/2013.
4. <http://www.cosbkup.gatech.edu/group/chem780/CHAPT2.pdf>. Retrieved 23/08/2013.
5. J. H. Espenson, *Chemical Kinetic and Reaction Mechanisms*, 2nd edition, McGraw-Hill, New York, **1995**, p. 1 - 80, 155 - 159, 161 – 162, 253 - 256.
6. M.L. Tobe and J. Burgess, *Inorganic Reaction Mechanisms*, Addison Wesley. Longman Ltd. Essex, **1999**, p. 30 - 43, 70, 112.
7. R. B. Jordan, *Reaction Mechanisms of Inorganic and Organometallic Systems*, Oxford University Press New York, **1991**, p. 1 - 17.
8. P. Atkins and J. de Paula, *Atkins' Physical Chemistry 8th edition*, Oxford University Press, Oxford, **2006**, p. 479 – 815, 791 - 829.
9. D. Benson, *Mechanisms of Inorganic Reactions in Solution*, McGraw-Hill, London, **1968**, p. 1 - 13.
10. M. G. Evans, M. Polanyi, *Trans. Faraday Soc.*, **1935**, 31, 875.
11. Laider, J. H. Meiser, *Physical Chemistry*, 4th edition. Houghton, Mifflin, New York, **2003**, p. 363 – 371, 373 – 393.
12. R. G. Wilkins, *Kinetics and Mechanisms of Reactions of Transition Metal Complexes*, VCH, Weinheim, **1991**, p. 41 - 43.
13. H. Eyring, *J. Chem. Phys.* **1935**, 3, 107.
14. S. Ašperger, *Chemical Kinetics and Inorganic Reaction Mechanisms 2nd edition.*, Kluwer Academic/ Plenum Publisher, New York, **2003**, p. 3, 7- 23.
15. F. Basolo and R. G. Pearson, *Mechanisms of Inorganic Reactions*, 2nd Ed., Wiley, New York, **1967**, p. 351 - 356.
16. L. Helm and A. E. Merbach, *Dalton. Trans.*, **2002**, 633.
17. D. Katakis and G. Gordon, *Mechanisms of Inorganic Reactions*, Wiley-Interscience, New York, **1987**, p. 58 – 66.
18. D. A. Skoog, D. M. West, F. J. Holler and S. R. Crouch, *Fundamentals of Analytical Chemistry*, 8th edition, Brooks/Cole – Thomson Learning, Inc., United States, **2004**, p. 718 - 734, 771 - 775, 878 - 894.
19. S. R. Logan, *Fundamentals of Chemical Kinetics*, Longman, Essex, **1996**, p. 24 - 37.

20. A. Mambanda, *PhD Thesis, Influence of Bridging Groups on the Reactivity of Dinuclear Platinum(II) Complexes with bis(2-pyridylmethyl)amine Chelate Headgroups*, University of KwaZulu-Natal, Pietermaritzburg, South Africa, **2009**, p. 82 – 88.
21. <http://teaching.shu.ac.uk/hwb/chemistry/tutorials/molspec/uvvisab3.htm>. Retrieved: 11/09/2013.

CHAPTER 4

Mechanistic Behaviour of Platinum(II) Complexes with Quinolyl and Pyridyl Moieties Using a Series of Bio-relevant Azole Nucleophiles

4.0. Abstract

The kinetic and mechanistic investigation of the chloride substitution from mononuclear tridentate platinum(II) complexes, viz., [Pt(2,2':6,2''-terpyridine)Cl]Cl.2H₂O, (**PtL1**), [Pt(1,3-di(2-pyridyl)benzene)Cl], (**PtL2**), [Pt(2,6-di-(2'-quinoliny)pyridine)Cl]Cl, (**PtL3**) and [Pt(1,3-di-(2'-quinoliny)benzene)Cl] (**PtL4**) using a series of five-membered N-donor heterocyclic nucleophiles, viz., imidazole (**Im**), 1-methylimidazole (**MIm**), 1,2-dimethylimidazole (**DIm**), pyrazole (**Pyz**) and 1,2,4-triazole (**Trz**) was conducted under *pseudo* first-order conditions as a function of concentration and temperature using UV/Vis spectroscopy and conventional stopped-flow techniques. The reactivity of the studied platinum(II) complexes followed the trend **PtL2** > **PtL4** > **PtL1** > **PtL3**. The lability of the chloride ligand was dependent on the strength of the π -back bonding between the tridentate ligand system and the metal centre which directly influences the electrophilicity of the metal centre. The presence of two *cis*-quinoline moieties on **PtL3** and **PtL4** result in a non-planar and flexible complex with a restricted electron flow. This causes an accumulation of electron density on the metal centre through a net σ -donation of the quinoline moieties towards the Pt centre. This electron-rich environment around the metal centre impedes the attack of incoming azole nucleophiles thus a lower reactivity compared to Pt(II) complexes with *cis*-pyridyl moieties. Moreover, by changing the *trans*-donor ring from pyridine (**PtL1** and **PtL3**) to phenyl (**PtL2** and **PtL4**), the kinetic *trans*-labilizing effect on such Pt(II)terpy-derivatives was accentuated. The reactivity trend of the azole nucleophiles was influenced by the basicity (**Im** > **Pyz** > **Trz**) and steric effects of the entering nucleophile (**MIm** > **Im** > **DIm**) for all complexes except for **PtL3** where **MIm** and **DIm** had similar reactivities. This was probably due to the difference in steric demands. The experimental data is well supported by DFT computational data. The negative entropy values and the dependence of the rate constants on the nucleophile concentration support an associative mechanism for all substitution reactions.

4.1. Introduction

Ligand substitution reactions of square planar Pt(II) complexes are amongst the well-studied systems following the recognition that the antitumour activity of cisplatin is derived from a simple act of substitution of its two *cis*-coordinated labile ligands.¹⁻³ In the majority of cases, the substitution of the labile ligands from the Pt(II) centre proceed *via* a trigonal bipyramidal transition state which is a hallmark for bimolecular and associatively activated mode of substitution. In-depth kinetic and mechanistic studies^{4-10,13-19} have shown that the electronic and structural properties of the non-labile ligands are key design tools for more effective future metal-based drugs, placing mechanistic and kinetic studies at the centre-stage for the design or search of candidate antitumour drugs of improved efficacy. Pt(II) complexes with tridentate polypyridyl ligands provide good study models in ligand exchange reactions since only the fourth coordinated group is labile. The π -conjugation extended along the plane of the tridentate polypyridyl ligand system help stabilise the Pt(II) complexes.⁴⁻⁶ Data from literature^{5,6,9,13-19} on tridentate coordinated Pt(II) complexes exemplified by [Pt(terpy)Cl], (where terpy = 2,2':6',2''-terpyridine) have shown how the rate of substitution of the labile ligand can be tuned by electronic (*trans* and *cis* effects of ancillary substitutions) and steric effects.⁷

For instance, a comparison of the chloro substitution from [Pt(dien)Cl], (where dien = diethylenetriamine) and [Pt(terpy)Cl] have clearly shown that π -back bonding of the terpy ligand enhances the reactivity of the complex. The terpy complex reacts by two to six orders of magnitudes faster than [Pt(dien)Cl].⁸⁻¹⁰ This large reactivity difference is due to the stabilization of the five-coordinate transition state of [Pt(terpy)Cl] brought about by the ability of the terpy ligand to receive electron density from the Pt(II) centre thereby making the metal centre electrophilic and thus more receptive to electron density from incoming nucleophiles.⁸⁻¹³

The π -acceptability of the tridentate ligand can be categorised further into the *trans* or *cis* π -effect. The reactivity trend with the investigated series of Pt(II) complexes was mostly due to the electrophilicity of the Pt metal centre which is a consequence of the amount of electron back-donation being directed towards the ligand orbitals. Complexes with higher electronic communication between the π -acceptor ligands have enhanced substitution rates compared to complexes in which the electronic communication has been disjointed.^{10,17}

However, this may not be always the case, for example, if strong σ -donor groups such as a phenyl ring separate the pyridyl rings of terpy. A study conducted by Hoffman *et al*¹⁹ reported substitution rates of labile chloro ligands of tridentate coordinated Pt(II) complexes with various number of pyridine and phenyl rings to depend on whether the σ -donor group is situated *cis*-/*trans*- to the leaving group.^{10,19} This involved the systematic replacement of one pyridine ring with a phenyl ring

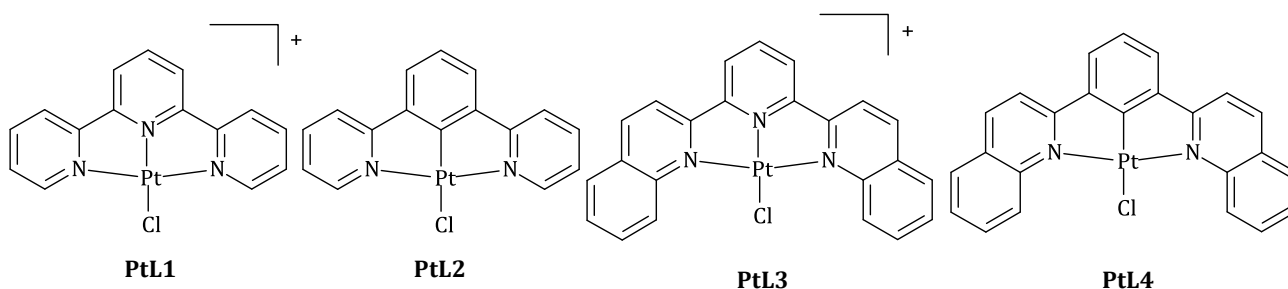
in both *cis*- and *trans*-positions on a Pt(II) terpy backbone and kinetically studying their substitution reactions with thiourea nucleophiles.¹⁹ In all three Pt(II) complexes the pyridine/phenyl ring was in-plane with the coordination plane and the π -acceptor abilities were regarded as similar in all complexes due to both phenyl and pyridyl rings having delocalised π -electrons. The Pt(II) complex with a phenyl group *cis* to the leaving group had a reduced substitution rate compared to Pt(terpy) and the rate constant was much smaller than that of Pt(II)(1,3-di(2-pyridyl)benzene), which has a phenyl group *trans*- to the leaving chloride.^{11,19} This was due to the strong σ -donor ability of the *cis*-phenyl which increases steric hindrance in the five-coordinate transition state and reduces nucleophilic discrimination which collaborate in decreasing reactivity. The contrary was observed for complex with a phenyl in the *trans*-position, reactivity was found to be orders of magnitude greater than that of the standard complex, Pt(terpy). This was due to less steric hindrance experienced by the entering nucleophile, the higher *trans*-effect of the phenyl ring but mostly due to the destabilization of the ground state.¹⁹

Previous studies reported by Jaganyi *et al.*¹⁴⁻¹⁶ showed that by introducing different ortho-substituted phenyl groups at the 4'-position of a terpyridine ligand system influences the π -back bonding strength of the ligand which affects the electrophilicity of the metal centre and thus its reactivity with nucleophiles. Also verified that the addition of electron donating substituents increases electron density on the Pt(II) centre in the transition state making it less electrophilic. In the process, it reduces the π -acceptability of the terpyridyl ligand thus decreases the rate of substitution. Electron-withdrawing substituents were found to have a contrary effect on the rate of substitution.^{14,15}

One other interesting aspect on the rate of substitution of these Pt(II) complexes has been the effect of π -conjugated systems.^{9,10,13-17,18} In most cases, the extended delocalised π -conjugation enhances the electronic communication due to increasing the strength of the π -back bonding ligand, thus making the metal centre more electrophilic and susceptible to nucleophilic attacks.^{13,17} However, current studies from our group have shown a contrasting trend during Pt(II) complex substitution reactions.^{5,6} When a isoquinolyl group replaces one of the *cis*-pyridyl rings of a terpy backbone, the rate was significantly slow by a factor of three which was intriguing.^{5,6} Extension of π -conjugation through the isoquinolyl group slowed down the rate of substitution at the metal centre due to the net electron donation into the π -acceptor ligand framework. Accumulation of electron density effectively decreases the electrophilicity of a metal centre.^{5,6}

In this study, we report the trends in the rate of substitution using four tridentate coordinated Pt(II) complexes structurally similar to those reported by Hoffman *et al.*¹⁹ however, in this case the *cis*-pyridyl rings are replaced by 2-quinolyl groups. This will enable us to quantify the effect of

extending the π -conjugation around the Pt(II) centre using the net π/σ -donating 2-quinoline moieties. The tridentate coordinated Pt(II) complexes were [Pt(2,2':6,2''-terpyridine)Cl]Cl.2H₂O, (**PtL1**), [Pt(1,3-di(2-pyridyl)benzene)Cl], (**PtL2**), [Pt(2,6-di-(2'-quinolinyl)pyridine)Cl](Cl), (**PtL3**) and [Pt(1,3-di-(2'-quinolinyl)benzene)Cl] (**PtL4**). Also, by changing the *trans* group from pyridine to phenyl, we intend on determining how the extended conjugation combined with the strong *trans*-effect of the phenyl ring influence substitution reactions. A series of five-membered heterocyclic azole nucleophiles were considered appropriate for this study due to their biological relevance, as for instance imidazole is part of the DNA which Pt complexes bind to.¹⁸



Scheme 4.1: Structural formulae of the investigated Pt(II) complexes (counterions omitted for clarity).

4.2. Experimental

4.2.1. Materials and procedures

The following chemicals, 1,3-dibromobenzene (98%), (2-pyridinyl)tributylstannane (98%), bis(triphenylphosphine)palladium(II) dichloride (98%), 1,3-diacetylbenzene (97%), 1,5-cyclooctadiene, COD (99%) and 2,2':6',2''-terpyridine (98%) were purchased from Sigma-Aldrich and used as received. The platinum(II) precursors, potassium tetrachloroplatinate, K₂PtCl₄ (99.99%) was obtained from Strem Chemicals. Dimethylsulfoxide and nitromethane were purchased from Sigma-Aldrich and Saarchem, respectively while the rest of the solvents were procured from Merck.

4.2.2. Synthesis of Ligands

The ligand, **1,3-di(2-pyridyl)benzene, L2** was synthesized following a literature method,^{19,20} but with a modified purification step.

A mixture of 1,3-dibromobenzene (0.272 mL, 2.25mmol), (2-pyridyl)tributylstannane (1.8 mL, 6.53 mmol), Pd(PPh₃)Cl₂ (5 mol %) and LiCl (810 mg, 22.6mmol) in anhydrous toluene was heated and reflux for 3 days at 100 °C under a flow of N₂ gas. After cooling to 23 °C, a saturated KF solution was

added and the mixture stirred for 35 minutes. Solid residues were filtered off and CH_2Cl_2 (100 mL) and 5% w/v NaHCO_3 (100 mL) were added to the filtrate. The mixture was shaken for 15 minutes and the organic layer separated, dried over anhydrous sodium carbonate. Purification was achieved using a silica gel chromatographic column eluted with a 60% hexane/ 40 % ethyl acetate mixture. The title compound was obtained as a bright yellow oil. Yield: 155 mg (25.5%). TOF MS ES^+ : $m/z = 255.09$ $[\text{M}+\text{Na}]$. ^1H NMR (400 MHz, CDCl_3) ppm $\delta = 8.69$ (d, 2H), 8.62 (t, 1H), 8.30 (dd, 2H), 7.81 (d, 2H), 7.73 (td, 2H), 7.56 (t, 1H), 7.21 (m, 2H).

Synthesis of **2, 6-di-(2'-quinolinyl) pyridine, L3** was synthesized using a literature method.²¹⁻²³

A mixture of 1,3-diacetylpyridine (300 mg, 1.8mmol), 2-aminobenzaldehyde (432 mg, 3.6 mmol), and KOH (1.2 g) in absolute EtOH (20 mL) was refluxed for 24 h. The mixture was then cooled to room temperature, and H_2O (20 mL) was added. The aqueous phase was extracted with CH_2Cl_2 (3 x 15 mL). The organic phase was dried over anhydrous MgSO_4 and the solvent evaporated yielding a residue which was recrystallized from ether/ CH_2Cl_2 (6:1) to give the desired product (**L3**) as light yellow needles. Yield: 279 mg (47%). TOF MS ES^+ : $m/z = 356.11$ $[\text{M}+\text{Na}]$. ^1H NMR (CDCl_3): $\delta = 8.82$ (d, 2H); 8.74 (d, 2H); 8.31 (d, 2H); 8.18 (d, 2H); 8.04 (t, 1H); 7.86 (d, 2H); 7.73 (t, 2H); 7.54 (td, 2H). ^{13}C NMR (CDCl_3 , 400 MHz): $\delta = 156.22$; 155.53; 147.96; 137.96; 136.74; 129.85; 129.59; 128.37; 127.65; 126.79; 122.10; 119.12.

The ligand, **1,3-di-(2'-quinolinyl)benzene, L4** was prepared following a method used to synthesize 2,6-di-(2'-quinolinyl) pyridine.^{21,23} instead 1,3-diacetylbenzene was used as the starting material.

A mixture of 1,3-diacetylbenzene (200 mg, 1.2 mmol), 2-aminobenzaldehyde (288 mg, 2.4 mmol), and KOH (800 mg) in absolute EtOH (40 mL) was refluxed for 24 h. The mixture was then cooled to room temperature, and H_2O (20 mL) was added. The aqueous phase was extracted with CH_2Cl_2 (3 x 15 mL). The organic phase was dried over anhydrous MgSO_4 and the solvent evaporated to provide a residue which was recrystallized from ether/ CH_2Cl_2 (6:1) to give the desired product (**L4**) as light yellow needles. Yield: 56% (224 mg). TOF MS ES^+ : $m/z = 355$ $[\text{M}+\text{Na}]$. ^1H NMR (CDCl_3): $\delta = 8.95$ (t, 1H), 8.33-8.27 (m, 4H), 8.21 (d, 2H); 8.02 (d, 2H), 7.84 (d, 2H), 7.74 (td, 2H), 7.68 (t, 1H), 7.53 (td, 2H). ^{13}C NMR (CDCl_3 , 400 MHz): $\delta = 157.0$, 148.1, 140.1, 137.2, 129.8, 129.6, 129.5, 128.7, 127.5, 127.3, 126.9, 126.5, 119.2. Anal. Calcd for $\text{C}_{24}\text{H}_{15}\text{N}_2$: C = 86.75, H = 4.82, N = 8.43%. Found C = 86.68, H = 4.83, N = 8.47%.

4.2.3. Synthesis of Platinum(II) Complexes

Synthesis of **[Pt(2,2:6,2''-terpyridine)Cl]Cl.2H₂O, PtL1** was done following a known literature procedure²⁴ and the $[\text{Pt}(\text{COD})\text{Cl}_2]$ precursor was synthesised following a literature method.²⁵

The ligand 2,2':6,2''-terpyridine (**L1**) (313 mg, 1.34 mmol) was added to a stirred suspension of [Pt(COD)Cl₂] (500 mg, 1.34 mmol) in water (30 mL) and the mixture was heated to between 40 and 50 °C. The mixture was dissolved to give an orange-red solution after about 20 minutes. The solution was allowed to cool to room temperature and filtered to remove any unreacted material. A red solid was obtained after concentrating the filtrate under reduced pressure. This red product, [Pt(terpy)Cl]Cl·2H₂O (**PtL1**), was filtered, washed with diethyl ether and air-dried to give the pure desired product. Yield: 0.64 g (89 %). TOF MS ES⁺: $m/z = 463.0$ [M⁺]. Anal. Calcd for C₁₅H₁₅N₃PtCl₂O₂: C = 33.71, H = 2.85, N = 7.88 %. Found C = 33.92, H = 3.09, N = 7.60 %.

[Pt(1,3-Di(2-pyridyl)benzene)Cl], PtL2 was synthesised according to a literature procedure.²⁰

A mixture of 1,3-di(2-pyridinyl)benzene (82.3 mg, 0.355 mmol) in 9 mL acetic acid and K₂PtCl₄ (147.2 mg, 0.355 mmol) in 1 mL H₂O was added into a reaction flask. This mixture was degassed and purged with nitrogen gas and then refluxed at 110 – 115 °C. After 3 days, the reaction mixture was cooled to 23 °C and the resulting yellow suspension was filtered off, washed with MeOH, EtOH, water and diethyl ether after which it was dried under vacuo to yield the desired product as a bright yellow solid. Yield: 124 mg (65 %). TOF MS ES⁺: $m/z = 463$ [M+2H⁺]. ¹H NMR (DMSO-*d*₆, 400 MHz): 9.12 (dd, 2H); 8.21 (td, 2H); 8.14 (br-d, 2H); 7.75 (d, 2H); 7.56 (ddd, 2H); 7.28 (t, 1H). ¹³C NMR (DMSO-*d*₆, 400 MHz): 167.06; 161.47; 151.73; 141.00; 140.92; 125.38; 124.58; 123.61; 120.89. Anal. Calcd for C₁₆H₁₁N₂PtCl: C = 41.61; H = 2.40; N = 6.06 %. Found C = 41.98; H = 2.41; N = 5.89 %.

Synthesis of **[Pt(2,6-di-(2'-quinolinyl)pyridine)Cl](Cl), PtL3**

The Pt(II) precursor used, *cis*-dichlorobis(dimethylsulfoxide)platinum(II) was synthesised using a literature procedure.²⁶

A mixture of **L3** (100 mg) and Pt(DMSO)₂Cl₂ (126 mg) in methanol (15 mL) was refluxed for three days under a flowing gas of inert atmosphere. The orange/yellow coloured precipitate was filtered off using a 0.45 μm millipore system and was washed with methanol, ethanol, diethyl ether and dichloromethane and dried under vacuum.²⁷

TOF MS ES⁺: Yield: 98 mg (58%) $m/z = 563$ [M⁺]. ¹H NMR (DMSO-*d*₆, 400 MHz): 9.55 (d, 2H); 9.12 (d, 2H); 8.81 (d, 2H); 8.67 (m, 3H); 8.23 (d, 2H); 8.04 (t, 2H); 7.89 (t, 2H). ¹³C NMR (DMSO-*d*₆, 400 MHz): 155.3; 154.8; 146.8; 138.2; 137.4; 132.3; 130.1; 129.0; 127.8; 127.2; 121.6; 118.8. ¹⁹⁵Pt NMR (DMSO-*d*₆, 500 MHz): -2961.6 ppm. Anal. Calcd for C₂₃H₁₅N₃PtCl: C = 47.40; H = 2.56; N = 4.61 %.

Found C = 47.08; H = 2.19; N = 4.33 %. IR (4000 - 650)[†] $\bar{\nu}$: 3097.8 (Pt-Cl stretch), 1622.7 (C=N, pyridyl), 1068.5 - 1021.7 (ClO₄ counter ion).

Synthesis of [Pt(1,3-di-(2'-quinolinyl)benzene)Cl], PtL4²⁷

A mixture of K₂PtCl₄ (104.3 mg, 0.242 mmol) and 1,3-di-(2'-quinolinyl)benzene (80 mg, 0.242 mmol) in 20 mL glacial acetic acid were refluxed at 110 °C for 24 h. The dark yellow solid was isolated by filtration, washed with chloroform, methanol, acetone, ethanol and diethyl ether and dried under vacuum.

Yield: 106 mg (78 %). TOF MS ES⁺: m/z = 526 [M⁺]. ¹H NMR (DMSO-*d*₆, 400 MHz): 8.97 (d, 1H); 8.84 - 8.75 (m, 2H); 8.59 - 8.48 (m, 3H); 8.40 (dd, 1H); 8.35 - 8.30 (m, 2H); 8.08 - 7.99 (m, 3H); 7.81 (td, 2H); 7.62 (td, 2H) ppm. Anal. Calcd for C₂₄H₁₅N₂PtCl: C = 51.34; H = 2.76; N = 5.08 %. Found: C = 51.20; H = 3.03; N = 5.52 %. IR (4000- 650)[†] $\bar{\nu}$: 3097.6 (Pt-Cl stretch), 1615.4 (C=N, pyridyl), 1068.8 - 1021.4 (ClO₄ counter ion).

4.2.4. Preparation of Complexes and Nucleophile Solutions for Kinetic Analysis

A 0.1 M ionic strength solution was prepared by dissolving the required amount of LiCF₃SO₃ and LiCl in methanol to afford a 0.1 M concentrated solution. This solution was used to dissolve complexes and nucleophiles for kinetic analysis. The triflate ion, was chosen because it does not coordinate to the Pt(II) metal centre.²⁸

To improve the solubility of the complexes in the medium, the required amount of the metal complex was first dissolved in 2 % DMF before it was made up to volume with a constant ionic strength solution to 100 mL.

The solutions of all the neutral nucleophiles, *viz.*, **Im**, **Pyz**, **Trz**, **MIm** and **DIm** were prepared by dissolving a known quantity of the nucleophile into the constant ionic strength methanol solution to an ultimate nucleophilic concentration that was *ca.* 50 times larger than the Pt(II) complex concentration. The ionic strength was kept constant at 0.1 M throughout all the kinetic reactions. From this stock solution, a series of subsequent dilutions were made of constant ionic strength to afford nucleophilic solutions of 10, 20, 30 and 40 times the concentration of the metal complex. Except for **PtL2** with **Im**, **MIm** and **DIm** of which the nucleophilic stock solutions were made to be 250 times that of the Pt(II) complex and diluted subsequently to create solutions in the order of, 50, 100, 150 and 200 times the concentration of the metal complex.

[†] vs = very strong, s = strong, m = medium, w = weak and b = broad.

4.2.5. Physical Measurements and Instrumentation

^1H , ^{13}C and ^{195}Pt spectra were recorded on a Bruker Avance III 500 or Bruker Avance III 400 at frequencies of 500 MHz or 400 MHz (^1H) and 125 MHz/100 MHz (^{13}C) using either a 5 mm BBOZ probe or a 5 mm TBIZ probe. All proton and carbon chemical shifts are reported relative to the relevant solvent signals at 30 °C unless stated otherwise. Elemental compositions of the ligands and complexes were performed on a Thermo Scientific Flash 2000. The mass spectral data of the ligands and complexes were acquired on a Waters Micromass LCT Premier spectrometer. All FTIR spectra were recorded on a Bruker Alpha FTIR spectrometer. The spectra were acquired by crushing the powder on the sample platform between the Diamond Heads. A total of about 25 spectra were averaged. Relevant information was obtained from the frequency range 4 000 to 400 cm^{-1} . The characterization spectra for the ligands and complexes are shown on **Figures S4.1 - S4.18** of the supporting information. Kinetic studies for fast reactions were monitored using an Applied Photophysics SX 20 stopped-flow spectrophotometer coupled to an online data acquisition system. Slow reactions were monitored using a Varian UV/Vis Cary 100 spectrophotometer. The temperature of these instruments was controlled throughout all kinetic experiments to ± 0.02 °C. Kinetic traces (see **Figure S4.19 - S4.23**) were graphically analysed using the Origin 7.5^{®29} software package.

4.2.6. Computational modelling

Computational modelling of the complexes, **PtL1**, **PtL2**, **PtL3** and **PtL4** as well as the nucleophiles, **Im**, **MIm**, **Dim**, **Pyz** and **Trz** were performed as ground state electronic structures in the gas phase using the computational software package, Gaussian 09W.³⁰ For all complexes, the density functional theory (DFT) method using the B3LYP functionals and a basis set of LANL2DZ was used to optimize the neutral and +1 charged Pt(II) complexes. For theazole nucleophiles computational calculations were performed with a basis set of 3-21G.

4.2.7. X-ray Crystallography

The single X-ray crystal data for the ligand, L4 was recorded on a Bruker Apex II Duo equipped with an Oxford Instrument Cryojet operating at 100 K and an Incoatec microsource operating at 30 W power. The data was collected with Mo $K\alpha$ radiation ($\lambda = 0.71073$ Å) at a crystal-to-detector distance of 50 mm. The following conditions were used for the Bruker data collection: omega and phi scans with exposures taken at 30 W X-ray power and 0.50° frame widths using APEX2.³¹ The programme, SAINT³¹ was used to reduce the data, using outlier rejection, scan speed scaling, as well as standard Lorentz and polarisation correction factors. Direct methods, SHELXS-97³² were used to solve the structure. Hydrogen atoms were located in the difference density map and refined

isotropically with SHELXL-97³² and were included as idealised contributors in the least squares process. To prepare the material for publication OLEX2, a complete structure solution, refinement and analysis program³³ was used. The ligand, **L4** crystallized in the monoclinic crystal system, in the space group, $P2_1/c$ and contained one complete molecule with $Z = 4$. The crystal structure is shown in **Figure 4.1** and a summary of the crystal data and structure refinement details are shown in **Table 4.1**.

Table 4.1: Crystal data and structural refinement for 1,3-di-(2'-quinolinyl)benzene, **L4**.

<i>Parameter</i>	
Chemical formula	$C_{24}H_{16}N_2$
M_r (g.mol ⁻¹)	332.39
Crystal system	Monoclinic
Space group	$P2_1/c$
Temperature (K)	100
a (Å)	34.334 (2)
b (Å)	3.8441 (3)
c (Å)	12.2227 (9)
α (°)	90
β (°)	97.160 (3)
γ (°)	90
V (Å ³)	1600.6 (2)
Z	4
μ (MoK α) (mm ⁻¹)	0.08
$F(000)$	696
Crystal size (mm)	0.26 x 0.09 x 0.05
θ range (°)	1.2–26.2
No. of measured, independent and observed [$I > 2\sigma(I)$] reflections	11191, 3047, 2488
R_{int}	0.030
No. of refined parameters and restraints	235, 0
H-atom treatment	by a mixture of independent and constrained refinement
$R[F^2 > 2\sigma(F^2)]$, $wR(F^2)$, S	0.030, 0.122, 1.08
$\Delta\rho_{max}$, $\Delta\rho_{min}$ (e Å ⁻³)	0.24, -0.22

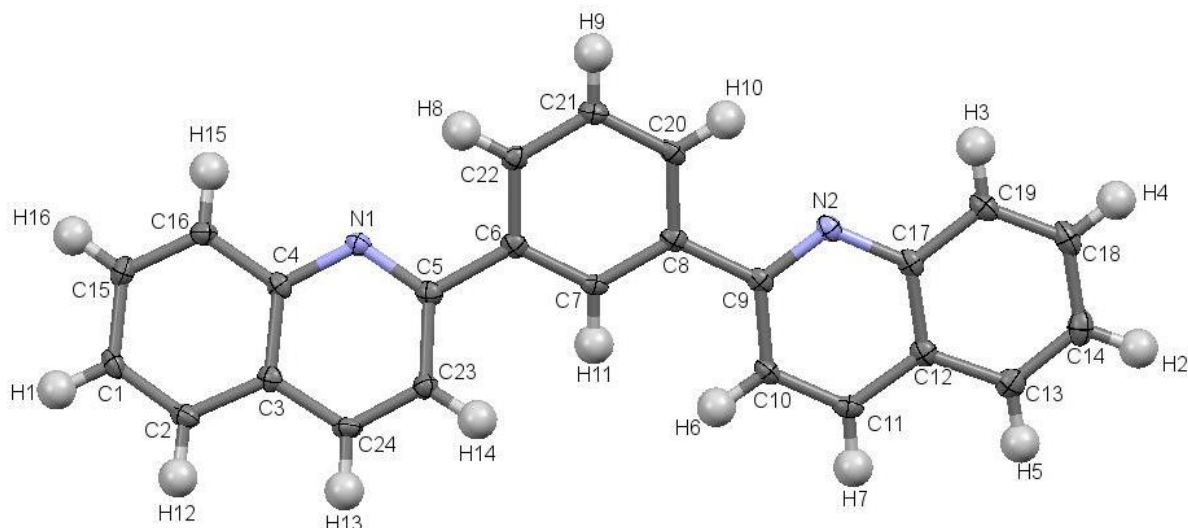


Figure 4.1: Molecular structure of the ligand, **L4** with thermal ellipsoids at the 50 % probability level.

4.2.8. Kinetic measurements

All kinetic measurements were performed under *pseudo* first-order conditions with the nucleophiles provided in concentrations of at least 10-fold excess over that of the Pt(II) complex. This ensured that the reaction goes to completion. All reactions were initiated by mixing equal volumes of pre-thermostated solutions of complex and nucleophile solutions placed into the two compartments of the quartz cuvettes (for **PtL1** and **PtL3**) or by directly mixing the solutions into a stopped-flow reaction analyser (for **PtL2** and **PtL4**). The changes in absorbance of each reaction mixture were recorded over the wavelength range 200 - 800 nm. All wavelengths suitable for kinetic studies were predetermined using a UV/Vis spectrophotometer and are summarised in **Table S4.1** of the supporting information. The kinetic traces obtained at suitable wavelengths were used to determine the observed rate constants, k_{obs} at different nucleophilic concentrations. These are represented in **Tables S4.2 – S4.6** of the supporting information. The temperature dependence of the rate of reaction was studied within the range of 15 - 40 °C at an interval of 5 °C. The data was fitted to the Eyring equation,³⁴ to calculate the activation parameters ΔH^\ddagger and ΔS^\ddagger from the slope and intercept of the plots, respectively.

4.3. Results





4.3.1. Computational Studies

In an effort to gain an in-depth understanding of the structural difference between the Pt(II) complexes, computational calculations were performed. A summary of the DFT calculated data is presented in **Table 4.2**, while the geometry-optimized structures, the frontier molecular orbital diagrams and electrostatic potential mappings are presented in **Table 4.3**.

The bond angles around each Pt(II) centre of each complex (**Table 4.2**) reflects a slightly distorted square planar coordination geometry. The computational data from **Table 4.2** also reveals that **PtL1** and **PtL2** with *cis*-pyridyl moieties on either side of the platinum centre adopts a C_{2v} symmetry whereas **PtL3** and **PtL4** with *cis*-quinoline moieties coordinated to either side of the metal centre adopted a C_s symmetry point group. Data in **Table 4.2** indicates that the Pt-Cl bond length is slightly longer for complexes with a C-donor atom *trans* to the chloro leaving group (**PtL2** = 2.504 and **PtL4** = 2.542) as compared to the complexes with N-donor atoms in the *trans* position (**PtL1** = 2.392 and **PtL3** = 2.419). Furthermore, the Pt-Cl bond length is the longest for complexes containing quinoline ligands *cis* to the leaving group as compared to similar complexes containing *cis*-pyridine rings. This elongation is due to electron density repulsion in the ground state.

The HOMO-LUMO energy gaps shown in **Table 4.2** show the Pt(II) complexes with *trans*-N donor groups **PtL1** and **PtL3** have a smaller energy gap as compared to Pt(II) complexes with *trans*-C-donor ligands **PtL4** and **PtL2**. The HOMO map is mainly on the *trans*-donor to the metal centre and down to the leaving group for **PtL1**, **PtL2** and **PtL4** and situated mostly on the quinoline rings for **PtL3**. This is an indication of where electron density is mostly located on the ground state. The LUMO orbitals which map the location in which electron density is transferred to, are mainly located on the aromatic rings for all complexes. The electronic chemical potential (μ), a calculated parameter describing the tendency of electrons to resist an equilibrium system was found to be greater for **PtL2** and **PtL4** following the trend **PtL2** > **PtL4** > **PtL3** > **PtL1**.^{35,36} This indicates that **PtL2** is the least stable thus should be the more reactive. Also represented on **Table 4.3** are the electrostatic potential mappings and the planarity structures of the complexes.

Table 4.2: A summary of the DFT calculated parameters for the investigated platinum(II) complexes.

Properties	PtL1	PtL2	PtL3	PtL4
				
Point groups	C_{2v}	C_{2v}	C_s	C_s
Bond Lengths				
Pt- C_{trans}/N_{trans}	1.963	1.932	2.024	1.933
Pt-Cl	2.392	2.504	2.419	2.542
Bond Angles				
Cl-Pt- N_{cis}	98.8	99.3	100.2	100.5
N_{cis} -Pt-N/ C_{trans}	81.2	80.7	80.3	79.9
Cl-Pt-N/ C_{trans}	180.0	180.0	162.5	160.0
N_{cis} -Pt- N_{cis}	162.3	161.5	159.6	158.9
Dihedral [‡]	-	-	27.4	30.1
Energy Gap				
HOMO (eV)	-9.54	-5.58	-9.16	-5.61
LUMO (eV)	-6.38	-2.17	-6.25	-2.42
$\Delta E_{LUMO-HOMO}$ (eV)	3.16	3.41	2.91	3.19
Electronic chemical Potential, μ (eV)	-7.962	-3.875	-7.705	-4.015
NBO charges				
Pt ²⁺	0.551	0.426	0.547	0.431
Cl ⁻	-0.396	-0.559	-0.392	-0.547
N/ C_{trans}	-0.462	-0.101	-0.460	-0.090
N_{cis}	0.492	-0.492	-0.483	-0.488
Dipole moment (Debye)	9.651	6.6476	8.1686	5.699

[‡] refers to the dihedral angle $C_{qui}-N_{cis}-Pt-Cl$

Table 4.3: DFT calculated (B3LYP/LANL2DZ) diagrams showing the HOMOs, LUMOs, electrostatic potential mappings and the planarity of the tridentate Pt(II) complexes.

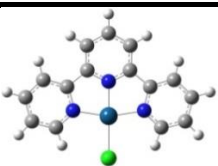
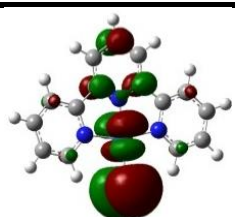
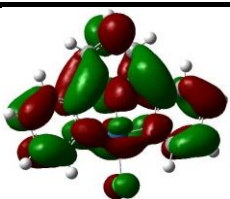

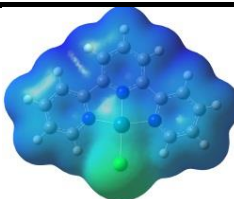
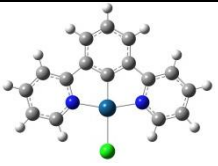
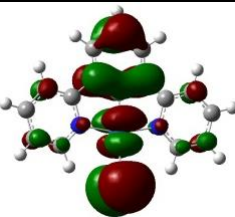
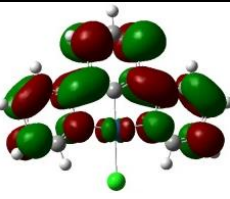

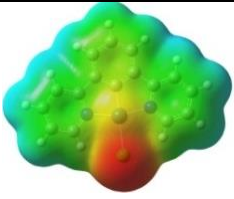
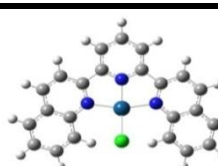
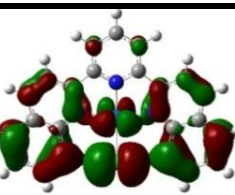
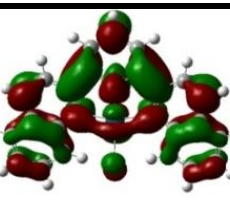

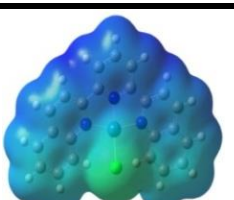
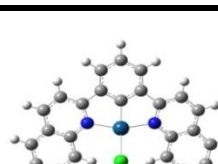
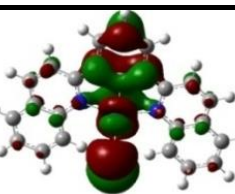
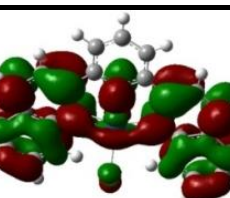

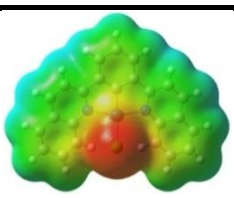
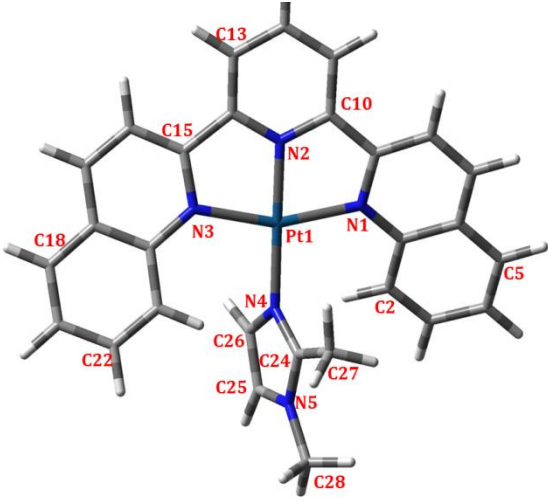
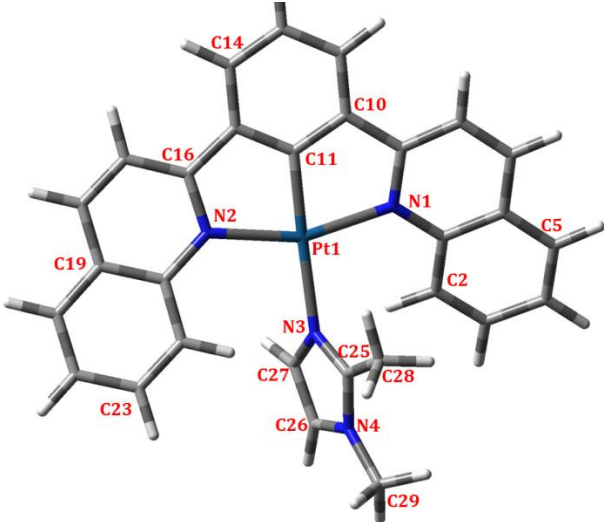
Complex Structures	HOMO	LUMO	Planarity	ESP Map
 PtL1				
 PtL2				
 PtL3				
 PtL4				

Table 4.4: DFT-calculated geometry-optimised structures of **PtL3** and **PtL4** coordinated **DIm** to compare levels of steric conflicts due to ion interactions.

PtL3-DIm		PtL4-DIm	
			
Distance (Å)			
C2-N4 = 3.096		C2-N3 = 3.080	
C2-C27 = 3.821		C2-C28 = 3.816	
H from C2 - H _{ax} from C27 = 3.918		H from C2-H _{ax} from C28 = 3.879	
Angles (°C)			
C24-N4-Pt1	127.7	C25-N3-Pt1	126.8
C27-C24-N4	127.1	C28-C25-N3	126.4
C2-C1-N1-Pt1	18.4	C2-C1-N1-Pt1	17.8

4.3.2. Kinetic and Mechanistic Studies

The substitution of the coordinated chloride from four monofunctional Pt(II) complexes was studied under *pseudo* first-order conditions using UV/Vis spectrophotometry and stopped-flow techniques. Neutral N-donor azoles of different basicities and steric constrains, *viz.*, **Im**, **MIm**, **DIm**, **Trz** and **Pyz** were used in the substitution reactions. Spectral changes resulting from mixing the complex and nucleophile solutions were recorded for the wavelength range 200 – 800 nm. **Figure 4.2** shows changes in the UV/Vis absorption spectra for the reaction of **PtL3** and **MIm** and the inset shows the corresponding kinetic trace at 370 nm. The presence of a distinct isobestic points in the spectra is evident that chloride is substituted by the nucleophile to form the desired product.³⁷ A representative kinetic trace for fast reactions is shown in **Figure 4.3** for the reaction between **PtL2** and **DIm**.

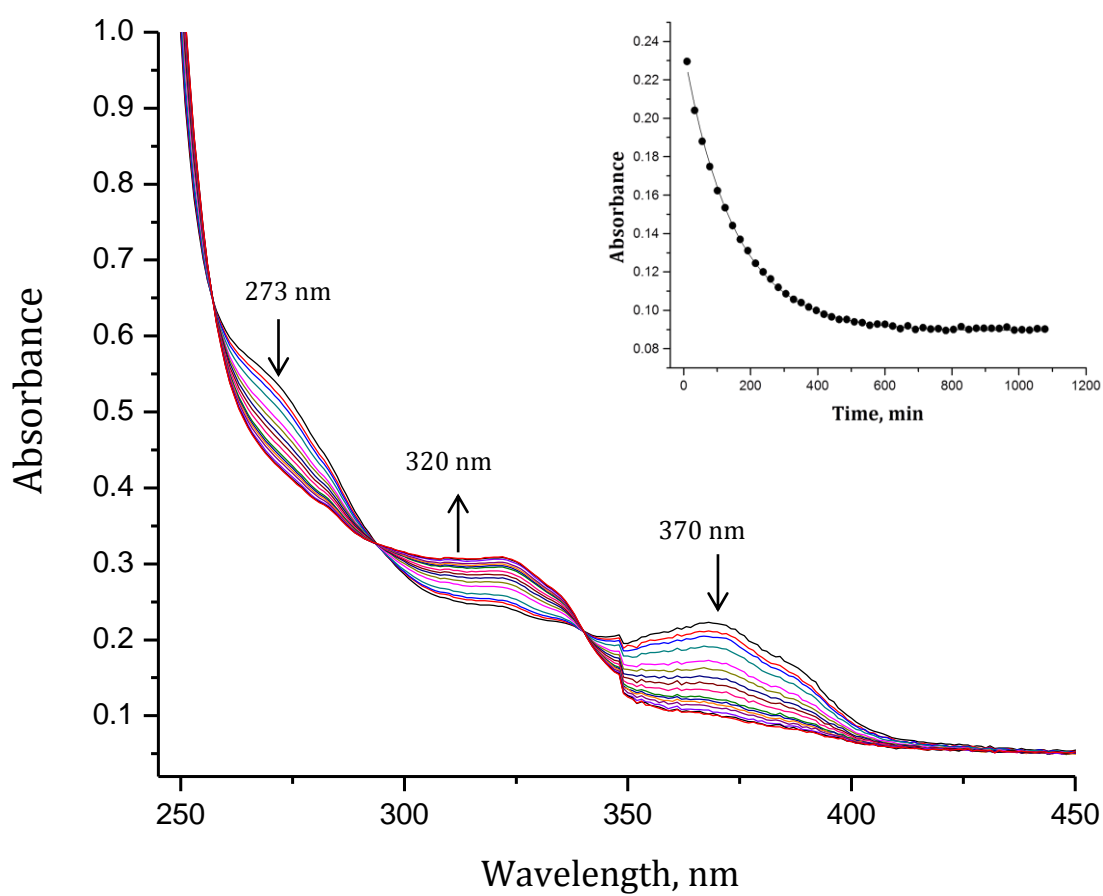


Figure 4.2: UV/Vis spectra for the reaction of **PtL3** (5.18×10^{-5} M) and **MIm** (1.04×10^{-3} M) at an ionic strength of 0.1 M (LiCF_3SO_3 and 0.01 M LiCl), at 298 K. *Inset:* kinetic trace at 370 nm.

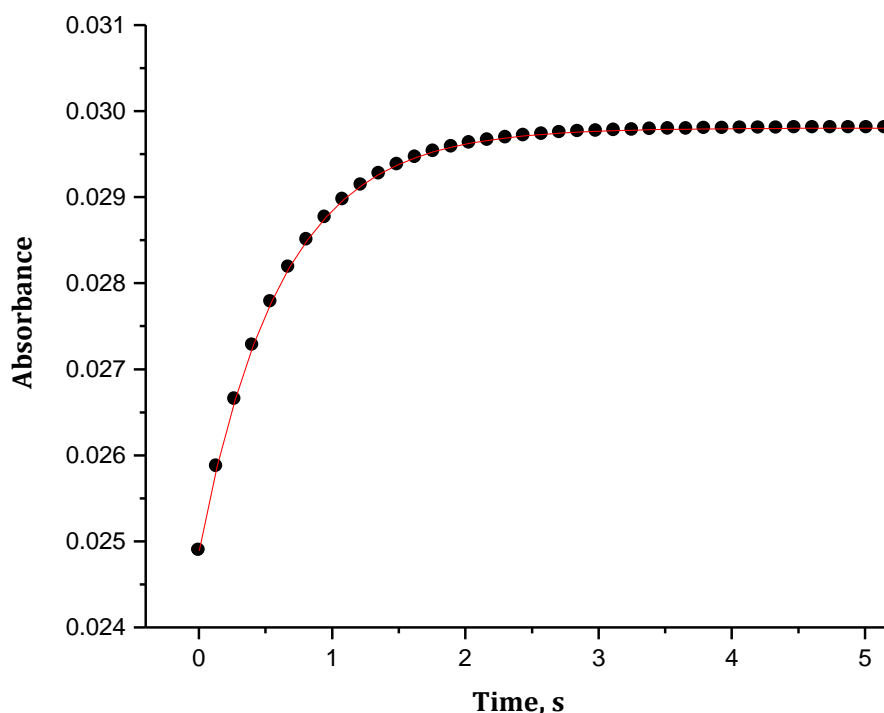


Figure 4.3: Typical stopped flow trace for the reaction between **PtL2** (3.70×10^{-5} M) and **DIIm** (5.55×10^{-3} M) in methanol followed at 318 nm, $I = 0.1$ M (LiCF_3SO_3 , LiCl) at $T = 298$ K.

The kinetic traces were fitted to a single exponential functional to obtain *pseudo* first-order rate constants, k_{obs} , (see inset in **Figure 4.2**). For stopped-flow reactions, an average k_{obs} value was calculated from a set of five to ten runs. The observed first-order rate constants were plotted against the nucleophile concentration according to the rate law represented by *Equation 4.1*.³⁹

$$k_{\text{obs}} = k_2[\text{Nu}] \quad (4.1)$$

where, k_2 represent the second-order rate constant for the direct substitution. The slopes of the plots of k_{obs} versus nucleophile concentration are numerically equal to the second-order rate constants, k_2 . These are shown in **Table 4.5** including literature values for **PtL1** used for comparison.⁶ **Figure 4.4** shows a representative plot of the concentration dependence of the rate of the substitution of **PtL4** with all five nucleophiles. The concentration dependence plots for **PtL2** and **PtL3** are shown on **Figures S4.24 - S4.26** of the supporting information.

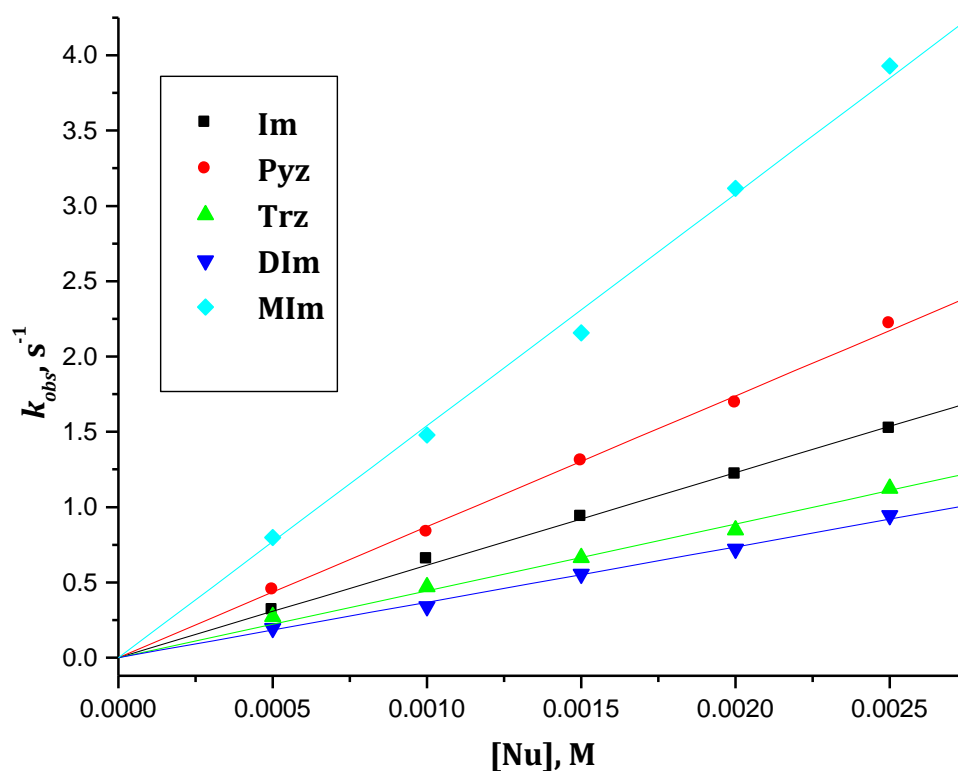
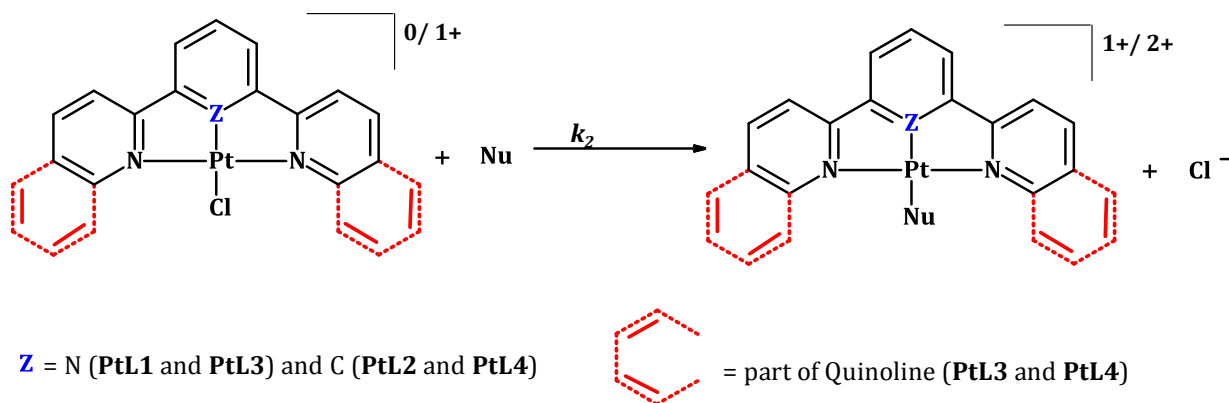


Figure 4.4: Concentration dependence of k_{obs} for the displacement of the chloro ligand in **PtL4** by the azole nucleophiles at $I = 0.1 \text{ M}$, $T = 298 \text{ K}$.

All the plots gave straight-line fits passing through the origin. This means that the substitution reactions proceed irreversibly *via* a direct attack by the nucleophile without any solvent intervention. **Scheme 4.2** illustrates the mechanistic pathway for the chloride substitution, *i.e.* the direct nucleophilic attack characterised by the rate constant, k_2 .³⁸



Scheme 4.2: Reaction scheme for the substitution mechanism all the investigated Pt(II) complexes.

The rates of reactions were measured at different temperatures ranging from 15 °C to 40 °C, at 5 °C intervals. The enthalpy of activation (ΔH^\ddagger) and entropy of activation (ΔS^\ddagger) were calculated according to the Eyring equation³⁹ represented by Equation 4.2 where R and T are the gas constant and temperature respectively.

$$\ln\left(\frac{k_2}{T}\right) = -\frac{\Delta H^\ddagger}{R}\left(\frac{1}{T}\right) + \left(23.8 + \frac{\Delta S^\ddagger}{R}\right) \quad (4.2)$$

The rates constant and activation data for nucleophilic substitution reactions are represented in Table 4.5 including the literature values for PtL1 as a comparison. An example of the Eyring plots for PtL4 with all nucleophiles is shown in Figure 4.5 and the Eyring plots for PtL2 and PtL3 with all nucleophiles are represented by Figures S4.29 and S4.30. Temperature dependence data used to obtain Eyring plots for all complexes is shown in Tables S4.8 to S4.12 of the supporting information.

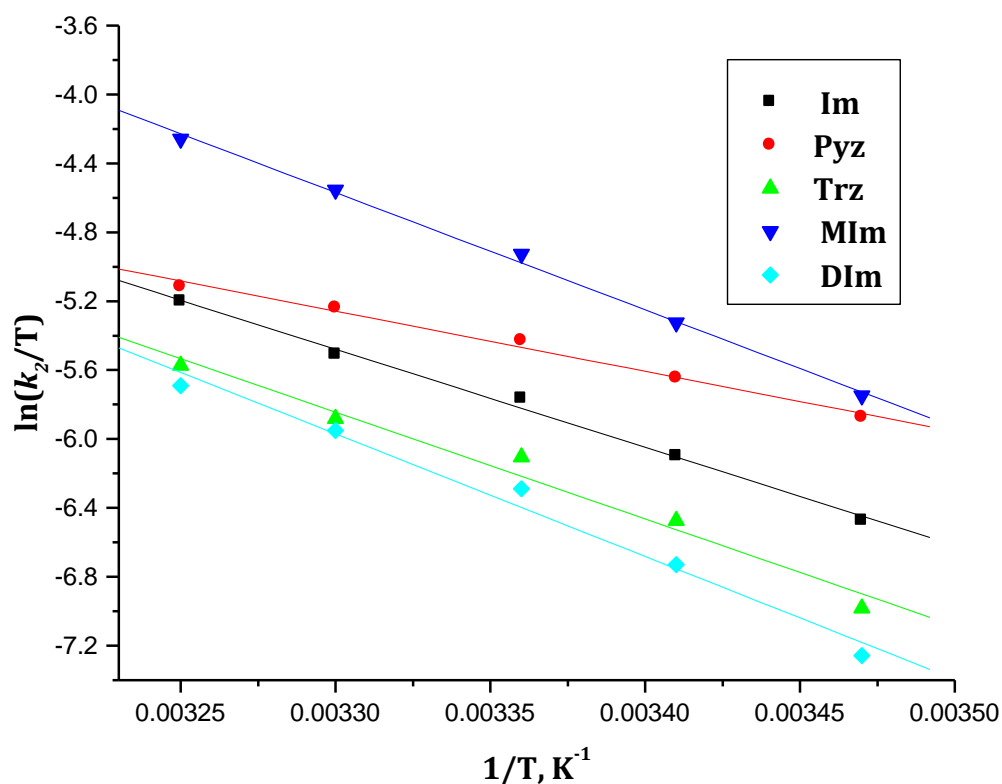
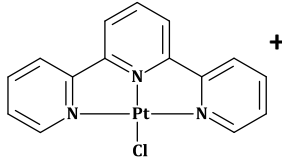
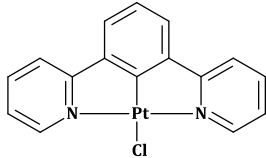
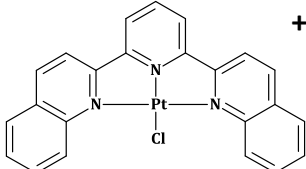
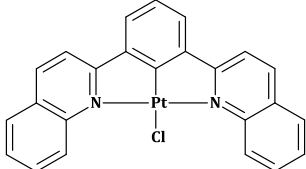
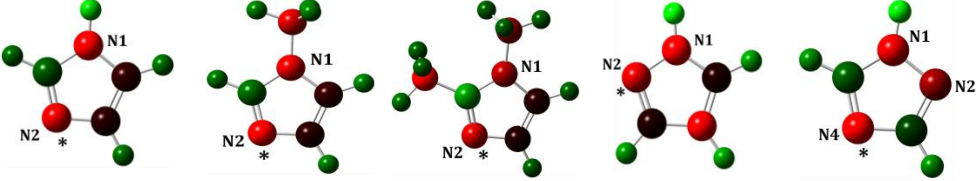


Figure 4.5: Plot of $\ln(k_2/T)$ versus $1/T$ for PtL4 with the azole nucleophiles in the temperature range 15 – 35 °C, $I = 0.1$ M.

Table 4.5: Second-order rate constants at 25 °C and the activation parameters for the chloride substitution from tridentate Pt(II) complexes by **Im**, **MIm**, **DIm**, **Trz** and **Pyz**azole nucleophiles in methanol [$I = 0.1 \text{ M}$ ($0.09 \text{ M LiCF}_3\text{SO}_3 + 0.01 \text{ M LiCl}$)].

Complexes	Nucleophiles	$k_2 \text{ (M}^{-1} \text{s}^{-1}\text{)}$	$\Delta H^\ddagger \text{ (kJ mol}^{-1}\text{)}$	$\Delta S^\ddagger \text{ (JK}^{-1} \text{mol}^{-1}\text{)}$
 <p>PtL1**</p>	Im	3.70 ± 0.04	50.9 ± 1	-67 ± 3
	MIm	3.79 ± 0.07	45.6 ± 1	-84 ± 4
	DIm	1.49 ± 0.03	56.4 ± 8	-53 ± 28
	Trz	0.85 ± 0.02	39.7 ± 3	-114 ± 10
	Pyz	1.26 ± 0.02	44.0 ± 1	-96 ± 4
 <p>PtL2</p>	Im	637 ± 8	58.2 ± 2	-39.6 ± 5
	MIm	1068 ± 75	30.6 ± 1	-139.4 ± 5
	DIm	269 ± 3	62.8 ± 2	-30.4 ± 7
	Trz	580 ± 28	36.6 ± 1	-125 ± 3
	Pyz	621 ± 23	43.4 ± 3	-104 ± 11
 <p>PtL3</p>	Im	0.046 ± 0.001	47.4 ± 3	-91 ± 5
	MIm	0.112 ± 0.002	55.4 ± 4	-58.0 ± 5
	DIm	0.116 ± 0.008	24.4 ± 4	-181 ± 14
	Trz	0.0040 ± 0.0001	57.5 ± 3	-137 ± 8
	Pyz	0.016 ± 0.0004	47.0 ± 2	-148 ± 16
 <p>PtL4</p>	Im	614 ± 6	46.2 ± 1	-91 ± 5
	MIm	967 ± 14	55.0 ± 2	-58.0 ± 5
	DIm	239 ± 3	43.0 ± 3	-109.8 ± 11
	Trz	444 ± 10	51.6 ± 4	-76.1 ± 15
	Pyz	549 ± 12	45.3 ± 4	-95.7 ± 14

** Values extracted from literature reference 6

Table 4.6: DFT-calculated NBO charges of investigated azole nucleophiles.


NBO charges	Im	MIm	DIm	Pyz	Trz
N1	-0.552	-0.415	-0.416	-0.351	-0.431
N2	-0.480	-0.494	-0.496	-0.294	-0.272
N3	-	-	-	-	-0.490
C1	0.181	0.190	0.357	-0.044	0.106
C2	-0.086	-0.078	-0.078	-0.344	0.167
C3	-0.104	-0.097	-0.095	-0.043	-
pK_a^{45}	7.00	7.33	8.00	2.52	2.19

4.4. Discussion

The current study involves the variation of two distinctive properties of Pt(II) complexes with tridentate terpyridine analogues. Firstly, the *trans*-group is varied from a strong π -accepting pyridine ring to a strong σ -donating phenyl ring. The second variation involves the replacement of electron deficient *cis*-pyridyl moieties with extended π -conjugated 2-quinoyl moieties on *cis*-positions of the Pt(II) centre. The observed reactivity trend for the chloride substitution follows the order **PtL2** > **PtL4** > **PtL1** > **PtL3** with most azole nucleophiles investigated as indicated in **Table 4.5**.

The complexes, **PtL1** and **PtL2** have *cis*-pyridine groups in common and only differ in their *trans*-groups. The same applies for **PtL3** and **PtL4**, having a common *cis*-quinoline moiety but vary in terms of pendant-groups. Thus, in order to interpret the observed reactivity trends their structural as well as electronic properties were compared.

For instance, the complexes bearing common *cis*-pyridyl moieties and different *trans*-groups show different reactivities with the azoles. **PtL2** with a *trans*-phenyl ring has second order rate constant

values, k_2 , that are two orders of magnitude higher than the rate constant values observed for **PtL1**.⁶ Furthermore **PtL4**, also with a *trans*-phenyl ring, has rate constant values that are about four orders of magnitude higher than the rate constants obtained for **PtL3** with most nucleophiles. The observed reactivity difference is expected for **PtL1** and **PtL2** and is in agreement with a similar study using thiourea nucleophiles.¹⁹ This is due to the strong σ -donor strength of the *trans*-phenyl group which effectively donates electron density towards the Pt(II) centre resulting in a stronger *trans*-labilization effect being experienced by the leaving chloride ligand.^{19,40} This is reflected on the Pt-Cl and Pt-N/C bond lengths represented in **Table 4.2**, which show that **PtL2** has a longer Pt-Cl bond (2.504 Å) and a slightly shorter Pt-C bond length (1.932 Å) compared to that of **PtL1** (Pt-Cl = 2.392 Å) and (Pt-N = 1.963). Likewise, the Pt-Cl bond of **PtL4** (2.542 Å) is longer than that of **PtL3** (2.419 Å) and its Pt-C bond (1.933 Å) is shorter than the Pt-N bond of **PtL3** (2.024 Å). The Pt-Cl bonds of the quinoline bearing complexes (**PtL3** and **PtL4**) are slightly longer than that of **PtL1** and **PtL2** with *cis*-pyridyl moieties due to H- and Cl- repulsion. The stronger σ -donor character of the *trans*-phenyl moieties is also supported by the NBO charges. **Table 4.2** shows decreased NBO charges for **PtL2** (0.426) and **PtL4** (0.431) as compared to the Pt(II) complexes with *trans*-pyridine rings, **PtL1** (0.551) and **PtL3** (0.547). This is due to the stronger σ -donor effect of the *trans*-phenyl ring; therefore causes an accumulation of electron density on the metal centre hence a less electrophilic Pt centre. This phenomenon is consistent with the notion that N-atoms are more electronegative than C-atoms, hence they pull away electron density from the Pt centre causing it to be more electrophilic. This is in agreement with the electrostatic potential mappings of the complexes shown in **Table 4.3**.

Moreover, previous studies have shown pyridine moieties are good π -acceptors.^{5,6,8,13-18} Thus the higher NBO charges for complexes with *trans*-pyridine moieties, *viz.*, **PtL1** and **PtL3**, corroborates with the dipole moment values shown on **Table 4.2**. For complexes with *trans*-pyridine rings, **PtL1** and **PtL3**, the dipole moment values are 9.651 D and 8.1686 D respectively, whereas complexes with *trans*-phenyl rings **PtL2** (6.648 D) and **PtL4** (5.699 D), the dipole moments decrease.⁴¹ Like the NBO charges, the dipole moments of **PtL1** and **PtL3** are accounted for by the ability of the pyridyl moiety to accept electron density from the metal centre through π -back donation leading to a more electrophilic centre but not necessarily higher reactivity compared to **PtL2** and **PtL4**.

It is worth to note that the HOMO-LUMO energy gap, ΔE , reflects a contradicting trend from that of the kinetic data. The Pt(II) complex with the least reactivity, **PtL3**, has the smallest HOMO-LUMO energy gap ($\Delta E = 2.91$ eV) while the most reactive complex, **PtL2**, has the highest energy gap ($\Delta E = 3.41$ eV). This is accounted for by the good π -acceptability of the *trans*-pyridine ring of **PtL3**.^{5,42,43} Also, due to the increase in conjugation through the fused aromatics of the quinoline moieties in

PtL3 the HOMO is elevated and the LUMO is lowered slightly. Thus, a smaller π - π^* energy gap is attained (**Table 4.2**).⁴⁴

The introduction of fused aromatics as *cis*-donor groups to the chelate ligand system of complexes, **PtL3** and **PtL4** provides an extended π -conjugation compared to complexes with *cis*-pyridyl moieties. The *cis*-quinolyl moieties of **PtL3** and **PtL4** infuse both π -acceptability of pyridine with the σ -donor ability of the phenyl ring.⁴⁵⁻⁴⁸ The k_2 values represented on **Table 4.5** shows that **PtL3** is two-three orders of magnitude less reactive than **PtL1**. This indicates that there is a net σ -donor effect that suppresses the π -acceptability of the quinoline bearing Pt(II) complexes thus less π -back donation occurs.⁴⁵⁻⁴⁸ This results in an accumulation of electron density on the metal centre which lowers the electrophilicity of the Pt(II) centre and destabilizes the five-coordinate transition state.^{5,6}

On the other hand when comparing the rate constant values of the complexes, **PtL2** and **PtL4**, represented on **Table 4.5**, an unexpected slight decrease in reactivity is observed. For instance, with imidazole as the nucleophile the rate constant of **PtL2** is $637 \pm 8 \text{ M}^{-1}\text{s}^{-1}$ and that of **PtL4** is $614 \pm 6 \text{ M}^{-1}\text{s}^{-1}$. This indicates that the ability of the *cis*-quinolyl moieties to effectively donate electron density to the Pt(II) centre is hindered by the presence of a stronger *trans*-labilizing phenyl moiety. So even though the reactivity decreases, the degree at which it is decreased is smaller for Pt(II) complexes with a *trans*-phenyl-pendant as compared to the difference in reactivity between **PtL1** and **PtL3**, which is two orders of magnitude.

In general the Pt(II) complexes with *cis*-pyridyl moieties are more reactive than the Pt(II) complexes with *cis*-quinolyl moieties. This is also mainly due to the fact that the complexes with *cis*-pyridyl moieties, **PtL1** and **PtL2**, adopt rigid and planar structures whereas **PtL3** and **PtL4** with *cis*-quinolyl moieties have flexible structures with the Pt-Cl bond deviating from planarity (**Table 4.3**). This uneven planarity affects the aromaticity of the complexes hence hinders the flow of electron. Therefore, as a result the π -acceptability of **PtL3** and **PtL4** is hampered causing a relatively low reactivity for quinoline-based complexes compared to pyridine-based complexes. **Figure 4.1** shows the X-ray crystal structure for the ligand, **L4**, from the diagram it is seen that the donor-atoms of the ligand system (N1, N2 and C7) are far apart from each other, indicating that the ligand has to twist in order for all the donor atoms to coordinate to the metal centre, resulting in a non-planar Pt complex.

Nevertheless, for all complexes the HOMOs are concentrated mainly over the *trans*-donor, metal centre and chloro atom except for **PtL3** where the HOMO is located mainly on the *cis*-quinoline moieties and the Pt(II) centre. This is expected for **PtL2** and **PtL4** since the *trans*-group is an electron donating phenyl group as shown by electron density in the ground state is along the N-Pt-

Cl axis, making the electron rich phenyl ring and the d_z -orbitals of Pt(II) centre the main source of electron density (**Table 4.3**). Conversely for **PtL3**, most electron density is situated on the highly σ -donating quinoline groups, further illustrating good σ -donor abilities of the conjugated quinoline systems. As a consequence, the ground state of the complex is destabilized resulting in a decrease in the reactivity. There is a similarity in the location of the LUMO molecular orbitals for all the Pt(II) complexes, the π^* orbitals are distributed evenly throughout the ligand system. However the LUMO map of **PtL4** shows no contribution from the electron-rich phenyl ring (**Table 4.3**).

The second-order rate constants of square planar platinum(II) complexes undergoing associative substitution reactions is highly dependent on the steric and/or electronic factors of the entering nucleophiles.^{9,49-52} In this case, the reactivity of the nucleophiles involved in this study depends on both their steric and electronic properties. In order to explain the reactivity trend of theazole nucleophiles, we divided them into two groups based on their structural similarities. For instance, the nucleophiles with no substituents (**Im**, **Pyz** and **Trz**) are categorised into one group and their reactivity trend with all complexes, **Im** > **Pyz** > **Trz**, mirrors on their basicity values.^{6,7,17,51} The pK_a values for **Im**, **Pyz** and **Trz** are 7.00, 2.52 and 2.19 respectively (**Table 4.6**), and the higher the pK_a value the more reactive is the nucleophile towards the metal complex (see **Figures S4.7** and **S4.28** of the supporting information). **Im** has a higher pK_a compared to **Pyz** and is thus more basic than **Pyz** because of the base weakening interactions of the adjacent pyrrolic-N.⁴⁵ The nucleophile with the lowest basicity reflected by the smallest pK_a value is **Trz** and has the slowest reactivity among nucleophiles with no substituents. This is due to the increased in aromaticity caused by the increased number of N-donor atoms in a five membered ring. Also, the slow reactivity can be accounted by the strong inductive effect of the α -N-donor atoms, N1 and N2 which readily withdraw electrons from the vicinal nitrogen causing N4 to be more electronegative.^{6,17,45} Previous studies have shown the pyridine-like N4 to be the most preferred site for binding.^{6,17}

Focusing on the other set of nucleophiles, the reactivity trend was **MIm** > **Im** > **DIm** for **PtL1**, **PtL2** and **PtL4** and for **PtL3** the reactivity of **MIm** and **DIm** were relatively the same. The pK_a values of **Im**, **MIm** and **DIm** are 7.00, 7.30 and 7.85, respectively.^{6,45}

MIm has the highest reactivity with all complexes and this is accounted for by the inductive donation of electron density by the methyl substituent on the N1-position of the heterocyclic ring which makes the binding pyridine-like nitrogen, N3 more basic and thus more reactive. Since the methyl-group is situated far from N3, chances of the methyl group on N1 sterically retarding the formation of the five-coordinate transition state are minimal.⁴⁹ However, in the case of **DIm**, the low reactivity of the nucleophile as compared to **Im** and **MIm** for complexes, **PtL1**, **PtL2** and **PtL4** is attributed to steric hindrance due to the *ortho*-methyl group which surpasses the inductive

donation into the ring. Although the methyl group on C1 inductively increases the basicity of **DIm**, steric congestion resulting from the group being situated α -N3 donor destabilizes the transition state and retards reactivity by a magnitude of four times with **PtL2** and **PtL4** compared to the most reactive nucleophile, **MIm** and by two magnitudes for **PtL1**. However, in the case of **PtL3**, steric retardation brought about by the α -methyl results in similar reactivity for **MIm** and **DIm** as indicated by the rate constant values shown on **Table 4.5** (0.112 ± 0.002 and 0.116 ± 0.008). This implies that the steric effect of **DIm** do not affect the reactivity of **PtL3** as much compared to other Pt(II) complexes. This was verified by DFT modelling of **PtL3** coordinated to **DIm**, **PtL3-DIm**, which were compared to that of **PtL4-DIm** and the steric hindrance of H-H, C-C and C-N interactions are shown on **Table 4.4**.

4.5. Conclusion

From this study we can conclude that the liability of the coordinated chloride ligand from the complexes **PtL1**, **PtL2**, **PtL3** and **PtL4**, is influenced to a great extent by the electrophilicity of the platinum(II) centre. The electronic communication at the metal centre is controlled by the strength of the π -back bonding through the extended π -conjugated aromatic ligand framework. The replacement of *cis*-pyridine rings with *cis*-2-quinoline groups led to slower reactivity. This attributed to the overall σ -donating effect of the 2-quinoline groups forming part of the tridentate ligand which causes an accumulation of electron density at the platinum centre thus decreasing the electrophilicity of the metal centre. This effect is more dominant in the *trans*-pyridine systems but is very minimal with *trans*-phenyl ring systems which have a strong σ -*trans* effect. Also, the result of this study confirm that when the central pyridyl ring of a terpy-type ligand system is replaced by a phenyl ring reactivity is enhanced due to the strong *trans* σ -donor effect of the carbon atom which destabilizes the ground state of the complexes. The reactivity of the neutral heterocyclic azole nucleophiles is influenced by steric effects and the basicity of the coordinating N-donor. This reactivity trend is supported by data from DFT computational calculations. Negative values of entropies of activation and positive values of enthalpies of activation for all reactions support an associate nature of the substitution process.

4.6. References

1. A. M. Fichtinger-Schepman, J. L. van der Veer, J. H. den Hartog, P. H. Lohman and J. Reedijk, *Biochemistry*, **1985**, *24*, 707 - 713.
2. B. Lippert, *Cisplatin: Chemistry and Biochemistry of a leading Anticancer Drug*, Wiley-VCH, New York, **1999**, p. 3 - 100, 184 - 190.
3. L. Kelland, *The Resurgence of Platinum-based Cancer Chemotherapy*, **2007**, 573 - 584.
4. Ž. D. Bugarčić, G. Liehr and R. van Eldik, *J. Chem. Soc., Dalton Trans.*, **2002**, 951.
5. P. Ongoma and D. Jaganyi, *Dalton Trans.*, **2012**, *41*, 10724.
6. A. Shaira, D. Reddy and D. Jaganyi, *Dalton Trans.*, **2013**, *42*, 8426 - 8436.
7. Ž. D. Bugarčić, B. Petrović, E. Zangrando, *Inorg. Chim. Acta*, **2004**, *357*, 2650 - 2656.
8. B. Pitteri, G. Marangoni, L. Cattalini and T. Bobbo, *J. Chem. Soc., Dalton Trans.*, **1995**, 3853.
9. B. Pitteri, G. Marangoni, L. Cattalini, F. Visentin, V. Bertolasi and P. Gilli, *Polyhedron*, **2001**, *20*, 869.
10. R. Romeo, M. R. Plutino, L. M. Scolaro, S. Stoccoro and G. Minghetti, *Inorg. Chem.*, **2000**, *39*, 4749.
11. R. Romeo, A. Grassi, L. M. Scolaro, *Inorg. Chem.* **1992**, *31*, 4383 - 4390.
12. R. Romeo, M. L. Tobe, *Inorg. Chem.* **1974**, *13*, 1991 - 1996.
13. D. Jaganyi, A. Hofmann and R. van Eldik, *Communi.*, **2001**, *40*, 9, 1680 - 1683.
14. D. Jaganyi, K-L. De Boer, J. Gertenbach, J. Perils, *Int. J. Chem. Kinet.*, **2008**, *40*, 808 - 818.
15. D. Reddy and D. Jaganyi, *Dalton Trans.*, **2008**, 6724 - 6731.
16. D. Jaganyi, D. Reddy, J. A. Gertenbach, A. Hofmann and R. van Eldik, *Dalton Trans.*, **2004**, 299 - 304.
17. A. Hofmann, D. Jaganyi, O. Q. Munro, G. Liehr and R. van Eldik, *Inorg. Chem.*, **2003**, *42*, 1688 - 1700.
18. D. Reddy, K. J. Akerman, M. P. Akerman, D. Jaganyi, *Transition Met. Chem.*, **2011**, *36*, 593.
19. A. Hofmann, L. Dahenburg and R. van Eldik, *Inorg. Chem.*, **2003**, *42*, 6528-6538.
20. D.J. Cardenas and A. M. Echavarren, *Organometallics*, **1999**, *18*, 3337-3341.
21. C. M. Harris, H.R.H. Matil, E. Sinn, *Inorg. Chem.*, **1969**, *8*, 101-104.
22. D.M. Klassen, C.W. Hudson, and E.L. Shaddix, *Inorg. Chem.*, **1975**, *14*, 2733-2736.
23. C. Bonnefous, A. Chouai and P. Thummel, *Inorg. Chem.*, **2001**, *40*, 5851 - 5859.
24. G. Annibale, M. Brandolisio and B. Pitteri, *Polyhedron*, **1995**, *14*, 3, 451 - 453.
25. J. X. McDermott, J. F. White and G. M. Whitesides, *J. Am. Chem. Soc.*, **1976**, *98*, 6521.

26. G. S. Hill, M. J. Irwin, C. J. Levy, L. M. Rendina and R. J. Puddephatt, *Inorganic synthesis*, **2007**, p. 149 and 154.
27. K. L. Garner, L. F. Parkes, J. D. Piper and J. A. G. Williams, *Inorg. Chem.*, **2010**, *49*, 476- 487.
28. T. G. Appleton, J. R. Hall, S. F. Ralph and C. S. M. Thompson, *Inorg. Chem.*, **1984**, *23*, 3521.
29. Origin7.5™ SRO, v7.5714 (B5714), Origin Lab Corporation, Northampton, One, Northampton, MA, 01060, USA, **2003**.
30. M. J. Frisch, G. W. Trucks, H. B. Schlegel, G. E. Scuseria, M. A. Robb, J. R. Cheeseman, G. Scalmani, V. Barone, B. Mennucci, G. A. Petersson, H. Nakatsuji, M. Caricato, X. Li, H. P. Hratchian, A. F. Izmaylov, J. Bloino, G. Zheng, J. L. Sonnenberg, M. Hada, M. Ehara, K. Toyota, R. Fukuda, J. Hasegawa, M. Ishida, T. Nakajima, Y. Honda, O. Kitao, H. Nakai, T. Vreven, J. A. Montgomery, Jr., J. E. Peralta, F. Ogliaro, M. Bearpark, J. J. Heyd, E. Brothers, K. N. Kudin, V. N. Staroverov, R. Kobayashi, J. Normand, K. Raghavachari, A. Rendell, J. C. Burant, S. S. Iyengar, J. Tomasi, M. Cossi, N. Rega, J. M. Millam, M. Klene, J. E. Knox, J. B. Cross, V. Bakken, C. Adamo, J. Jaramillo, R. Gomperts, R. E. Stratmann, O. Yazyev, A. J. Austin, R. Cammi, C. Pomelli, J. W. Ochterski, R. L. Martin, K. Morokuma, V. G. Zakrzewski, G. A. Voth, P. Salvador, J. J. Dannenberg, S. Dapprich, A. D. Daniels, O. Farkas, J. B. Foresman, J. V. Ortiz, J. Cioslowski, and D. J. Fox, *Gaussian 09, Revision C.1*, **2010**, Gaussian Inc., Wallingford CT.
31. Bruker APEX2, SAINT and SADABS. Bruker AXS Inc., **2010**, Madison, Wisconsin, USA.
32. G.M. Sheldick, *A short history of SHELX. Acta. Crystallogr. Sec. A*, **2008**, *64*, 112 - 122.
33. O.V. Dolomanov, L.J. Bourhis, R.J. Gildea, J.A.K. Howard, H. Puschmann, *J. Appl Cryst.* **2009**, *42*, 229.
34. H. Eyring, *J. Chem. Phys.*, **1935**, *3*, 107.
35. P. K. Chattaraj and B.J. Maiti, *Am. Chem. Soc.*, **2003**, *125*, 2705.
36. C. A. Mebi, *J. Chem. Sci.*, **2011**, *123*, *5*, 727 - 731.
37. M. Ray, S. Bhattacharya and P. Banerjee, *Polyhedron*, **1999**, *18*, 1569.
38. H. B. Gray and R. J. Olcott, *Inorg. Chem.*, **1962**, *1*, 481.
39. J. D. Atwood, *Inorganic and Organic Reaction Mechanisms* 2nd edition. Wiley- VCH Inc., New York, **1997**, 43 - 46.
40. S. Lanza, F. Nicolò and G. Tresoldi, *Eur. J. Inorg. Chem.* **2002**, 1049 - 1055.
41. D.P. Rillema, A.J. Cruz, C. Moore, K. Siam, A. Jehan, D. Base, T. Nguyen and W. Huang, *Inorg. Chem.*, **2013**, *52*, p. 596 - 607.
42. R. Buchner, J. S. Field, R. J. Haines, G. C. Summerton and D. R. McMillin, *Inorg. Chem.*, **1997**, *36*, 3952.

-
43. D. R. McMillin and J. J. Moore, *Coord. Chem. Rev.*, **2002**, 229, 133.
 44. J. C-H. Chan, W. H. Lam, H-L.Wong, N. Zhu, W-T.Wong and V. W-W.Ya, *J. Am. Chem. Soc.*,**2011**, 133, 12690 - 12705.
 45. A.R. Katritzky, A.F. Pozharski, *Handbook of Heterocyclic Chemistry 2nd edition* Pergamon/Elsevier, **2000**, p. 177 - 178, 379, 377.
 46. J. M. Khurana, *Organic Chemistry: Chemistry of Heterocyclic Compounds*, **2006**, p. 4 - 7.
 47. T. L. Gilchrist, *Heterocyclic Chemistry 3rd edition*, Longman England, **1998**, p. 158 - 172.
 48. J. A. Joule and G. F. Smith, *Heterocyclic Chemistry 2nd edition* **1978**, Van Nostrand Reinhold Co. Ltd., New York, p. 82 - 120.
 49. B. Pitteri and M. Bortoluzzi, *Polyhedron*, **2006**, 25, 2698 - 2704.
 50. B. Pitteri and M. Bortoluzzi, *Eur. J. Inorg. Chem.*, **2007**, 28, 4456.
 51. M. Bellicini, L. Cattalini, G. Marangoni and B. Pitteri, *J. Chem. Soc. Dalton Trans.*, **1994**, 1805.
 52. C. F. Weber, and R. van Eldik, *Eur. J. Inorg. Chem.*, **2005**, 23, 4755.

4.7. Supporting Information 4

Mass, NMR and IR spectra, stopped flow and UV/ Vis kinetic traces for **PtL2**, **PtL3** and **PtL4**, a summary of wavelengths for kinetic measurements, tables summarizing k_{obs} values determine for reactions at various concentrations, representative concentration dependence plots, LFER plots for all complexes, tables summarizing values used to obtain Eyring plots and representative temperature dependence plots.

Elemental Composition Report

Single Mass Analysis

Tolerance = 500.0 PPM / DBE: min = -1.5, max = 50.0

Element prediction: Off

Number of isotope peaks used for i-FIT = 3

Monoisotopic Mass, Even Electron Ions

17 formula(e) evaluated with 1 results within limits (all results (up to 1000) for each mass)

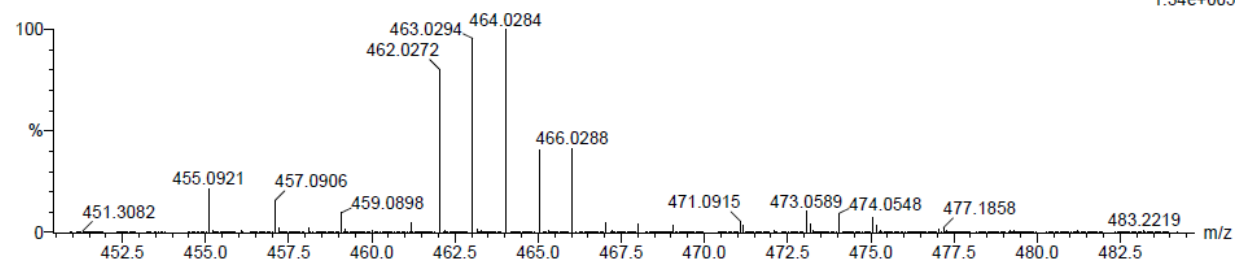
Elements Used:

C: 10-15 H: 10-15 N: 0-5 Cl: 0-1 Pt: 0-1

Sli

Pt terpy Recry 9 (0.136) Cm (1:31)

TOF MS ES+
1.34e+005



Minimum:

Maximum: 5.0 500.0 -1.5

Mass	Calc. Mass	mDa	PPM	DBE	i-FIT	i-FIT (Norm)	Formula
463.0294	463.0289	0.5	1.1	12.5	571.7	0.0	C15 H11 N3 Cl Pt

Figure S4.1: Mass spectrum of **[Pt(2,2':6',2''-terpyridine)Cl](SO₃CF₃)**, **PtL1**.

Elemental Composition Report

Page 1

Single Mass Analysis

Tolerance = 5.0 PPM / DBE: min = -1.5, max = 50.0

Element prediction: Off

Number of isotope peaks used for i-FIT = 3

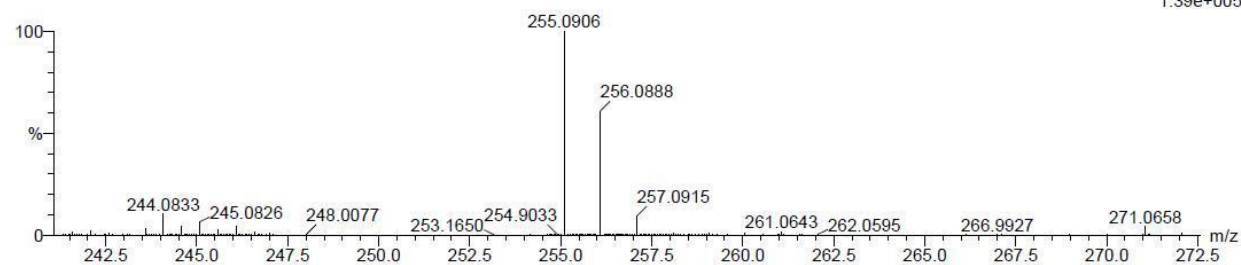
Monoisotopic Mass, Even Electron Ions

7 formula(e) evaluated with 1 results within limits (all results (up to 1000) for each mass)

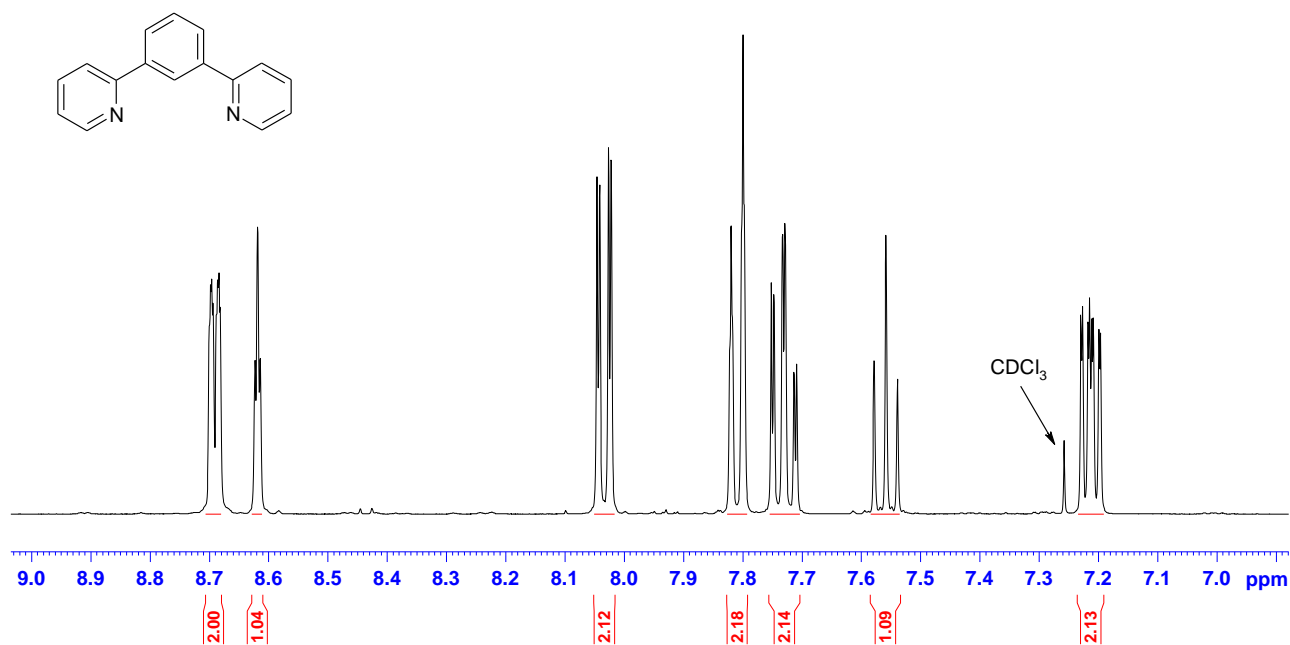
Elements Used:

C: 15-20 H: 10-15 N: 0-5 Na: 0-1

NCN 2.4 (0.052) Cm (1:30)

TOF MS ES+
1.39e+005

Mass	Calc. Mass	mDa	PPM	DBE	i-FIT	i-FIT (Norm)	Formula
255.0906	255.0898	0.8	3.1	11.5	646.7	0.0	C16 H12 N2 Na

Figure S4.2: Mass spectrum of [Pt(1,3-di(2-pyridyl)benzene)Cl]₂.Figure S4.3: ¹H NMR spectrum of [Pt(1,3-di(2-pyridyl)benzene)Cl]₂ in deuterated chloroform.

Elemental Composition Report

Page 1

Single Mass Analysis

Tolerance = 5.0 PPM / DBE: min = -1.5, max = 50.0

Element prediction: Off

Number of isotope peaks used for i-FIT = 3

Monoisotopic Mass, Odd and Even Electron Ions

28 formula(e) evaluated with 1 results within limits (all results (up to 1000) for each mass)

Elements Used:

C: 15-20 H: 10-15 N: 0-5 Cl: 0-1 Pt: 0-2

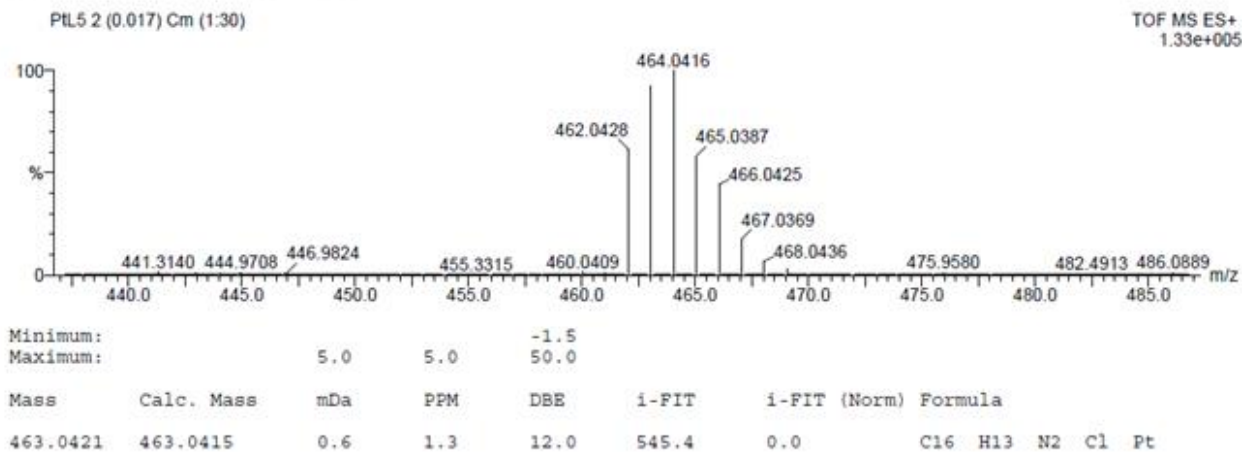
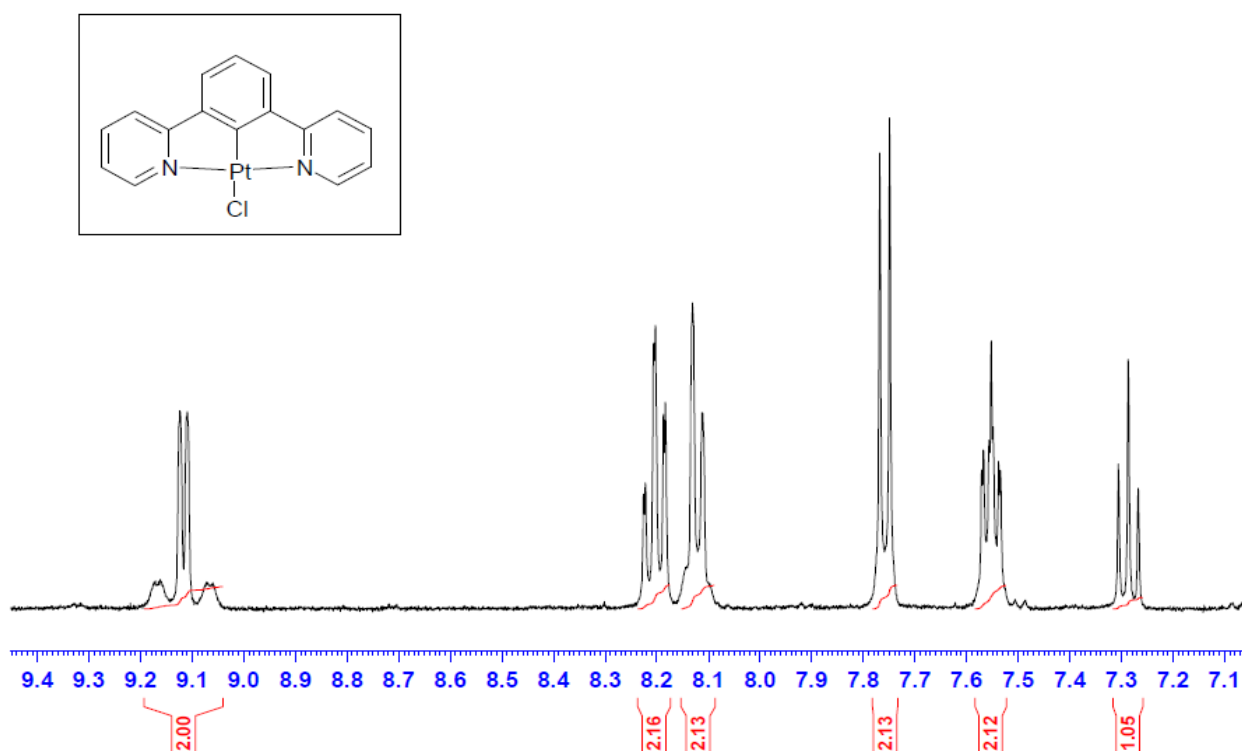


Figure S4.4: Mass spectrum of [Pt(1,3-di(2-pyridyl)benzene)Cl], PtL2.

Figure S4.5: ^1H NMR spectrum of [Pt(1,3-di(2-pyridyl)benzene)Cl], PtL2 in $\text{DMSO-}d_6$.

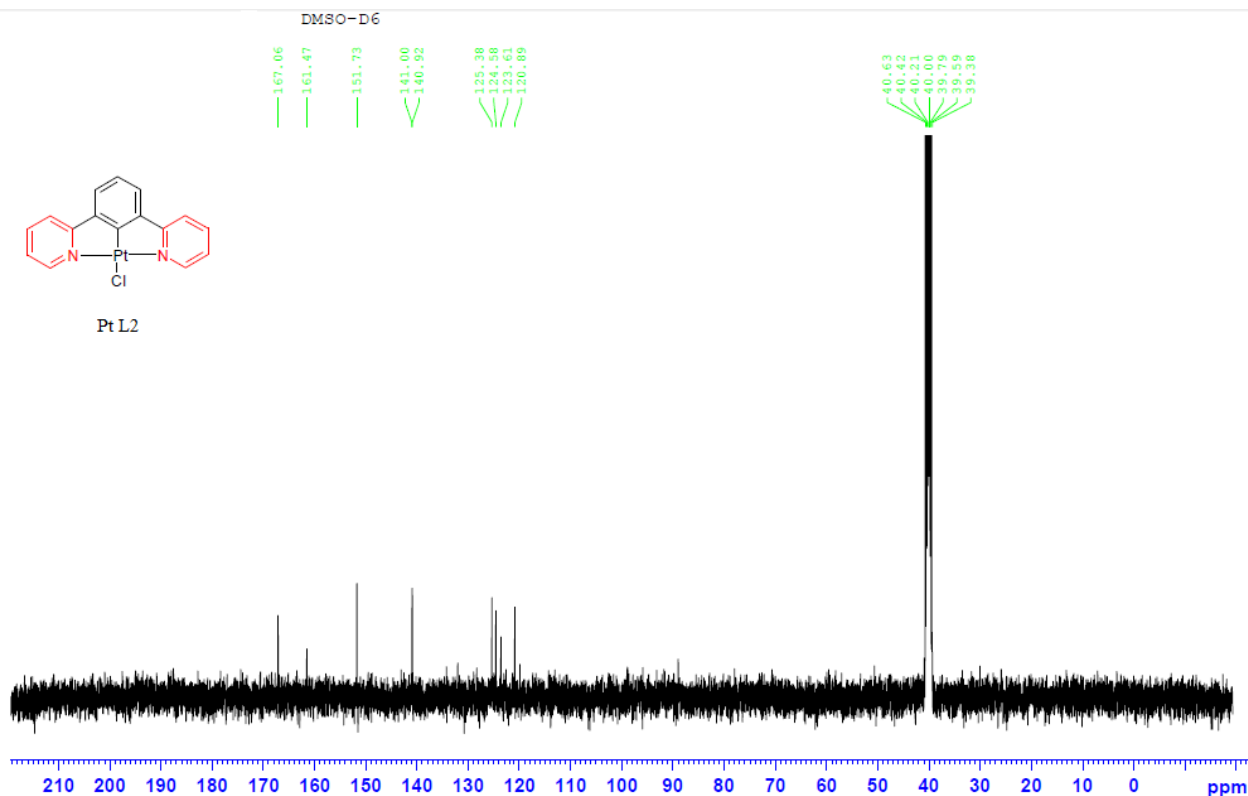


Figure S4.6: ^{13}C NMR spectrum of $[\text{Pt}(1,3\text{-di}(2\text{-pyridyl})\text{benzene})\text{Cl}]$, PtL2 in $\text{DMSO-}d_6$.

Elemental Composition Report

Page 1

Single Mass Analysis

Tolerance = 5.0 PPM / DBE: min = -1.5, max = 50.0

Element prediction: Off

Number of isotope peaks used for i-FIT = 3

Monoisotopic Mass, Even Electron Ions

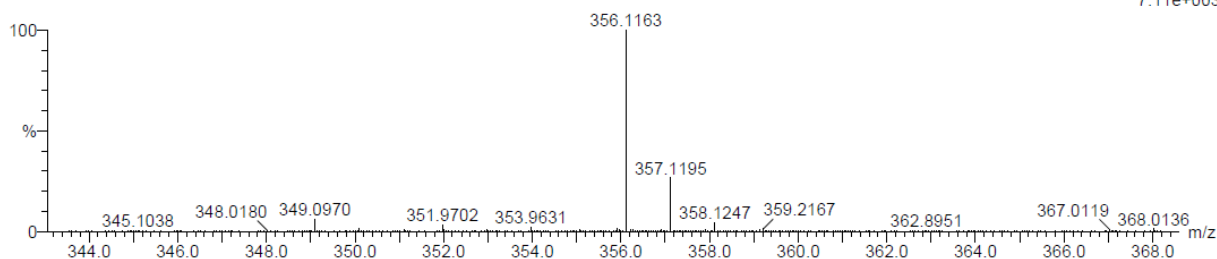
8 formula(e) evaluated with 1 results within limits (all results (up to 1000) for each mass)

Elements Used:

C: 20-25 H: 10-20 N: 0-5 Na: 0-1

DBtpy 2 (0.017) Cm (1:30)

TOF MS ES+
7.11e+003



Minimum:

Maximum: 5.0 5.0 -1.5

Mass Calc. Mass mDa PPM DBE i-FIT i-FIT (Norm) Formula

356.1163 356.1164 -0.1 -0.3 17.5 315.3 0.0 C23 H15 N3 Na

Figure S4.7: Mass spectrum of $2,6\text{-di-(2'-quinoliny)pyridine}$, L3.

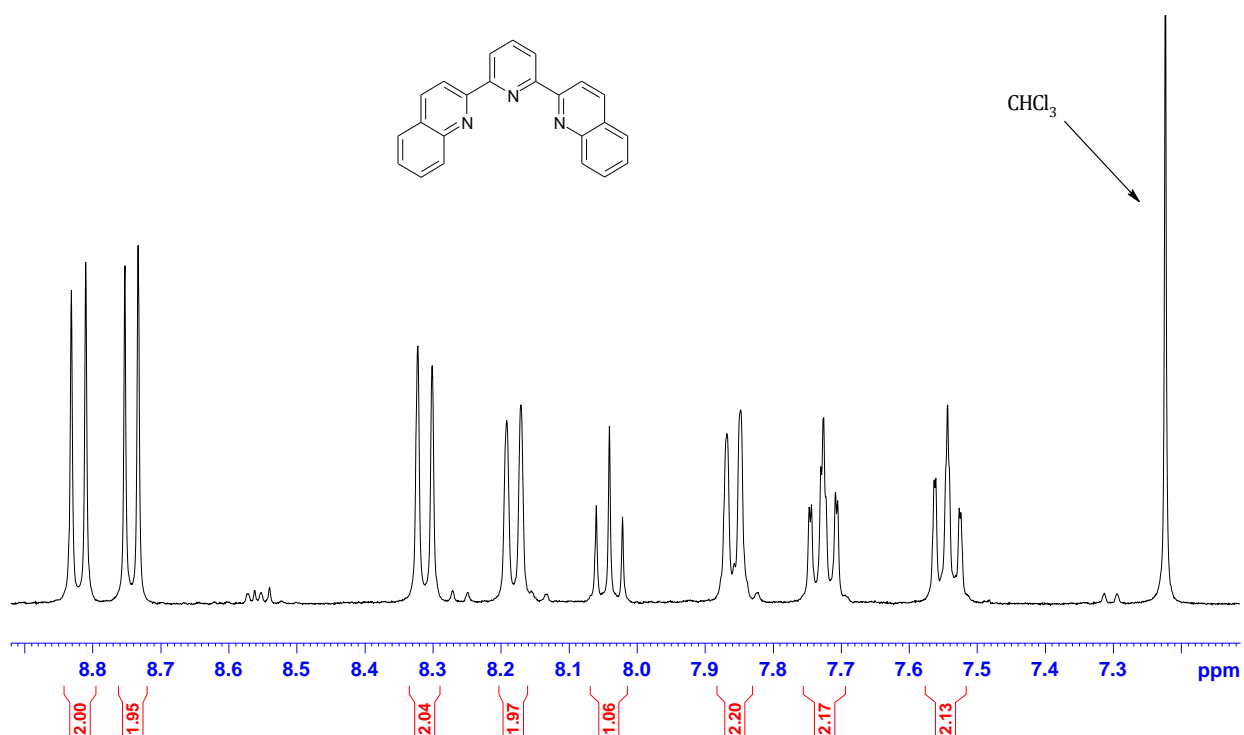


Figure S4.8: ^1H NMR spectrum of 2,6-di-(2'-quinoliny)pyridine, L3 in deuterated chloroform.

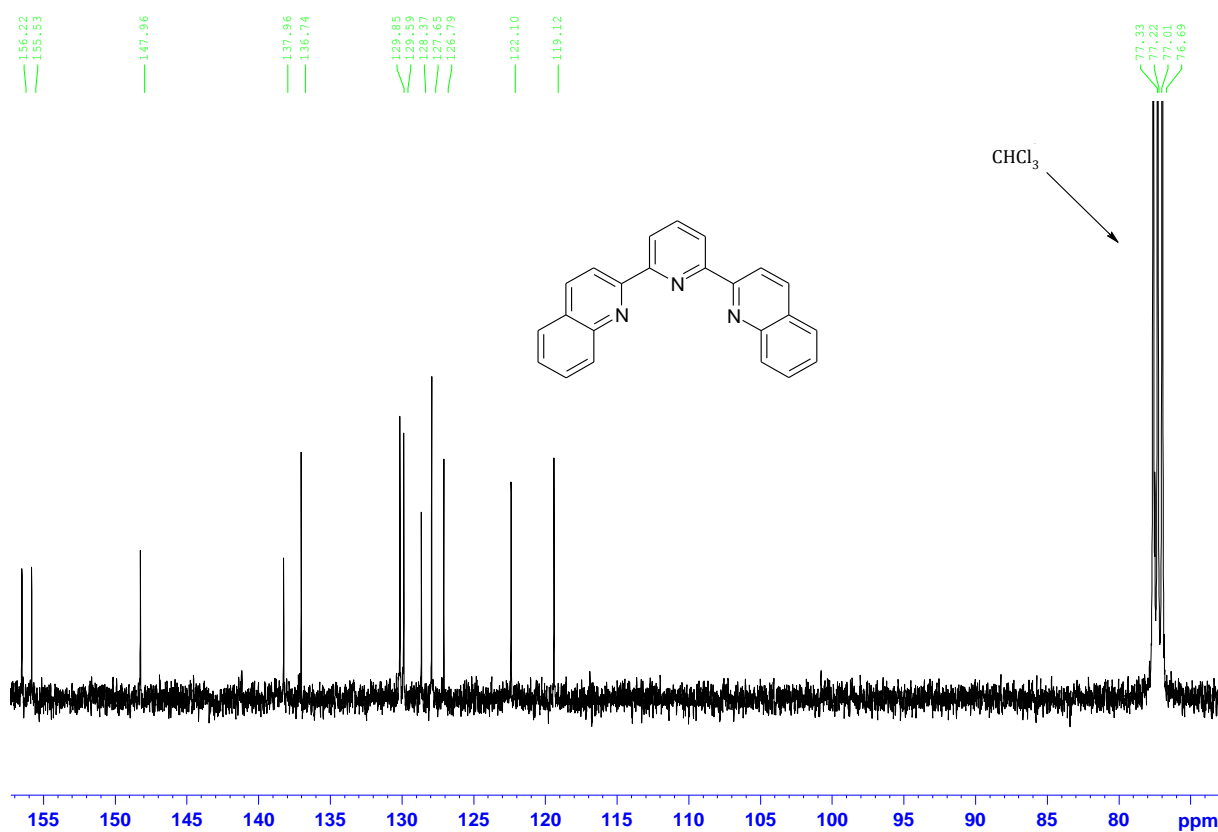


Figure S4.9: ^{13}C NMR spectrum of 2,6-di-(2'-quinoliny)pyridine, L3 in deuterated chloroform.

Elemental Composition Report

Page 1

Single Mass Analysis

Tolerance = 5.0 PPM / DBE: min = -1.5, max = 50.0

Element prediction: Off

Number of isotope peaks used for i-FIT = 3

Monoisotopic Mass, Even Electron Ions

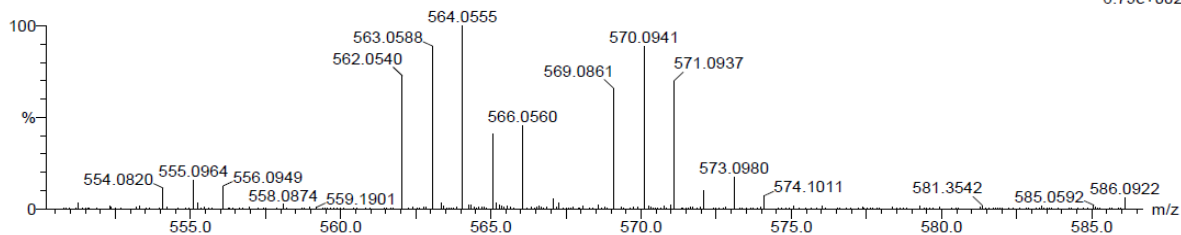
9 formula(e) evaluated with 1 results within limits (all results (up to 1000) for each mass)

Elements Used:

C: 20-25 H: 10-15 N: 0-5 Cl: 1-1 Pt: 0-1

Sli

Pt NNN dbtpy 12 (0.187)

TOF MS ES+
6.79e+002

Minimum:

Maximum: 5.0 5.0 -1.5

Mass	Calc. Mass	mDa	PPM	DBE	i-FIT	i-FIT (Norm)	Formula
563.0588	563.0602	-1.4	-2.5	18.5	131.0	0.0	C23 H15 N3 Cl Pt

Figure S4.10: Mass spectrum of [Pt(2,6-di-(2'-quinolinyl)pyridine)Cl](Cl), PtL3.

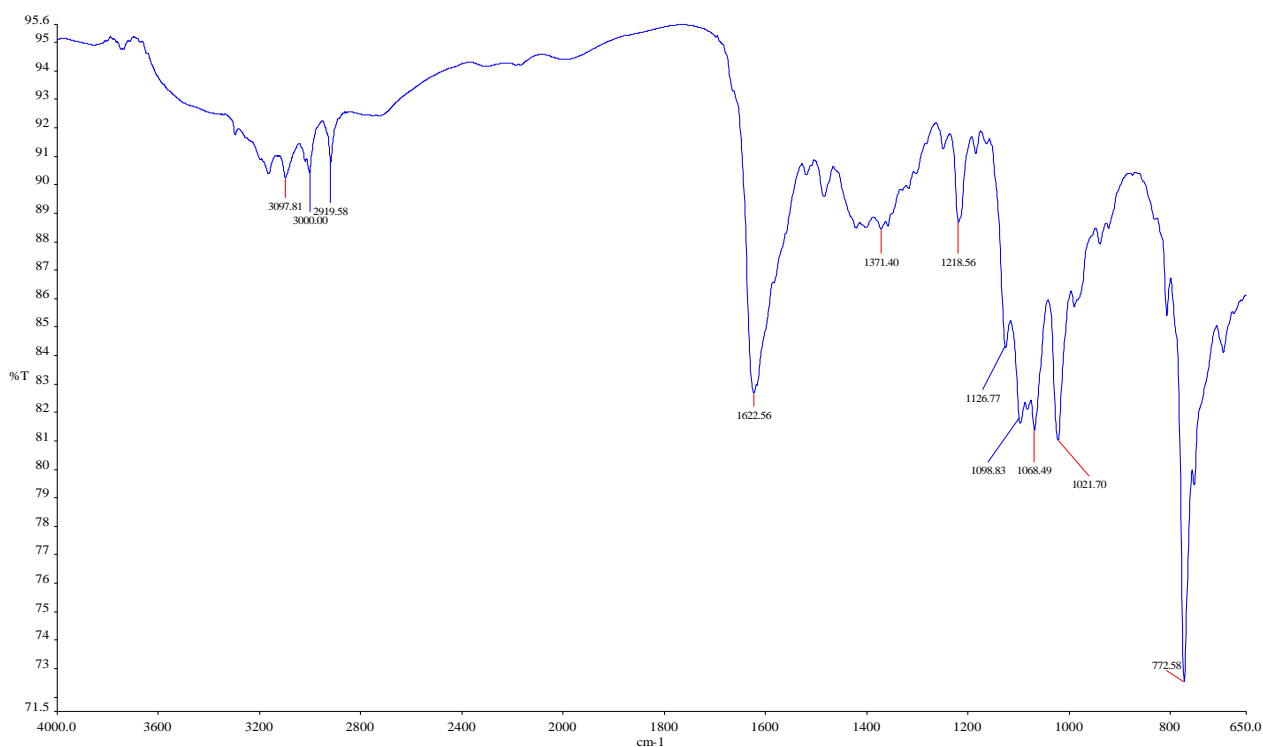


Figure S4.11: Infrared spectrum of [Pt(2,6-di-(2'-quinolinyl)pyridine)Cl](Cl), PtL3.

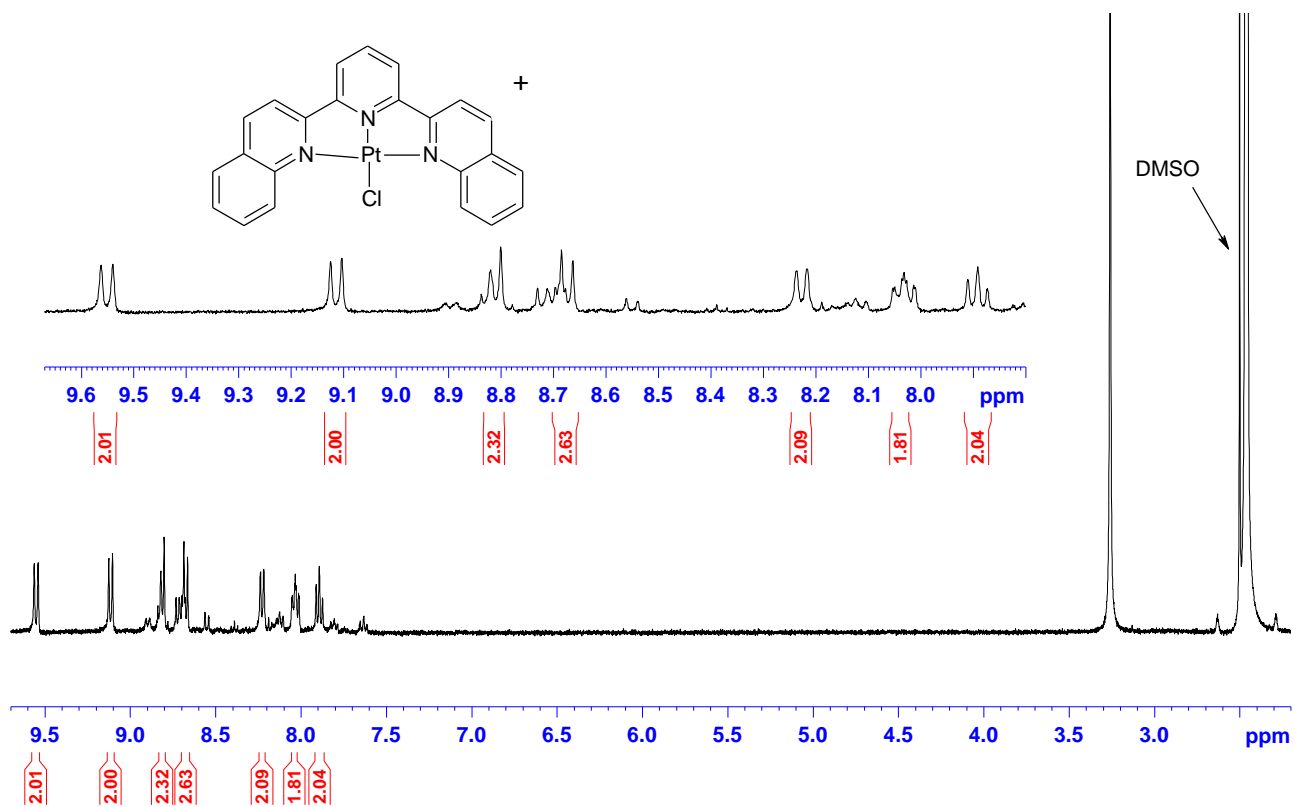


Figure S4.12: ^1H NMR spectrum of $[\text{Pt}(2,6\text{-di-(2'-quinolinyl)pyridine})\text{Cl}](\text{Cl})$, PtL3 in $\text{DMSO-}d_6$.

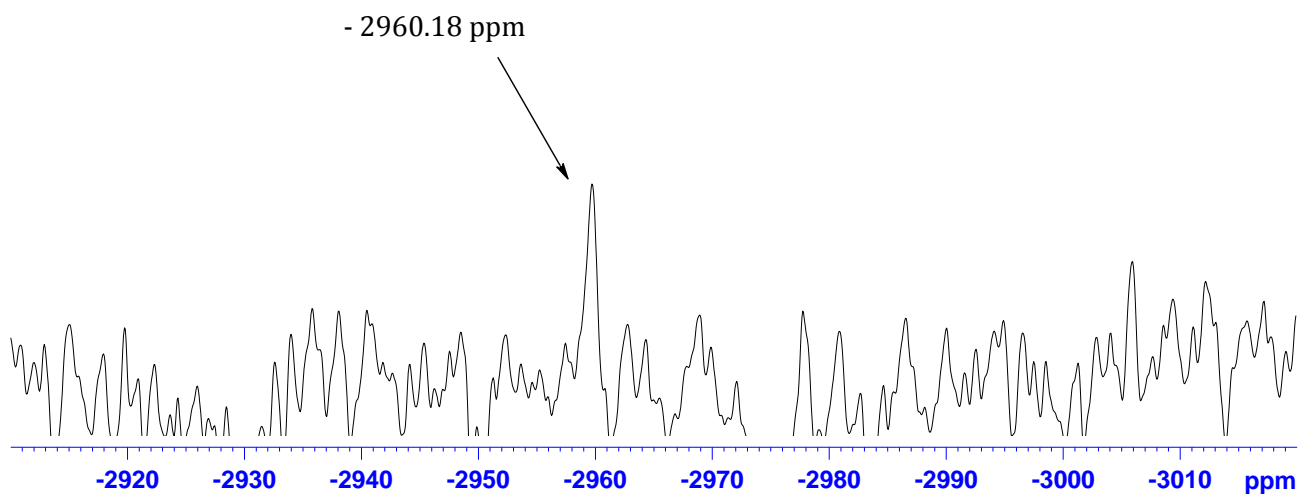


Figure S4.13: ^{195}Pt NMR spectrum of $[\text{Pt}(2,6\text{-di-(2'-quinolinyl)pyridine})\text{Cl}](\text{Cl})$, PtL3 in $\text{DMSO-}d_6$.

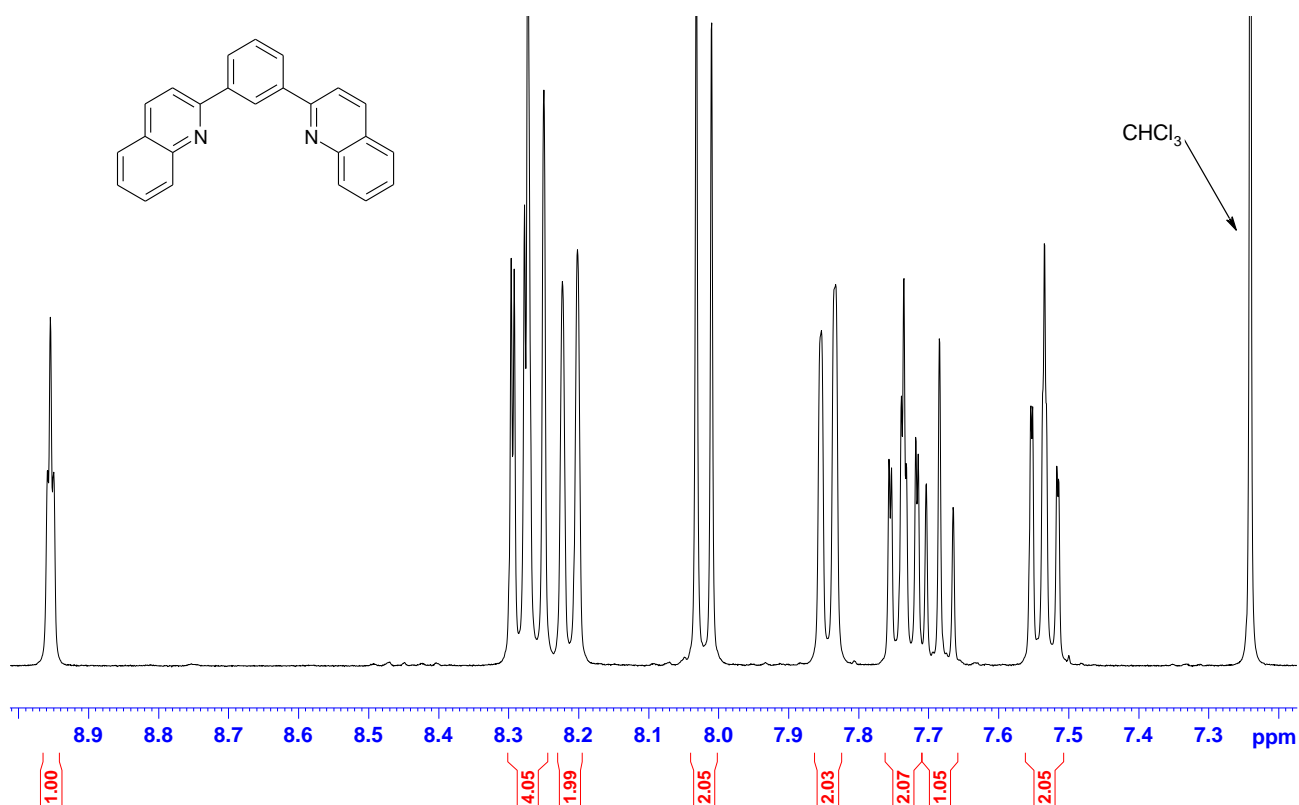


Figure S4.14: ^1H NMR spectrum of 1,3-di-(2'-quinolinyl)benzene, L4 in deuterated chloroform.

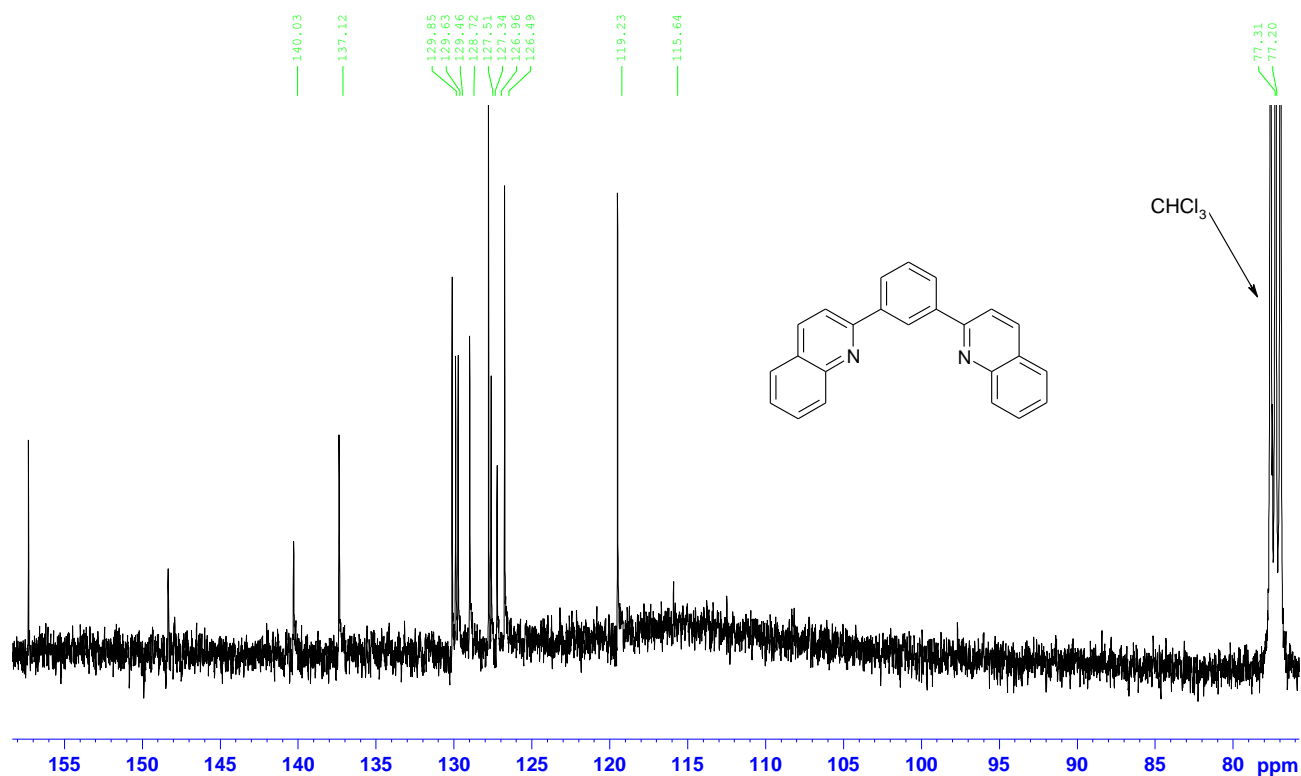


Figure S4.15: ^{13}C NMR spectrum of 1,3-di-(2'-quinolinyl)benzene, L4 in deuterated chloroform.

Elemental Composition Report

Page 1

Single Mass Analysis

Tolerance = 15.0 PPM / DBE: min = -1.5, max = 50.0

Element prediction: Off

Number of isotope peaks used for i-FIT = 3

Monoisotopic Mass, Even Electron Ions

10 formula(e) evaluated with 1 results within limits (all results (up to 1000) for each mass)

Elements Used:

C: 20-25 H: 10-20 N: 0-5 Pt: 0-1

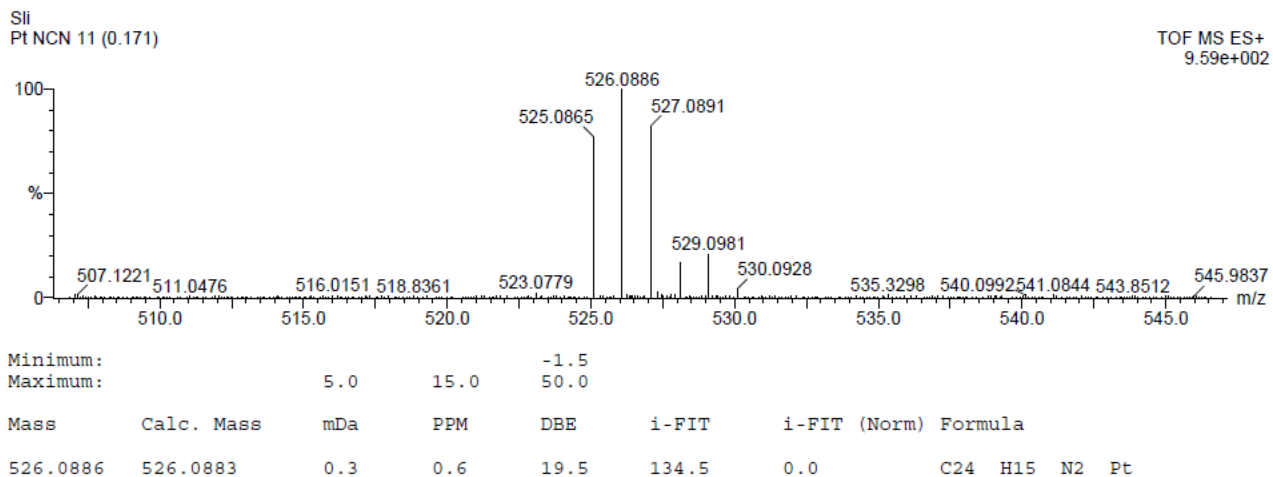


Figure S4.16: Mass spectrum of [Pt(1,3-di-(2'-quinolinyl)benzene)Cl], PtL4.

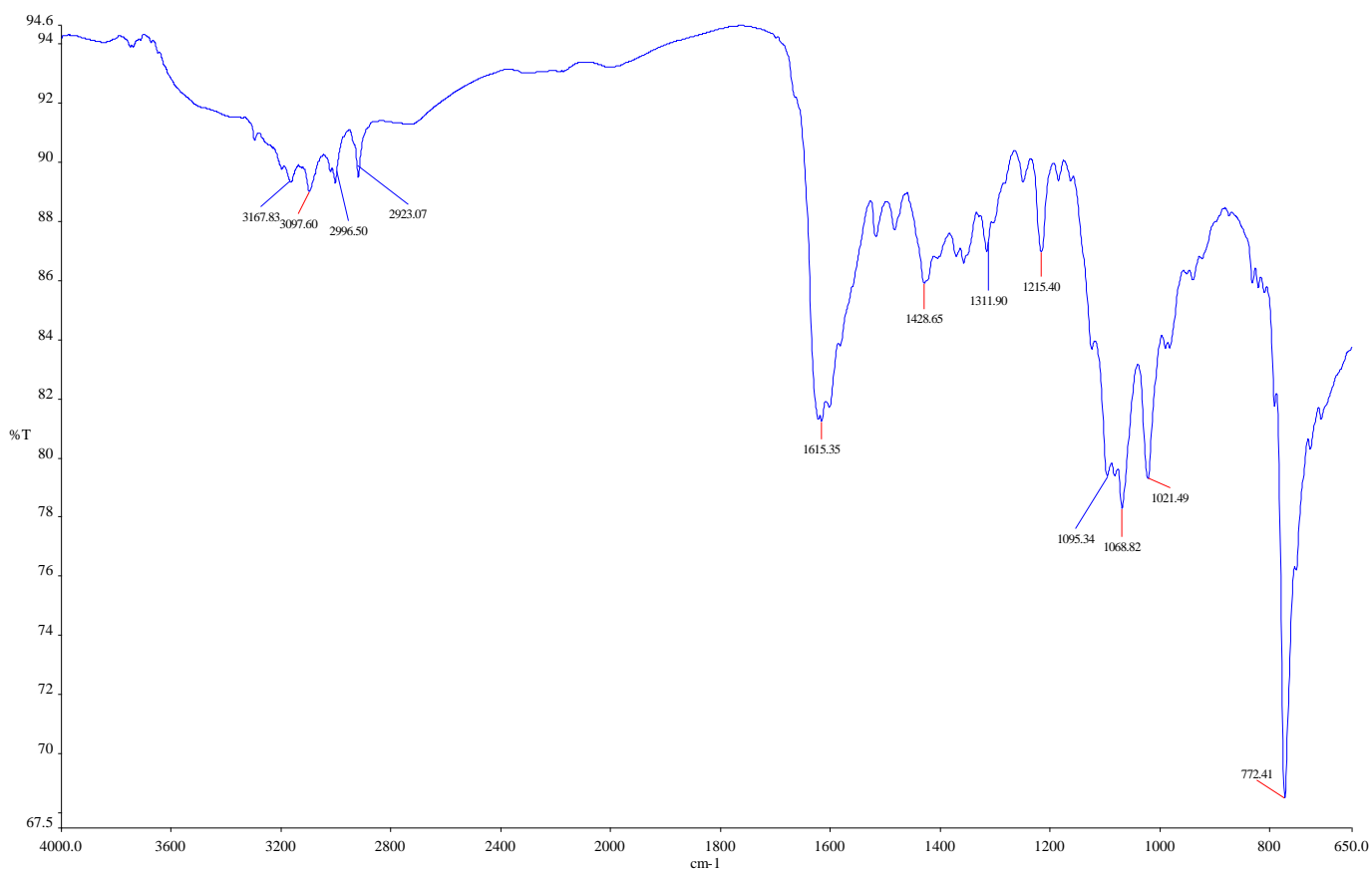


Figure S4.17: Infrared spectrum of [Pt(1,3-di-(2'-quinolinyl)benzene)Cl], PtL4.

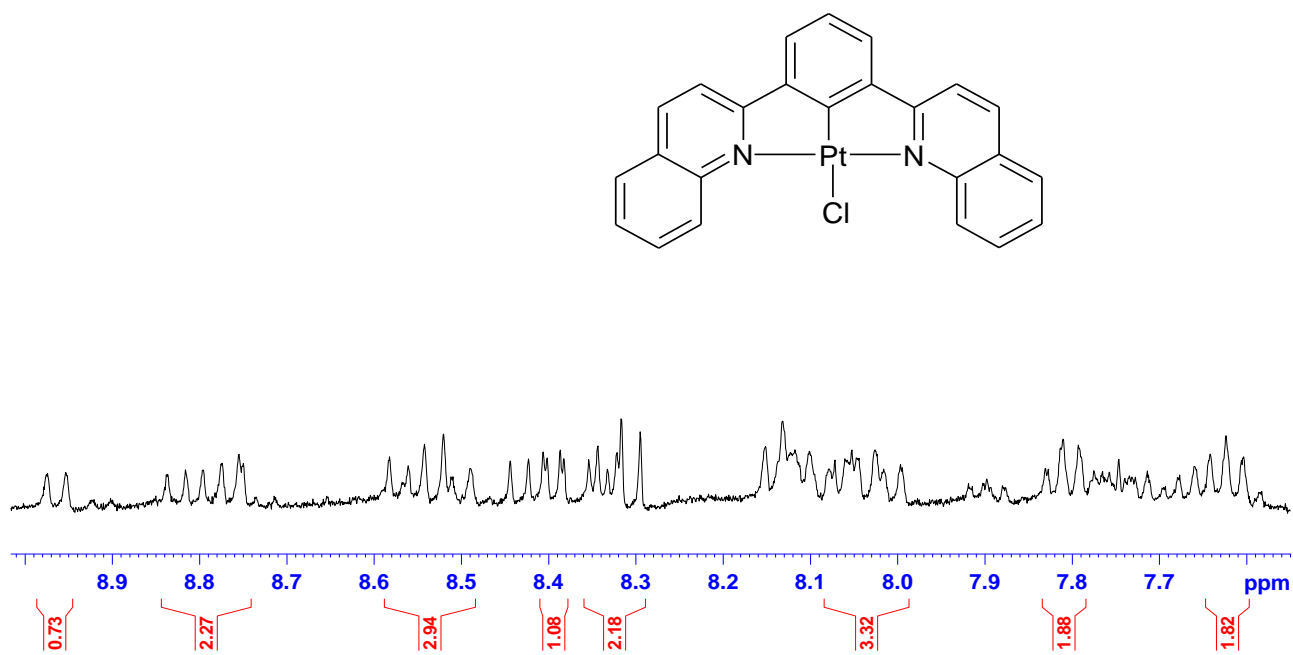


Figure S4.18: ¹H NMR spectrum of [Pt(1,3-di-(2'-quinolinyl)benzene)Cl], PtL4 in DMSO-d₆.

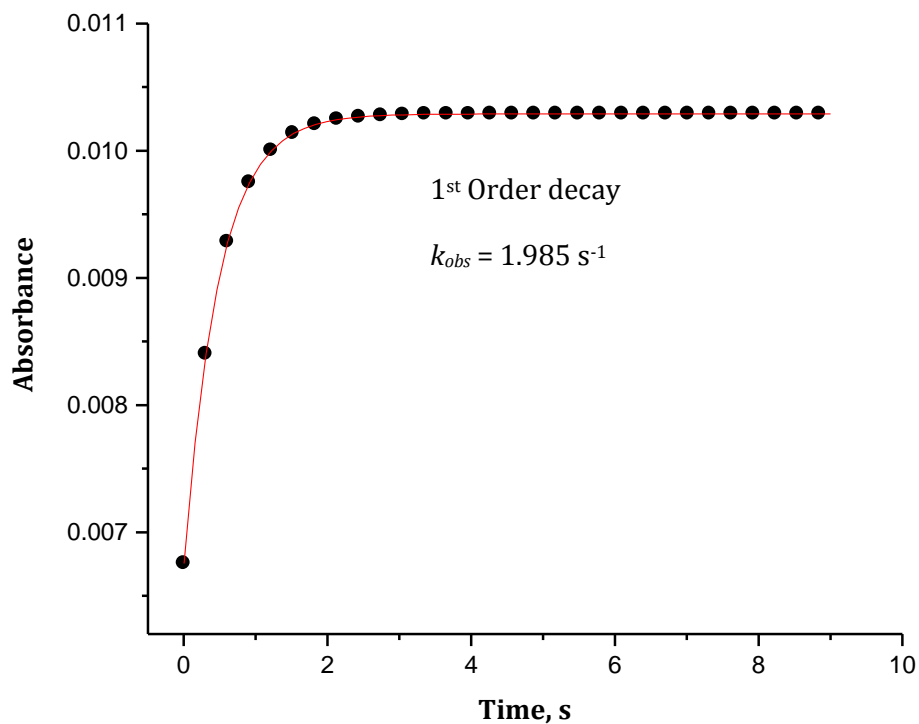


Figure S4.19: Stopped-flow kinetic trace of **PtL2** ($3.69 \times 10^{-5} \text{ M}$) with methylimidazole ($3.69 \times 10^{-3} \text{ M}$ (100 fold) taken at 273 nm and at 298 K.

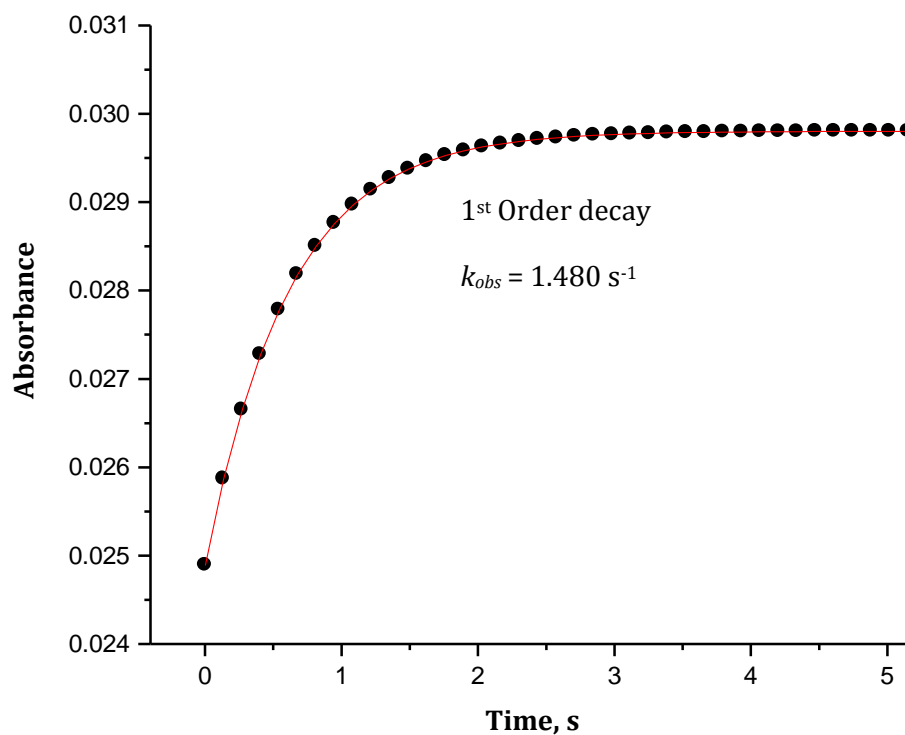


Figure S4.20: Stopped-flow kinetic trace of **PtL2** ($3.69 \times 10^{-5} \text{ M}$) with dimethylimidazole ($5.35 \times 10^{-3} \text{ M}$ (150 fold) taken at 318 nm and at 298 K.

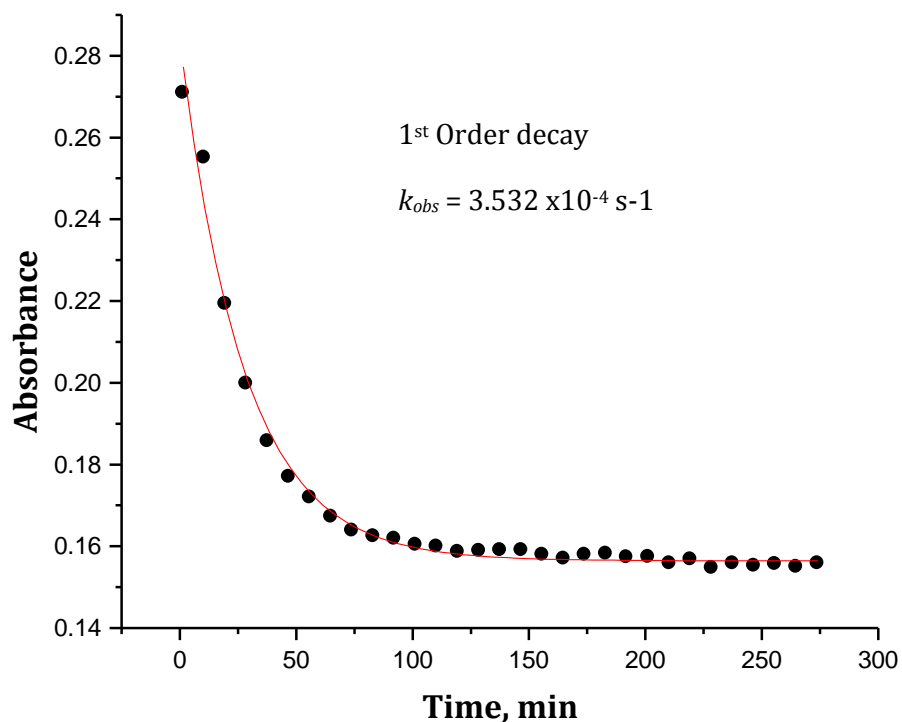


Figure S4.21: UV/Visible absorption versus time kinetic trace of **PtL3** (5.18×10^{-5} M) with dimethylimidazole (2.59×10^{-3} M (50 fold)) taken at 388 nm and at 298 K.

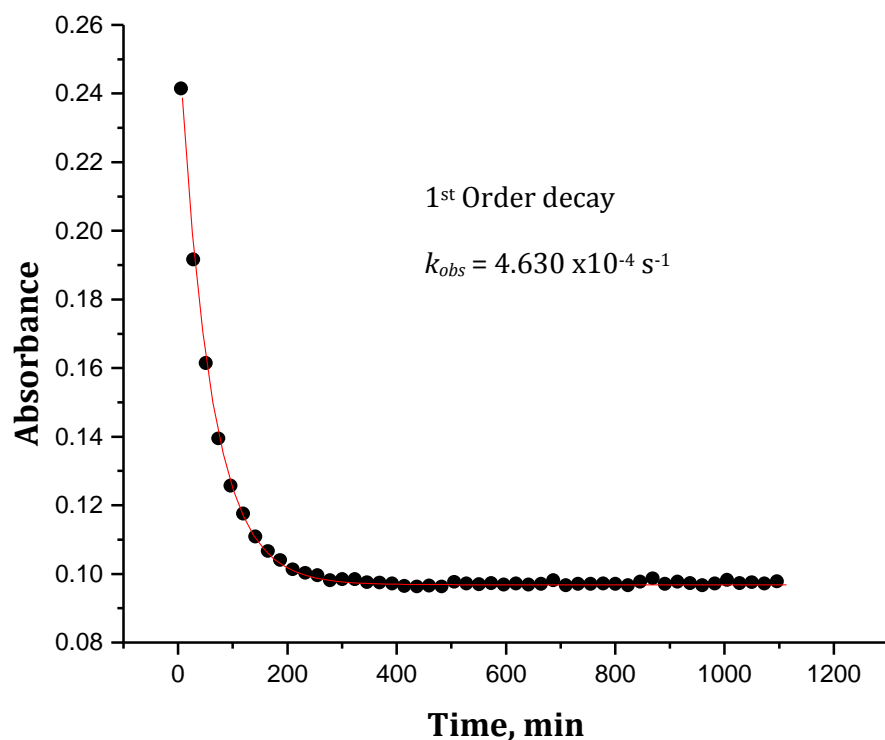


Figure S4.22: UV/Visible absorption versus time kinetic trace of **PtL3** (5.18×10^{-5} M) with methylimidazole (2.59×10^{-3} M (50 fold)) taken at 370 nm and at 298 K.

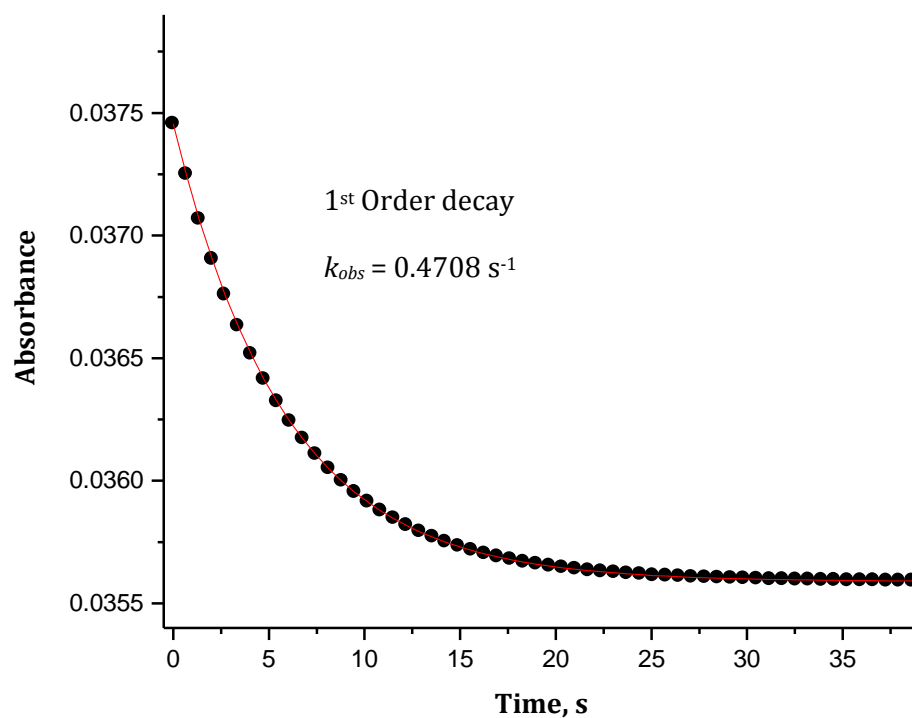


Figure S4.23: UV/Visible absorption versus time kinetic trace of **PtL4** ($5.00 \times 10^{-5} \text{ M}$) with triazole ($1.04 \times 10^{-3} \text{ M}$ (20 fold)) taken at 425 nm and at 298 K.

Table S4.1: Summary of the wavelengths (nm) used to observe the reaction between the platinum(II) complexes and the azole nucleophiles.

Wavelength, λ (nm)			
Nucleophile	PtL2	PtL3	PtL4
Imidazole	275	388	480
Pyrazole	400	390	470
Triazole	400	390	425
Methyl imidazole	273	370	480
Dimethyl imidazole	318	388	485

Table S4.2: Average observed rate constants, $k_{\text{obs}}, \text{s}^{-1}$ for the substitution of chloride from **PtL2**, **PtL3** and **PtL4** by imidazole, T = 298 K, I = 0.10 M (LiCF₃SO₃ + LiCl).

PtL2		PtL3		PtL4	
[Im], M	$k_{\text{obs2}}, \text{s}^{-1}$	[Im], M	$k_{\text{obs2}}, \text{s}^{-1}$	[Im], M	$k_{\text{obs2}}, \text{s}^{-1}$
0.00185	1.079	0.000518	0.00003157	0.00050	0.3154
0.00369	2.408	0.00104	0.00004895	0.0010	0.6534
0.00535	3.580	0.00155	0.00006741	0.0015	0.9353
0.00738	4.595	0.00207	0.00009402	0.0020	1.217
0.00923	5.858	0.00259	0.0001194	0.0025	1.520

Table S4.3: Average observed rate constants, $k_{\text{obs}}, \text{s}^{-1}$ for the substitution of chloride from **PtL2**, **PtL3** and **PtL4** by pyrazole, T = 298 K, I = 0.10 M (LiCF₃SO₃ + LiCl).

PtL2		PtL3		PtL4	
[Pyz], M	$k_{\text{obs2}}, \text{s}^{-1}$	[Pyz], M	$k_{\text{obs2}}, \text{s}^{-1}$	[Pyz], M	$k_{\text{obs2}}, \text{s}^{-1}$
0.000369	0.2089	0.000518	0.00001042	0.00518	0.4492
0.000738	0.3872	0.00104	0.00001763	0.00104	0.8329
0.00111	0.6465	0.00155	0.00002348	0.00155	1.308
0.00148	0.8513	0.00207	0.00003248	0.00207	1.692
0.00185	1.123	0.00259	0.00004268	0.00259	2.219

Table S4.4: Average observed rate constants, $k_{\text{obs}}, \text{s}^{-1}$ for the substitution of chloride from **PtL2**, **PtL3** and **PtL4** by 1,2,4-triazole, $T = 298 \text{ K}$, $I = 0.10 \text{ M}$ ($\text{LiCF}_3\text{SO}_3 + \text{LiCl}$).

PtL2		PtL3		PtL4	
[Trz], M	$k_{\text{obs2}}, \text{s}^{-1}$	[Trz], M	$k_{\text{obs2}}, \text{s}^{-1}$	[Trz], M	$k_{\text{obs2}}, \text{s}^{-1}$
0.000369	0.1888	0.000518	0.00001334	0.000518	0.2708
0.0007384	0.4334	0.00104	0.00001539	0.00104	0.4708
0.00111	0.6459	0.00155	0.00001709	0.00155	0.6646
0.00148	0.7987	0.00207	0.00001953	0.00207	0.8459
0.00185	1.077	0.00259	0.00002155	0.00259	1.125

Table S4.5: Average observed rate constants, $k_{\text{obs}}, \text{s}^{-1}$ for the substitution of chloride from **PtL2**, **PtL3** and **PtL4** by 1-methylimidazole, $T = 298 \text{ K}$, $I = 0.10 \text{ M}$ ($\text{LiCF}_3\text{SO}_3 + \text{LiCl}$).

PtL2		PtL3		PtL4	
[MIm], M	$k_{\text{obs2}}, \text{s}^{-1}$	[MIm], M	$k_{\text{obs2}}, \text{s}^{-1}$	[MIm], M	$k_{\text{obs2}}, \text{s}^{-1}$
0.00185	1.118	0.000518	0.00004730	0.000518	0.7972
0.00369	1.985	0.00104	0.0001108	0.00104	1.478
0.00535	2.815	0.00155	0.0001691	0.00155	2.157
0.00738	3.726	0.00207	0.0002364	0.00207	3.116
0.00923	5.177	0.00259	0.0002907	0.00259	3.930

Table S4.6: Average observed rate constants, $k_{\text{obs}}, \text{s}^{-1}$ for the substitution of chloride from **PtL2**, **PtL3** and **PtL4** by 1,2-dimethylimidazole, $T = 298 \text{ K}$, $I = 0.10 \text{ M}$ ($\text{LiCF}_3\text{SO}_3 + \text{LiCl}$).

PtL2		PtL3		PtL4	
[DIm], M	$k_{\text{obs2}}, \text{s}^{-1}$	[DIm], M	$k_{\text{obs2}}, \text{s}^{-1}$	[DIm], M	$k_{\text{obs2}}, \text{s}^{-1}$
0.00185	0.4777	0.000518	0.0003532	0.00050	0.1923
0.00369	0.9644	0.00104	0.0004214	0.0010	0.3368
0.00535	1.480	0.00155	0.0004773	0.0015	0.5536
0.00738	1.932	0.00207	0.0005165	0.002	0.7200
0.00923	2.529	0.00259	0.0006061	0.0025	0.9415

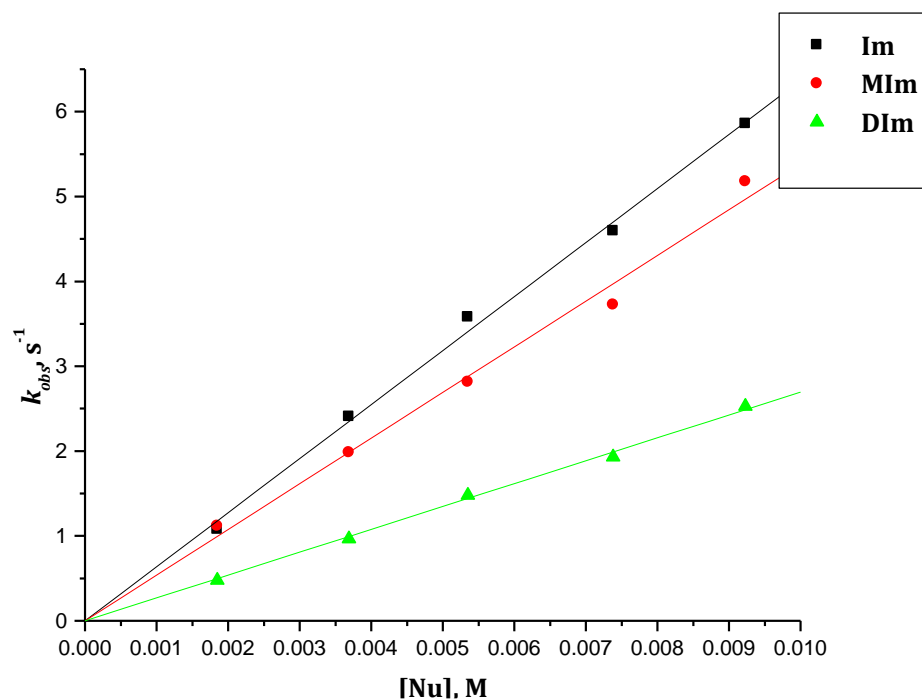


Figure S4.24: Plots of *pseudo*-first order rate constants (k_{obs}) against concentration of nucleophiles (**Im**, **MIm** & **DIm**) for the chloride substitution reaction on **PtL2** in a methanol solution ($I= 0.10$ M ($LiCF_3SO_3 + LiCl$)) at 298 K.

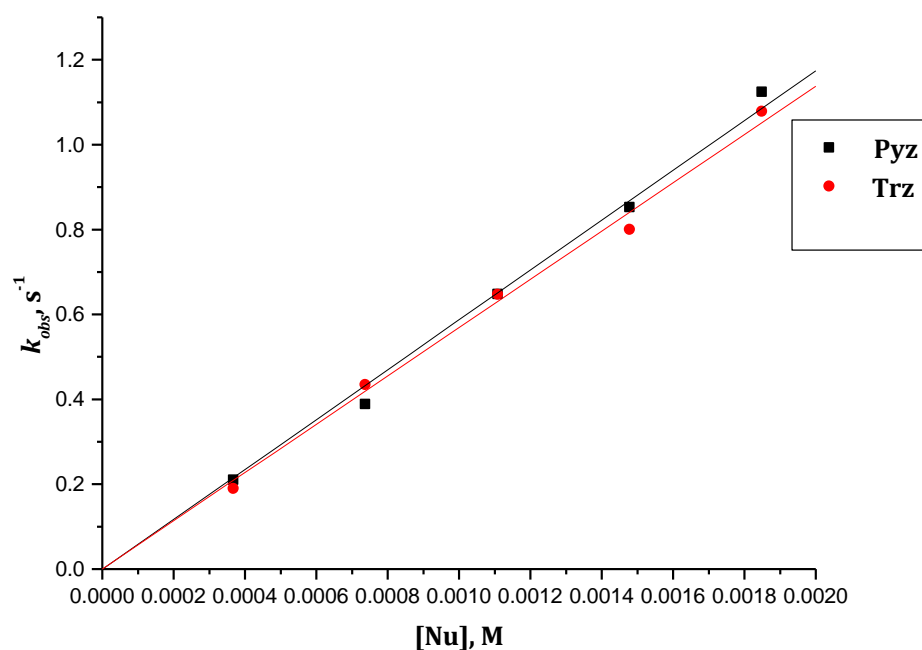


Figure S4.25: Plots of *pseudo*-first order rate constants (k_{obs}) against concentration of nucleophiles (**Pyz** & **Trz**) for the chloride substitution reaction on **PtL2** in an ethanol solution ($I= 0.10$ M ($LiCF_3SO_3 + LiCl$)) at 298 K.

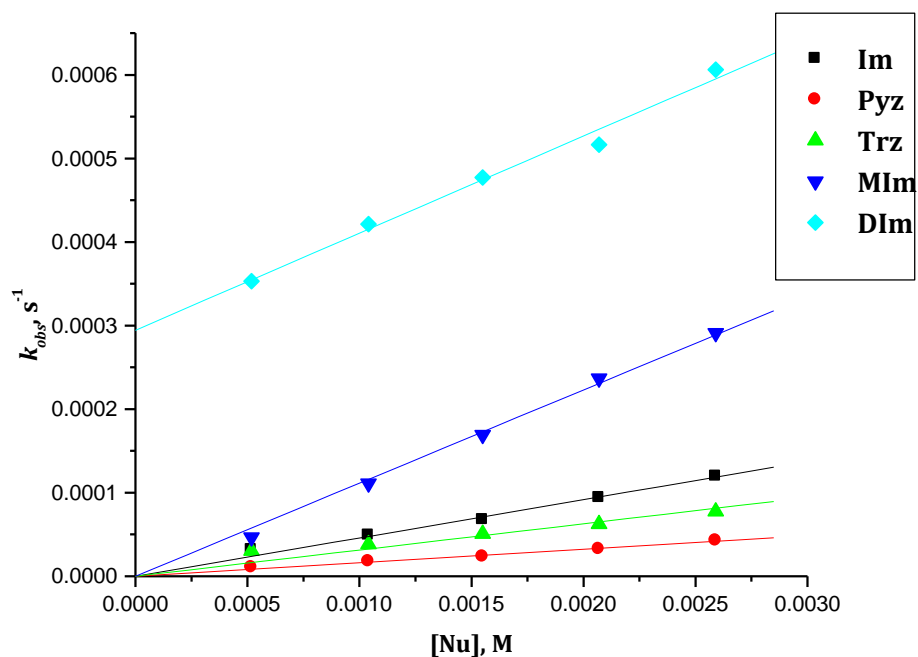


Figure S4.26: Plots of pseudo-first order rate constants (k_{obs}) against concentration of all nucleophiles (**Im**, **Pyz**, **Trz**, **MIm** & **DIm**) for the chloride substitution reaction on **PtL3** in a methanol solution ($I = 0.10$ M ($\text{LiCF}_3\text{SO}_3 + \text{LiCl}$)) at

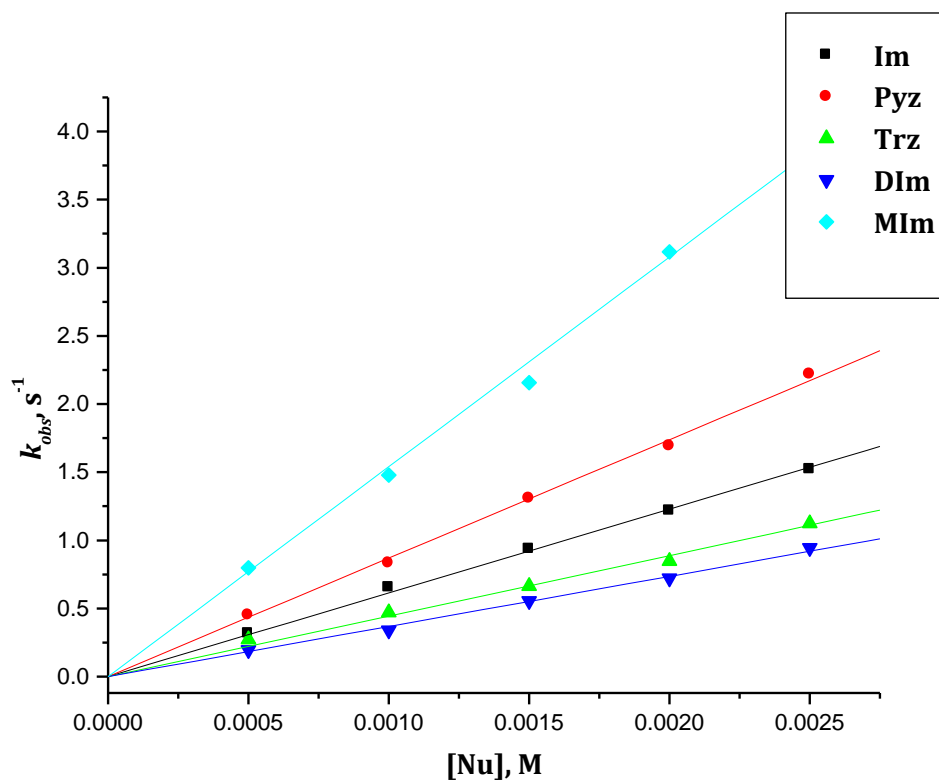


Figure S4.27: Plots of pseudo-first order rate constants (k_{obs}) against concentration of all nucleophiles (**Im**, **Pyz**, **Trz**, **MIm** & **DIm**) for the chloride substitution reaction on **PtL4** in a methanol solution ($I = 0.10$ M ($\text{LiCF}_3\text{SO}_3 + \text{LiCl}$)) at

Table S4.7: The log of the second order rate constants, k_2 , of the studied reactions with Pt(II) complexes and the pK_a values of the nucleophiles.

Nu	pK_a	$\log k_2$			
		PtL1	PtL2	PtL3	PtL4
Pyz	2.19	-0.07058	2.76343	-2.40121	2.64738
Trz	2.52	0.10037	2.79309	-1.79317	2.73957
Im	7.00	0.5682	2.8041	-1.33913	2.78817
MIm	7.33	0.57864	3.02747	-0.95078	2.98543
DIm	8.00	0.17319	2.42975	-0.93554	2.3784

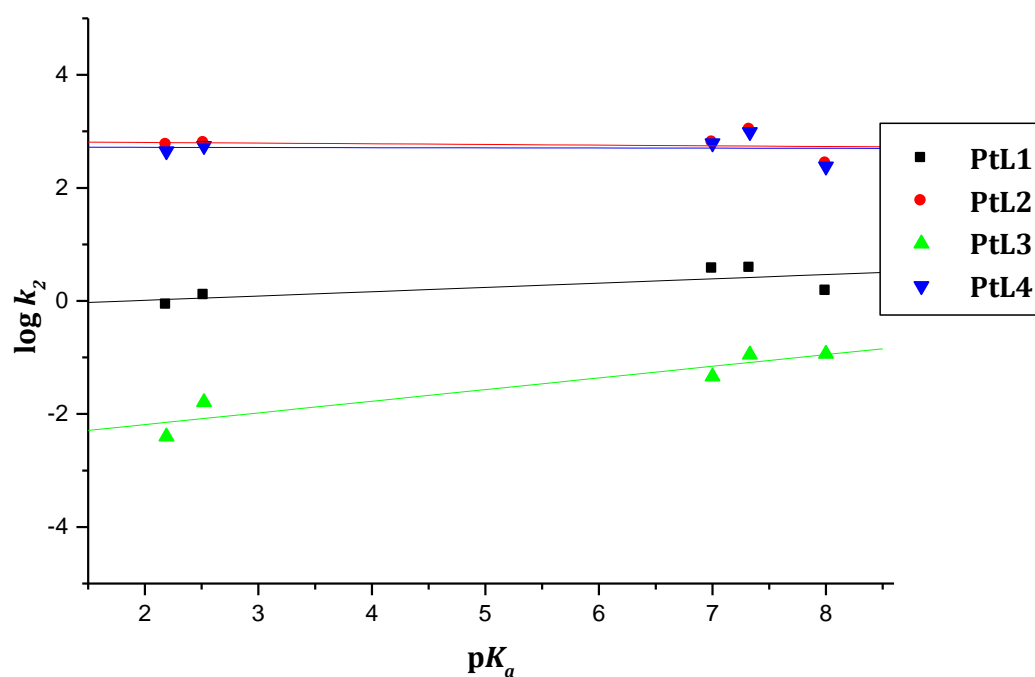


Figure S4.28: Plots of $\log k_2$ achieved from the substitution reactions of the Pt(II) complexes against the pK_a values of the nucleophiles investigated

Table S4.8: Temperature dependence of k_2 , $M^{-1} s^{-1}$, for the displacement of the chloride by Imidazole in a methanol solution, $I = 0.1$ ($LiCF_3SO_3 + LiCl$).

PtL2		PtL3		PtL4	
1/T	ln (k_2/T)	1/T	ln (k_2/T)	1/T	ln (k_2/T)
0.00347	-5.396058	0.00347	-15.85449	0.00347	-6.47299
0.00341	-4.875674	0.00341	-15.58702	0.00341	-6.09859
0.00336	-4.406548	0.00336	-15.30187	0.00336	-5.76401
0.00330	-4.10120	0.00330	-14.9620	0.00330	-5.50953
0.00325	-3.659225	0.00325	-14.55719	0.00325	-5.20121
0.00317	-3.181256				

Table S4.9: Temperature dependence of k_2 , $M^{-1} s^{-1}$, for the displacement of the chloride by pyrazole in a methanol solution, $I = 0.1$ ($LiCF_3SO_3 + LiCl$).

PtL2		PtL3		PtL4	
1/T	ln (k_2/T)	1/T	ln (k_2/T)	1/T	ln (k_2/T)
0.00347	-6.8349	0.00347	-16.93629	0.00347	-5.87367
0.00341	-6.42229	0.00341	-16.59817	0.00341	-5.64502
0.00336	-6.28355	0.00336	-16.35638	0.00336	-5.42878
0.00330	-5.94302	0.00330	-15.95887	0.00330	-5.23972
0.00325	-5.6046	0.00325	-15.66071	0.00325	-5.11598

Table S4.10: Temperature dependence of k_2 , $M^{-1} s^{-1}$, for the displacement of the chloride by 1,2,4-triazole in a methanol solution, $I = 0.1$ ($LiCF_3SO_3 + LiCl$).

PtL2		PtL3		PtL4	
1/T	ln (k_2/T)	1/T	ln (k_2/T)	1/T	ln (k_2/T)
0.00347	-6.53519	0.00347	-16.75858	0.00347	-6.9836
0.00341	-6.29051	0.00341	-16.29386	0.00341	-6.475
0.00336	-6.05843	0.00336	-11.21855	0.00336	-6.1056
0.00330	-5.8003	0.00330	-15.4712	0.00330	-5.88296
0.00325	-5.53899	0.00325	-15.22388	0.00325	-5.57264

Table S4.11: Temperature dependence of k_2 , $M^{-1} s^{-1}$, for the displacement of the chloride by 1-methylimidazole in a methanol solution, $I = 0.1$ ($LiCF_3SO_3 + LiCl$).

PtL2		PtL3		PtL4	
1/T	ln (k_2/T)	1/T	ln (k_2/T)	1/T	ln (k_2/T)
0.00353	-4.37358	0.00347	-15.06628	0.00347	-5.74949
0.00341	-3.88858	0.00341	-14.719	0.00341	-5.3263
0.00336	-3.70382	0.00336	-14.38196	0.00336	-4.92821
0.00330	-3.55404	0.00330	-14.0018	0.00330	-4.55682
0.00325	-3.28268	0.00325	-13.53779	0.00325	-4.26044

Table S4.12: Temperature dependence of k_2 , $M^{-1} s^{-1}$, for the displacement of the chloride by 1,2-dimethylimidazole in a methanol solution, $I = 0.1$ ($LiCF_3SO_3 + LiCl$).

PtL2		PtL3		PtL4	
1/T	ln (k_2/T)	1/T	ln (k_2/T)	1/T	ln (k_2/T)
0.00347	-6.05641	0.00347	-8.31681	0.00347	-7.25834
0.00341	-5.6454	0.00341	-7.94952	0.00341	-6.72838
0.00336	-5.27842	0.00336	-7.84971	0.00336	-6.28843
0.00330	-4.64547	0.00330	-7.69394	0.00330	-5.94976
0.00325	-4.25887	0.00325	-7.62755	0.00325	-5.69064

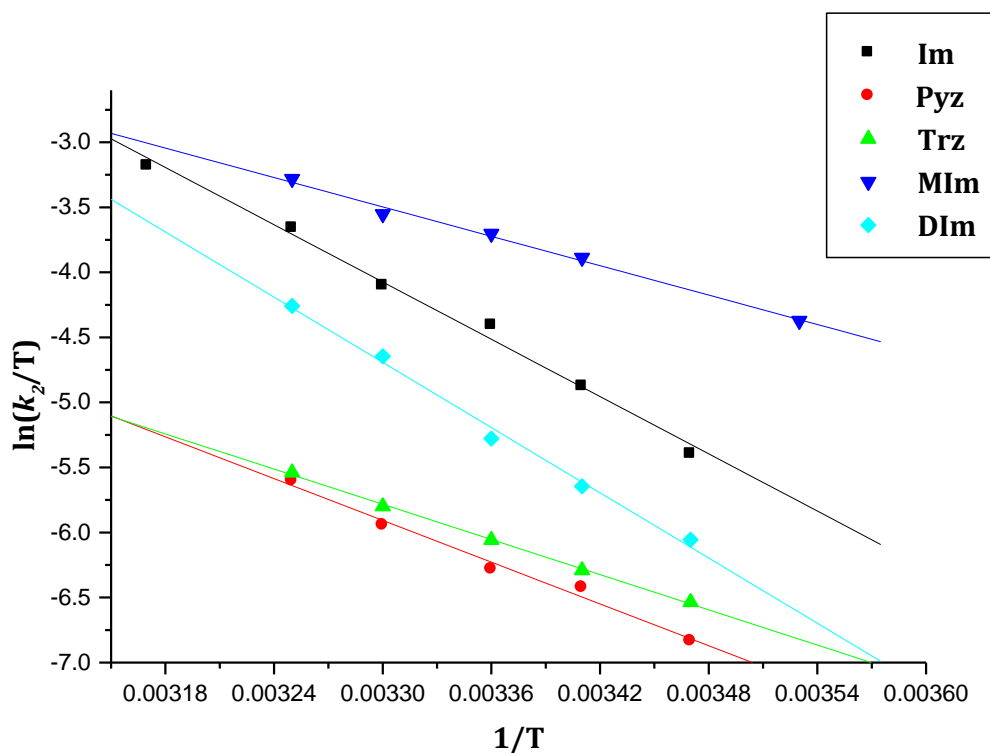


Figure S4.29: Temperature dependence plot of **PtL2** with all nucleophiles, **Im**, **Pyz**, **Trz**, **MIm** and **DIm** in a methanol solution, $I = 0.10$ M.

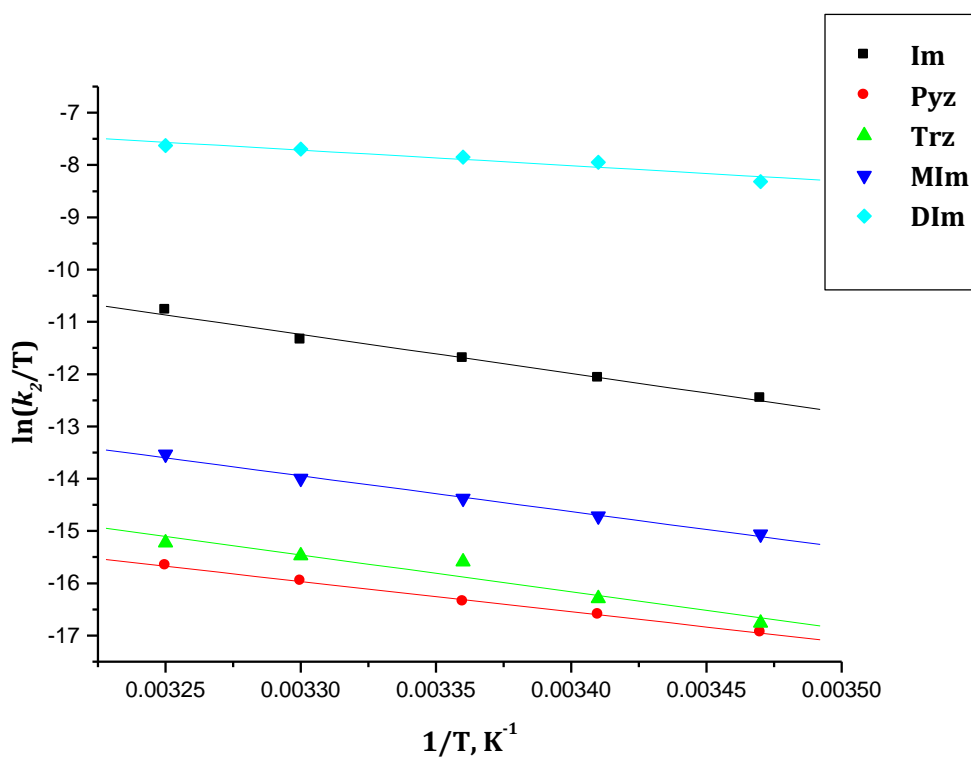


Figure S4.30: Temperature dependence plot of **PtL3** with all nucleophiles, **Im**, **Pyz**, **Trz**, **MIm** and **DIm** in a methanol solution, $I = 0.10$ M.

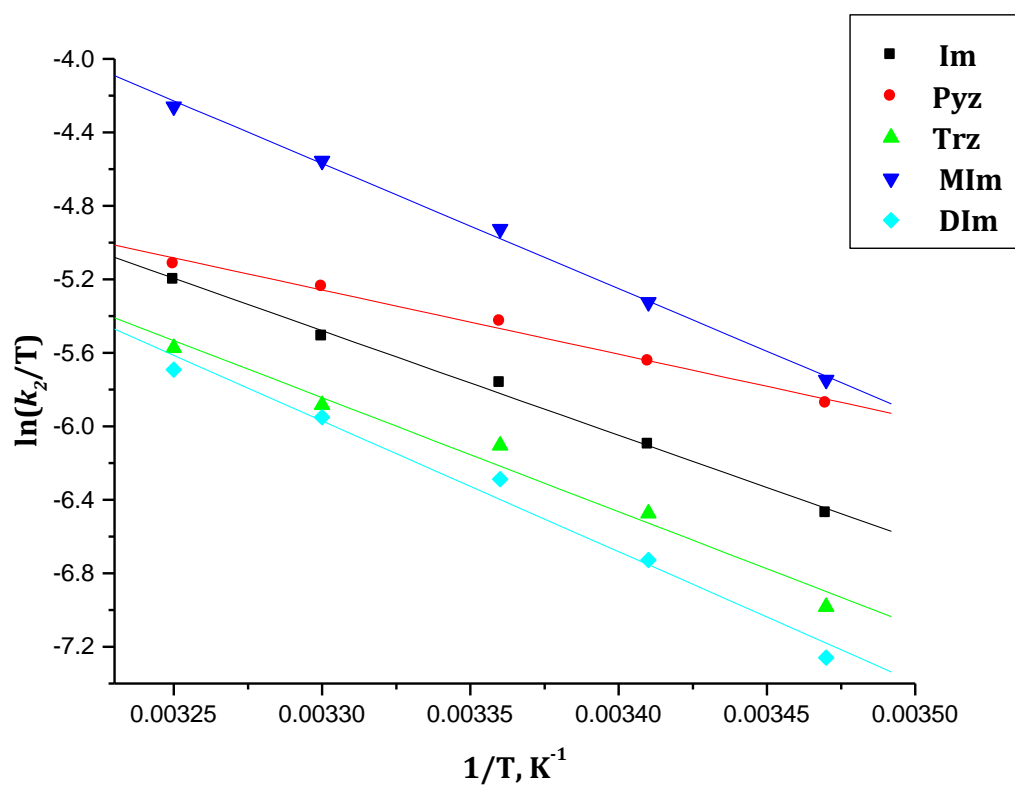


Figure S4.31: Temperature dependence plot of **PtL4** with all nucleophiles, **Im**, **Pyz**, **Trz**, **MIm** and **DIm** in a methanol solution, $I = 0.10$ M.

CHAPTER 5

A Detailed Kinetic and Mechanistic Study of the Substitution Reactions of Platinum(II) Complexes with N^N- and N^S-donor Chelates using Azole Nucleophiles. Crystal structure of [Pt(bis(2-pyridylmethyl)sulfide)Cl]ClO₄.

5.0. Abstract

The substitution kinetics of the complexes [Pt(bis(2-pyridylmethyl)amine)OH₂](ClO₄)₂, **Ptdpa** and [Pt(bis(2-pyridylmethyl)sulfide)OH₂](ClO₄)₂, **Ptdps**, with a series of azole nucleophiles: Imidazole (**Im**), 1-methylimidazole (**MIm**), 1,2-Dimethylimidazole (**DIm**), 1,2,4-triazole (**Trz**) and pyrazole (**Pyz**), were studied in an aqua medium at constant ionic strength (0.1 M). The substitution of the coordinated water ligand on the platinum(II) complexes by the azoles were studied under *pseudo*-first order conditions as a function of the incoming nucleophiles concentration and temperature using either stopped-flow techniques or UV/Vis spectroscopy. **Ptdps** was found to be more reactive (three magnitude higher) than **Ptdpa**. The second-order rate constant, k_2 , for all the nucleophiles ranged between 0.087 ± 0.005 and 0.926 ± 0.05 M⁻¹ s⁻¹ for **Ptdpa** and between 146 ± 4 and 1458 ± 10 M⁻¹ s⁻¹ for **Ptdps**. The rate of substitution of the aqua ligand is dependent on the strength of the σ -donor character and the π -acceptability of the *trans* atom to the leaving group. The observed reactivity trend for the azoles with each platinum(II) complex followed the trend, **MIm** > **Im** > **DIm** > **Trz** > **Pyz**. This reactivity trend is in accordance with the basicity, steric and electrophilic effects of the nucleophiles. This is in agreement with the linear free energy relationship of each complex for all the nucleophiles. The temperature dependence studies support an associative nature of activation which is expected for low-spin d^8 square-planar platinum(II) complexes. The X-ray crystal structure of **Ptdps-Cl** is presented.

5.1. Introduction

Substitution reactions of square planar d^8 complexes, in particular Pt(II) complexes have interested many coordination kineticists. This has been so ever since the serendipitous discovery of the anti-tumor activity of *cis*-[PtCl₂(NH₃)₂] and in particular that antitumor activity of such Pt(II) based drugs comes about from their ability to covalently bind or interchelate to certain fragments of nucleic acids.¹⁻⁴

However, due to drug resistance and severe side effects associated with the use of cisplatin, non-classical Pt(II) complexes with varied structural properties have been developed recently and their kinetic and mechanistic behavior of nucleophilic substitution reactions also studied.^{3,4} Examples coming from recent studies include mechanistic investigation of dinuclear and trinuclear Pt(II) complexes.^{5,6} The most notable anticancer agent has been trinuclear Pt(II) complex, BBR 3464 synthesized by Farrell *et al.*⁵ This Pt(II) complex has shown remarkable therapeutic success in clinical trials due to its ability to form different adducts with DNA from those of the parent drug thus overcoming drug resistance.^{5,6}

Central to this body of knowledge, has been the kinetic data from mononuclear Pt(II) and Pd(II) complexes with tridentate N^NN-donor chelate ligands such as diethylenetriamine (dien),^{7,8} bis(2-pyridylmethyl)amine (bpma)⁹⁻¹² and 2,2':6'2''-terpyridine (terpy).¹³⁻¹⁶ These model compounds have provided useful kinetic information on substitution behavior of square planar complexes in general due to their high stability and simplicity of their substitution kinetics.^{10,17,18} Their kinetic data on tuning the electronic and/or steric ancillary fragments of the non-labile chelate ligand systems have provided useful insight on the reactivity and how ligand modifications could affect the fate of the metal complexes under biological conditions, especially their *in vivo* reactions with DNA biomolecules.¹⁷

Hofmann and co-workers¹⁶ were able to distinguish between the *trans* and *cis* π / and σ effect on reactivity for a series of Pt(II) complexes bearing chelating ligands with extended π molecular orbital systems. In the study the pyridyl nitrogen donor of a terpy ligand backbone was replaced with a phenyl carbon donor, on the *trans* and *cis*-positions in order to investigate the influence of having a strong σ -donor group on either *cis* or *trans* to the leaving group on the substitution reactions of the Pt(II) complexes. The Pt(II) complex with the phenyl carbon donor in the *cis*-position resulted in a decrease in the substitution rate due to the accumulation of electron density at the metal centre.^{16,19} Unlike this complex, its isomeric analogue with the phenyl ring on the *trans* position showed a significant increase in reactivity compared to the Pt(II) terpy complex. This was due to the high destabilization of the ground state *via* the *trans* influence and its own additional π -acceptor contribution on the chelate.¹⁶

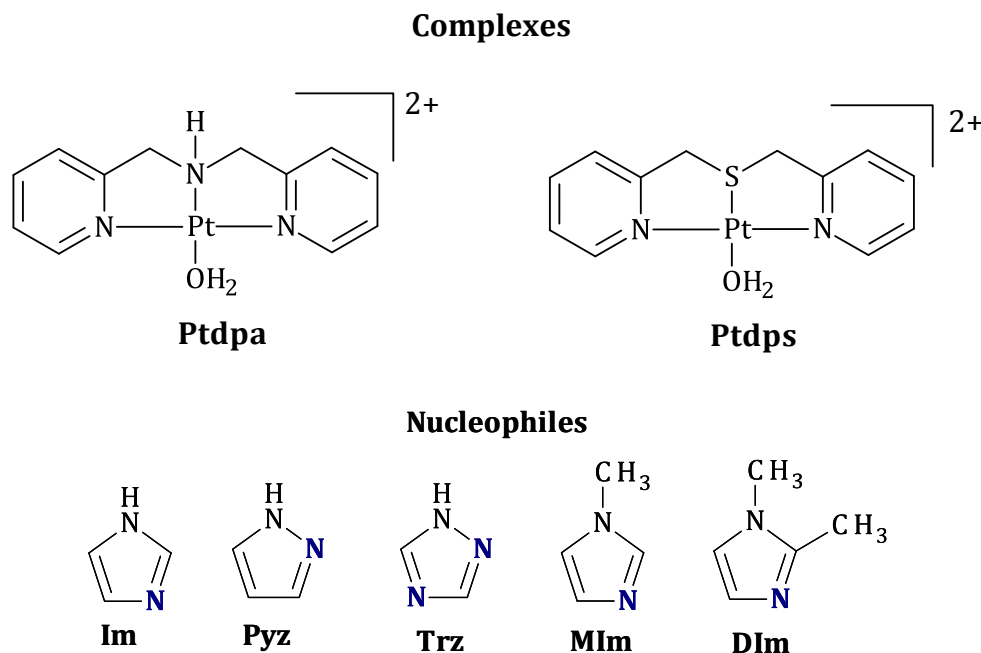
Work conducted by Mambanda *et al.*¹⁸ showed that attaching alkyl hydrocarbon groups of varying chain lengths on the *trans*-N donor atoms of Pt(Cl) bis(2-pyridylmethyl)amine complex enhances the substitution reactivity of the parent complex. This was due to the additional σ -inductive donation brought about by the alkyl chain. The increase in reactivity was dependent on the chain length and branching of the alkyl groups.¹⁸

Furthermore, work reported by Hochreuther *et al.*²⁰ on the diaqua complex [Pt(2-methylthiomethylpyridine)(OH₂)₂]²⁺, Pt(mtp) confirmed that the first substitution occurs at the aqua ligand *trans* to the strong σ -donor sulfur atom ahead of the one coordinated to the strong π -acceptor pyridine ring of the 2-methylpyridine ligand.^{20,21} However, a study conducted by Pitteri *et al.*,¹⁴ on the substitution reactions of Pt(II) complexes with a bis(2-pyridylmethyl) sulfide non leaving group and terpy using halide nucleophiles showed comparable reactivities between them. The results meant that the *trans*-labilizing effect of a coplanar pyridine ring of terpy was almost the same as that of the thioether sulfur atom.¹⁴ Another study conveyed by this group involved the kinetic substitution of pyridine in [Pt(bis(methylthiomethyl)pyridine)]; [Pt(bis(2-pyridylmethyl)amine)pyridine] and [Pt(bis(2-pyridylmethyl)sulfide)pyridine] by a series of anionic and neutral nucleophiles.²² The results obtained showed that second-order rate constant for substituting the pyridine from [Pt(bis(2-pyridylmethyl)sulfide)pyridine] was greater than that from [Pt(bis(methylthiomethyl)pyridine)] and was even greater than that from [Pt(bis(2-pyridylmethyl)amine)pyridine].²² It was clear that the *trans* effect of the sulfur atom of the thioether and to a lesser extent, the π -acceptability of this *cis* pyridine rings controlled the reactivity of the Pt(II) complex.

To extend this understanding on the factors influencing the reactivity when one changes the *trans*-donor group of chelated Pt(II) complexes, we studied the substitution reactions of [Pt(bis(2-pyridylmethyl) amine)(H₂O)](ClO₄)₂ (**Ptdpa**) and [Pt(bis(2-pyridylmethyl) sulphide)H₂O](ClO₄)₂ (**Ptdps**) with neutral nitrogen donor azole nucleophiles.

The nucleophiles used are, *viz.* imidazole (**Im**), 1-methylimidazole (**MIm**), 1,2-dimethylimidazole (**DIm**), pyrazole (**Pyz**) and 1,2,4-triazole (**Trz**). The five-membered neutral heterocyclic nucleophiles containing either 2 or 3 N-atoms (azoles) are of important models from a bioinorganic point of view. Studies have shown that Pt(II) complexes prefer binding to DNA through the N7 atom of guanine (part of its ring structure is an azole) instead of adenine, leading to a distorted DNA strand.²³⁻²⁷ Furthermore, the imidazole groups of histidine residues act as a ligand in most haemoproteins that regulates oxygen uptake and electron transfer *via* the cytochromes in living organisms.^{23,28-31}

In addition, the pK_a value of **Ptdps** was determined and the crystal structure of [Pt(bis(2-pyridylmethyl)sulfide)Cl](ClO₄)(CH₃NO₂), **Ptdps-Cl** is reported. Computational calculations were also conducted and are in excellent agreement with the kinetic data obtained. The structures of the investigated complexes and nucleophiles are illustrated in **Scheme 1**.



Scheme 5.1 Structures of the Pt(II) complexes and nucleophiles used in the study.

5.2. Experimental

5.2.1. Chemicals and reagents

Thiosemicarbazide (99%), 2-picolyl chloride hydrochloride (98%), di-(2-picolyl) amine (99%), sodium perchlorate (NaClO₄), silver perchlorate (AgClO₄), pyrazole (98%), 1,2,4-triazole (98%), 1-methylimidazole and 1,2-dimethylimidazole were purchased from Aldrich and were used as received.

The platinum(II) precursor complexes, dichlorobis(benzonitrile)platinum(II), ([Pt(Ph(CN)₂Cl₂]) (99%) and potassium tetrachloroplatinate, K₂PtCl₄ (99.99%) were purchased from Strem Chemicals and were used as supplied.

All organic solvents along with the acids, (HClO₄, HCl) were supplied by Merck except for nitromethane which was purchased from Saarchem.

5.2.2. Synthesis of (bis(2-pyridylmethyl) sulphide), **dps**

The ligand, **dps**, was synthesized following a literature method.³² Thiosemicarbazide (0.46 g, 6.1 mmol) was dissolved in 150 mL distilled H₂O. To the solution, was added 2-picolyyl chloride hydrochloride (3.30 g, 20.1 mmol) followed by NaOH (8.09 g, 202 mmol). The resulting mixture was stirred at room temperature for 24 hours and the unreacted material was removed by filtration. The filtrate was extracted using 3 portions of 50 mL CHCl₃ and the combined organic extracts were dried over anhydrous MgSO₄. After filtering off the MgSO₄, the solvent was removed completely under *vacuo*. The desired ligand (**dps**) was obtained as brown oil.

Yield: 1.15 g (87%). TOF MS ES⁺: m/z = 239.06 [M+Na]. ¹H NMR (CDCl₃, 400 MHz): δ/ppm = 8.51 (1H, d), 7.60(1H, td), 7.34 (d, 1H). 7.12(ddd, 1H), 3.80(s, 2H), 2.59(s, 2H).

5.2.3. Synthesis of Pt(II) complexes

5.2.3.1. Synthesis of [Pt(bis(2-pyridylmethyl) amine)Cl](ClO₄), **Ptdpa-Cl**

The complex, **Ptdpa-Cl** was synthesized according to a well-known procedure.³⁴ To a solution of K₂PtCl₄ (0.205 g, 0.48 mmol) dissolved in 0.005 M HCl (100 mL), the ligand, di-(2-picolyyl) amine; **dpa** (0.087 mL, 0.48 mmol) was added. The mixture was refluxed for 3 days and during this period; a yellow suspension formed which redissolved later. The yellow mixture was cooled to room temperature then filtered and the filtrate was reduced to about 10 mL. Addition of saturated NaClO₄ (3 mL) precipitated the desired complex as a yellow colloid. This was collected by filtration, washed with small amounts of water, ethanol and ether and was dried under vacuum.

Yield: 242 mg (95%). Anal. Calcd for C₁₂H₁₃N₃O₄PtCl₂: C = 27. 23; H = 2.48; N = 7.94. Found: C = 26. 73; H = 2.45; N = 7.62. TOF MS ES⁺: m/z = 430.0519 (M⁺⁺Na). ¹H NMR (DMSO-*d*₆, 400 MHz) δ/ppm: 8.75 (d, 2H); 8.57 (br s, 1H); 8.18 (t, 2H); 7.71 (d, 2H); 7.57 (t, 2H); 4.88 (m, 2H); 4.55(dd, 2H). ¹³C NMR (DMSO-*d*₆, 400 MHz) δ/ppm: 167.5; 147.5; 139.5; 124.0; 121.3; 57.6. ¹⁹⁵Pt NMR (DMSO-*d*₆, 500 MHz) δ/ppm: -2346.2. IR (4000- 650)[†] $\bar{\nu}$: 3095.9(mb), 2919.6(w), 1614.6(sb), 1482.5(w), 1435.7(mb), 1218.9(m), 1081.9(vs), 1021.2(m), 765.1(vs).

5.2.3.2. Synthesis of [Pt(bis(2-pyridylmethyl) sulfide)Cl](ClO₄), **Ptdps-Cl**

The complex, **Ptdps-Cl** was obtained following a literature method.³³ To [Pt(Ph(CN)₂ Cl₂] (1.50 g, 3.0 mmol) dissolved in a minimum amount of CH₂Cl₂ was added a solution of the ligand (0.649

[†] vs = very strong, s = strong, m = medium, w = weak and b= broad.

g, 3 mmol in 10 mL CH₂Cl₂) drop wise. The mixture was refluxed for 2 hours, and during this time a yellow precipitate gradually appeared. The crude product was filtered off under *vacuo* as a yellow solid. The product was recrystallized from a supersaturated and boiling aqueous solution of LiClO₄. The desired compound was slowly cooled to room temperature and filtered using a 0.45 μm nylon filter membrane.

Yield: 1.05 g (64%). Anal. Calcd for C₁₂H₁₂N₂SO₄PtCl₂: C = 26.38; H = 2.21; N = 5.13. Found: C = 25.91; H = 2.06; N = 5.47. TOF MS ES⁺: m/z = 239 [M+Na]. ¹H NMR (CDCl₃, 400 MHz) δ/ppm: 8.92(d, 2H); 8.20(t, 2H); 7.84(d, 2H); 7.61(t, 2H); 5.75(d, 2H); 4.81(d, 2H). ¹³C NMR (DMSO-d₆, 400 MHz) δ/ppm: 165.3; 150.6; 140.9; 125.4; 124.9; 44.2. ¹⁹⁵Pt NMR (DMSO-d₆, 500 MHz) δ/ppm: -2694.02. IR (4000- 650)⁺ $\bar{\nu}$: 3297.2(w), 3166.7(wb), 2918.0(m), 1622.3(sb), 1476.1(w), 1444.6(w), 1357.6(w).

5.2.3.3. Crystallization of [Pt(bis(2-pyridylmethyl) sulphide)Cl](ClO₄)-CH₃NO₂, Ptdps-Cl

The crystal, **Ptdps-Cl** was synthesised by dissolving [Pt(bis(2-pyridylmethyl) sulphide)Cl](ClO₄) in 3 mL nitromethane to make a saturated solution and undissolved materials were filtered through a 0.45 μm nylon filter membrane. The brown crystal was grown through slow vapour diffusion of ether into the solution contained in a special designed chamber.

5.2.4. Preparation of aqua complex solutions

The solution of the aqua complexes, **Ptdpa** and **Ptdps** were prepared as described in the literature,³⁴ by reacting an appropriate amount of AgClO₄ with the corresponding chloro complexes. The chloro Pt(II) complex and AgClO₄ (1:1 molar ratio) were dissolved in 0.10 HClO₄ solution and the mixture was stirred under a flow of nitrogen at 40 - 50 °C in the dark for 24 hours. The silver chloride precipitate which formed was filtered off using a 0.45 μm nylon filter membrane. The filtrate was collected and diluted with 0.10 M HClO₄ solution, to give solutions of complexes with final concentrations which were 2.06 x 10⁻⁵ M and 2.08 x 10⁻⁵ M for **Ptdpa** and **Ptdps**, respectively.

5.2.5. Instrumentation & Physical Measurements

The NMR spectra were recorded on a Bruker Avance III 500 or Bruker Avance III 400 at frequencies of 500 MHz or 400 MHz (¹H) and 125 MHz/100 MHz (Pt) using either a 5 mm BBOZ probe or a 5 mm TBIZ probe. All proton and carbon chemical shifts are reported relative to the relevant solvent signals at 30 °C unless stated otherwise. Elemental compositions of the ligands

and complexes were performed on a Thermo Scientific Flash 2000. The pH of the aqueous solutions of the complex, **Ptdps**, was measured using a Jenway 4330 Conductivity/pH meter equipped with a Micro 4.5 μm diameter glass electrode. The electrode was calibrated at 25 $^{\circ}\text{C}$ using standard buffer solutions of pH 4.0; 7.0 and 10.0 (Merck). The electrolyte of pH electrode was replaced with 3.0 M NaCl instead of KCl to prevent precipitation of KClO_4 during pH measurement. The mass spectral data of the ligands and complexes were acquired on a Waters Micromass LCT Premier spectrometer. All FTIR spectra were recorded on a Bruker Alpha FTIR spectrometer. The spectra were acquired by crushing the powder on the sample platform between the Diamond Heads. A total of about 25 spectra were averaged. Relevant information acquired and within the frequency range 4 000 to 650 cm^{-1} .

An Applied Photophysics SX 20 stopped-flow spectrophotometer coupled to an online data acquisition system was used to monitor fast reactions. Slow reactions were monitored using a Varian UV/Vis Cary 100 spectrophotometer. The temperature of these instruments was controlled throughout all kinetic measurements to ± 0.02 $^{\circ}\text{C}$. $\text{p}K_{\text{a}}$ and kinetic traces were graphically analysed using the Origin 7.5^{®35} software package.

5.2.6. Determination of the $\text{p}K_{\text{a}}$ value of **Ptdps**

Spectrophotometric pH titrations of the aqua complex, **Ptdps** with the base, NaOH were performed in the pH range of 1 - 10 and monitored using an UV/Vis spectrophotometer. To avoid dilution effects, a large complex solution volume of 150 mL was used and crushed NaOH pellets were added to increase the pH stepwise from pH 1 until pH 3. Further increases in pH were achieved by drop wise additions of a series of NaOH solutions of the concentrations ranging from 0.01 M to 0.5 M. 2.0 mL aliquots from the complex solution were withdrawn for pH measurement; these were discarded to avoid *in situ* contamination by chloride ions released from the pH electrode. To test the reversibility of the system, drops of diluted solutions of HClO_4 were used.

The UV/Vis spectra for the pH titration along with the plot of the absorbance versus pH at 300 nm as the inset are shown in **Figure 5.1**.

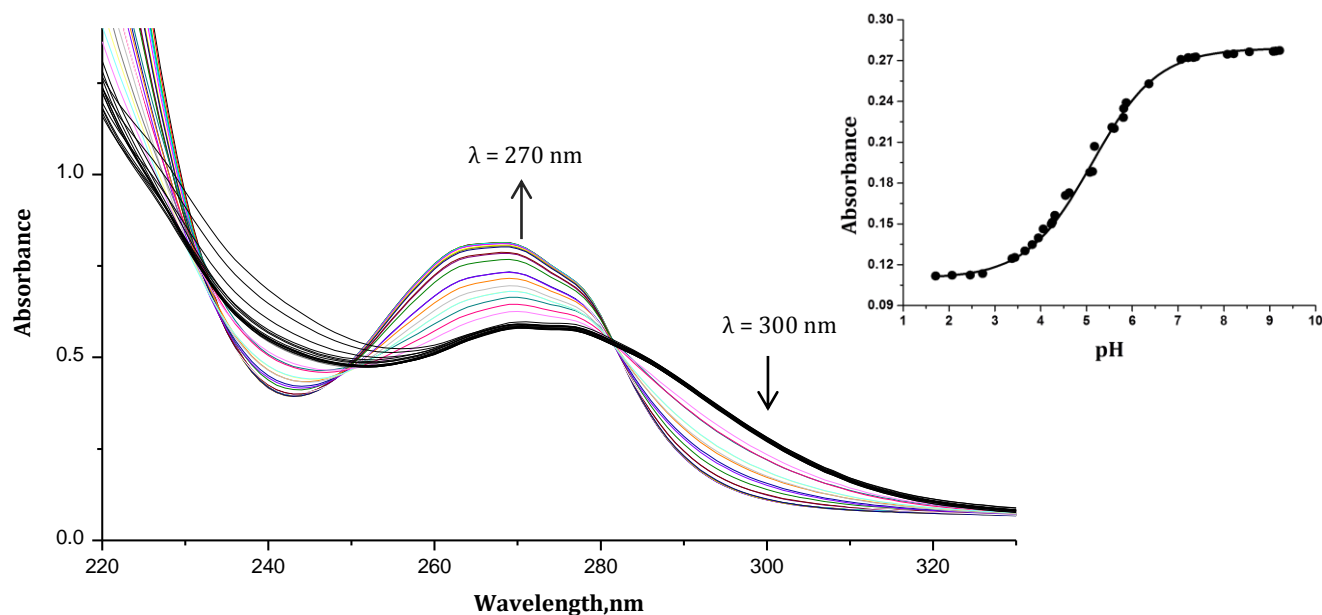


Figure 5.1: UV/Vis spectra for the titration of 0.1 mM **Ptdps** with NaOH, pH range 1–10, $T = 298$ K. *Inset:* Plot of absorbance vs. pH at 300 nm.

5.2.7. Computational Details

The density functional theoretical (DFT) calculations of the complexes, **Ptdpa**; **Ptdps** and **Ptdps-Cl** modelled as cations and in the gas phase were performed with the Gaussian 09W computational software³⁶ using the B3LYP functional in the basis set of LANL2DZ for the electronic structures at the ground state. The computed data of **Ptdps-Cl** was used to gauge the accuracy of the computation in the gaseous phase. A summary of the computational data is illustrated in **Table 5.2** while the HOMO-LUMO diagrams depicted in **Figure 5.2**.

5.2.8. X ray Crystallography

The single crystal X-ray data for the metal complex was recorded on a Bruker Apex II Duo equipped with an Oxford Instrument Cryojet operating at 100 K and an Incoatec microsource operating at 30 W power. The data was collected with Mo $K\alpha$ ($\lambda = 0.71073$ Å) radiation at a crystal-to-detector distance of 50 mm. The following conditions were used for the Bruker data collection: omega and phi scans with exposures taken at 30 W X-ray power and 0.50° frame widths using APEX2.³⁷ The data was reduced with the programme SAINT³⁷ using outlier rejection, scan speed scaling, as well as standard Lorentz and polarisation correction factors. Direct methods, SHELXS-97³⁸ were used to solve the structure. Hydrogen atoms were located in

the difference density map and refined isotropically with SHELXL-97³⁸ and were included as idealised contributors in the least squares process. OLEX2, a complete structure solution, refinement and analysis program³⁹ was used to prepare the material for publication. The complex, **Ptdps-Cl** crystallized in the monoclinic space group, P2₁/c and contained one complete molecule with Z = 4. The crystal structure is shown in **Figure 5.7** and a summary of the crystal data and structure refinement details are available in **Table 5.1**.

Table 5.1: Crystallographic data and structure refinement for [**Ptdps-Cl**](ClO₄)·CH₃NO₂

<i>Parameter</i>	
Chemical formula	C ₁₂ H ₁₂ ClN ₂ PtS•ClO ₄ •CH ₃ NO ₂
<i>M_r</i> (g mol ⁻¹)	607.33
Crystal system	Monoclinic
Space group	P2 ₁ /c
Temperature (K)	100
<i>a</i> (Å)	14.6795 (5)
<i>b</i> (Å)	7.2800 (3)
<i>c</i> (Å)	17.2174 (6)
β (°)	103.086 (2)
<i>V</i> (Å ³)	1792.19 (11)
<i>Z</i>	4
Radiation type	Mo K α
Crystal size (mm)	0.28 × 0.20 × 0.10
<i>T_{min}</i> / <i>T_{max}</i>	0.205, 0.491
No. of measured, independent and observed [<i>I</i> > 2 σ (<i>I</i>)] reflections	18487, 5463, 5101
<i>R_{int}</i>	0.026
($\sin \theta/\lambda$) _{max} (Å ⁻¹)	0.715
<i>R</i> [<i>F</i> ² > 2 σ (<i>F</i> ²)], w <i>R</i> (<i>F</i> ²), <i>S</i>	0.026, 0.066, 1.05
No. of parameters	236
No. of restraints	0
H-atom treatment	H-atom parameters constrained
$\Delta\rho_{\max}$, $\Delta\rho_{\min}$ (e Å ⁻³)	3.41, -3.07

5.2.9. Kinetic measurements

All substitution reactions were performed under *pseudo* first-order conditions. To ensure all kinetic reactions go to completion, all nucleophiles were provided in concentrations of at least 10-fold excess over the metal complex. A pH of 2.0 and an ionic strength of 0.1 M NaClO₄ were maintained throughout all kinetic experiments. Suitable wavelengths at which kinetic measurements were collected were predetermined spectrophotometrically by monitoring the

change in absorbance of the mixture of the Pt(II) complex and the nucleophile as a function of time and these are summarised in the supporting information. The temperature dependence studies for all the reactions were studied within temperatures ranging from 15 to 40 °C at an interval of 5 °C.

5.3. Results

5.3.1. Computational Studies

In order to gain further insight and to understand the structural and electronic differences between the complexes, computational calculations were performed at the DFT level of theory and the data is summarised in **Table 5.2** and **Figure 5.2**. Data on the planarity and ESP diagrams for both complexes are included in the supporting information, **Table S5.3**.

To gauge the accuracy of the calculated data in the gaseous state, X-ray data of **Ptdps-Cl** was compared with the computed data for **Ptdps-Cl** in the gaseous state. The calculated bond lengths and angles for **Ptdps-Cl** showed a good match with those obtained for the crystal structure within the experimental error.

When looking at the frontier molecular orbital mapping of the HOMO in the ground state for both complexes depicted in **Figure 5.2**, they are both similar. The HOMO orbitals are situated mainly on the metal centre, indicating that electron density is transferred mainly from the Pt(II) centre. However, the LUMO orbital diagrams show distinct variations between the frontier molecular orbital mappings. For **Ptdpa**, electron density from the Pt 5d HOMO orbitals is transferred to the π^* LUMO orbitals situated around the pyridine and methylene moieties of the ligand system. This is expected since studies have shown pyridine rings to be good π -electron acceptors.^{18,20,40,41} For **Ptdps**, a slightly different LUMO diagram is observed. The π^* orbitals are situated mostly on the S_{trans} -Pt-O bonds and extended towards the methylene groups and pyridine groups on either side to a lesser extent.

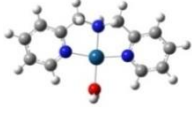


The reason for this is that the *trans* S-atom of **Ptdps** has empty accessible 3d orbitals which are available to accommodate electron density from the HOMO orbitals. Unlike the N donor atom of **Ptdpa** which has no d-orbitals and is therefore unable to transfer charge and has to only use its pyridine rings for π -acceptability. Since it is known that large cations with smaller electrical charges prefer ($d \rightarrow d$) π interactions,⁴² the charge at the Pt ion is transferred into the empty d-orbitals of the *trans* S-atom resulting in a more positive electrophilicity index of the system as shown by the DFT calculations.⁴³ This π -interaction is more favourable than the ($d-p$) π back

donation of **Ptdpa** because it involves orbitals of the same symmetry and similar size ($5d$ and $3d$). This phenomenon is supported by the strong σ -donating character of the *trans*-S-atom which effectively donates electron density to the metal centre.^{20,22} As a consequence, combined influence of the σ -donation and π -acceptability of the S-atom of the thioether causes the substitution process for **Ptdps** to be more stabilized at the transition state than that of **Ptdpa** resulting in an escalated the rate of substitution.^{40,41}

Also shown in **Figure 5.2**, is an overlap of the HOMO and LUMO orbitals for both complexes. This occurs due to the interactions between the $5d$ -orbitals of the metal and the π^* anti bonding orbitals of the ligand, suggesting electronic communication amongst the HOMO and LUMO orbitals of each complex resulting in greater π -acceptor abilities. However, for **Ptdps** there is a greater electronic communication as compared to **Ptdpa** due to a higher overlapping.

In addition, an increase in the calculated dipole moment of **Ptdpa** (0.270 D) moving to **Ptdps** (3.663 D) is noted. This big change is due to the thioether group being a better π -acceptor as the S-atom in **Ptdps** is able to use its vacant d -orbitals to accept electron density compared to **Ptdpa**.⁴⁴

Table 5.2: A summary of the DFT calculated structural data for the investigated tridentate Pt(II) complexes, **Ptdpa** and **Ptdps** at B3LYP/LANL2DZ level of theory.

Properties	Ptdpa	Ptdps	Ptdps-Cl	X-ray Data
				
BOND LENGTHS (Å)				
Pt–N/ <i>S</i> _{trans}	2.022	2.356	2.396	2.2277(6)
Pt–O/Cl	2.105	2.122	2.442	2.3228(6)
BOND ANGLES (°)				
O–Pt–N _{cis}	96.67	93.04	94.61	93.62(7)
O–Pt–N/ <i>S</i> _{trans}	180.0	177.22	175.2	178.31(2)
N _{cis} –Pt–N _{cis}	166.4	167.8	168.6	168.24(10)
ENERGY GAP, ΔE (eV)				
HOMO	-7.19	-7.36		
LUMO	-2.44	-2.86		
ΔE/eV	4.75	4.49		
CHEMICAL HARDNESS, η (eV)				
η	2.38	2.25		
ELECTROPHILICITY INDEX, ω (eV)				
ω	4.88	5.80		
NBO CHARGES				
Pt ²⁺	0.775	0.604		
O ²⁻	-0.924	-0.921		
N/ <i>S</i> _{trans}	-0.629	0.443		
N _{cis}	-0.517	-0.513		
DIPOLE MOMENT (Debye)				
	0.270	3.663		

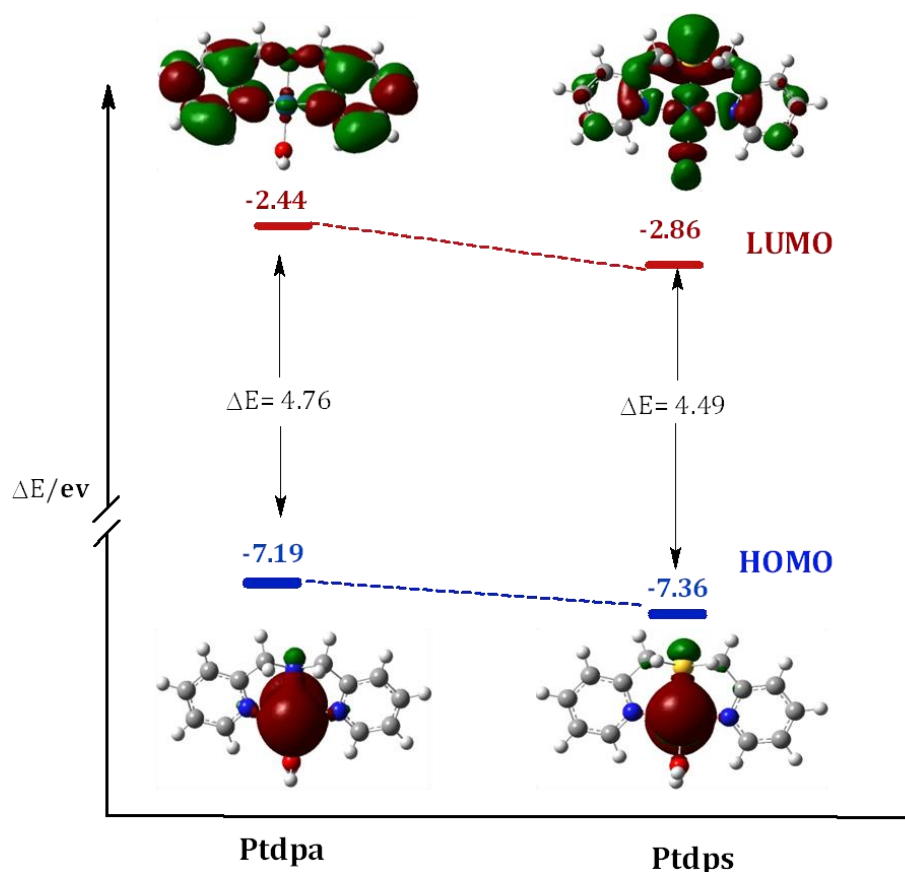


Figure 5.2: Density functional theoretical (DFT) minimum energy structures, HOMO and LUMO frontier molecular orbitals for the complexes **Pt dpa** and **Pt dps**.

5.3.2. Kinetic Studies

The substitution of the coordinated aqua ligands from Pt(II) tridentate complexes, **Pt dpa** and **Pt dps** by five azole nucleophiles, **Im**, **MIm**, **DIm**, **Trz** and **Pyz** were investigated as a function of concentration and temperature. Both conventional UV/Vis and stopped-flow techniques were used to monitor the reactions under pseudo first-order conditions. Substitution reactions of **Pt dpa** with all nucleophiles were studied using a UV/Vis spectrophotometer of which an absorption spectrum of wavelengths ranging from 200 - 800 nm was obtained and by selecting the wavelength with the greatest change in absorbance, a kinetic trace was attained. **Figure 5.3** shows typical changes in the absorption spectra of **Pt dpa** and a kinetic trace at 275 nm is shown as an inset to the figure. Substitution reactions of **Pt dps** were all followed using stopped-flow spectrophotometry and all kinetic traces obtained were described by single exponential fits. A typical stopped-flow trace for **Pt dps** with methyl imidazole, **MIm** at 298 K is presented in **Figure 5.4**.

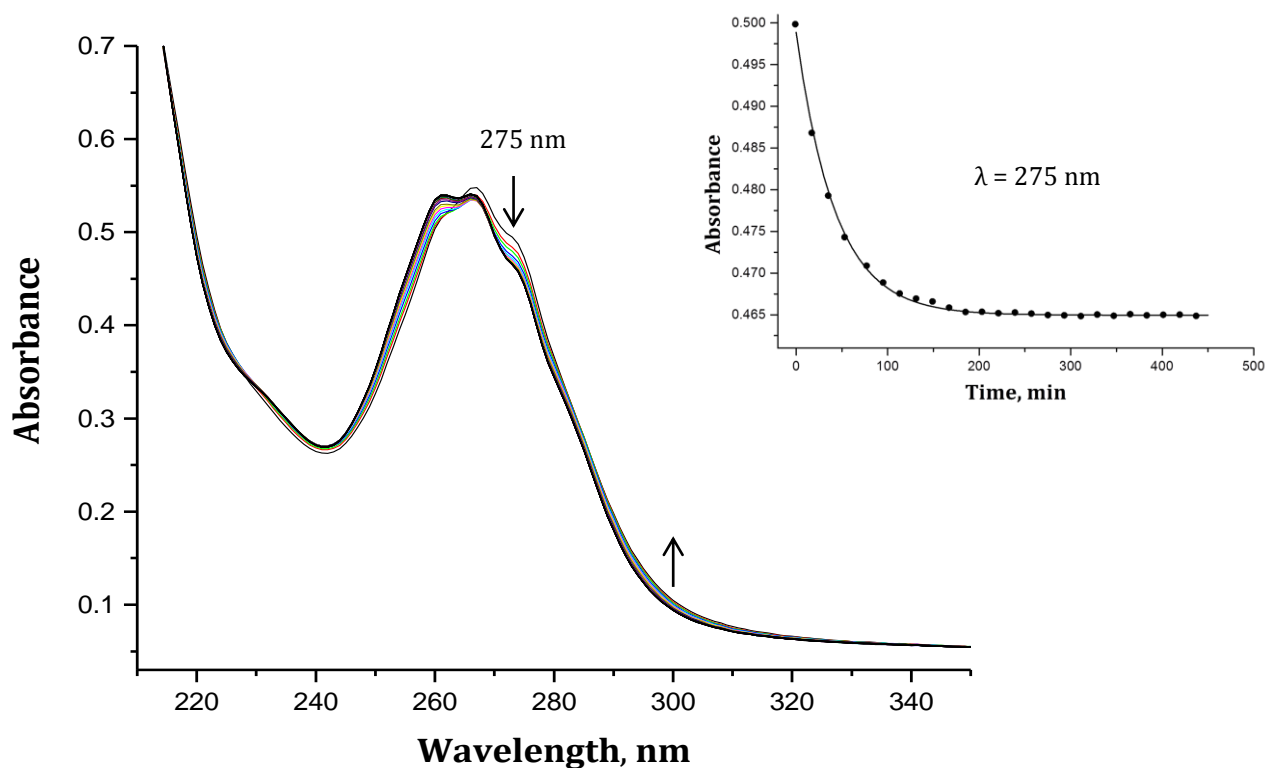


Figure 5.3: UV-Vis absorbance spectra for **Ptdpa** (1.032×10^{-4} M) and **Trz** (1.03×10^{-3} M) at an ionic strength of 0.1 M (NaClO_4), at 298 K. *Inset:* kinetic trace at 275 nm.

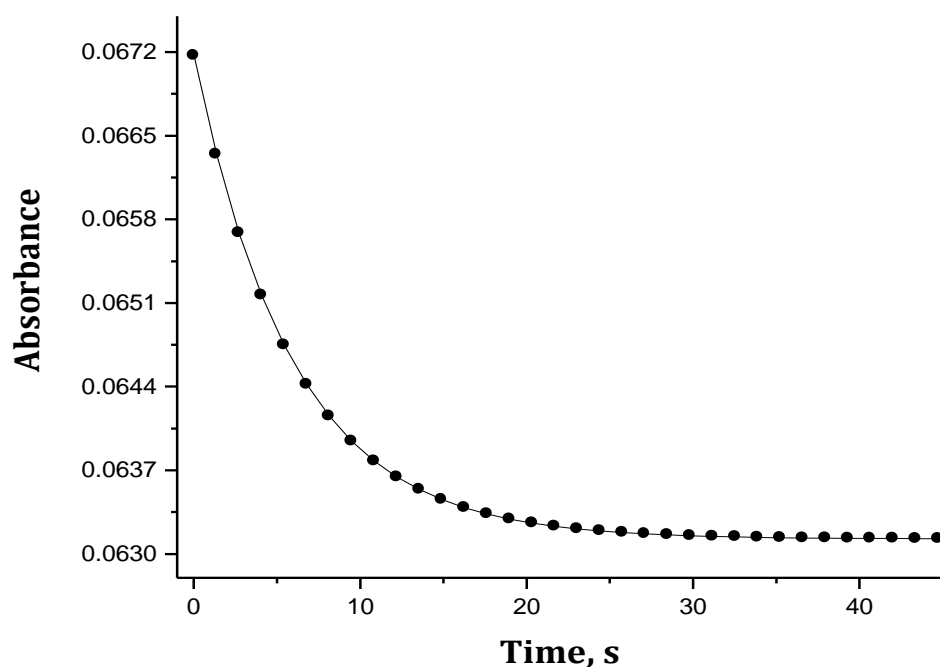


Figure 5.4: Stopped-flow kinetic trace at 285 nm for the substitution reaction of **Pyz** with **Ptdps** at 298 K.

The *pseudo* first-order rate constants, k_{obs} , were calculated from the kinetic traces and **Figure 5.5** illustrates the plot of the dependence of the *pseudo* first-order rate constant (k_{obs}) for **Ptdps**

on the entering nucleophile concentration. For both complexes, straight lines with zero intercepts were obtained with all nucleophiles. This suggests that all reactions were irreversible and independent of the solvent effect.

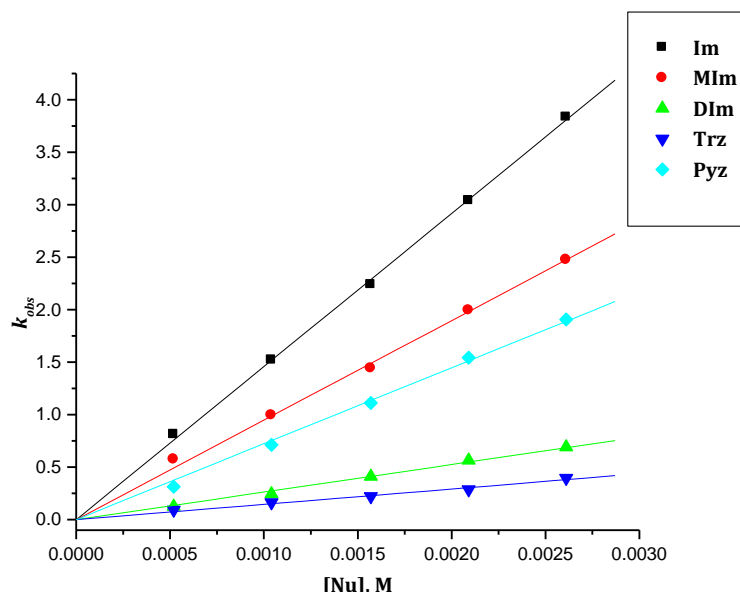


Figure 5.5: Concentration dependence plot for the displacement of the aqua ligand from **Ptdps** (1.04×10^{-4} M) by azole nucleophiles at 298 K.

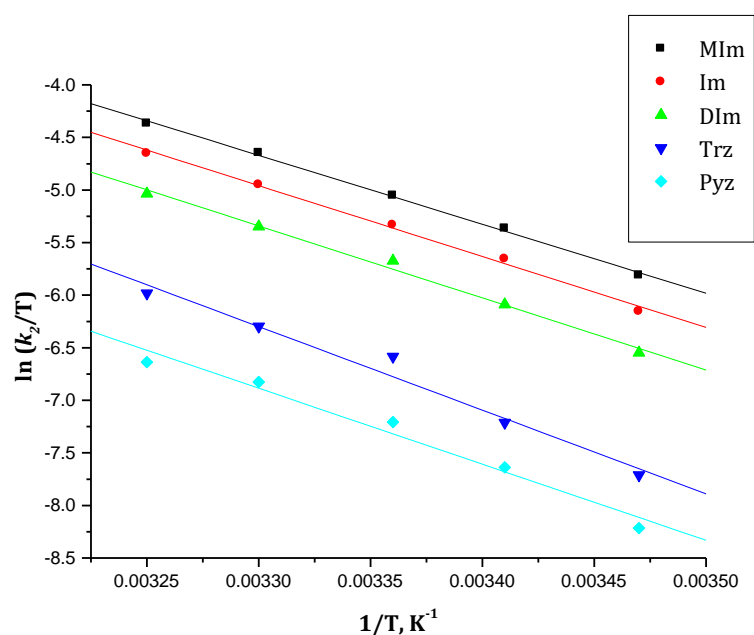
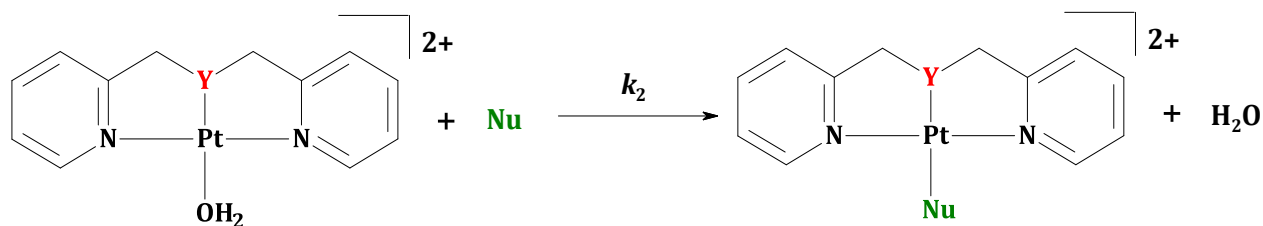


Figure 5.6: Temperature dependence of $k_2/ \text{M}^{-1} \text{s}^{-1}$, for the displacement of the aqua ligand in **Ptdps** (1.04×10^{-4} M) by a series of azole nucleophiles.

Therefore a general mechanism of the aqua substitution by the azole can be illustrated as shown in **scheme 5.2**. The direct nucleophilic attack by the azoles is characterised by the rate

constant, k_2 , for all reactions of **Ptdps** and **Ptdpa**. The overall rate law is according to *Equation 5.1*, with k_2 .



Y = NH (**Ptdpa**) and S (**Ptdps**)

Nu = **Im**, **MIm**, **DIm**, **Pyz**, **Trz**

Scheme 5.2: Proposed substitution mechanism for the removal of the aqua group from the investigated complexes by a series of azole nucleophiles.

The second-order rate constants for the direct nucleophilic attack, k_2 , and the second-order rate constants for the solvolysis path, k_{-2} , were calculated from the slope and the y-intercept of the concentration dependence plots of the reactions at 25 °C, respectively and the data is summarized in **Table 5.3**.

$$k_{obs} = k_2[Nu] \quad (5.1)$$

Also represented in **Table 5.3**, are the activation parameters, ΔH^\ddagger and ΔS^\ddagger values calculated using the Eyring plots from the temperature dependence studies at varying temperatures ranging from 15 – 40 °C.^{24,25}

Table 5.3: Rate constants and activation parameters for substitution reactions of **Ptdpa** and **Ptdps** with azole nucleophiles at $T = 298$ K, pH = 2 (**Ptdpa**) or 3 (**Ptdps**), $I = 0.1$ M (HClO_4 adjusted with NaClO_4).

	Nu	k_2 ($\text{M}^{-1}\text{s}^{-1}$)	ΔH^\ddagger (kJ mol^{-1})	ΔS^\ddagger ($\text{J K}^{-1}\text{mol}^{-1}$)
Ptdpa	Im	0.451 ± 0.01	49 ± 3	-87 ± 10
	MIm	0.926 ± 0.05	53 ± 10	-202 ± 2
	DIm	0.311 ± 0.007	63 ± 3	-43 ± 11
	Trz	0.267 ± 0.008	57 ± 4	-69 ± 13
	Pyz	0.087 ± 0.005	71 ± 4	-33 ± 12
Ptdps	Im	949 ± 12	54 ± 3	-58 ± 9
	MIm	1458 ± 10	52 ± 2	-65 ± 6
	DIm	724 ± 11	56 ± 2	-59 ± 7
	Trz	263 ± 5	63 ± 5	-41 ± 17
	Pyz	146 ± 4	12 ± 0.7	-155 ± 2

Thermodynamic data: pK_a values:

Ptdpa = $5.53 \pm 0.07^\ddagger$ **Ptdps** = $5.12 \pm 0.04^\S$

[‡] Value extracted from literature, reference 34.

[§] Value from current study

5.3.3. Crystal Structure of [Pt*dps*-Cl](ClO₄)·CH₃NO₂

The molecular structure of [Pt*dps*-Cl] was confirmed by X-ray crystal structure determination and is represented in **Figure 5.7**.

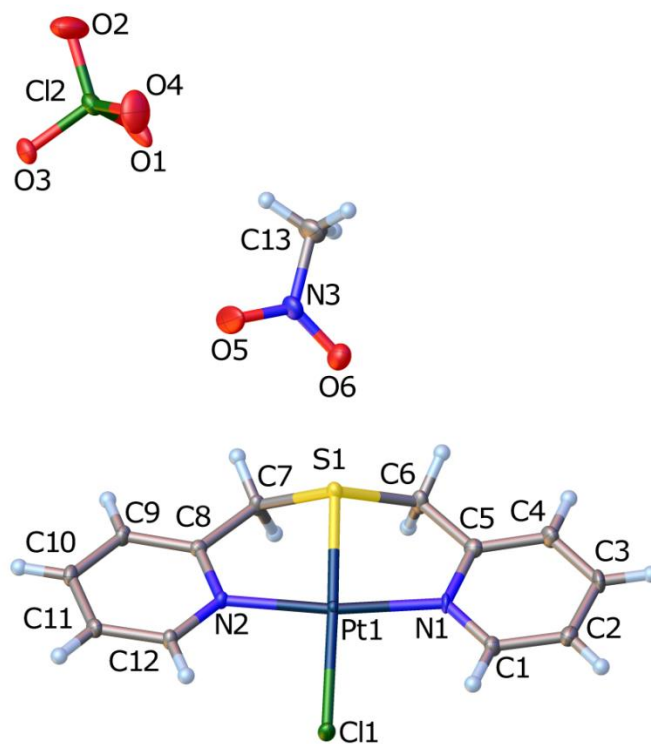


Figure 5.7: Thermal ellipsoid diagram (50% probability surfaces) of the molecular structure of **Pt*dps*-Cl (ClO₄) · CH₃NO₂**

The crystal structure of the brown crystalline rectangular blocks, **Pt*dps*-Cl** was solved. It crystallises with (ClO₄) as a counter ion and (CH₃NO₂) as solvent molecule. The thermal ellipsoid at 50% probability level is represented in **Figure 5.7** while **Table 5.4** lists the selected bond lengths and angles for the structure. **Figure 5.7** shows the tridentate ligand, **dps**, coordinated to the Pt(II) centre by the nitrogen atoms on the *cis*-positioned pyridine rings and the S-donor of the *trans*-situated thioether group while the fourth position is occupied by a chloride ion. The coordination geometry of the complexes is a slightly distorted square planar. Due to the bigger size of the S-atom, the thioether group is forced out of the plane containing the rest of the molecule as a way of minimizing electron-electron repulsions. As a result, the methylene groups of the chelate are located on one side and the chloro leaving group tipped over on the other side exposing it to nucleophilic attacks. This can be seen clearly from **Figure 5.8**.

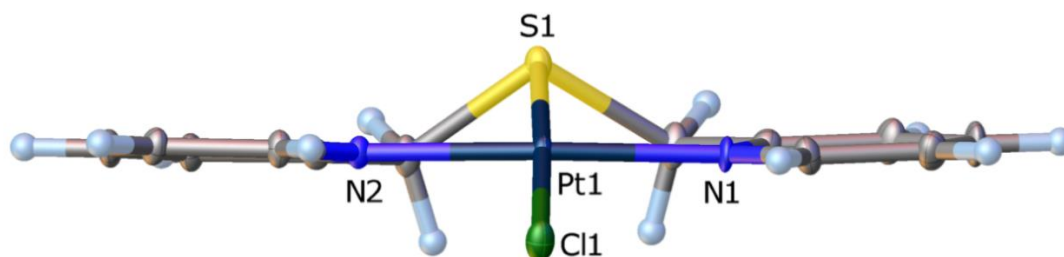


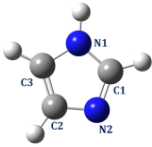
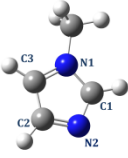
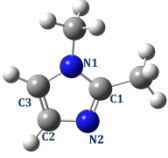


Figure 5.8: Top edge view of the monocation, **Ptdps-Cl** showing the *trans* S-donor atom being out-of-plane.

From **Table 5.4** it is noticeable that the Pt–Cl bond (2.323(6) Å) is significantly longer than that of the bond *trans* to it, Pt1–S1 (2.228(6) Å). In the solid and also in solution, the elongation of the Pt–Cl bond results from the strong *trans* influence of the sulfur atom. This is in line with the big size of the sulfur atom and high diffusivity of its atomic orbitals which leads to a strong bond formation with the soft Pt(II) atom. This weakens the Pt–Cl bond *trans* to the thioether. In addition it tips off the leaving group from the molecule plane making it prone to aerial attack on one side. Also, from the bond angles of the crystal structure represented in **Table 5.4**, **Ptdps-Cl** acquires a distorted square planar geometry. The N2–Pt1–N1 bite angle has deviated from linearity to an angle of 168.2(10)°. The N2–Pt1–S1 angle is 84.7(7)° while the N1–Pt1–S1 angle is similar to it at 85.3(7)°. The S1–Pt–Cl angle is slightly lower than 180° at 178.3(2)°.

Table 5.4: Selected X-ray determined bond lengths (Å) and angles (°) for **Ptdps-Cl**

Bond lengths (Å)			
Pt1–N2	2.015 (2)	C7–C8	1.503 (4)
Pt1–N1	2.027 (2)	C7–H7A	0.9900
Pt1–S1	2.2277 (6)	C7–H7B	0.9900
Pt1–Cl1	2.3228 (6)	C8–C9	1.389 (3)
Angles (°)			
N2–Pt1–N1	168.24 (10)	C8–C7–S1	106.79 (18)
N2–Pt1–S1	84.70 (7)	C8–C7–H7A	110.4
N1–Pt1–S1	85.33 (7)	S1–C7–H7A	110.4
S1–Pt1–Cl1	178.31 (2)	H7A–C7–H7B	108.6

Table 5.5: The pK_a values and NBO charges for the donor atoms of the nucleophiles studied.

					
	Im	MIm	DIm	Pyz	Trz
N1	-0.552	-0.415	-0.416	-0.351	-0.431
N2	-0.480	-0.494	-0.496	-0.294	-0.272
N3	-	-	-	-	-0.490
C1	0.181	0.190	0.357	-0.044	0.106
C2	-0.086	-0.078	-0.078	-0.344	0.167
C3	-0.104	-0.097	-0.095	-0.043	-
pK_a^{52 **}	7.00	7.33	8.00	2.52	2.19

5.4. Discussion

In this study, two Pt(II) complexes, **Ptdpa** and **Ptdps** were synthesized and their substitution reactivity with a set of azole nucleophiles was investigated in order to understand the effect of changing the *trans*-donor from an amine to a thioether group. Data from **Table 5.3** shows the aqua substitution by N-donor nucleophiles is about three orders of magnitudes greater for **Ptdps** than it is for **Ptdpa**. For instance, the reaction between **Ptdps** and **MIm** is 1.6×10^3 times faster than **Ptdpa**. A similar comparison shows that a reaction between **Ptdps** and **Trz** is in fact 2.6×10^3 times faster than **Ptdpa**. Therefore it is clear that the reactivity trend among the two Pt(II) complexes is electronically controlled. The substitution reactivity trend for all the nucleophiles investigated follows the order **MIm** > **Im** > **DIm** > **Trz** > **Pyz** for both complexes reflecting that the nucleophilicity trend was both sterically and electronically controlled.

The high reactivity of **Ptdps** towards the N-donor nucleophiles is attributed to the strong σ -donor S-atom *trans* to the leaving group which significantly labializes the *trans* water ligand due to the increased *trans* effect.²⁰ This is in agreement with the work reported by Pitteri et al.²² using a series of neutral and anionic nucleophiles. As explained, the strong σ -*trans* effect of the thioether elongates the Pt–O bond of the aqua (2.122 Å) as compared to the Pt–O bond in **Ptdpa** (2.105 Å), as reflected in the DFT-calculated bond lengths at the ground state shown in **Table**

** pK_a values from reference 56.

5.2. This is in excellent agreement with previous studies showing that when the σ -donor ability of the *trans* ligand is enhanced so does the *trans* labialization effect of the metal-to-leaving group bond.^{22,45,51} Another factor to consider is that sulfur is a much larger atom than nitrogen; therefore it is easily polarizable due to its high diffusivity of the atomic orbitals compared to that of nitrogen which further explains the higher reactivity of **Ptdps** to that of **Ptdpa**.²²

Due to the presence of pyridyl moieties in the *cis*-position of both the complexes, their π -back bonding ability is similar as supported by the DFT calculated NBO charges on the N_{*cis*} atoms shown on **Table 5.2**, (-0.517) for **Ptdpa** and (-0.513) for **Ptdps**.

However, the NBO charge on the Pt(II) centre of **Ptdps** is smaller than that of **Ptdpa**. Meaning the metal centre of **Ptdpa** (0.775) reflect a more electropositive charge than that of **Ptdps** (0.604). This decrease in positivity of the metal centre from **Ptdpa** to **Ptdps** can be accounted for by the strong σ -donor character of the *trans*-thioether moiety in **Ptdps**. Electrons are donated from the strong S- or N-donor *via* the σ -bond to the metal centre in **Ptdps** or **Ptdpa** respectively. However, due to *trans*-N- being more electronegative than *trans*-S- group, the amine moiety in **Ptdpa** is a weaker electron donor resulting in less π -back donation from the metal centre. As a consequence, the NBO charge on the metal centre in **Ptdpa** is more positive than the NBO charge on the metal centre in **Ptdps**. The results show that the *trans*-effect is much stronger than the repulsion effect of the incoming nucleophile due to a higher electron density on the Pt-atom.

Apart from the σ -donor ability of the *trans*-S atom of the thioether group, the high reactivity of **Ptdps** as to **Ptdpa** is also due to its ability to receive electron density. The S-atom of **Ptdps** is able to accept electron density from the metal centre through π -back bonding using the low lying vacant *d*-orbitals of the sulfur atom. Therefore, in this case, the S-atom of the thioether group of **Ptdps** acts as both σ -donor and π -acceptor. This is supported by the DFT calculated global electrophilicity index and the p*K*_a values which is an indication of the electronic distribution around the metal centre.^{20,46}

It is known that the substitution reactions of square planar Pt(II) complexes depend highly on the nature of the entering nucleophile.⁴⁷⁻⁴⁹ As such, the nucleophilicity of the nucleophiles selected for this study depends on both their electronic and steric properties. To explain the reactivity trend of the nucleophiles, the investigatedazole nucleophiles were separated into two groups based on their structural similarities. The first group comprises of imidazoles which differed only in the number of methyl substituents on the ring, *viz.*, imidazole (**Im**), 1-methyl imidazole (**MIm**) and 1,2-dimethyl imidazole (**DIm**). The other group consists of azoles with no substituents, **Im**, **Pyz** and **Trz**. Of the imidazoles used, **DIm** represents the most sterically

hindered nucleophile in the series due to the steric effect of its 2-methyl substituent. As a result, **DIm** showed the slowest reactivity with both Pt(II) complexes when compared to **MIm** and **Im**, which have one and no substituents on their rings.

In contrast, **MIm** is more reactive than **Im** despite the steric hindrance due to the substituent on the former. The higher reactivity of **MIm** as compared to **Im** is attributed to the σ -effect due to the methyl substituent presented in the N1 atom.^{27,50} The methyl group inductively donates electrons to the ring system, causing the N3- donor to be more basic. Due to the methyl group being situated far from the expected N3 binding position, steric hindrance is minimal.^{47,50} Thus, the overall order in reactivity for the imidazoles follows the trend **MIm** > **Im** > **DIm**. The negative entropy values, ΔS^\ddagger and positive enthalpy values, ΔH^\ddagger support an associative mechanism that is typical of Pt(II) d^8 square planar complexes.^{7,24,51}

However, other studies conducted with these nucleophiles have shown the reactivity trend to depend upon the basicity of the nitrogen which coordinates to the Pt(II) centre during substitution reactions.^{27,47,50} Since azoles are potential ambidentate ligands, assurance as to which binding site is more preferred for coordination is essential. For this reason, computational DFT studies were performed on the nucleophiles in the gaseous phase and the data obtained is represented in **Table 5.5**. From the NBO charges, it is clear that in all nucleophiles the pyridinic-N (N2 in **Table 5.5**) has a more negative charge than the pyrrolic-N (N1 in **Table 5.5**). This is due to the ability of the pyrrolic-N to donate electrons towards the electronic ring system, making the pyridinic-N more negative and thus more reactive towards electrophilic centres.^{50,52} As far as **Trz** is concerned, the N3-pyridinic position is more preferred for binding to electrophiles than the N1 and N2 position since the NBO charge of N3 (-0.490) is more negative than the NBO charges of N1 (-0.431) and N2 (-0.272). Furthermore, the crystal structures of azole coordinated Pt(II) complexes have been obtained and are in line with the binding sites predicted by the computational data.^{50,53,54}

The reactivity of the azole nucleophiles with no substituents, **Pyz**, **Im** and **Trz**, were found to follow the trend **Im** > **Trz** > **Pyz**. This trend is in line with the basicity of the nucleophiles, whose pK_a values are **Im** = 7.00, **Pyz** = 2.52 and **Trz** = 2.19 as represented in **Table 5.5**.^{55,56}

Since the rate of substitution reactions of square planar Pt(II) complexes is highly dependent on the entering nucleophile, a relation between basicity of the nucleophile and its reactivity with the investigated Pt(II) complexes was determined using the Linear Free Energy Relationship (LFER) *Equation 5.2*:

$$\log k_2 = \alpha(pK_a) + b \quad (5.2)$$

where α and b are parameters representing electronic and steric effects.^{14,47}

A plot of $\log k_2$ versus pK_a of the nucleophiles is shown in **Figure 5.9** using data from **Table 5.3** and **5.5**. A linear fit of the rate constant of each complex to the pK_a of the entering nucleophiles were obtained. The slopes of each linear fit represent the ability of each platinum centre to discriminate the incoming nucleophiles.^{14,47,50} In the current study **Ptdps** is more sensitive to the nature of the incoming nucleophile than **Ptdpa**.

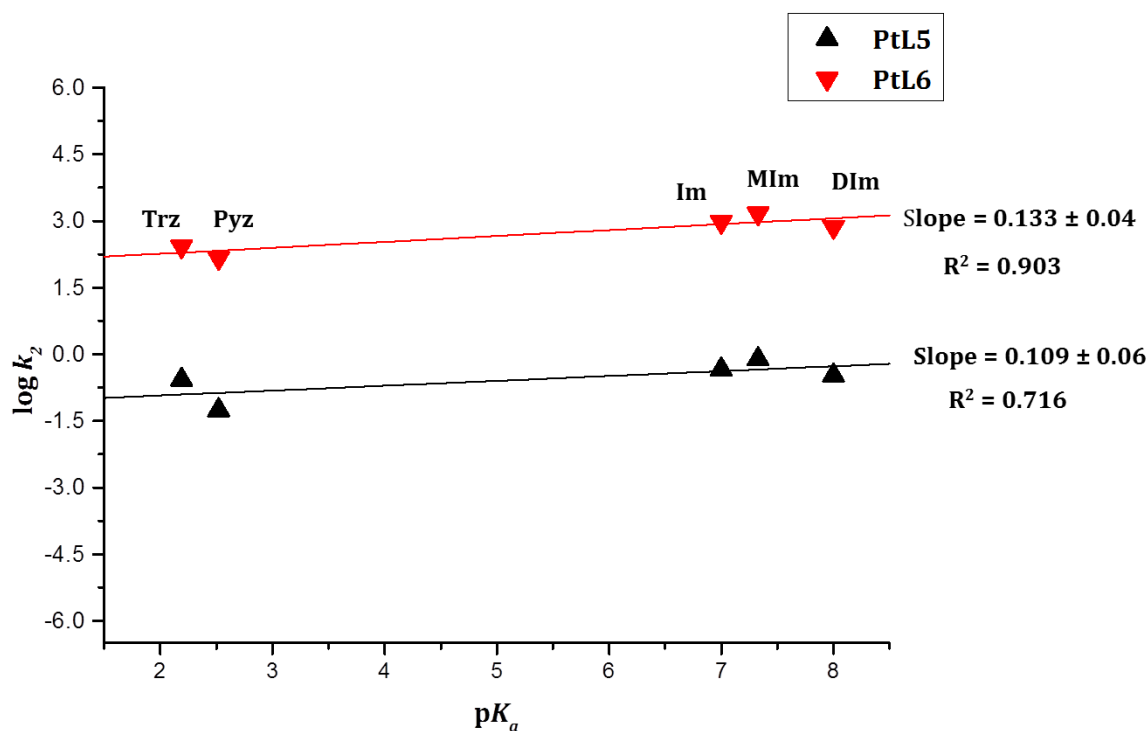


Figure 5.9: Plots of $\log k_2$ achieved from the substitution reactions of the Pt(II) complexes against the pK_a values of the nucleophiles investigated.

5.5. Conclusion

The results of this study reveals that the lability of the aqua ligand from the complexes **Ptdpa** and **Ptdps** is strongly influenced by the strength of the σ -donation character of the atom *trans* to the leaving group. In the current study, the S-atom in **Ptdps** is both σ -donor and a π -acceptor. Using its unoccupied *d*-orbitals for π -back bonding allowing electron density from the metal to be transferred to these *d*-orbitals, leading to a more electrophilic Pt-centre, stabilizes the transition state and leads to a higher reactivity. The higher reactivity in **Ptdps** compared to **Ptdpa** is due to a strong *trans*-effect in combination with the π -back bonding. The kinetic data is supported by the DFT calculations.

The reactivity of the nucleophiles investigated was found to be influenced by both steric factors (**DIm**, **MIm** and **Im**) and electronic factors (**Im**, **Pyz** and **Trz**). The LFER for all the heterocyclic nucleophiles investigated showed that **Ptdps** was more sensitive to changes in the nature of the nucleophiles than **Ptdpa**.

The observed activation parameters, ΔH^\ddagger and ΔS^\ddagger , in both complexes as well as the dependence of the second-order rate constants, k_2 on concentration of the nucleophiles further support the associative mechanism.

5.6. References

1. B. Rosenberg, L. Van Champ, J. E. Trosko, V.H. Mansour, *Nature*, **1969**, 222, 384.
2. B. Rosenberg, *Cancer*, **1985**, 55, 2303 – 2316.
3. B. Lippert, *Cisplatin: Chemistry and biochemistry of a Leading Anticancer Drug*, Wiley-VCH, New York, **1999**, p.1-100, 184-190.
4. E. Wong and C. M. Giandomenico, *Chem. Rev.*, **1999**, 99, 2451.
5. N. Farrell, *Comments Inorg. Chem.*, **1995**, 16, 6, 373.
6. M. S. Davies, J. W. Cox, S. J. Berners-Price, W. Barklage, Y. Qu, and N. Farrell, *Inorg. Chem.*, **2000**, 39, 1710-1715.
7. F. Basolo, J. Chat, H.B. Gray, R.G. Pearson and B.L. Shaw, *J. Chem. Soc.*, **1961**, 2207.
8. M. Schmulling, A.D. Ryabov and R. van Eldik, *J. Chem. Soc., Chem. Commun.*, **1992**, 1609.
9. D. Jaganyi and F. Tiba, *Transition Met. Chem.*, **2003**, 28, 803.
10. D. Jaganyi, F. Tiba, O.Q. Munro, B. Petrović and Z. D. Bugarčić, *Dalton Trans.*, **2006**, 2943.
11. Ž. D. Bugarčić, G. Liehr and R. van Eldik, *J. Chem. Soc., Dalton Trans.*, **2001**, 2825.
12. Ž. D. Bugarčić, G. Liehr and R. van Eldik, *J. Chem. Soc., Dalton Trans.*, **2002**, 951.
13. B. Pitteri, E. I. J. Breet and R. van Eldik, *Inorg. Chim. Acta.*, **1983**, 301, 76.
14. B. Pitteri, G. Marangoni, L. Cattalini and T. Bobbo, *J. Chem. Soc., Dalton Trans.*, **1995**, 3853.
15. G. Annibale, M. Brandolisio, Ž. D. Bugarčić and L. Cattalini, *Transition Met. Chem.*, **1998**, 23, 715.
16. A. Hofmann, L. Dahlenburg and R. van Eldik, *Inorg. Chem.*, **2003**, 42, 6528.
17. Petrović, B., Bugarčić, Ž. D., Dees, A., Ivanović-Burmazović, I., Heinemann, F. W., Puchta, R., Steinmann, S. N., Corminboeuf, C., van Eldik, R., *Inorg. Chem.*, **2012**, 51, 1516.
18. A. Mambanda and D. Jaganyi, *Dalton Trans.*, **2011**, 40, 79.
19. D. Jaganyi, D. Reddy, J. A. Gertenbach, A. Hofmann and R. van Eldik, *Dalton Trans.*, **2004**, 0, 299.
20. S. Hochreuther, S. T. Nandibewoor, R. Puchta and R. van Eldik, *Dalton Trans.*, **2012**, 41, 512.
21. G. Bogdanović, V. Kojić, T. Srdić, D. Jakimov, M. Djuran, Ž. D. Bugarčić M. Baltić and V. V. Baldić, *Met.-Based Drugs*, **2002**, 9, 33.
22. B. Pitteri, M. Bortoluzzi and G. Marangoni, *Transition. Met. Chem.*, **2005**, 30, 1008.
23. L.R. Kelland, N.P. Farrell, *Platinum-Based Drugs in Cancer Therapy*, **2000**, Humana Press, p. 321-337.

24. J.D. Atwood, *Inorganic & Organometallic Reaction Mechanisms 2nd edition*, Wiley-VCH, New York Inc., Canada, **1997**, p. 43-62.
25. R.G. Wilkinson, *Kinetics and Mechanism of Reactions at Transition Metal Complexes, 2nd edition*, VCH, Weinheim, **1991**, p. 199-201, 232-242.
26. P. Banerjee, *Coord. Chem.*, **1999**, 190-192, 19 - 28.
27. D. Reddy, K. J. Akerman, M. P. Akerman, D. Jaganyi, *Transition Met. Chem.*, **2011**, 36, 593.
28. R.J. Sundberg and R. B. Martin, *Chem. Rev.*, **1974**, 74, 471.
29. C. A. Hitchcock, *Biochem. Soc. Trans.*, **1991**, 19, 782.
30. M. A. Jalil, S. Fujinami, H. Senda and H. Nishikawa, *J. Chem. Soc., Dalton Trans.*, **1999**, 1655.
31. R. Contreras, A. Flores-Parra, E. Mijangos, F. Telles, H. Lopez-Sandoval, N. Barba-Behenens, *Coord. Chem., Reviews*, **2009**, 253, 1979.
32. N.-D. Sung, K.-Y. Choi, H.-H. Lee, K.-C. Lee, M.-J. Kim, *Transition Met. Chem.*, **2005**, 30, 273.
33. B. Pitteri, G. Marangoni and L. Cattalini, *Polyhedron*, **1995**, 14, 17-18, 2331.
34. A. Hofmann, D. Jaganyi, O.Q. Munro, G. Liehr and R. van Eldik, *Inorg. Chem.*, **2003**, 42, 1688.
35. Origin7.5TM SRO, v7.5714 (B5714), Origin Lab Corporation, Northampton, One, Northampton, MA, 01060, USA, **2003**.
36. M. J. Frisch, G. W. Trucks, H. B. Schlegel, G. E. Scuseria, M. A. Robb, J. R. Cheeseman, G. Scalmani, V. Barone, B. Mennucci, G. A. Petersson, H. Nakatsuji, M. Caricato, X. Li, H. P. Hratchian, A. F. Izmaylov, J. Bloino, G. Zheng, J. L. Sonnenberg, M. Hada, M. Ehara, K. Toyota, R. Fukuda, J. Hasegawa, M. Ishida, T. Nakajima, Y. Honda, O. Kitao, H. Nakai, T. Vreven, J. A. Montgomery, Jr., J. E. Peralta, F. Ogliaro, M. Bearpark, J. J. Heyd, E. Brothers, K. N. Kudin, V. N. Staroverov, R. Kobayashi, J. Normand, K. Raghavachari, A. Rendell, J. C. Burant, S. S. Iyengar, J. Tomasi, M. Cossi, N. Rega, J. M. Millam, M. Klene, J. E. Knox, J. B. Cross, V. Bakken, C. Adamo, J. Jaramillo, R. Gomperts, R. E. Stratmann, O. Yazyev, A. J. Austin, R. Cammi, C. Pomelli, J. W. Ochterski, R. L. Martin, K. Morokuma, V. G. Zakrzewski, G. A. Voth, P. Salvador, J. J. Dannenberg, S. Dapprich, A. D. Daniels, O. Farkas, J. B. Foresman, J. V. Ortiz, J. Cioslowski, and D. J. Fox, *Gaussian 09, Revision C.1*, **2010**, Gaussian Inc., Wallingford CT.
37. Bruker APEX2, SAINT and SADABS. Bruker AXS Inc., **2010**, Madison, Wisconsin, USA.
38. G.M. Sheldick, *A short history of SHELX. Acta. Crystallogr. Sec. A*, **2008**, 64, 112 - 122.
39. O.V. Dolomanov, L.J. Bourhis, R.J. Gildea, J.A.K. Howard, H. Puschmann, *J. Appl. Cryst.* **2009**, 42, 229.

-
40. P. Ongoma and D. Jaganyi, *Dalton Trans.*, **2012**, *41*, 10724.
 41. D. Jaganyi, K-L. De Boer, J. Gertenbach, J. Perils, *Int. J. of Chem. Kinetics*, **2008**, 808.
 42. J.C. Bailar, H.J. Emeléus, R. Nyholm, A.F. Trotman-Dickenson, *Comprehensive Inorganic Chemistry*, Pergamon press, Oxford, New York, **1973**, p. 795 - 931.
 43. F.A. Cotton, G. Wilkinson, *Advanced Inorganic Chemistry 5th edition*, Wiley-Interscience, New York, **1988**, p.491 - 543.
 44. D.P. Rillema, A.J. Cruz, C. Moore, K. Siam, A. Jehan, D. Base, T. Nguyen and W. Huang, *Inorg. Chem.*, **2013**, *52*, p. 596.
 45. M. Schmulling, D.M. Grove, G. van Koten, R. van Eldik, N. Veldman and A.L. Spek, *Organometallics*, **1996**, *15*, 1384.
 46. L. Dadci, H. Elias, U. Frey, A. Hörnig, U. Koelle, A.E. Merbach, H. Paulus, J.S. Schneider, *Inorg. Chem.*, **1995**, *34*, 306.
 47. B. Pitteri and M. Bortoluzzi, *Polyhedron*, **2006**, *25*, 2698.
 48. B. Pitteri, G. Marangoni, L. Cattalini, F. Visentin, V. Bertolasi and P. Gilli, *Polyhedron*, **2001**, *20*, 869.
 49. B. Pitteri and M. Bortoluzzi, *Eur. J. Inorg. Chem.*, **2007**, *28*, 4456.
 50. A. Shaira, D. Reddy and D. Jaganyi, *Dalton Trans.*, **2013**, *42*, 8426.
 51. U. Belluco, L. Cattalini, F. Basolo, R.G. Pearson and A. Turco, *J. Am. Chem. Soc.*, **1965**, *87*, *2*, 241.
 52. A.R. Katritzky, A.F. Pozharski, *Handbook of Heterocyclic Chemistry 2nd edition* Pergamon/Elsevier, **2000**, p. 177, 377.
 53. M. Akerman, K. Akerman, D. Jaganyi and D. Reddy, *Acta Cryst.*, 2011, E67, m1075.
 54. M. Akerman, K. Akerman, D. Jaganyi and D. Reddy, *Acta Cryst.*, 2010, C67, m290.
 55. A.R. Katritzky, C.W. Rees, *Comprehensive heterocyclic chemistry, vol 5*. Pergamon Press, Oxford, **1984**, p. 35 - 50, 169 - 225.
 56. T. Eicher and S. Hauptmann, *The Chemistry of Heterocycles*, Wiley-VCH Verlas GmbH & Co. KGaA, Weinheim, **2003**, p. 165 - 173, 179 - 184, 208 - 212.

5.7. Supporting Information 5

This includes NMR, IR and mass spectra, a summary of the selected wavelengths used in kinetic measurements, kinetic traces, tables representing a summary of all k_{obs} values determined, concentration dependence and Eyring plots for determination of second-order rate constant and activation parameters respectively, electrostatic potential surfaces and planarity diagrams of the complexes, additional X-ray crystal diagrams and X-ray crystallographic data in a CIF file.

Elemental Composition Report

Single Mass Analysis

Tolerance = 5.0 PPM / DBE: min = -1.5, max = 50.0

Element prediction: Off

Number of isotope peaks used for i-FIT = 3

Monoisotopic Mass, Odd and Even Electron Ions

22 formula(e) evaluated with 1 results within limits (all results (up to 1000) for each mass)

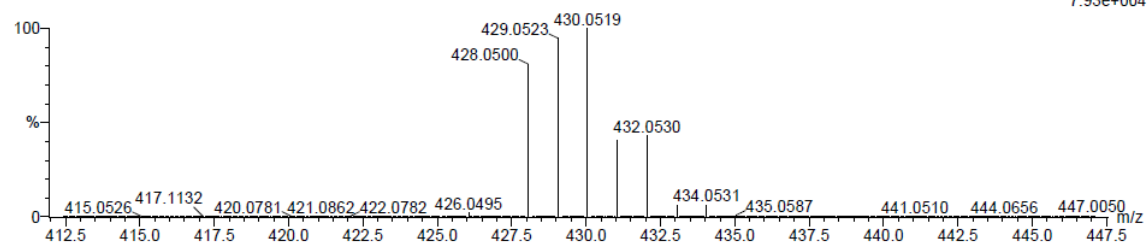
Elements Used:

C: 10-15 H: 10-15 N: 0-5 Cl: 0-1 Pt: 0-2

Sli

Pt dpa 4 (0.051) Cm (1:31)

TOF MS ES+
7.93e+004



Minimum:

Maximum: 5.0 5.0 -1.5

5.0 5.0 50.0

Mass	Calc. Mass	mDa	PPM	DBE	i-FIT	i-FIT (Norm)	Formula
430.0519	430.0524	-0.5	-1.2	8.0	542.4	0.0	C12 H14 N3 Cl Pt

Figure S5.1: Mass spectrum of the complex, [Pt(bis(2-pyridylmethyl) amine)Cl](ClO₄), Ptdpa.

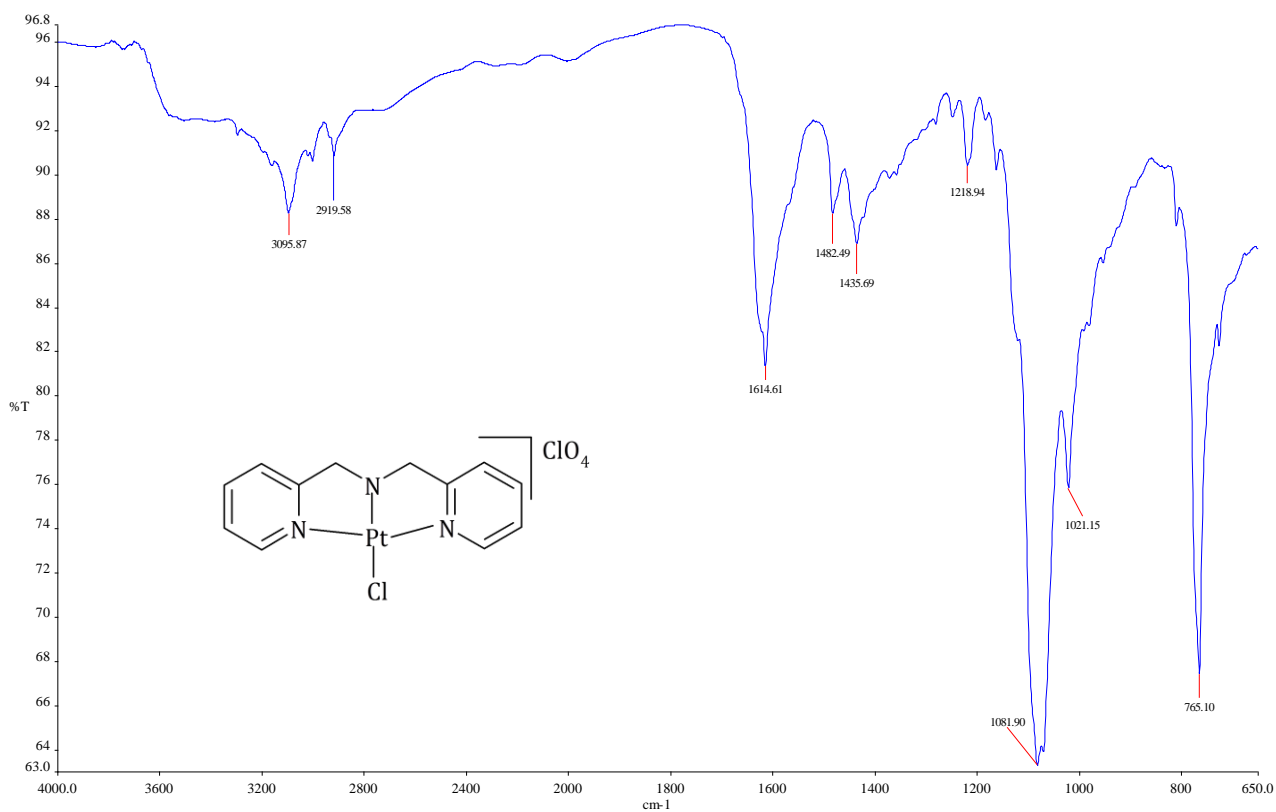


Figure S5.2: Infrared spectrum of [Pt(bis(2-pyridylmethyl) amine)Cl](ClO₄), **Ptdpa**.

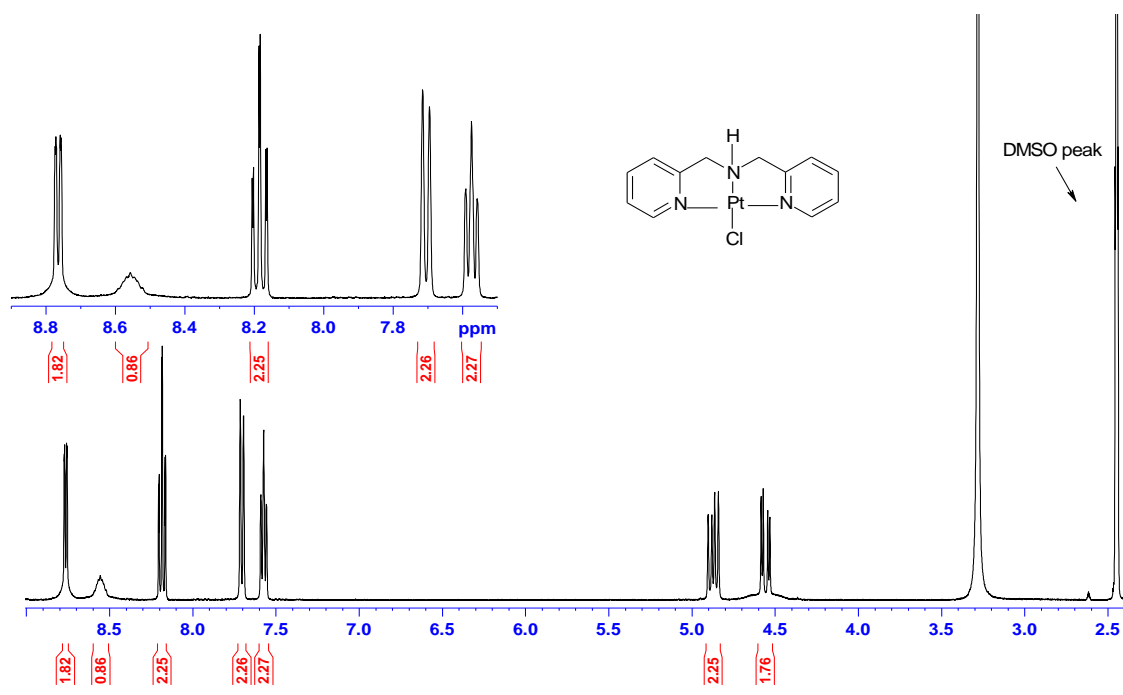


Figure S5.3: ¹H NMR of [Pt(bis(2-pyridylmethyl) amine)Cl](ClO₄), **Ptdpa** in DMSO-*d*₆.

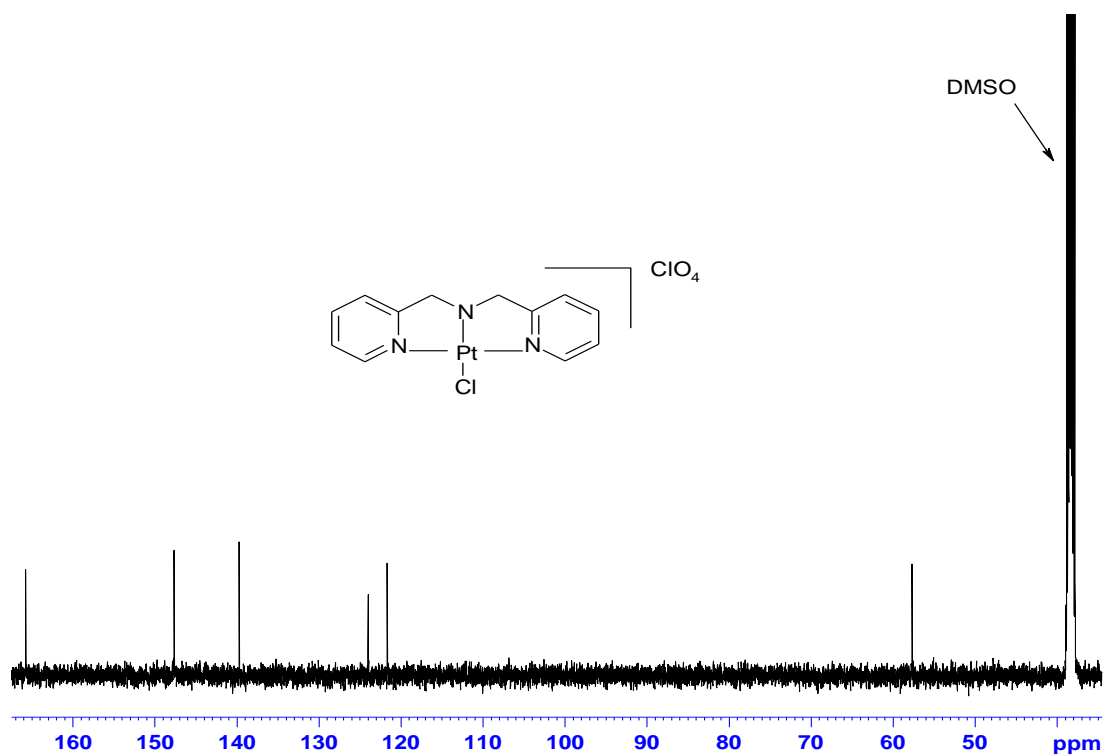


Figure S5.4: ¹³C NMR spectrum of [Pt(bis(2-pyridylmethyl) amine)Cl](ClO₄), **Ptdpa** in DMSO-*d*₆.

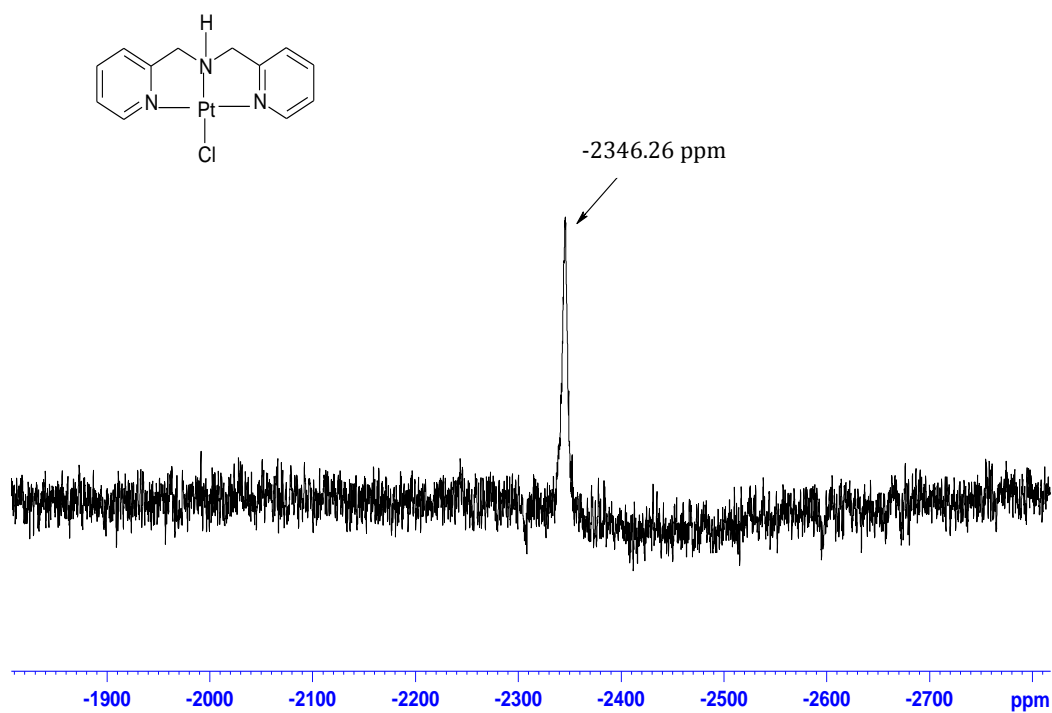


Figure S5.5: ¹⁹⁵Pt NMR spectrum of [Pt(bis(2-pyridylmethyl) amine)Cl](ClO₄), **Ptdpa** in DMSO-*d*₆.

Single Mass Analysis

Tolerance = 5.0 PPM / DBE: min = -1.5, max = 50.0

Element prediction: Off

Number of isotope peaks used for i-FIT = 3

Monoisotopic Mass, Even Electron Ions

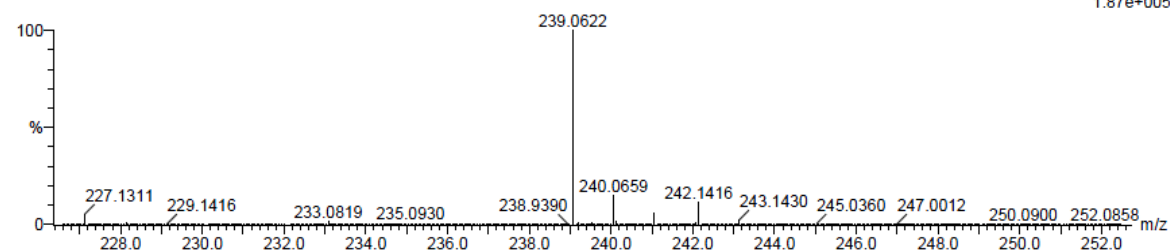
9 formula(e) evaluated with 1 results within limits (all results (up to 1000) for each mass)

Elements Used:

C: 10-15 H: 10-15 N: 0-5 Na: 0-1 S: 0-1

Sli

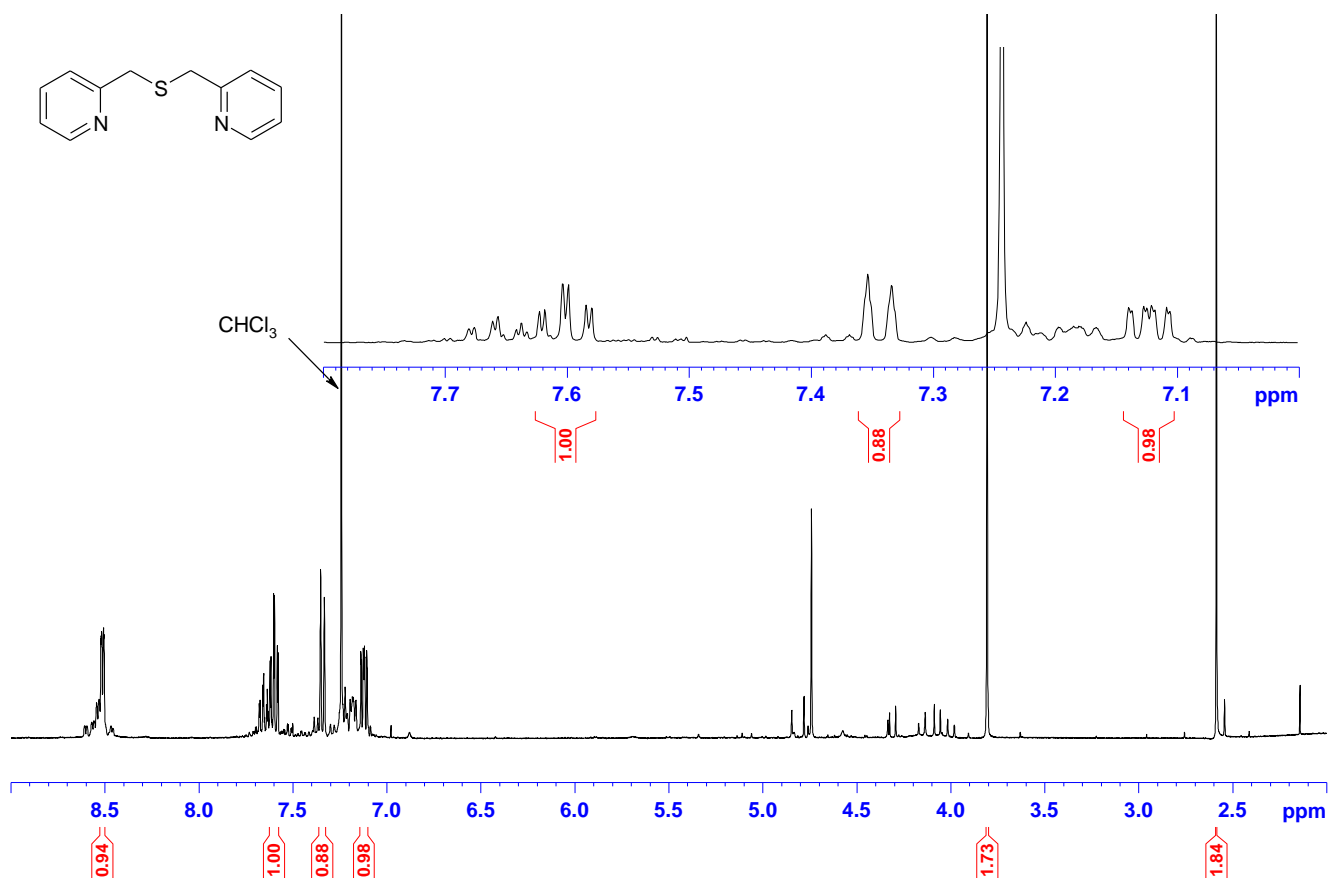
dps 10 (0.153) Cm (1:31)

TOF MS ES+
1.87e+005

Minimum:

Maximum:

Mass	Calc. Mass	mDa	PPM	DBE	i-FIT	i-FIT (Norm)	Formula
239.0622	239.0619	0.3	1.3	7.5	630.1	0.0	C12 H12 N2 Na S

Figure S5.6. Mass spectrum of the ligand, (bis(2-pyridylmethyl) sulfide) **dps**.Figure S5.7: ^1H NMR spectrum of the ligand, (bis(2-pyridylmethyl) sulphide) **dps** in CDCl_3 .

Single Mass Analysis

Tolerance = 5.0 PPM / DBE: min = -1.5, max = 50.0

Element prediction: Off

Number of isotope peaks used for i-FIT = 3

Monoisotopic Mass, Odd and Even Electron Ions

33 formula(e) evaluated with 1 results within limits (all results (up to 1000) for each mass)

Elements Used:

C: 10-15 H: 10-15 N: 0-5 S: 0-1 Cl: 0-1 Pt: 0-1

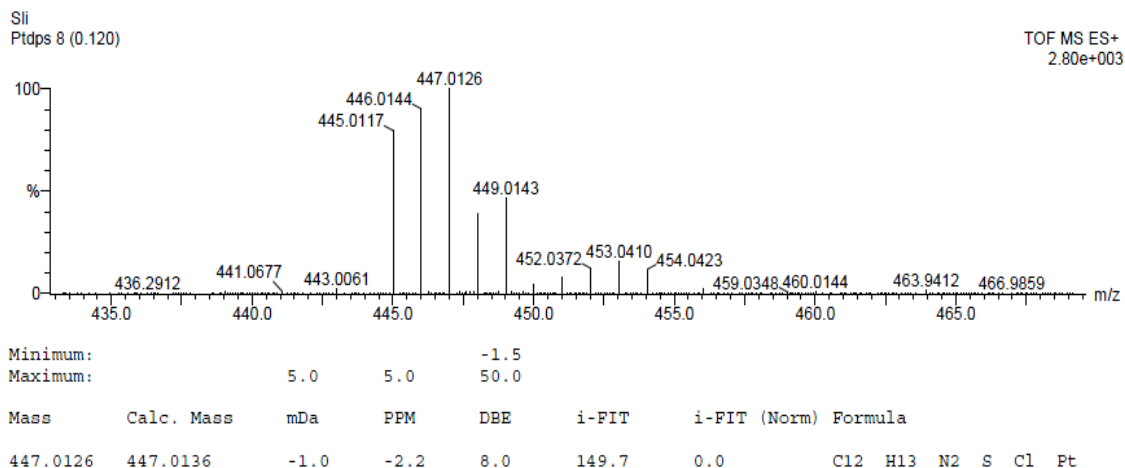


Figure S5.8: Mass spectrum for the complex, [Pt(bis(2-pyridylmethyl)sulfide)Cl](ClO₄) Ptdps.

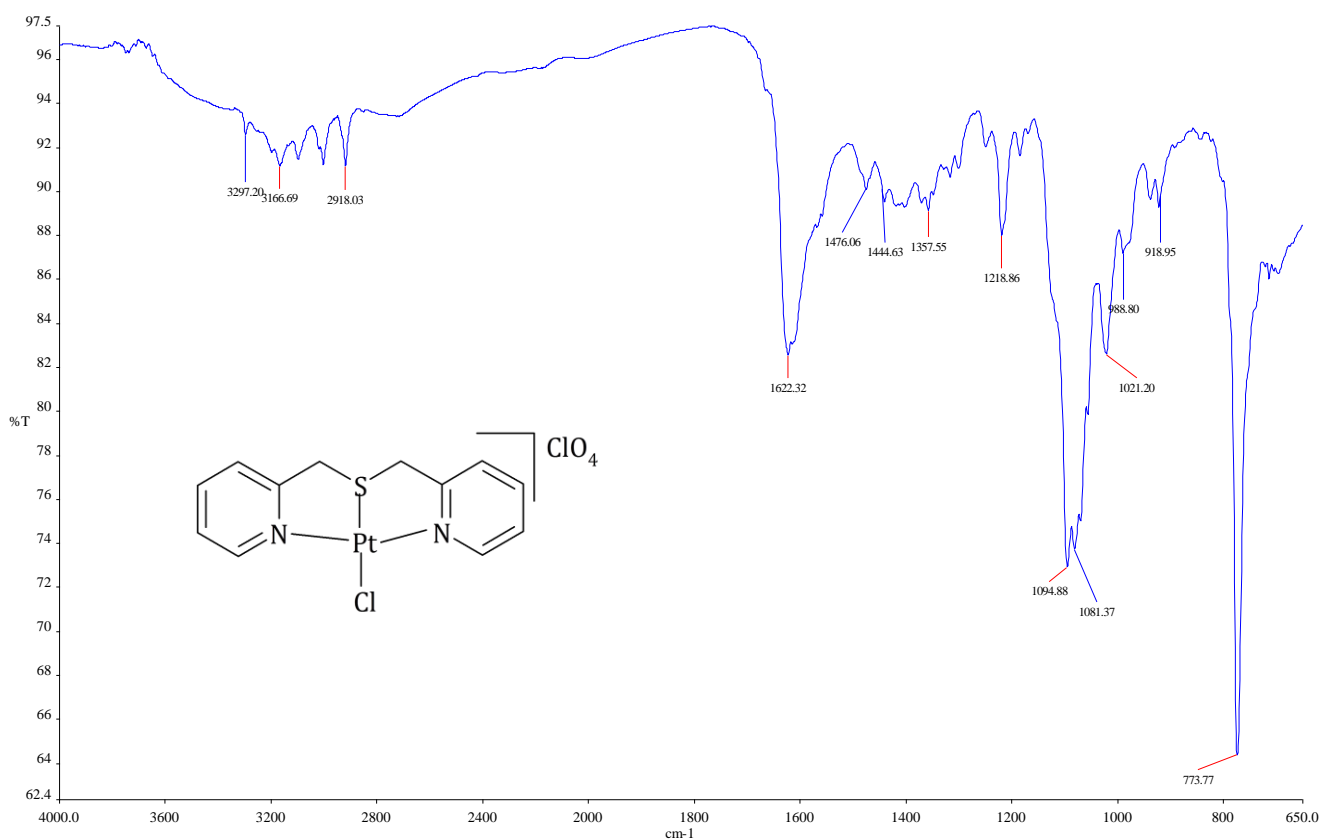


Figure S5.9: Infrared spectrum of [Pt(bis(2-pyridylmethyl) sulfide)Cl](ClO₄), Ptdps.

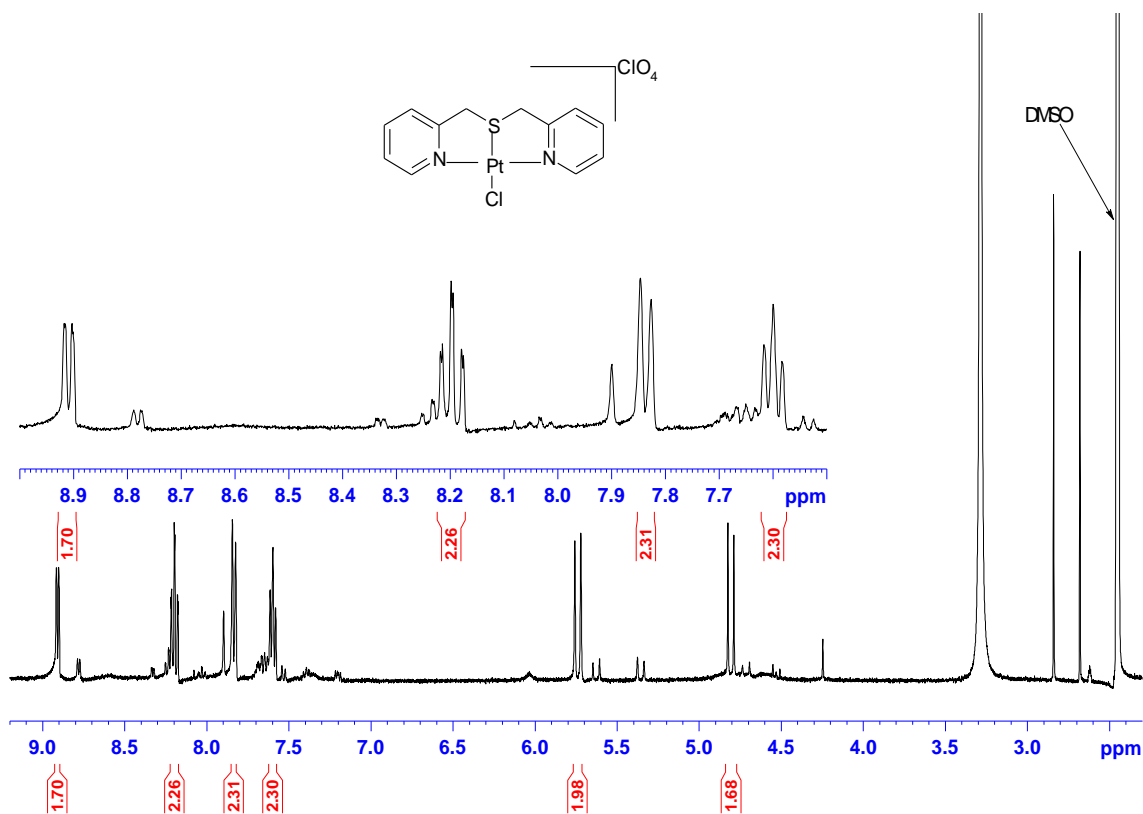


Figure S5.10: ^1H NMR spectrum of $[\text{Pt}(\text{bis}(2\text{-pyridylmethyl})\text{ sulfide})\text{Cl}](\text{ClO}_4)$, **Ptdps** in $\text{DMSO-}d_6$.

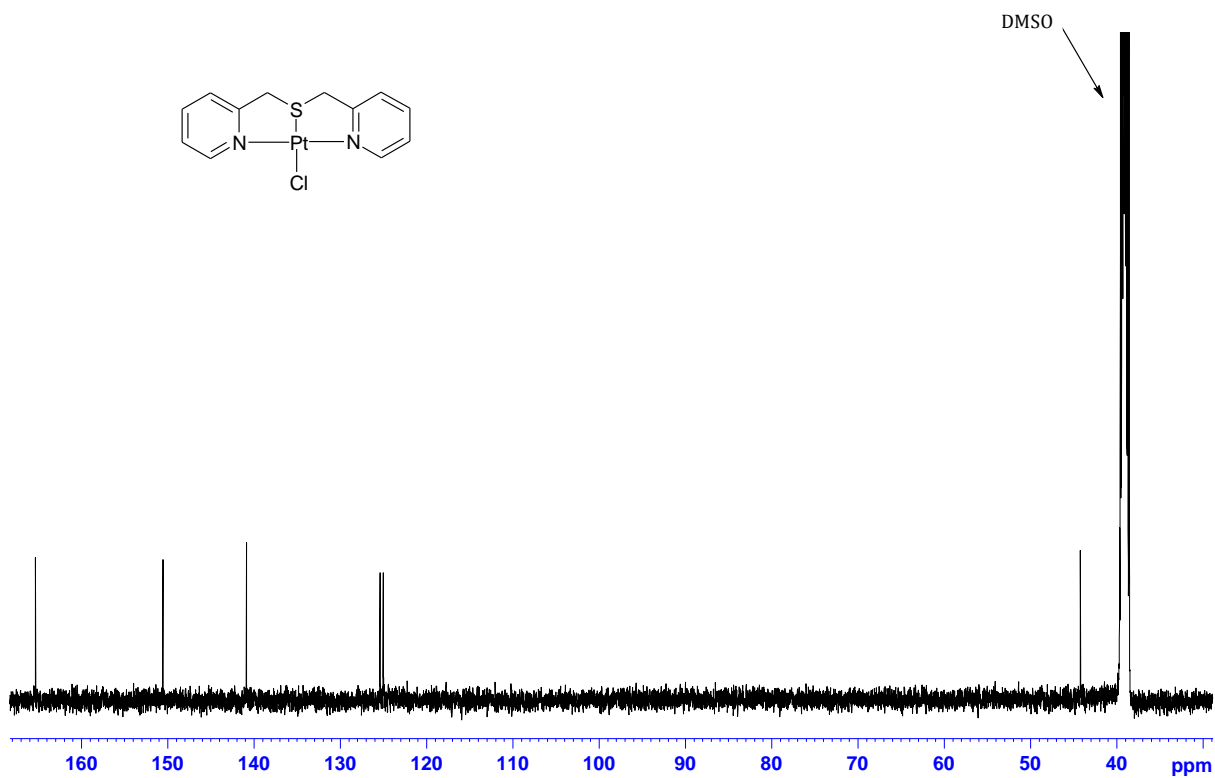


Figure S5.11: ^{13}C NMR spectrum of $[\text{Pt}(\text{bis}(2\text{-pyridylmethyl})\text{ sulfide})\text{Cl}](\text{ClO}_4)$, **Ptdps**.

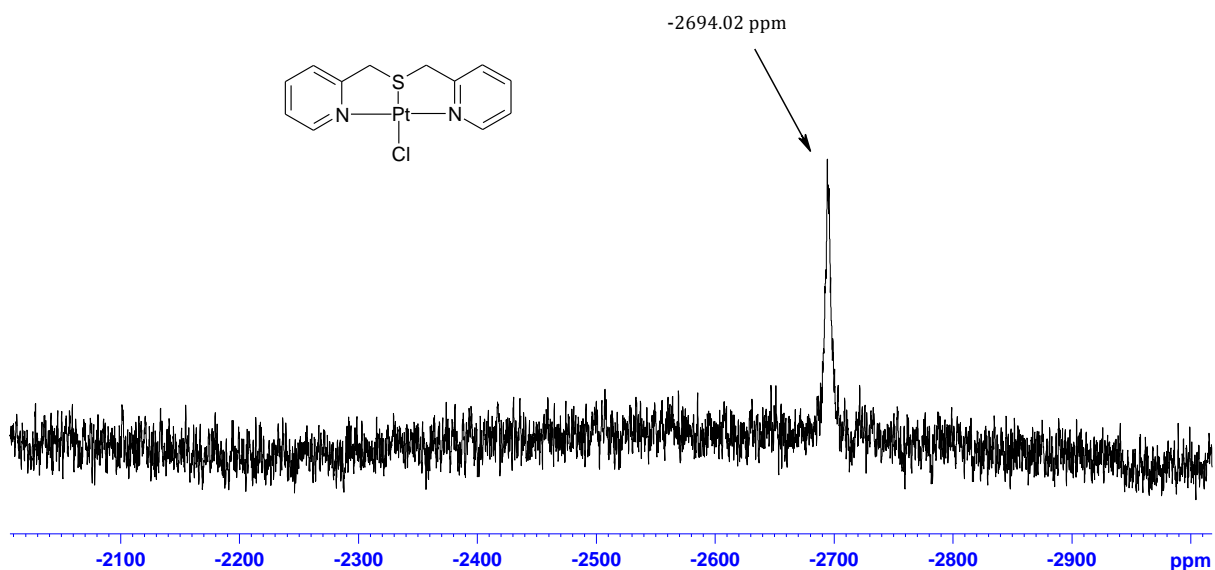


Figure S5.12: ¹⁹⁵Pt NMR of [Pt(bis(2-pyridylmethyl) sulfide)Cl](ClO₄), **Ptdps** in DMSO-*d*₆.

Table S5.1: X-ray crystallographic details for [PtdpsCl](ClO₄)·CH₃NO₂

Crystal data

Chemical formula	C ₁₂ H ₁₂ ClN ₂ PtS·ClO ₄ ·CH ₃ NO ₂
Mr (g mol ⁻¹)	607.33
Crystal system	Monoclinic
Space group	P21/c
Temperature (K)	100
a (Å)	14.6795 (5)
b (Å)	7.2800 (3)
c (Å)	17.2174 (6)
β (°)	103.086 (2)
V (Å ³)	1792.19 (11)
Z	4
Radiation type	Mo Kα
Crystal size (mm)	0.28 × 0.20 × 0.10

Data collection

Diffractometer	Bruker APEX II Duo diffractometer
Absorption correction	Multi-scan
T _{min} / T _{max}	0.205, 0.491
No. of measured, independent	18487, 5463, 5101

and observed [$I > 2\sigma(I)$] reflections

R_{int} 0.026

$(\sin \theta/\lambda)_{\text{max}}$ (\AA^{-1}) 0.715

Refinement

$R[F_2 > 2\sigma(F_2)], wR(F_2), S$ 0.026, 0.066, 1.05

No. of reflections 5463

No. of parameters 236

No. of restraints 0

H-atom treatment H-atom parameters constrained

$\Delta_{\text{max}}, \Delta_{\text{min}}$ ($e \text{\AA}^{-3}$) 3.41, -3.07

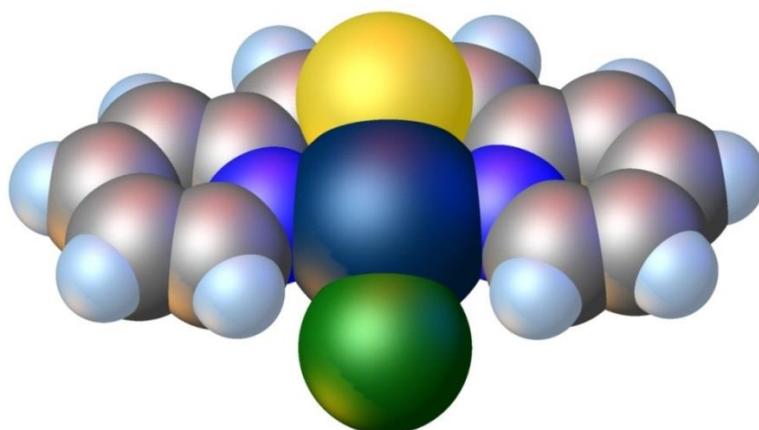


Figure S5.13: Space-fill plot of the cation in **Ptdps_Cl**.

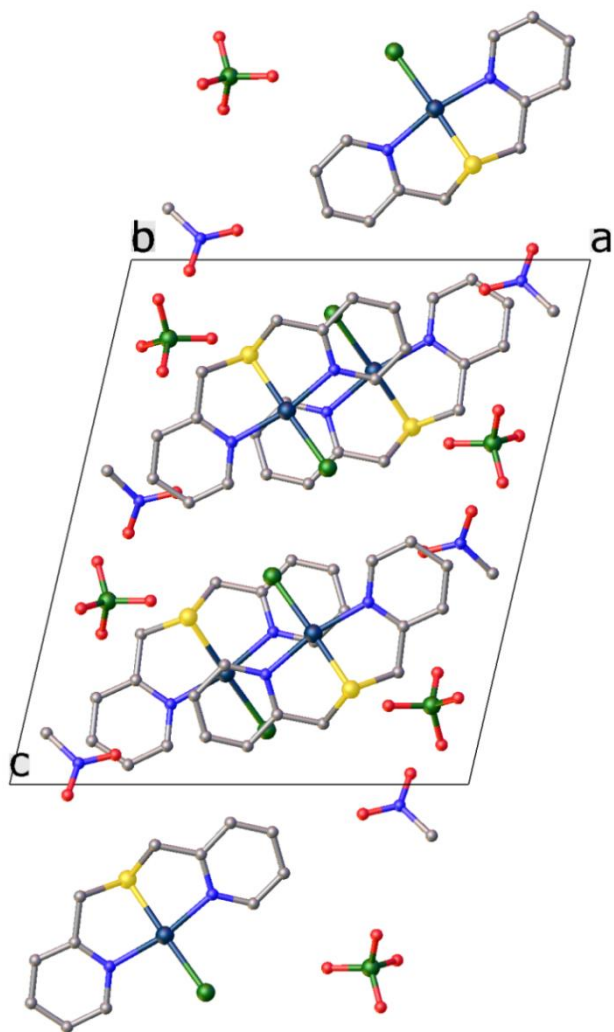


Figure S5.14: Unit cell contents viewed along $[0,1,0]$ of **Ptdps**. H-atoms have been omitted for clarity.

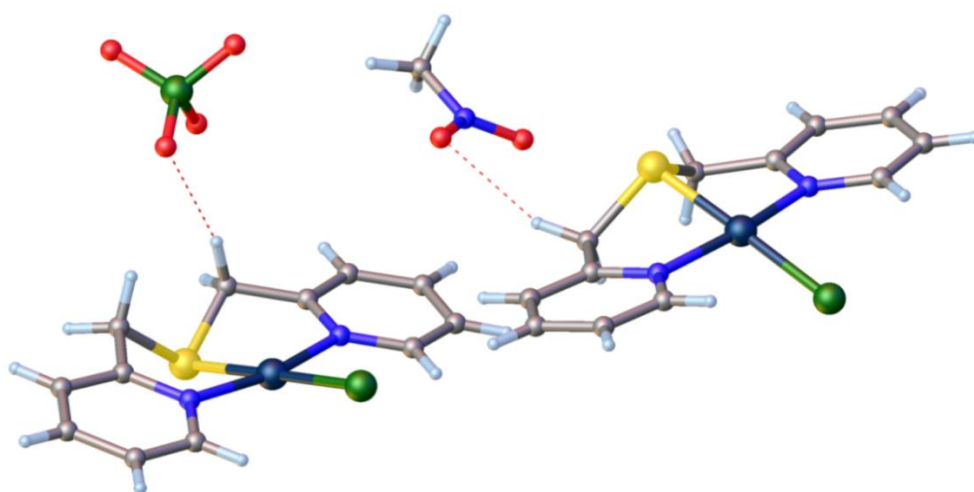


Figure S5.15: Cation to anion and cation to solvent contacts within the crystal structure.

Table S5.2: Selected X-ray determined geometric parameters (Å, °) for **Ptdps_Cl**

Pt1—N2	2.015 (2)	C7—C8	1.503 (4)
Pt1—N1	2.027 (2)	C7—H7A	0.9900
Pt1—S1	2.2277 (6)	C7—H7B	0.9900
Pt1—Cl1	2.3228 (6)	C8—C9	1.389 (3)
S1—C6	1.831 (3)	C9—C10	1.377 (4)
S1—C7	1.836 (3)	C9—H9	0.9500
N1—C1	1.353 (3)	C10—C11	1.391 (4)
N1—C5	1.362 (4)	C10—H10	0.9500
N2—C12	1.355 (3)	C11—C12	1.381 (4)
N2—C8	1.361 (3)	C11—H11	0.9500
C1—C2	1.382 (4)	C12—H12	0.9500
C1—H1	0.9500	C12—O2	1.429 (3)
C2—C3	1.389 (4)	C12—O4	1.435 (3)
C2—H2	0.9500	C12—O1	1.435 (3)
C3—C4	1.391 (4)	C12—O3	1.446 (2)
C3—H3	0.9500	O5—N3	1.220 (3)
C4—C5	1.387 (4)	O6—N3	1.219 (4)
C4—H4	0.9500	N3—C13	1.474 (4)
C5—C6	1.500 (4)	C13—H13A	0.9800
C6—H6A	0.9900	C13—H13B	0.9800
C6—H6B	0.9900	C13—H13C	0.9800
N2—Pt1—N1	168.24 (10)	C8—C7—S1	106.79 (18)
N2—Pt1—S1	84.70 (7)	C8—C7—H7A	110.4
N1—Pt1—S1	85.33 (7)	S1—C7—H7A	110.4
N2—Pt1—Cl1	93.62 (7)	C8—C7—H7B	110.4
N1—Pt1—Cl1	96.36 (7)	S1—C7—H7B	110.4
S1—Pt1—Cl1	178.31 (2)	H7A—C7—H7B	108.6
C6—S1—C7	105.46 (14)	N2—C8—C9	120.8 (2)
C6—S1—Pt1	94.69 (9)	N2—C8—C7	117.8 (2)
C7—S1—Pt1	93.09 (9)	C9—C8—C7	121.3 (2)
C1—N1—C5	119.6 (2)	C10—C9—C8	119.7 (2)
C1—N1—Pt1	124.59 (19)	C10—C9—H9	120.1
C5—N1—Pt1	115.63 (19)	C8—C9—H9	120.1
C12—N2—C8	119.5 (2)	C9—C10—C11	119.1 (2)
C12—N2—Pt1	125.30 (19)	C9—C10—H10	120.4
C8—N2—Pt1	115.21 (18)	C11—C10—H10	120.4

N1—C1—C2	121.5 (3)	C12—C11—C10	119.4 (3)
N1—C1—H1	119.3	C12—C11—H11	120.3
C2—C1—H1	119.3	C10—C11—H11	120.3
C1—C2—C3	119.9 (3)	N2—C12—C11	121.4 (3)
C1—C2—H2	120.1	N2—C12—H12	119.3
C3—C2—H2	120.1	C11—C12—H12	119.3
C2—C3—C4	118.1 (3)	O2—C12—O4	109.3 (2)
C2—C3—H3	120.9	O2—C12—O1	110.3 (2)
C4—C3—H3	120.9	O4—C12—O1	109.3 (2)
C5—C4—C3	120.4 (3)	O2—C12—O3	109.74 (17)
C5—C4—H4	119.8	O4—C12—O3	109.23 (17)
C3—C4—H4	119.8	O1—C12—O3	109.01 (16)
N1—C5—C4	120.4 (3)	O6—N3—O5	122.8 (3)
N1—C5—C6	118.3 (3)	O6—N3—C13	119.0 (3)
C4—C5—C6	121.2 (3)	O5—N3—C13	118.2 (3)
C5—C6—S1	107.6 (2)	N3—C13—H13A	109.5
C5—C6—H6A	110.2	N3—C13—H13B	109.5
S1—C6—H6A	110.2	H13A—C13—H13B	109.5
C5—C6—H6B	110.2	N3—C13—H13C	109.5
S1—C6—H6B	110.2	H13A—C13—H13C	109.5
H6A—C6—H6B	108.5	H13B—C13—H13C	109.5
N2—Pt1—S1—C6	-141.84 (13)	Pt1—N1—C5—C4	176.7 (2)
N1—Pt1—S1—C6	31.91 (13)	C1—N1—C5—C6	179.4 (3)
Cl1—Pt1—S1—C6	-149.0 (9)	Pt1—N1—C5—C6	-4.7 (3)
N2—Pt1—S1—C7	-36.05 (12)	C3—C4—C5—N1	-0.2 (5)
N1—Pt1—S1—C7	137.71 (12)	C3—C4—C5—C6	-178.8 (3)
Cl1—Pt1—S1—C7	-43.2 (9)	N1—C5—C6—S1	34.7 (3)
N2—Pt1—N1—C1	-173.0 (4)	C4—C5—C6—S1	-146.7 (2)
S1—Pt1—N1—C1	154.9 (2)	C7—S1—C6—C5	-136.7 (2)
Cl1—Pt1—N1—C1	-25.1 (2)	Pt1—S1—C6—C5	-42.1 (2)
N2—Pt1—N1—C5	11.4 (6)	C6—S1—C7—C8	141.27 (19)
S1—Pt1—N1—C5	-20.75 (19)	Pt1—S1—C7—C8	45.54 (18)
Cl1—Pt1—N1—C5	159.28 (19)	C12—N2—C8—C9	-0.4 (4)
N1—Pt1—N2—C12	175.4 (4)	Pt1—N2—C8—C9	-178.8 (2)
S1—Pt1—N2—C12	-152.5 (2)	C12—N2—C8—C7	179.4 (3)
Cl1—Pt1—N2—C12	27.3 (2)	Pt1—N2—C8—C7	1.0 (3)
N1—Pt1—N2—C8	-6.4 (6)	S1—C7—C8—N2	-35.0 (3)
S1—Pt1—N2—C8	25.79 (19)	S1—C7—C8—C9	144.8 (3)
Cl1—Pt1—N2—C8	-154.4 (2)	N2—C8—C9—C10	0.6 (5)

C5—N1—C1—C2	-0.6 (4)	C7—C8—C9—C10	-179.1 (3)
Pt1—N1—C1—C2	-176.1 (2)	C8—C9—C10—C11	-0.3 (5)
N1—C1—C2—C3	-0.3 (5)	C9—C10—C11—C12	-0.2 (5)
C1—C2—C3—C4	0.9 (5)	C8—N2—C12—C11	-0.2 (4)
C2—C3—C4—C5	-0.7 (5)	Pt1—N2—C12—C11	178.0 (2)
C1—N1—C5—C4	0.8 (4)	C10—C11—C12—N2	0.5 (4)

CIF Check Report for Ptdps Cl

Check CIF/PLATON report (basic structural check)

Datablock: mo_dj_sli_ptl6_cl_0m

Bond precision: C-C = 0.0040 Å	Wavelength=0.71073	
Cell: a=14.6795 (5) b=7.2800 (3) c=17.2174 (6)		
alpha=90 beta=103.086 (2) gamma=90		
Temperature: 100 K		
	Calculated	Reported
Volume	1792.19 (12)	1792.19 (11)
Space group	P 21/c	P21/c
Hall group	-P 2ybc	-P 2ybc
Moiety formula	C12 H12 Cl N2 Pt S, Cl O4, C H3 N O2	C12 H12 Cl N2 Pt S, Cl O4, C H3 N O2
Sum formula	C13 H15 Cl2 N3 O6 Pt S	C13 H15 Cl2 N3 O6 Pt S
Mr	607.33	607.33
Dx, g cm ⁻³	2.251	2.251
Z	4	4
Mu (mm ⁻¹)	8.281	0.000
F000	1160.0	1160.0
F000'	1155.62	
h, k, lmax	20, 10, 24	21, 10, 24
Nref	5511	5463
Tmin, Tmax		0.205, 0.491
Tmin'		
Correction method= MULTI-SCAN		
Data completeness= 0.991 Theta(max)= 30.560		
R(reflections)= 0.0255 (5101)	wR2(reflections)= 0.0662 (5463)	
S = 1.045	Npar= 236	

The following ALERTS were generated. Each ALERT has the format

test-name_ALERT_alert-type_alert-level.

Click on the hyperlinks for more details of the test.

● Alert level C

[PLAT244 ALERT 4 C](#) Low 'Solvent' Ueq as Compared to Neighbors of Cl2

[PLAT250 ALERT 2 C](#) Large U3/U1 Ratio for Average U(i,j) Tensor 2.2

Alert level G

[PLAT232 ALERT 2 G](#) Hirshfeld Test Diff (M-X) Pt1 -- Cl1 .. 5.7 su

[PLAT232 ALERT 2 G](#) Hirshfeld Test Diff (M-X) Pt1 -- S1 .. 8.3 su

[PLAT710 ALERT 4 G](#) Delete 1-2-3 or 2-3-4 Linear Torsion Angle ... # 3

CL1 -PT1 -S1 -C6 -149.00 0.90 1.555 1.555 1.555 1.555

[PLAT710 ALERT 4 G](#) Delete 1-2-3 or 2-3-4 Linear Torsion Angle ... # 6

CL1 -PT1 -S1 -C7 -43.20 0.90 1.555 1.555 1.555 1.555

PLATON version of 05/11/2012; check.def file version of 05/11/2012

Datablock mo_dj_sli_ptl6_cl_0m - ellipsoid plot

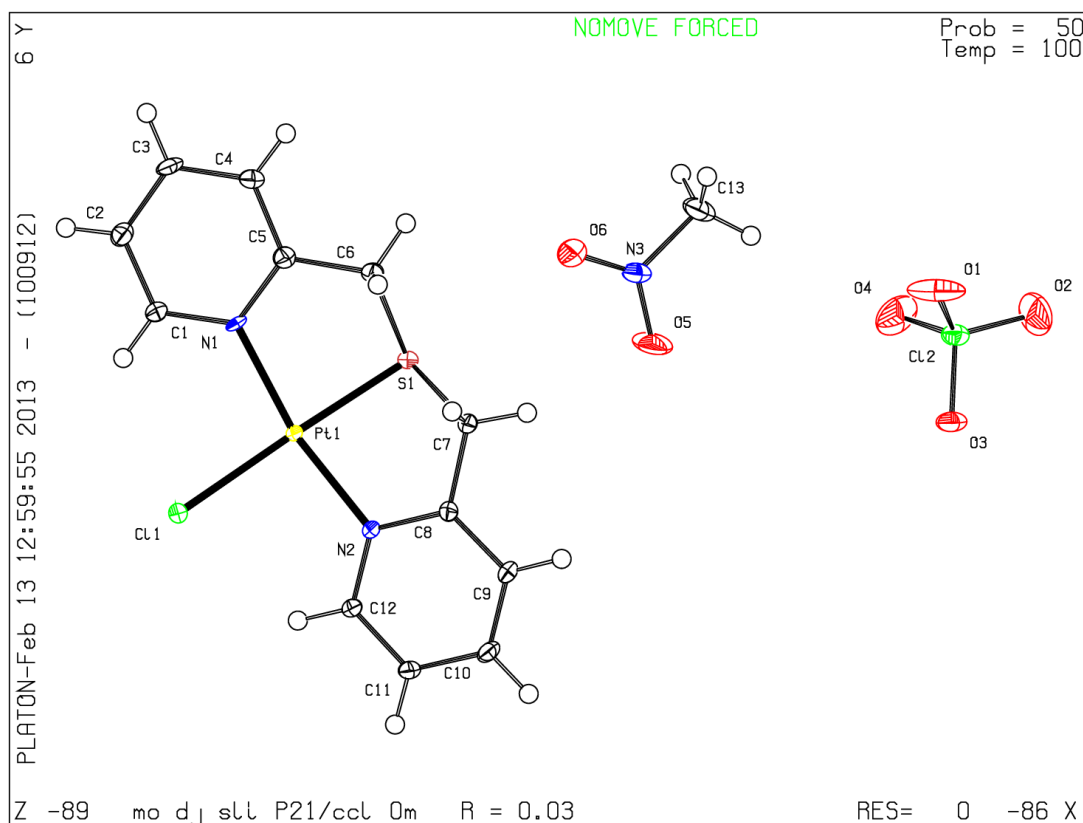
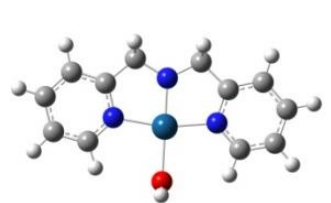




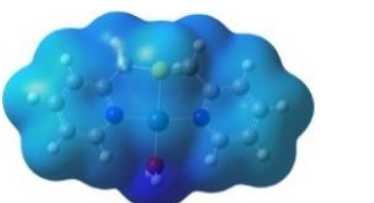


Table S5.3: DFT calculated electrostatic potential surfaces (ESP) and planarity of the platinum(II) complexes investigated.

COMPLEXE STRUCTURE	PLANARITY	ESP MAPPING
		 <p style="text-align: center;">Electronegativity →</p>
Ptdpa		
		
Ptdps		

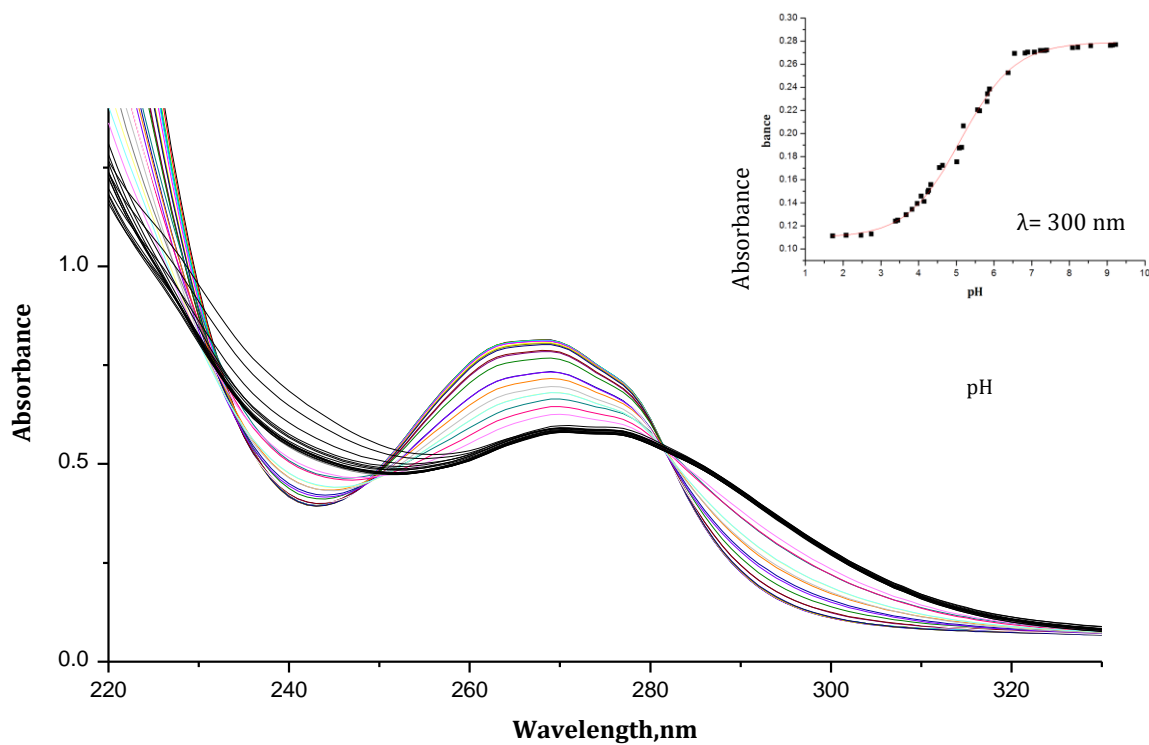


Figure S5.16: UV-visible spectra for the titration of 0.1 mM **Ptdps** with NaOH, pH range 1–10, $T= 298$ K. Inset: Plot of absorbance vs. pH at the specified wavelength.

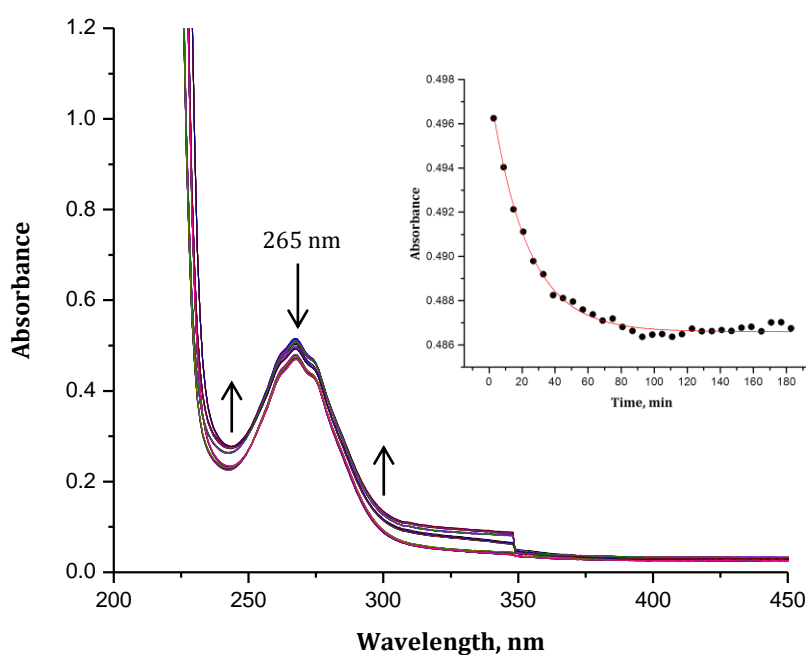


Figure S5.17: UV-visible absorbance spectra of **Ptdpa** (1.03×10^{-4} M) and **MIm** (2.58×10^{-3} M) at an ionic strength of 0.1 M, at 298 K. Inset is a kinetic trace at 264 nm.

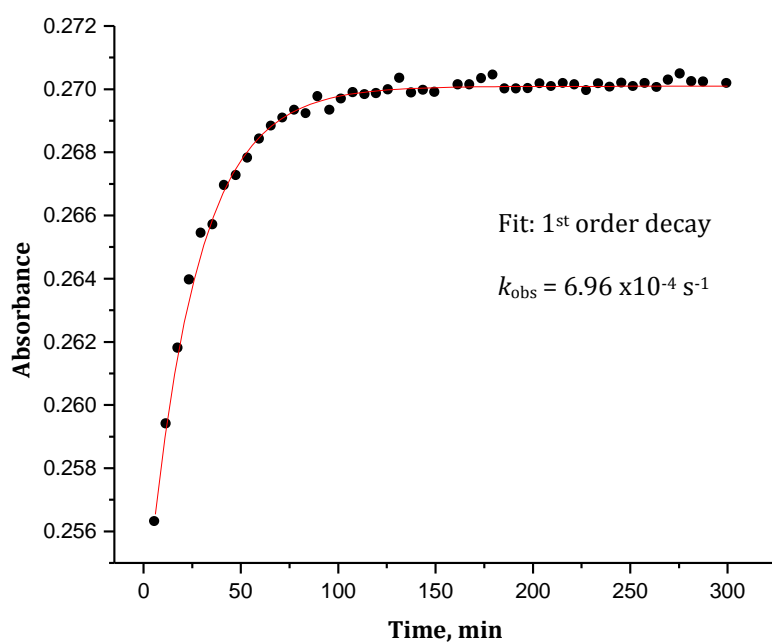


Figure S5.18: UV/Visible absorption versus time kinetic trace of **Ptdpa** (1.03×10^{-4} M) with imidazole (1.54×10^{-3} M (30 fold)) taken at 290 nm, at T = 298 K.

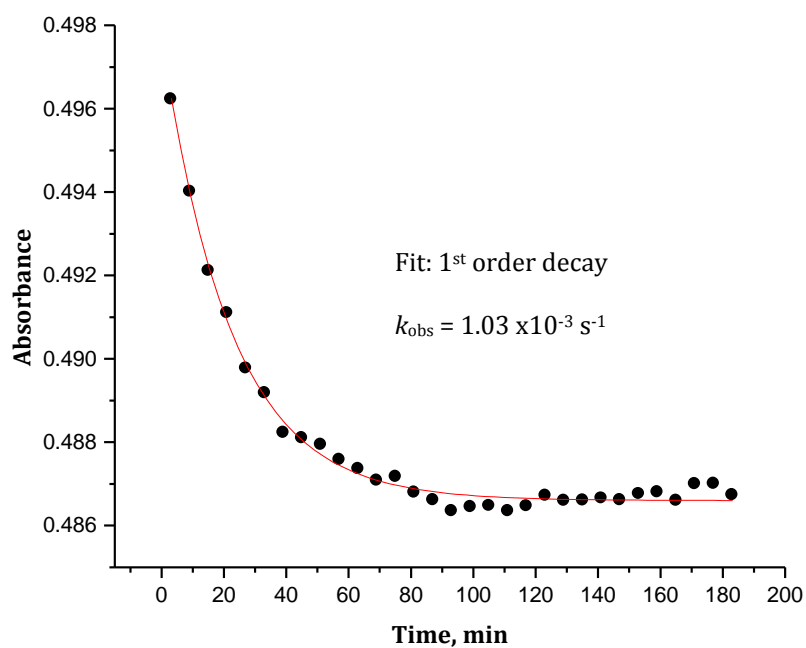


Figure S5.19: UV/Visible absorption versus time kinetic trace of **Ptdpa** ($1.03 \times 10^{-4} \text{ M}$) with 1-methylimidazole ($1.03 \times 10^{-3} \text{ M}$ (20 fold) taken at 264 nm and at 298 K.

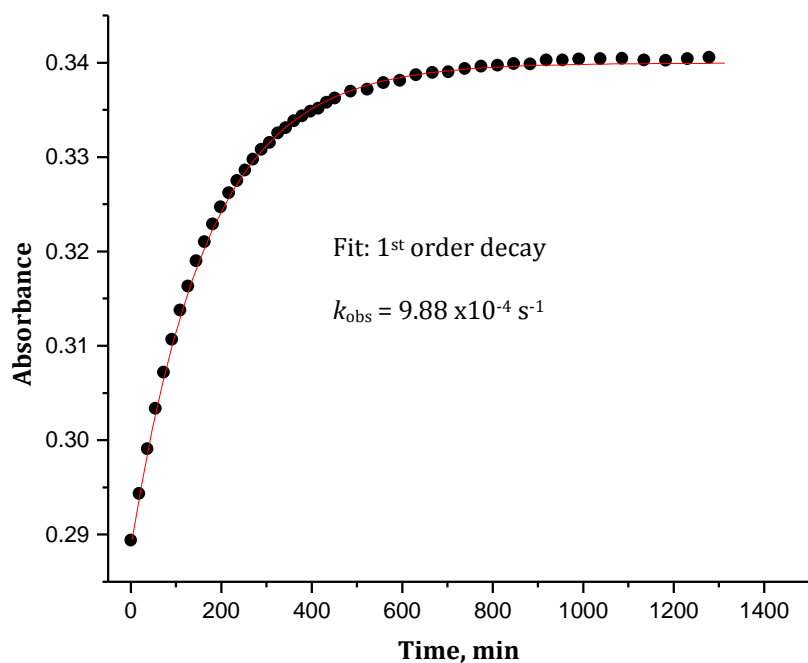


Figure S5.20: UV/Visible absorption versus time kinetic trace of **Ptdpa** ($1.03 \times 10^{-4} \text{ M}$) with pyrazole ($5.14 \times 10^{-3} \text{ M}$ (10 fold) taken at 250 nm and at 298 K.

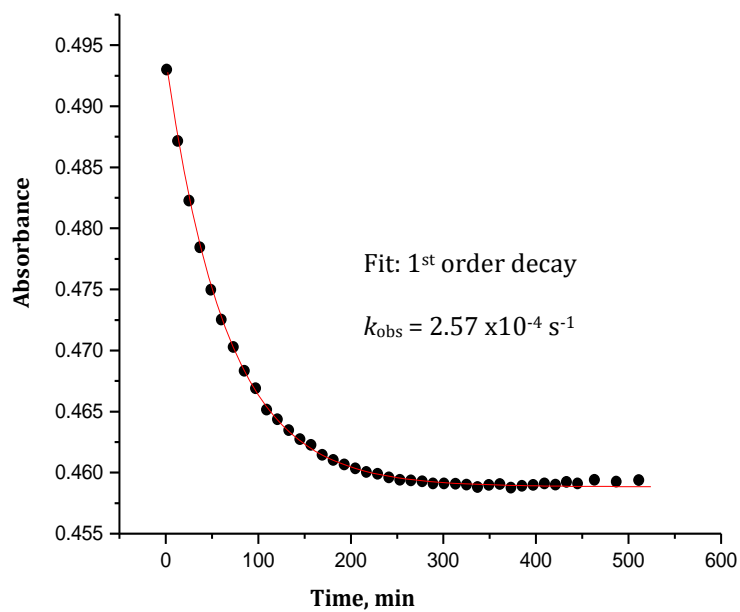


Figure S5.21: UV/Visible absorption versus time kinetic trace of **Ptdpa** ($1.03 \times 10^{-4} \text{ M}$) with 1,2,4-triazole ($1.03 \times 10^{-3} \text{ M}$ (20 fold)) taken at 273 nm, at $T = 298 \text{ K}$.

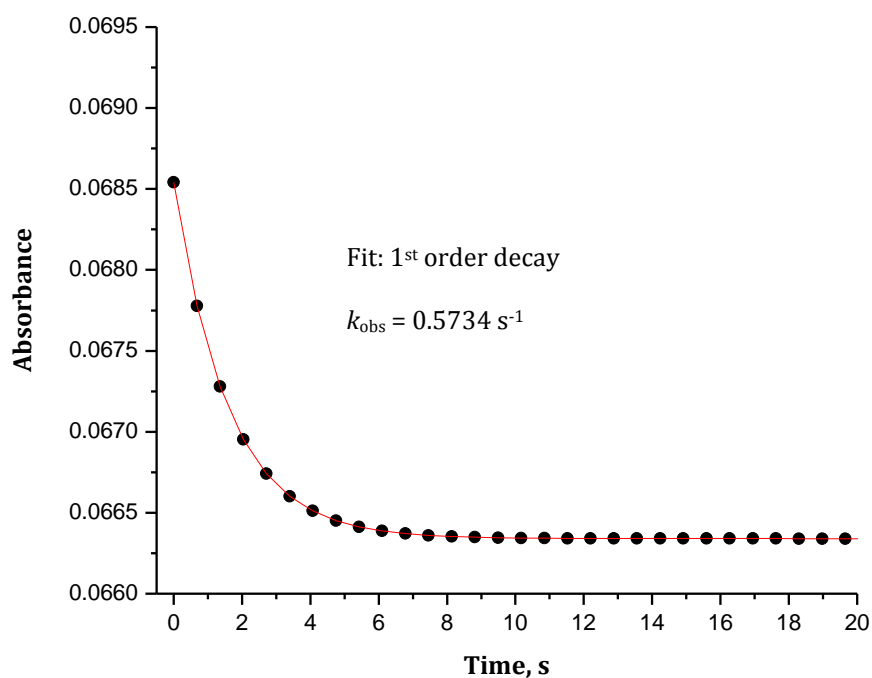


Figure S5.22: UV/Visible absorption versus time kinetic trace of **Ptdps** ($1.04 \times 10^{-4} \text{ M}$) with imidazole ($1.04 \times 10^{-3} \text{ M}$ (10 fold)) taken at 265 nm, at $T = 298 \text{ K}$.

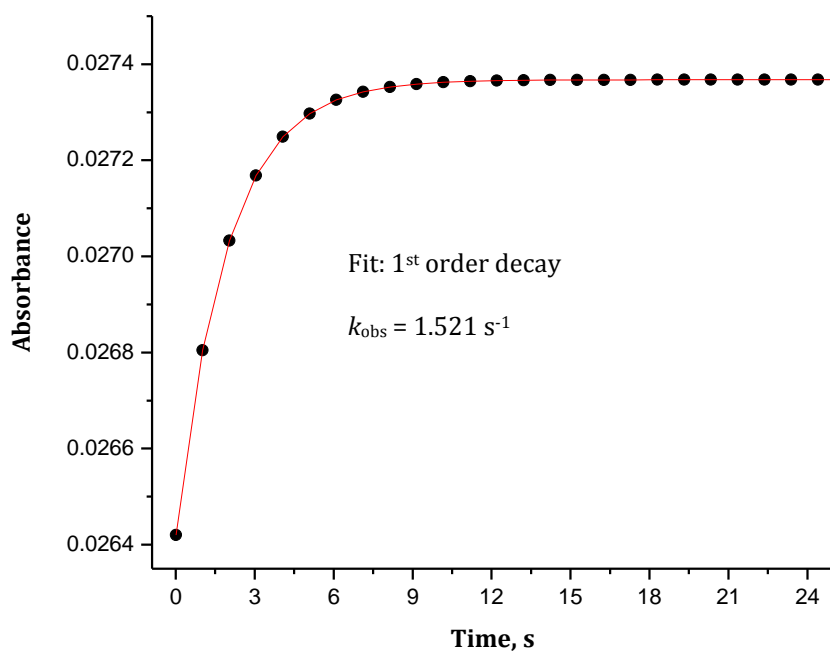


Figure S5.23: UV/Visible absorption versus time kinetic trace of **Ptdps** ($1.04 \times 10^{-4} \text{ M}$) with methyl imidazole ($2.08 \times 10^{-3} \text{ M}$ (20 fold)) taken at 295 nm, at $T = 298 \text{ K}$.

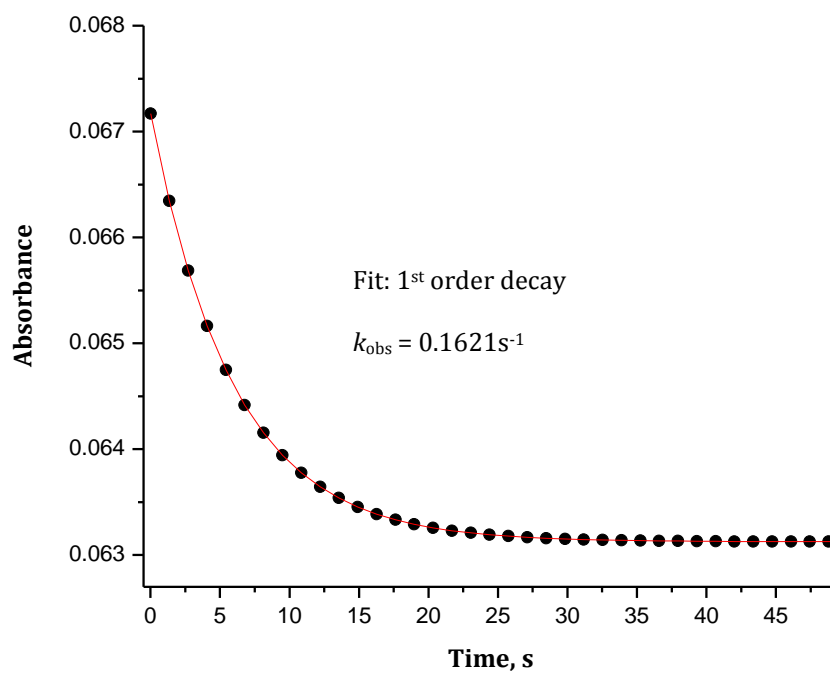


Figure S5.24: UV/Visible absorption versus time kinetic trace of **Ptdps** ($1.04 \times 10^{-4} \text{ M}$) with pyrazole ($2.08 \times 10^{-3} \text{ M}$ (20 fold)) taken at 285 nm, at $T = 298 \text{ K}$.

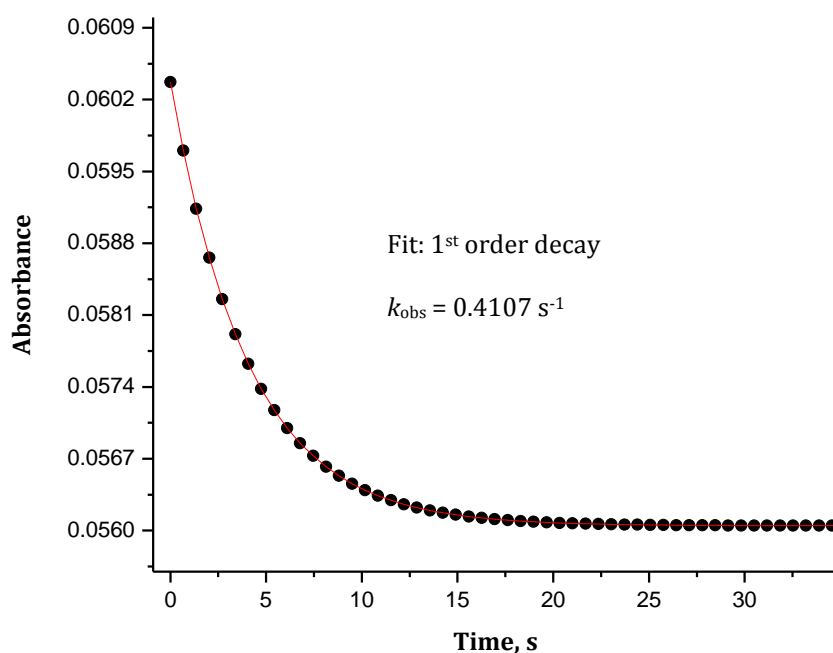


Figure S5.25: UV/Visible absorption versus time kinetic trace of **Ptdps** ($1.04 \times 10^{-4} \text{ M}$) with 1,2,4-triazole ($3.12 \times 10^{-3} \text{ M}$ (30 fold)) taken at 283 nm, at $T = 298 \text{ K}$.

Table S5.4: Summary of the wavelengths (nm) used to observe the reaction between the platinum(II) complexes and the neutral azole nucleophiles investigated.

Complex	Nucleophile	Wavelength, λ (nm)
Ptdpa	Im	290
	Pyz	250
	Trz	273
	MIm	264
	DIm	272
Ptdps	Im	260
	Pyz	286
	Trz	264
	MIm	295
	DIm	295

Table S5.4: Average observed rate constants, $k_{\text{obs}}, \text{s}^{-1}$ for **Ptdpa** (I = 0.1 M) and **Ptdps** (I = 0.01 M) by imidazole (**Im**), T = 298 K, {adjusted with NaClO_4 }.

Ptdpa		Ptdps	
[Im], M	$k_{\text{obs2}}, \text{s}^{-1}$	[Im], M	$k_{\text{obs2}}, \text{s}^{-1}$
0.000515	0.0003092	0.000520	0.5734
0.00103	0.0005038	0.00104	0.9930
0.00154	0.0006962	0.00157	1.440
0.00206	0.0009246	0.00209	1.994
0.00258	0.001130	0.00261	2.476

Table S5.5: Average observed rate constants, $k_{\text{obs}}, \text{s}^{-1}$ for **Ptdpa** (I = 0.1 M) and **Ptdps** (I = 0.01 M) by pyrazole (**Pyz**), T = 298 K, {adjusted with NaClO_4 }.

Ptdpa		Ptdps	
[Pyz], M	$k_{\text{obs2}}, \text{s}^{-1}$	[Pyz], M	$k_{\text{obs2}}, \text{s}^{-1}$
0.000515	0.0000777	0.000520	0.09297
0.00103	0.0000997	0.00104	0.1621
0.00154	0.0001317	0.00157	0.2213
0.00206	0.0001837	0.00209	0.2856
0.00258	0.0002091	0.00261	0.3938

Table S5.6: Average observed rate constants, $k_{\text{obs}}, \text{s}^{-1}$ for **Ptdpa** (I = 0.1 M) and **Ptdps** (I = 0.01 M) by 1,2,4-triazole (**Trz**), T = 298 K, {adjusted with NaClO_4 }.

Ptdpa		Ptdps	
[Trz], M	$k_{\text{obs2}}, \text{s}^{-1}$	[Trz], M	$k_{\text{obs2}}, \text{s}^{-1}$
0.000515	0.0001266	0.000520	0.1246
0.00103	0.0002566	0.00104	0.2439
0.00154	0.0003882	0.00157	0.4107
0.00206	0.0005206	0.00209	0.5629
0.00258	0.0007362	0.00261	0.6898

Table S5.7: Average observed rate constants, k_{obs} , s^{-1} for **Ptdpa** ($I = 0.1 \text{ M}$) and **Ptdps** ($I = 0.01 \text{ M}$) by 1-methylimidazole (**MIm**), $T = 298 \text{ K}$, {adjusted with NaClO_4 }.

Ptdpa		Ptdps	
[MIm], M	$k_{\text{obs2}}, \text{s}^{-1}$	[MIm], M	$k_{\text{obs2}}, \text{s}^{-1}$
0.000515	0.0005952	0.000520	0.8105
0.00103	0.001032	0.00104	1.521
0.00154	0.001343	0.00157	2.239
0.00206	0.001630	0.00209	3.038
0.00258	0.002611	0.00261	3.833

Table S5.8: Average observed rate constants, k_{obs} , s^{-1} for **Ptdpa** ($I = 0.1 \text{ M}$) and **Ptdps** ($I = 0.01 \text{ M}$) by 1,2-dimethylimidazole (**Dim**), $T = 298 \text{ K}$, {adjusted with NaClO_4 }.

Ptdpa		Ptdps	
[Dim], M	$k_{\text{obs2}}, \text{s}^{-1}$	[Dim], M	$k_{\text{obs2}}, \text{s}^{-1}$
0.000515	0.0005376	0.000520	0.3131
0.00103	0.0006410	0.00104	0.7134
0.00154	0.000794	0.00157	1.112
0.00206	0.001282	0.00209	1.543
0.00258	0.001590	0.00261	1.908

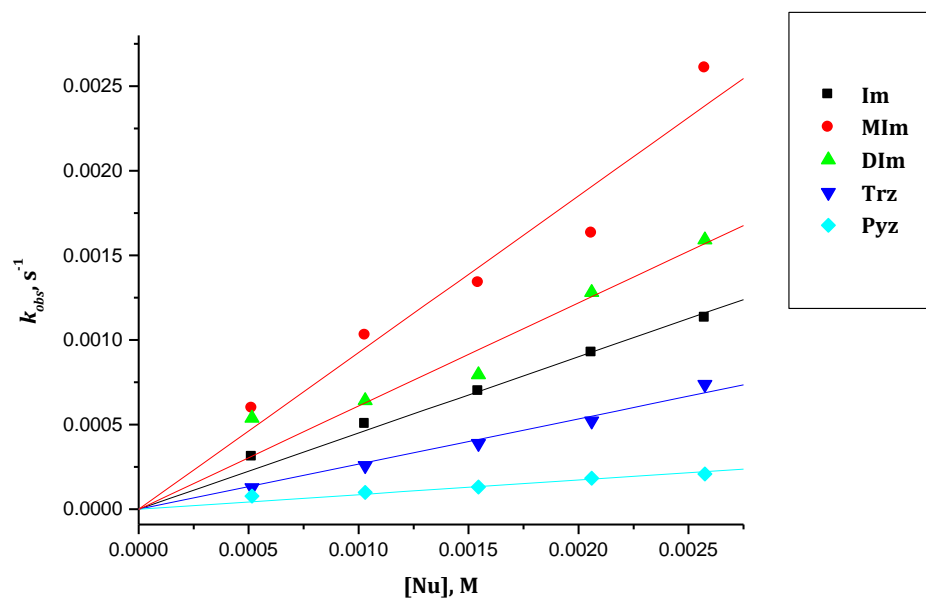


Figure S5.26: Plots of pseudo-first order rate constants (k_{obs}) against concentration of azole nucleophiles (**Im, Pyz, Trz, MIm & DIm**) for the aqua substitution reaction on **Ptdpa** in a pH 2, 0.010 M $HClO_4$ solution ($I= 0.10$ M ($HClO_4+ NaClO_4$)) at 298 K.

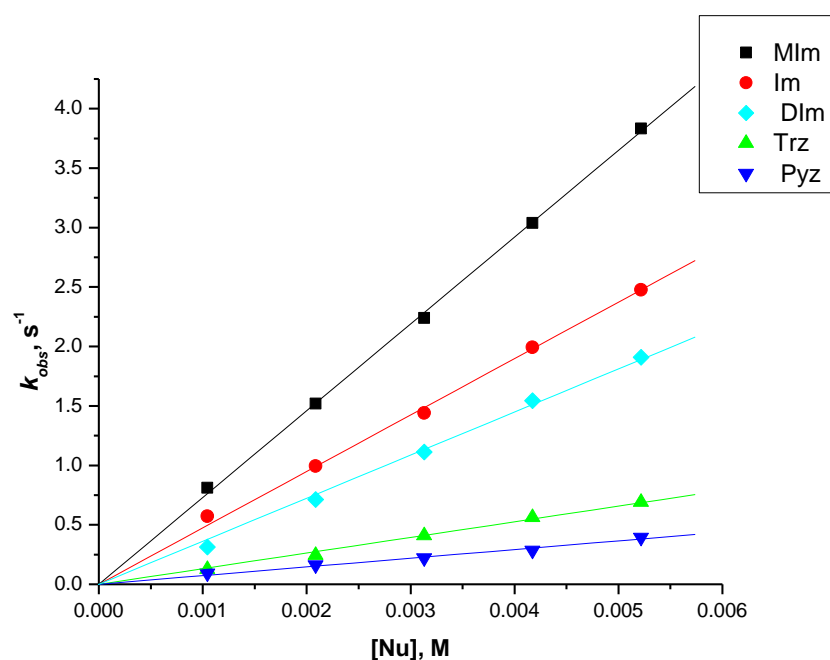


Figure S5.27: Plots of pseudo-first order rate constants (k_{obs}) against concentration of nucleophiles (**Im, Pyz, Trz, MIm & DIm**) for the aqua substitution reaction on **Ptdps** in a pH 3, 0.0010 M $HClO_4$ solution ($I= 0.010$ M ($HClO_4+ NaClO_4$)) at 298 K.

Table S5.9: Temperature dependence of k_2 , $M^{-1} s^{-1}$, for the displacement of the aqua ligand in **Ptdpa** ($I = 0.1 M$) and **Ptdps** ($I = 0.01 M$) by imidazole, {adjusted with $NaClO_4$ }.

Ptdpa		Ptdps	
1/T	ln (k_2/T)	1/T	ln (k_2/T)
0.00341	*	0.00347	-6.1547
0.00336	-6.7564	0.00341	-5.6559
0.0033	-6.4930	0.00336	-5.3326
0.00325	-6.1726	0.00330	-4.9500
0.00319	-5.8074	0.003247	-4.6542

Table S5.10: Temperature dependence of k_2 , $M^{-1} s^{-1}$, for the displacement of the aqua ligand in **Ptdpa** ($I = 0.1 M$) and **Ptdps** ($I = 0.01 M$) by pyrazole, {adjusted with $NaClO_4$ }.

Ptdpa		Ptdps	
1/T	ln (k_2/T)	1/T	ln (k_2/T)
10.0033	-8.3622	0.00347	-8.2158
0.00325	-7.9434	0.00341	-7.6373
0.00322	-7.8152	0.00336	-7.2055
0.00319	-7.4609	0.00330	-6.8267
*	*	0.00325	-6.6371

Table S5.11: Temperature dependence of k_2 , $M^{-1} s^{-1}$, for the displacement of the aqua ligand in **Ptdpa** ($I = 0.1 M$) and **Ptdps** ($I = 0.01 M$) by 1,2,4-triazole, {adjusted with $NaClO_4$ }.

Ptdpa		Ptdps	
1/T	ln (k_2/T)	1/T	ln (k_2/T)
0.00341	-7.9821	0.00347	-7.7146
0.00336	-7.6351	0.00341	-7.2144
0.0033	-7.1119	0.00336	-6.5871
0.00325	*	0.00330	-6.2998
0.00319	-6.5069	0.00325	-5.9843

Table S5.12: Temperature dependence of k_2 , $M^{-1} s^{-1}$, for the displacement of the aqua ligand in **Ptdpa** ($I = 0.1$ M) and **Ptdps** ($I = 0.01$ M) by 1-methylimidazole, {adjusted with $NaClO_4$ }.

Ptdpa		Ptdps	
1/T	ln (k_2/T)	1/T	ln (k_2/T)
0.00347	-8.28149	0.00347	-5.8130
0.00341	-7.629	0.00341	-5.3654
0.00336	-7.542	0.00336	-5.0552
0.0033	-7.404	0.00330	-4.6491
0.00325	-7.292	0.00325	-4.3693
0.00319	-7.194		

Table S5.13: Temperature dependence of k_2 , $M^{-1} s^{-1}$, for the displacement of the aqua ligand in **Ptdpa** ($I = 0.1$ M) and **Ptdps** ($I = 0.01$ M) by 1, 2-dimethylimidazole, {adjusted with $NaClO_4$ }.

Ptdpa		Ptdps	
1/T	ln (k_2/T)	1/T	ln (k_2/T)
0.00341	-7.1875	0.00347	-6.5486
0.00336	-6.7555	0.00341	-6.0888
0.00330	-6.3503	0.00336	-5.6733
0.00325	-5.8532	0.00330	-5.3484
0.00319	-5.5514	0.00325	-5.0351

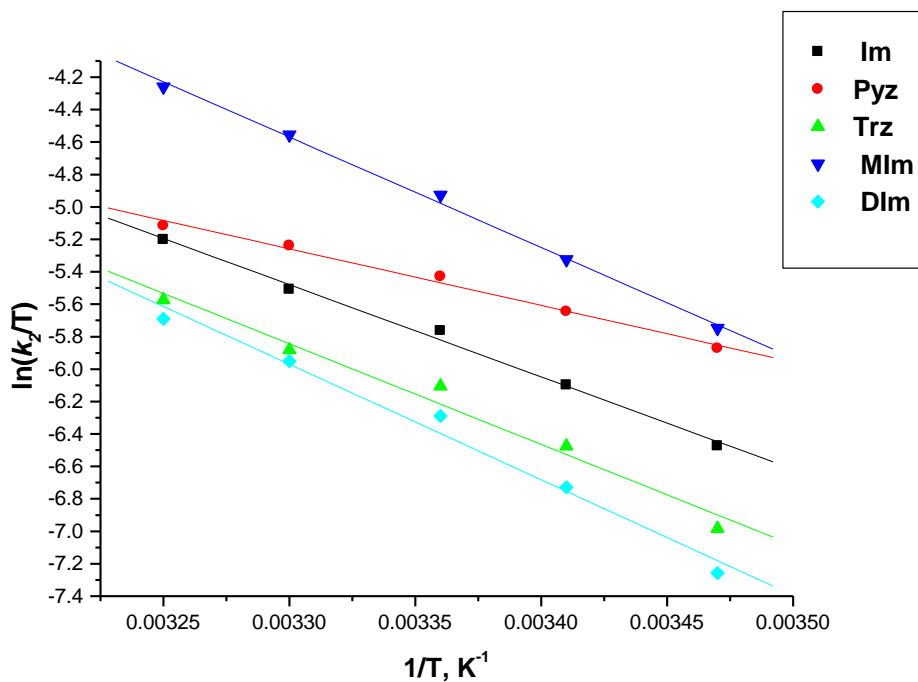


Figure S5.28: Temperature dependence plot of **Ptdpa** with all nucleophiles, **Im**, **Pyz**, **Trz**, **MIm** and **DIm**.

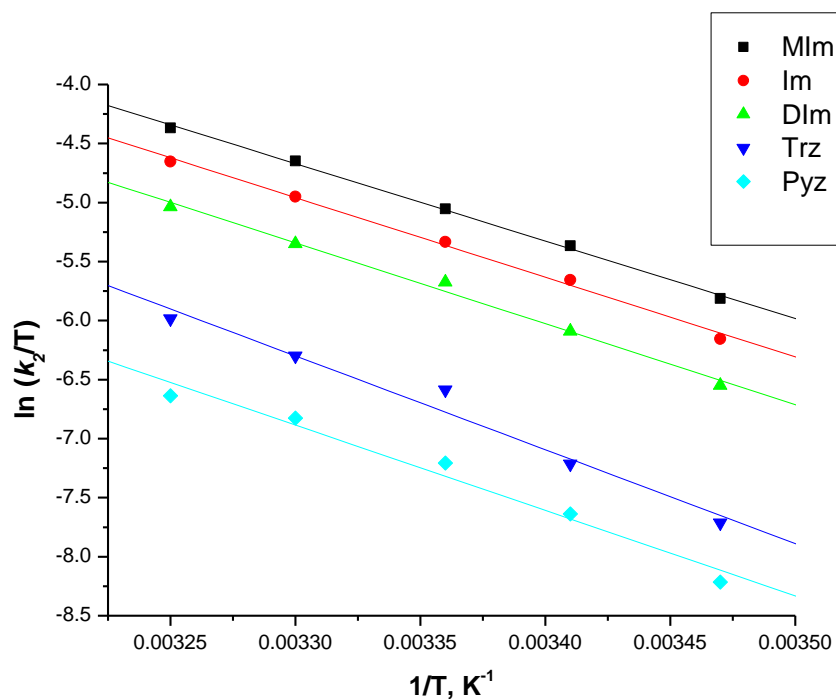


Figure S5.29: Temperature dependence plot of **Ptdps** with all nucleophiles, **Im**, **Pyz**, **Trz**, **MIm** and **DIm**.

CHAPTER 6

Summary and Future Work

6.1. Summary

Encouraged by the need to develop new Pt(II) complexes that exhibit improved anticancer activity, this primary aim of this study was to gain further insight into the kinetic properties of substitution reactions of square planar Pt(II) complexes with varying tridentate chelated ligand systems.

- When comparing the reactivity of a series of Pt(II) complexes with varying pyridyl and phenyl *trans*-ligands in the presence of *cis*-pyridyl and *cis*-quinolyl moieties. It was verified that Pt(II) complexes with *trans*-phenyl rings are more reactive than Pt(II) complexes with *trans*-pyridyl rings. However, it was intriguing to discover that this increase is reduced by the addition of quinolyl groups in the *cis*-positions. This is due to the overall σ -donation effect of the quinolyl moieties that counteracts the stronger *trans*-effect of the phenyl ring.^{1,2,3}
- The rate of aqua substitution for the Pt(II) complexes containing N^NN and N^SN ligand systems were compared and the reactivity of the complex with the *trans*-thioether donor was highly reactive due it being a good σ -donor and a π -acceptor.^{4,5,6}

By using bio-relevant heterocyclic *N*-donor azole nucleophiles for both aspects of this study, we have an idea of the bioinorganic reactions that could occur in the body when Pt(II) complexes of this kind reach the targeted DNA portion resembled by the azole nucleophile in this study.

6.2. Future Work

For the work reported in **Chapter 4**, we intend on extending the kinetic study by including a set of biological (glutathione and cysteine) and anionic nucleophiles (I^- , Br^- and SCN^-). This would allow us to get a better understanding of how these Pt(II) complexes will react with sulfur-containing components (glutathione and cysteine) found predominately in the biological system.^{7,8,9} Since the Pt centre is soft, it prefers coordinating to softer donor atoms such as sulfur instead of harder N-donor atoms. The interaction of the Pt(II) complex with S-containing molecules in the biological system prevent a large percentage of the Pt(II) complex from reaching the targeted DNA. The anionic nucleophiles will be included to determine how the rate of reactivity is affected by the polarizability of the incoming nucleophile.

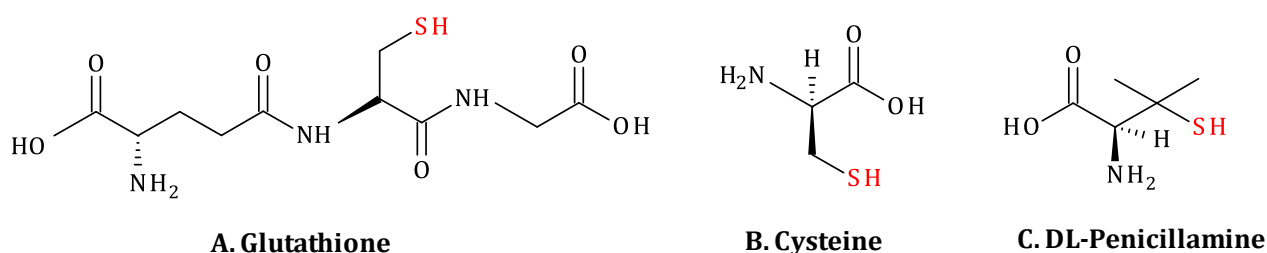


Figure 6.1: Sulfur-containing Biological Nucleophiles.

For the investigation reported in **Chapter 5**, we intend on extending the complexes studied and include two complexes each with *cis*-quinoline moiety and determine how this change affects the rate of substitution with theazole nucleophiles in comparison to **Ptdpa** and **Ptdps**

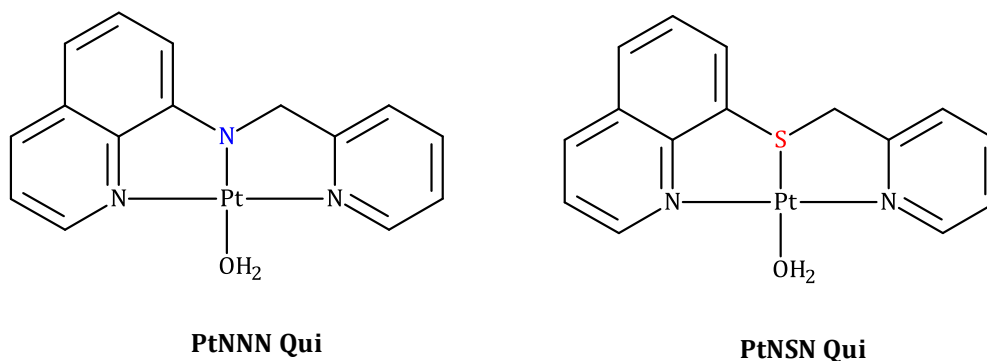


Figure 6.2: Two additional complexes to extend on **Chapter 5**.

We aim to evaluate all the Pt(II) complexes for cytotoxicity to determine if they could be active against certain human cancer types.

6.3. References

1. P. Ongoma and D. Jaganyi, *Dalton Trans.*, **2012**, *41*, 10724.
2. A. Shaira, D. Reddy and D. Jaganyi, *Dalton Trans.*, **2013**, *42*, 8426 – 8436.
3. A. Hofmann, L. Dahenburg and R. van Eldik, *Inorg. Chem.*, **2003**, *42*, 6528-6538.
4. B. Pitteri, M. Bortoluzzi and G. Marangoni, *Transition. Met. Chem.*, **2005**, *30*, 1008.
5. S. Hochreuther, S. T. Nandibewoor, R. Puchta and R. van Eldik, *Dalton Trans.*, **2012**, *41*, 512.
6. B. Pitteri and M. Bortoluzzi, *Polyhedron*, **2006**, *25*, 2698.
7. L.R. Kelland, N.P. Farrell, *Platinum-Based Drugs in Cancer Therapy*, **2000**, Humana Press, p. 321-337.
8. X Wang and Z. Guo, *Anticancer Agents in Medical Chemistry*, **2007**, *7*, 19-34.
9. B. Rosenberg, *Fundamental Study with Cisplatin*, **1984**.